UNIVERSITÀ
DEGLI STUDI
DI PADOVA

Sede Amministrativa: Università degli Studi di Padova

Dipartimento di Scienze del Farmaco

CORSO DI DOTTORATO DI RICERCA IN: **SCIENZE MOLECOLARI**
CURRICOLO: **SCIENZE FARMACEUTICHE**
CICLO: **XXIX**

MOLECULAR MECHANISMS OF RECOGNITION OF COAGULATION FACTORS

Coordinatore: Ch.mo Prof. Antonino Polimeno

Supervisore: Ch.mo Prof. Vincenzo De Filippis

Dottoranda: Giulia Pontarollo

Contents

ABSTRACT

The biochemical pathways sustaining living organisms, traditionally regarded as independently organized systems, are actually extensively connected by non-canonical protein interactions. The disruption of this finely regulated homeostasis, largely yet to unravel, results in various pathological manifestations.

Haemostasis (**Chapter 1**) is a defence response triggering after vessel walls injuries, which is articulated in the cascade activation of the blood coagulation factors, resulting in the generation of a localized clot. The central reaction of the coagulation cascade is prothrombin activation to mature α-thrombin by FXa, through the generation of the physiologically relevant intermediate prethrombin-2. Active α-thrombin is an ellipsoidal protein, composed of two six-stranded β-barrels encompassing, at their interface, the catalytic triad (His57, Asp102, Ser195). Opposite to the negatively charged active site, two extra positive regions of binding, named exosite I and exosite II, mediate the recognition with several physiologic ligands and substrates. Mature α-thrombin plays a pivotal role in haemostasis, entailing both procoagulant functions (platelets aggregation, fibrin generation) and an anticoagulant one (protein C activation). Beyond coagulation, this serine protease acts at the interface between inflammation, cellular proliferation, and neurodegenerative diseases.

The interplay between α-thrombin and proteins traditionally belonging to the central nervous system is undoubtedly a pioneering and yet unexplored topic (**Chapter 2.1**). When present at high cerebral concentrations α-thrombin triggers a pathologic pro-inflammatory state in the brain, which may be involved in the onset of neurodegenerative diseases. In detail, we refer to as *synucleinopathies* for a branch of diseases (i.e. Parkinson's disease) in which intracellular proteinaceous aggregates, mainly composed of α-synuclein, localize both in neurons and in glia. α-synuclein is an abundant presynaptic protein, belonging to the family of naturally unfolded proteins (NUPs), whose physiologic function is still matter of debate. Strikingly, beyond central nervous system, α-synuclein has been detected in plasma and in the haematopoietic lineage, particularly in platelets. Surprisingly, patients suffering from Parkinson's disease, featuring high α-synuclein concentrations, are characterized by lower ischaemic attacks, due to platelets abnormalities and impaired aggregation. Being these cells the main trigger of α-thrombin, we purposed to investigate the interaction between this enzyme and α-synuclein (**Chapter 2.2**). Our data clearly demonstrate that the two proteins bind with an affinity physiologically relevant for the concentrated microenvironment surrounding platelets. In the binary complex, α-synuclein interacts promiscuously with α-thrombin exosites by its negatively charged de-structured C-terminus, thus scavenging hyper-aggregation phaenomena.

In this intricate network, positive upregulation between coagulation and inflammation has been well established and extensively studied (**Chapter 3.1**). During sepsis, systematically activated immune response results in an exaggerated and detrimental inflammation, usually coupled to disseminated intravascular coagulation. In this scenario, exogenous proteases may play a relevant role during the early stages of the infection by directly activating coagulation. Several pathogen microorganisms express and secrete subtilisin-like serine proteases (subtilases), characterized by a broad specificity of cleavage. We purposed to investigate the effects of subtilases-catalysed proteolysis of thrombin zymogens prethrombin-2 (**Chapter 3.2**) and prothrombin (**Chapter 3.3**) by using the commercially available subtilisin Carlsberg, as a prototype for the superfamily. From the proteolysis and enzymatic assays data, it strikingly emerged that subtilisin activates both the zymogens to a novel thrombin-like specie, by the non-canonical hydrolysis of Ala470(149a)-Asn471(149b) peptide bond. The novel active specie, we named σPre2, is a non-covalent complex featuring the same α-thrombin cleavage specificity, with a catalytic efficiency ≈150-fold inferior to the physiologic enzyme. From fluorescence titrations and surface binding resonance, it emerged that σPre2 is characterized by a fully competent exosite II, an imperfect exosite I and a correctly moulded active site, which however features an impaired mechanism of substrate conversion.

Both experimental and clinical evidences clearly demonstrate the crucial importance of maintaining coagulation homeostasis, which, in physiologic conditions, is slightly unbalanced towards a haemorrhagic state to keep blood fluid in the intact vessels. A disruption of this equilibrium due to increase of functioning leads to pathological manifestations generically referred to as *thrombosis* (**Chapter 4.1**). Unfortunately, classical anticoagulant therapy presents well-documented limitations and bleeding side effects, driving the continuous efforts to develop new, safer drugs. In the late years, a hot research topic is represented by the engineering of natural anticoagulants from hematophagous organisms. Among all, anticoagulant hirudin from the medicinal leeches is the most popular compound, being α-thrombin most potent and specific natural inhibitor. In this work, we propose a novel strategy for hirudin production in *E. coli*, by conjugation to SUMO (small ubiquitin-like modifier protein), a eukaryotic chaperon which enhances protein folding and solubility (**Chapter 4.2**). The so-obtained recombinant hirudin is characterized by the same folding, spectroscopic features, and anti-thrombin activity of the natural variant.

In conclusion, coagulation is undoubtedly one of the most articulated and fascinating physio-pathologic systems regulating body homeostasis, displaying several connections with other biochemical pathways. The molecular mechanisms of recognition of the coagulation factors, yielding traditional or original protein interactions, is still a highly unexplored topic.

INTRODUCTION

CHAPTER 1

The Biochemistry of Coagulation

The Coagulation Cascade

Haemostasis is an extremely complex and finely regulated biochemical response that triggers after vascular damage of vessel walls and exposure of subendothelial tissue to the blood. This process, involving both cellular responses and enzymatic events, is organized in two consequent and synergic steps. During *primary haemostasis*, activated platelets adhere to subendothelial collagen and aggregate in a localized clot. In *secondary haemostasis*, an insoluble fibrin network anchors the platelets and further stabilizes the clot.

In particular, the coagulation cascade [**1**] is a flow of enzymatic reactions performed by blood zymogens mutually activated by limited proteolysis: the coagulation factors (FI-FXIII). The cascade is articulated in the *intrinsic* pathway, starting from FXII in the blood, and in the more relevant *extrinsic* pathway, from subendothelial tissue factor (TF), interacting with FVII/FVIIa. Both the intrinsic and the extrinsic cascades converge in the common pathway, to the activation of prothrombin (FII) to active α-thrombin (FIIa) (**Fig. 1**).

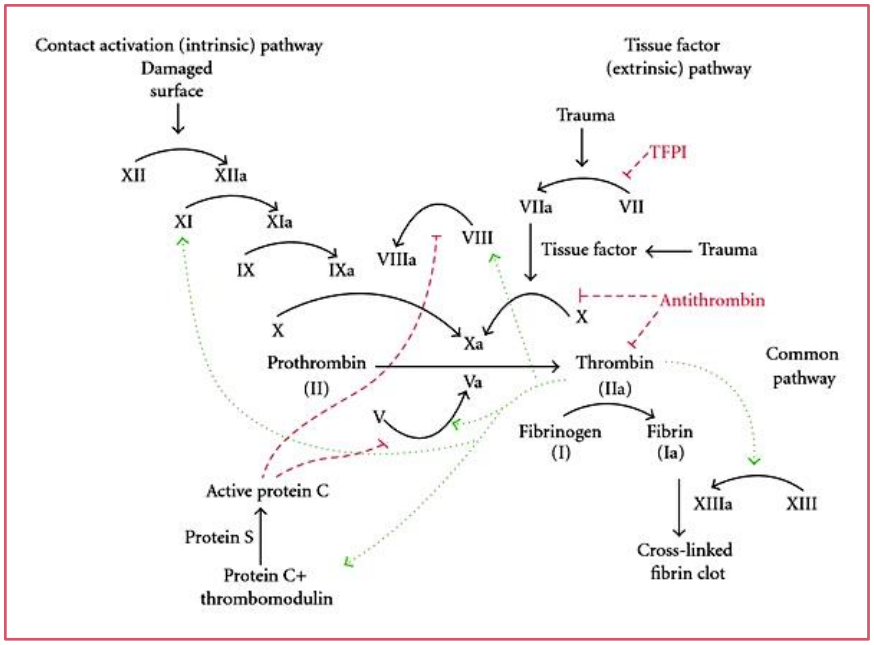

Figure 1. Schematic diagram of the coagulation cascade. The conversion of the coagulation factors (indicated by the roman numbers from I to XIII) from zymogens to the respective active (a) form is highlighted by black arrows. Red dashed lines stress the natural anticoagulant pathways, while green dots arrows indicate thrombin-activated reactions.

Prothrombin Structure

Human prothrombin (ProT) is a vitamin K-dependent zymogen, synthetized in the liver as a prepro-enzyme. Before secretion in the blood, this precursor undergoes a variety of posttranslational modifications: removal of the signal pre-peptide; conversion of ten Glu to γ-carboxyglutamic acid (Gla) residues on the N-terminal of ProT [**2**]; removal of the pro-peptide; attachment of three N-linked carbohydrate chains at N78, N100 and N373.

Mature ProT (579aa, 72.3kDa) circulates in plasma at 0.1 mg/ml, and it is characterized by a half-life of about 60 hours [**3**]. This single chain glycoprotein can be structurally divided in fragment 1 (1-155), fragment 2 (156-271) and the protease domain (272-579). Fragment 1 contains Gla domain (1-46) and kringle-1 (K1, residues 65-143), fragment 2 contains kringle-2 (K2, residues 170-248), while the protease domain encompasses A chain (285-320) and B chain (321-579).

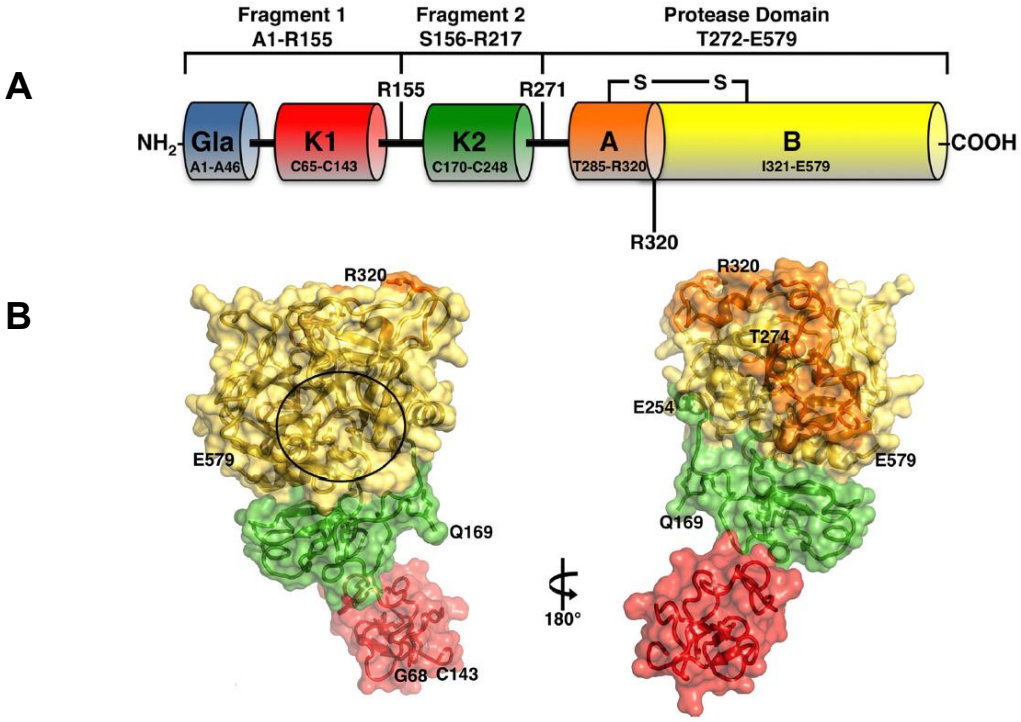

Figure 2 [from Pozzi et al., 2014]. (A) Schematic representation of human ProT in its colour coded architecture domains. Gla domain (1-46) in blue, and K1 (65-143) in red, compose fragment 1 (1-155); fragment 2 (156-271) encompasses K2 (170-248) in green; the protease domain (272-579) comprises A chain (285-320) in orange, and B chain (321-579) in yellow, linked by a disulphide bridge. The three flexible linkers are shown as thick black segments. **(B) Three-dimensional structure of S525A mutant of Gla-domainless ProT (45-579) (pdb: 4hzh).** ProT domains are displayed in the same colours as in **panel A**; α-thrombin active site is stressed by a black circle. None of the linkers could be resolved in the electron density map. Overall, the molecule is 80Å long, with fragment 2 coaxial with the protease domain and fragment 1 bent with a 36-degrees angle relative to the main axis.

All these regions are connected by flexible linkers, referred to as Lnk1, Lnk2 and Lnk3. Lnk1 (47-64) connects Gla to K1, Lnk 2 (144-169) connects K1 to K2, while Lnk3 (249-284) connects K2 to the protease domain (**Fig. 2A**). Overall, ProT bears twelve disulphide bridges: two in Gla domain, three both in the highly compact K1 and in K2, and four in the protease region, of which one connects A to B chain [**4**].

Until only few years ago, the three-dimensional architecture of ProT (intimately connected to its activation mechanism) was still elusive. In 2013, Pozzi and co-workers reported the first x-ray crystal structure of Gla-domainless (GD) ProT (45-579), at 3.3Å resolution. The structure (pdb: 4hzh), carrying an Ala replacement of the catalytic Ser525, features an overall 80Å bent conformation, in which the domains are not vertically stacked. In detail, while fragment 2 is coaxial to the protease domain, fragment 1 is positioned at a 36-degrees angle relative to the main axis. Notably, none of the three Lnk could be resolved in the electron density map (**Fig. 2B**). By luminescence resonance energy transfer (LRET) measurements, two distinct ProT conformations, populated in a 3:2 ratio, were detected: one fully extended (K1-K2 = 54 ± 2Å) and the other partially collapsed (K1-K2 < 34Å), as suggested by the crystal structure [**5**].

Beyond its well-established role in the coagulation cascade, ProT is involved in embryonic development [**6**;**7**], it has been detected in the cerebrospinal fluid of patients suffering from progressive neurodegenerative diseases [**8**], and it is the target of antibodies in the antiphospholipid syndrome (APS) [**9**].

The Prothrombinase Complex

In the penultimate step of the coagulation cascade, ProT (579aa, 72.3kDa) is proteolitically converted to active α-thrombin (295aa, 36.7kDa) by the prothrombinase complex, comprising FXa, FVa, Ca^{2+} and phospholipids [**10**] (**Fig. 3**). FXa functions as the enzymatic component, while the other cofactors all augment the rate of the FXa-catalysed cleavage. With respect to FXa alone, the catalytic constant k_{cat} of ProT conversion in the prothrombinase complex is more than 3000-fold enhanced. Notably, only in the cumulative presence of all the actors, FXa rate of hydrolysis is efficient under normal physiologic conditions (**Table 1**). In order to unravel the molecular mechanism of this multipart enzymatic activation, in 1979 Nesheim and colleagues investigated the role of each component of the complex. In detail, Ca^{2+} favours the anchoring of the highly negative Gla domains of both ProT and FXa to the phospholipid bilayer. The role of the membrane is simply to provide an active surface on which the catalysis occurs. As a proof of this hypothesis, the effect of activated platelets on the rate of hydrolysis is indistinguishable from synthetic vesicles made of

phosphatidylcholine and procoagulant phospholipids as phosphatidylserine. The role of FVa is particularly intriguing, because the zymogen FV can be activated by freshly generated α-thrombin, with a positive feedback amplification of the clotting. In effect, pro-cofactor FV interacts with the other components in a similar fashion to the activated factors, and possesses minimal but measurable procoagulant activity. Overall, the prothrombinase complex, in spite of its remarkable complexity, formally behaves as a typical enzyme, obeying to the Michaelis-Menten model [**11**].

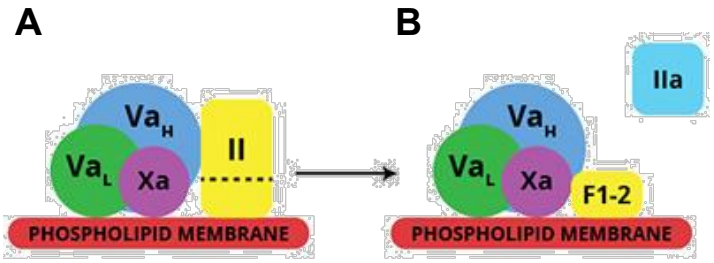

Figure 3. Schematic representation of the prothrombinase complex. The phospholipid membrane, on which the catalysis occurs, is represented in red. Both FXa, in violet, and ProT (FII), displayed in yellow in **panel A**, anchor to the bilayer by their Gla domain. FVa, in its light (in green) and heavy (in blue) chain, provides a scaffold on which the enzyme and the substrate can align properly. After the proteolysis, ProT fragments 1-2 still maintain a certain affinity for the complex, while α-thrombin (FIIa, displayed in cyan in **panel B**) is released in the surrounding environment.

Additions	Relative Rate[a]
Xa	1.0
Xa, PCPS	1.0
Xa, $Ca2^+$	2.3
Xa, Ca^{2+}, PCPS	22
Xa, Ca^{2+}, Va	356
Xa, Ca^{2+}, PCPS, Va	278000
Xa, Ca^{2+}, PCPS, Va[b]	480000

Table 1. Relative rates of ProT activation in the presence, in turn, of the different components of the prothrombinase complex [adapted from Nesheim et al., 1979]. All the measurements were performed in physiologic conditions at 22°C, keeping FVa as the limiting factor. PCPS: surface of phosphatidylcholine /phosphatidylserine, either synthetic or on activated platelets. [a] The rate of α-thrombin generation, relative to FXa alone, is expressed as moles of α-thrombin per minute per moles of FXa. [b] Velocity of the reaction at V_{max}.

Recent investigations shed new light on the mechanism of ProT activation. During the proteolysis *in vivo*, both ProT and FXa anchor to the platelets membrane through their Gla domain. In this scenario, cofactor FVa provides a scaffold on which enzyme and substrate may align for the catalysis. Mutagenesis studies have identified possible epitopes for the interaction of ProT with the

prothrombinase complex. K1, K2 [**12**;**13**], as well as α-thrombin regions, like exosite I [**14**] and the autolysis loop [**15**] interact with cofactor Va. On the other side, K2 [**16**], Gla domain [**17**] and α-thrombin exosite II [**18**] bind to the enzymatic FXa. According to a recent model, removal of Lnk2 may mimic the effect of FVa on ProT activation. The deletion mutant ProTΔ146-167 presents a contorted architecture, in which the domains are not vertically stacked: K1 comes close to the protease domain, while K2 contacts Gla domain. Since this distorted architecture reduces the enhancement of the catalysis from >3000-fold to only 60-fold in the presence of FVa, ProTΔ146-167 may be a close representation of the substrate conformation in the prothrombinase complex. In other words, the flexibility of Lnk2 allows ProT to explore multiple conformations, constituting an entropic barrier for optimal interaction with FXa [**19**]. Binding of FVa, in concert with the membrane, relieves this entropic cost by compressing ProT in a proper conformation for the cleavage [**4**].

Prothrombin Activation to Mature α-Thrombin

ProT is proteolytically activated to mature α-thrombin by hydrolysis at two sites: R271, after fragments 1 and 2 (F1·2), and R320, between the light A and the heavy B chain, generating the active site. Since this activation proceeds along two mutually exclusive pathways, two different intermediates are achieved, depending on which cleavage is performed first (**Fig. 4**). If the first hydrolysis occurs at R271, F1·2 is released, with the generation of inactive prethrombin-2 (308aa, 38.2kDa). On the other hand, if the first cleavage occurs at R320, the protein is all held together by the disulphide bridge between A and B chain, with the generation of active meizothrombin (579aa, 72.3kDa). The process is completed with the second cleavage at R271/R320 by FXa, and by an auto-proteolysis performed by active thrombin at R284 [**20**]. Mature (285-579) α-thrombin (295aa, 36.7kDa) accomplishes a further cleavage at R155, between fragment 1 and fragment 2.

Since both sites of cleavage (R271, R320) are exposed to the solvent and equally accessible to the proteolytic attack, the mechanism through which protrombinase selects the pathway of activation is still matter of debate. It has been reported that on the surface of platelets activation through prethrombin-2 (Pre2) is the preferred pathway [**21**]. By contrast, on red blood cells surfaces or on synthetic phospholipids vesicles, the activation proceeds through the active meizothrombin (mIIa) intermediate [**22**]. The directionality of the cleavage is likely to be influenced long range by ProT Gla domain *via* Lnk1 and Lkn2, in response to the nature of the membrane. As a proof of this hypothesis, deletion of Lnk1 switches on ProT activation through Pre2 intermediate. In detail, Lnk1 contains two helices connected by a disulphide bridge between C47 and C60.

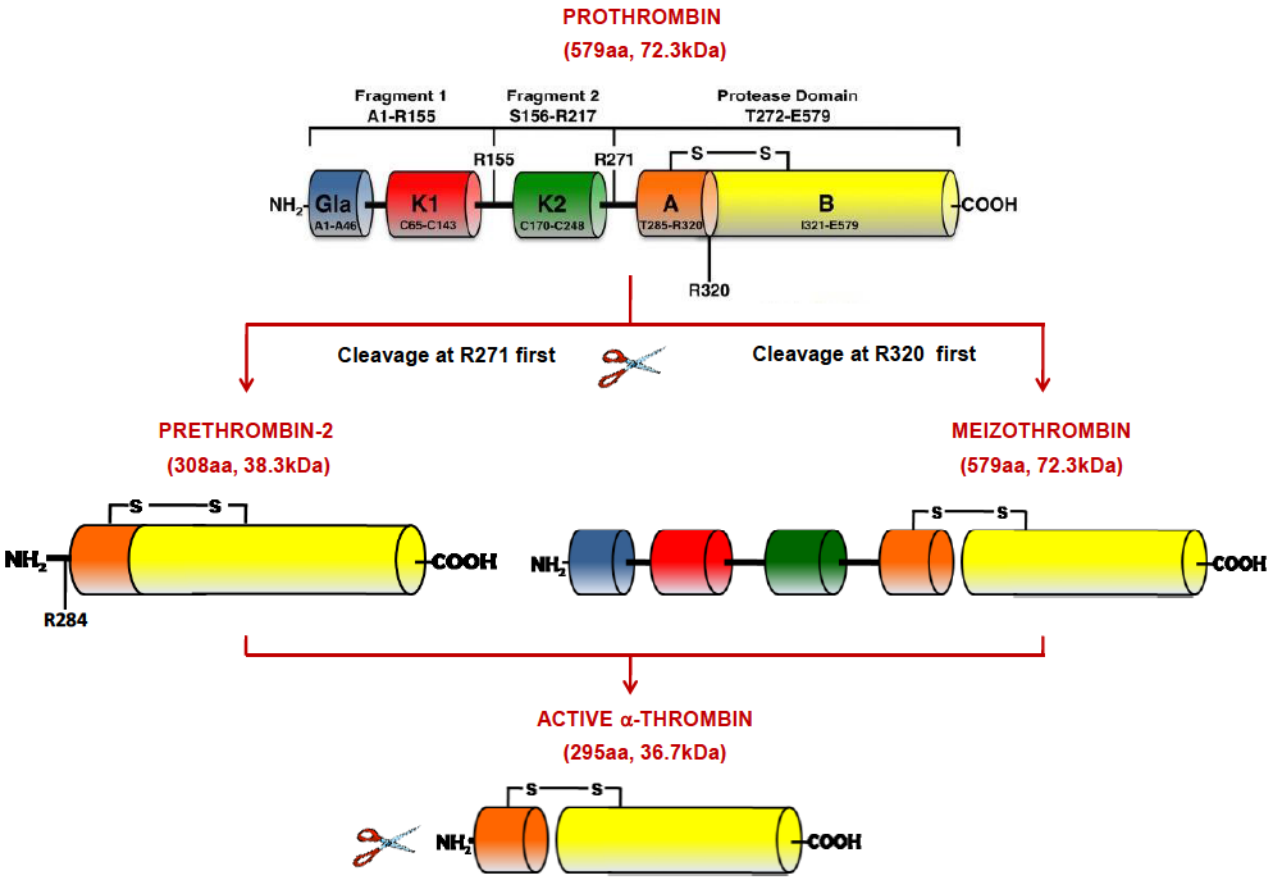

Figure 4. Alternative pathways of ProT activation by FXa. ProT is represented in its colour coded architecture domains, like in **Fig. 2A**. Two cleavages are necessary to achieve mature α-thrombin: R271, between K2 and the protease domain, and R320, between A and B chain. If cleavage at R271 is performed first, inactive prethrombin-2 is generated. On the other hand, if the first cleavage occurs at R320, active meizothrombin intermediate is achieved. The activation process is completed by the missing cleavage, and by an additional cleavage performed at R284 by thrombin itself, through an auto-proteolysis mechanism. Mature α-thrombin is composed by the light A and the heavy B chains, held together by a disulphide bridge.

Through this region, the Gla domain, anchored to the phospholipids bilayer, influences K1 position and propagates the conformational changes to the site of cleavage, located 80Å away, through flexible Lnk2 [**23**]. In an analogue way, removal of Lnk2 turns off the activation pathway through mIIa [**4**]. Moreover, specific receptors of FVa and FXa are present on the surface of activated platelets [**24**; **25**;**26**]. It is likely that the primary biological surface on which the prothrombinase complex assembles is that of the activated platelets. The resulting procoagulant effect is ensured by the fact

that inactive Pre2 is formed, but not released from the platelets-associated complex until the second cleavage at R320.

On the other hand, the prothrombinase complex is quite inefficient in completing α-thrombin generation through mIIa intermediate. In detail, in 40% of cases active mIIa is released in the surrounding environment, while only 60% is channelled *via* a concerted mechanism through its activation process [**27**]. The intermediate mIIa features an overall anticoagulant activity: it keeps the same efficiency (93%) for the generation of anticoagulant active protein C, while it retains only 7% and 2% productively in fibrin generation and platelets activation, respectively [**28**]. Meizothrombin production (and release) has been reported during atherosclerosis. After the rupture of the atherosclerotic plaques, lipid rafts and cellular debris assemble in vesicles somehow similar to the synthetic ones, providing an active surface on which the prothrombinase complex assembles [**29**]. In conclusion, while in physiologic conditions ProT hydrolysis on active platelets promotes an overall procoagulant response [**30**], in pathological manifestations in which an anticoagulant homeostasis is required, alternative phospholipid surfaces direction prothrombinase activity toward the production and release of active mIIa.

In vivo, the dynamic concentration of free α-thrombin after its generation is estimated to vary from 1nM (0.1 U/ml) to over 100-500nM in the coagulation burst, depending on detection methods and experimental conditions [**31**]. Whether this enzyme can reach such extraordinary concentrations remains an un-answered question. In return, α-thrombin half-life *in vivo* is very short.

Thrombin Functions

Mature α-thrombin (αT), the final protease of the coagulation cascade, is the key enzyme of haemostasis, exerting both pro- and anticoagulant functions through the interaction with numerous binders and substrates. Procoagulant roles entail fibrin generation and platelets aggregation, while the only anticoagulant action is protein C activation [**32**]. Moreover, αT promotes massive amplification of the coagulation cascade by proteolitically converting FV, FVIII and FXI to their active forms, leading eventually to its own generation by a positive feedback mechanism [**2**] (**Fig. 5**).

The conversion of soluble fibrinogen (FI) to an insoluble fibrin clot (FIa) is undoubtedly αT most specific function, and it proceeds through many steps. Human fibrinogen circulates in the plasma (2.6 mg/ml) as a heterodimer of three chains $(A\alpha B\beta\gamma)_2$, covalently linked by disulphide bonds. The overall protein structure is stretched, displaying a central *E* nodule and two terminal *D* knobs [**33**].

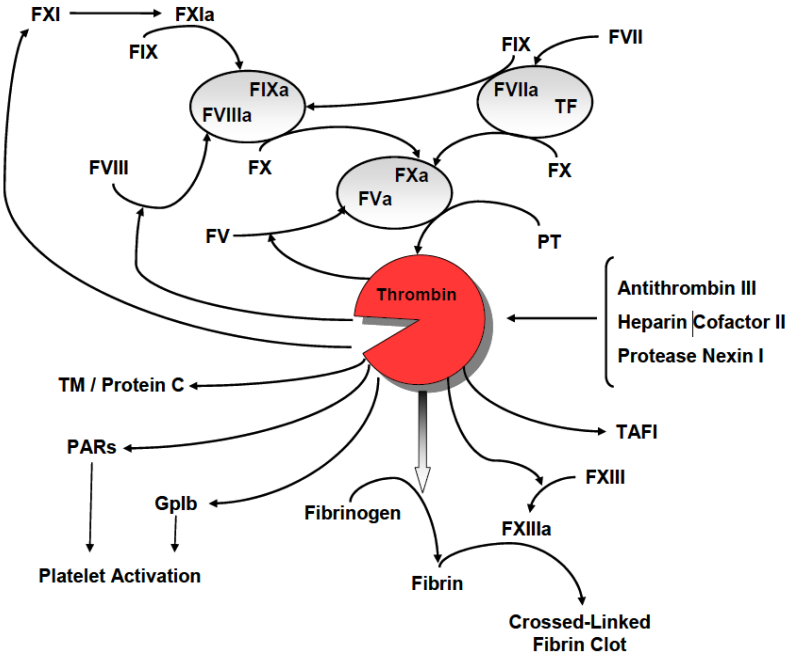

Figure 5. Thrombin central role in the coagulation cascade. After its release in the bloodstream, αT promotes the generation of a localized clot at the site of injury by platelets activation (through binding to GpIbα and cleavage of PARs) and fibrin generation, further stabilized by FXIIIa. Thrombin amplifies the coagulation cascade through the activation of FV, FVIII and FXI; on the other hand, it promotes its own down-regulation by protein C activation pathway. Antithrombin III, heparin cofactor II and protease nexin I are the main serine proteases inhibitors, acting in different body districts.

αT attacks the Aα chains first, with the release of two fibrinopeptides A (FpA, 16aa) and fibrin I monomer. The latters undergo longitudinal elongation through non-covalent staggered associations between *D* and *E* knots, assembling in protofibrils. After proteolysis by αT at the Bβ chains, with the release of two fibrinopeptides B (FpB, 14aa), protofibrils aggregate laterally through stacking interactions, resulting in insoluble fibrin fibres [**34**]. The scaffolds of the ensuing clot are further stabilized by αT-activated FXIIIa. This transglutaminase imparts structural integrity to the fibrin network by covalent cross-linking of Glu and Lys residues on adjacent fibrin molecules.

During primary haemostasis αT triggers platelets aggregation through the proteolysis of surface protease activated receptors (PARs), which are members of the G-protein-coupled-receptors superfamily [**35**]. Two PARs are involved in the haemostatic process: PAR-1 is the first receptor encompassed, whose activity is reinforced by PAR-4 at higher αT concentrations [**36**]. The protease cleaves PARs within the extracellular N-terminal domain, generating a newly exposed N-terminus, which binds itself on the receptor body promoting signal transduction [**37**] (**Fig. 6**).

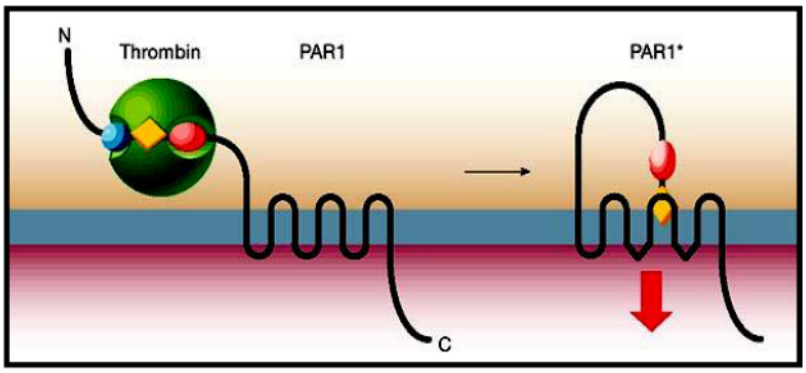

Figure 6. Platelets activation by thrombin-mediated PAR-1 cleavage. αT recognizes and cleaves PAR-1 N-terminal extracellular domain. The newly generated N-terminus acts itself as a ligand, bending on the receptor body.

After activation, platelets expand, generate sticky protuberances called *pseudopods*, degranulate and express on their surface the receptors GpIIb/IIIa, promiscuous for both fibrinogen and von Willebrand factor [**38**]. Platelets present two kinds of granules: δ-granules (Ca^{2+}, ADP, ATP, serotonin) [**39**] and α-granules (containing several coagulations mediators) whose release is driven by Ca^{2+} and determines an overall proaggregant effect [**40**]. Finally, platelets membrane becomes a highly active surface by expression of procoagulant phospholipids as phosphatidylserine. αT binds platelets by the surface glycoprotein GpIbα, which acts as a cofactor in cleavage of PAR-1, but may also mediate platelets activation in a non-proteolytic manner [**41**].

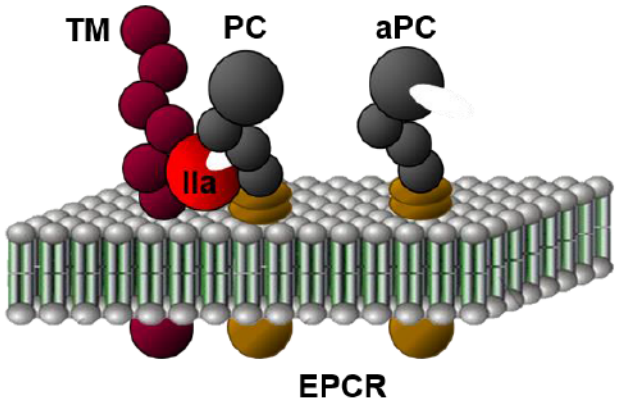

Figure 7. Thrombin anticoagulant activation of protein C. The activation of the zymogen (PC) to the active form (aPC) by αT (IIa) is a thousand-fold enhanced by endothelial thrombomodulin (TM) and by PC binding to its endothelial cells receptor (EPCR).

By contrast, αT promotes its own down-regulation by activating the protein C (PC) pathway. Upon contact with thrombomodulin (TM), which is an integral membrane protein present on the vascular endothelial cells, the specificity constant of the enzyme towards the zymogen protein C is greater than thousand-fold enhanced. A further increase of the reaction rate is provided by the presence of a specific endothelial cell protein C receptor (EPCR) [**42**] (**Fig. 7**). Activated protein C (aPC) cleaves and inactivates FVa and FVIIIa, two essential co-factors for the amplification of the coagulation cascade. Hijacking of αT by TM and activation of PC in the microcirculation constitute the natural anticoagulant pathway that prevents massive intravascular conversion of fibrinogen into an insoluble clot upon αT generation.

Beyond coagulation, αT elicits its action on many cells other than platelets, mainly mediated by activation of surface PARs. This serine protease stimulates a variety of responses in endothelial cells, including expression of growth factors, and the secretion of cytokines and adhesion molecules. αT also promotes cytokine elaboration by smooth muscle cells and stimulates the proliferation of both smooth muscle cells and fibroblasts.

Since αT is involved in a variety of biochemical pathways, a compelling regulation of its activity is essential to prevent excessive or improperly clot formation. Some members of the serine protease inhibitor (serpin) superfamily hinder αT catalytic activity, like antithrombin (originally called antithrombin III, ATIII), heparin cofactor II (HCII) and protease nexin I (PNI). For all the serpins, the rate of inhibition reaction is greatly accelerated in the presence of glycosamminoglycans such as heparin, heparan sulphate, and dermatan sulphate [**43**]. ATIII, circulating in the blood at 2.3μM, is the main inhibitor of intravascular coagulation, acting on several serine procoagulant proteases. In contrast, HCII is highly specific for αT, and regulates its activity in extravascular tissues following vascular injury, whereas PNI is likely to inhibit αT at or near the surface of a variety of cell types, but especially in the brain [**44**]. In addition to these endogenous αT inhibitors, several potent exogenous ones have been isolated from hematophagous organisms, including hirudin and haemadin from the leeches *Hirudo medicinalis*, *Hirudinaria manillensis* and *Haemadipsa sylvestris*, respectively.

Despite αT extremely short half-life *in vivo*, non-physiologic autolytic degradation products may be generated *ex vivo*. Upon prolonged storage in solution, human αT is first autolytically converted to β-thrombin (βT) by the cleavages at R75-Y76 and R77a-N78 bonds (chymotrypsinogen numbering - see **Appendix B**). If βT undergoes additional cleavage of the K149e-G150 bond, γ-thrombin (γT) is generated. Although the catalytic activities of α-, β-, and γ-thrombin are roughly

similar with respect to the hydrolysis of small chromogenic substrates, βT and γT are significantly less active towards physiologic macromolecular substrates such as fibrinogen.

In conclusion, αT absolutely plays a pivotal role in the maintaining of haemostasis, acting at the interface between coagulation and other physio-pathological interfaces. The molecular mechanism of recognition of such numerous molecular partners relies on thrombin unique structural features.

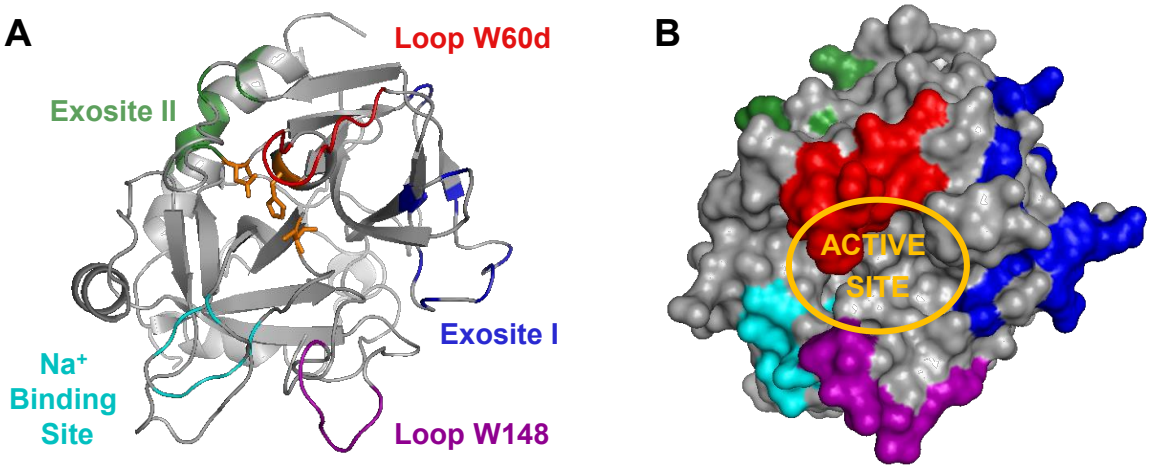

Figure 8. αT three-dimensional structure. αT (pdb: 1ppb-des PPACK) is shown in grey in the classical Bode [**45**] orientation, either in cartoon **(A)** or surface **(B)** representations. Significant regions are displayed with different colours: loop W60d (Y60a-T60i) in red; loop W148, or autolysis loop (W148-K149e) in violet; Na^+ binding site (D189, E217, D221, R221a, D222, K224, Y225) in cyan; exosite I (F34, K36, R67, K70, R73, R75, Y76, R77a, K81) in blue; exosite II (H91, R93, R101, R126, R165, R233, L234, K235, K236, K240) in green. In **panel A**, side chains of H57, D102 and S195 are highlighted in orange as sticks, while in **panel B** the active site is stressed by an orange circle. Both the exosites and the Na^+ binding site are located 15-20Å away from the catalytic cleft.

Thrombin Structure

Mature αT is a serine protease belonging to the chymotrypsin family, with which it shares 49% degree of similarity, and 35% degree of identity. Consequently, αT sequence numbering follows the numeration related to chymotrypsinogen (see **Appendix B**). Since αT bears some insertions that do not find a counterpart in chymotrypsin prototypic sequence, they are identified by the chymotrypsinogen number followed by a letter, indicative for their relative position [**45**].

Active αT is composed by a light A chain (36aa) and by a heavy B chain (259aa), held together by a disulphide bridge between C1 and C122. Overall, the protein contains four disulphide bridges, resulting in a globular fold. The B chain, which carries the functional epitopes of the enzyme, is

composed by two similar six-stranded β-barrels that pack together to accommodate the residues of the catalytic triad H57, D102, S195, at their interface (**Fig. 8**). The catalytic triad polarizes the side chain of the active S195 for a nucleophilic attack on the Cα atom in the scissile bond of the substrate. In the transition state the C atom, converted in a tetrahedral intermediate, is stabilized by hydrogen bonds between its carbonyl O atom and the amine hydrogen atoms of S195 and G193, which together form the oxyanionic hole. After transfer of a proton to H57, S195A acylates the substrate with its Oγ, releasing the substrate C-terminal fragment.

Nucleophilic attack by a water molecule catalyses deacylation, releasing the N-terminal fragment of the substrate, which restores the catalytic triad. D102 anchors H57 in the correct orientation for proton transfer from and to S195, compensating for the developing positive charge.

Active Site Cleft and Direct Substrate/Inhibitor Interactions

Numerous insertions are present in αT, relative to trypsin or chymotrypsin, shaped as loops connecting the β-strands in the B chain. Particularly, the active site residues H57, D102 and S195 are nestled in the centre of a narrow cleft framed in the upper side by the loop W60d, and in the bottom side by the loop W148. These two insertions profile and constrain the access to the catalytic site. The nine-residues loop W60d (Y60a-I60i) protrudes into the solvent with the tryptophan bulky side chain, screening H57 and S195 from the solvent [**32**]. Opposite to the W60d loop, the seven-residues W148 loop, or autolysis loop (W148-K149e), is a highly exposed and flexible region, crucial for fibrinogen recognition. It is still unclear whether the heterogeneous conformations observed for the W148 loop represent real responses to different ligands or if they are an artefact from crystal packing.

Due to its active site architecture, αT cleavage specificity is well characterized. The trypsin-like specificity for basic residues at P1 (based on the nomenclature of Schetcher and Berger, 1967) (**Fig. 9**) is conferred by D189, located deeply in the S1 site, occupying the bottom of the catalytic pocket. However, in contrast to trypsin pocket, αT increased flexibility allows accommodation of more hydrophobic or even uncharged P1 groups, conferring strong preference for Arg over Lys residues. Relatively unique to αT, the acidic E192 residue, located at the entrance of the catalytic pocket, bears a charged side chain not compensated by hydrogen bonds or ion pair interactions with neighbour residues. This uncompensated negative chain discriminates against substrates carrying acidic groups near the scissile bond, like PC or PAR-1 [**46**]. Based on the W215 indole moiety, a hydrophobic surface groove extends on top of the S1 pocket, which is partially delimited by the W60d loop. The conjunction of hydrophobic residues together with the pavement of the active site forms an apolar binding region, subdivided into the S2 cavity and the aryl binding site/S4 groove. This latter

site hosts P4 side chain of all L-amino acid substrates, whereas the P3 side chain extends alongside E192, away from the active site. The S1′ site of αT is limited in size by the bulky K60f side chain, and therefore it is particularly suited to accommodate small polar P1′ residues. The S2′ site is of medium size and mainly hydrophobic, so that bulky apolar P2′ residues are preferred. Finally, the S3′ site is open and slightly acid, resulting in a weak preference for basic P3′ side chains (**Table 2**).

On these bases, a P4 to P3′ consensus sequence of an optimal αT polypeptide substrate should contain a P4-Phe/Leu, any P3 residue, a P2-Pro/Val, a P1-Arg, a P1′-Ser/Gly, a P2′-Phe, and a P3′-Arg residue. Although most αT substrates follow the proposed scheme, important exceptions occur with fibrinogen A chain, FXIII, PC and HCII. Notably, another crucial feature that supports and governs the polypeptide presentation to the active site is its eventual interaction with the two exosites. These two electropositive patches provide additional favourable contacts with thrombin ligands, and virtually all the relevant physiological substrates/inhibitors interact with αT by contacting exosite I and/or exosite II.

Exosite I or ABE I

The prominent loop centred on K70 is called exosite I, and it is homologous to the Ca^{2+}-binding loop of the cognate proteases trypsin and chymotrypsin. In these pancreatic proteases, Ca^{2+} stabilizes the folding and increases the resistance to proteolytic digestion. In αT, the need for Ca^{2+} is removed by the insertion of K70, the side chain of which mimics the bound Ca^{2+} and obliterates the cavity available for binding this cation. In fact, αT does not bind Ca^{2+} up to mM concentrations.

Exosite I (Anion Binding Exosite I, ABE I), located about 10-15Å away from the active site, is placed mainly on the R67 to I82 loop, and bordered by the 37-loop and by the segment K109-K110. In this domain, four charged residues (R67, K70, E77, E80) form a salt bridge cluster, which is buried well below the surface of the exosite, substantially contributing to the rigidity of the loop [**47**]. Over this buried charged spot, several non-compensated cationic residues (R73, R75, R77a, K81) provide a strong electropositive field.

Exosite I is the recognition site for many macromolecular ligands, such as fibrin(ogen), TM, PAR-1, HCII, FV, FVIII, FXIII and the C-terminus of anticoagulant hirudin [**48-52**]. It is hypothesized that the positive exosite I electrical field could pre-orient the enzyme for a productive interaction ("electrostatic steering"). In addition, this region and the active site are allosterically coupled: the interaction to this extended recognition region communicates changes to the catalytic moiety of the enzyme. It has been reported that the binding of peptides derived from HCII [**53**], thrombin receptor I [**54**] or hirudin C-terminal domain [**55**] influence αT catalytic activity.

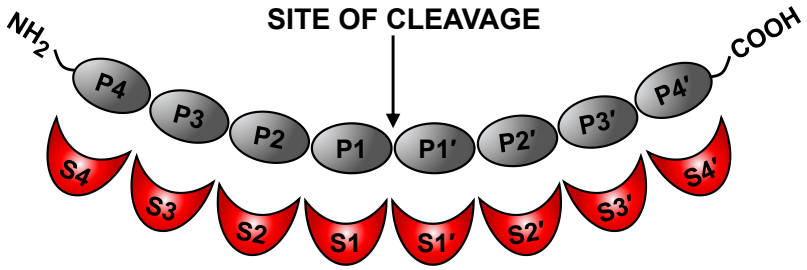

Figure 9. Schetcher-Berger nomenclature. Scheme of the interaction of a polypeptide substrate (in grey) with the active site of an enzyme (in red) before the proteolytic cleavage. Usually at least an eight-residue segment (P4-P4′) substrate interacts by its side chain residues with the correspondent subsites (S4-S4′) of the enzyme. The major determinant for enzyme specificity is the interaction between P1 and S1; generally, proteases cleave at the carboxy-terminal side of the scissile bond.

	P4	P3	P2	P1	P1′	P2′	P3′	Cofactor and Exosite
Fibrinogen A	Gly	Gly	Val	Arg	Gly	Pro	Arg	1
Fibrinogen B	Phe	Ser	Ala	Arg	Gly	His	Arg	1
FV (709)	Leu	Gly	Ile	Arg	Ser	Phe	Arg	1 and 2
FV (1018)	Leu	Ser	Pro	Arg	Thr	Phe	His	1 and 2
FV (1545)	Trp	Tyr	Leu	Arg	Ser	Asn	Asn	1 and 2
FVIII (372)	Ile	Gln	Ile	Arg	Ser	Val	Ala	1 and 2
FVIII (740)	Ile	Glu	Pro	Arg	Ser	Phe	Ser	1 and 2
FVIII (1618)	Gln	Ser	Pro	Arg	Ser	Phe	Gln	1 and 2
FXIII	Gly	Val	Pro	Arg	Gly	Val	Asn	None
PAR-1	Leu	Asp	Pro	Arg	Ser	Phe	Leu	1
PAR-4	Pro	Ala	Pro	Arg	Gly	Tyr	Pro	None
FXI	Ile	Lys	Pro	Arg	Ile	Val	Gly	1
PC	Val	Asp	Pro	Arg	Ile	Val	Gly	TM (1)
TAFI	Val	Ser	Pro	Arg	Ala	Ser	Ala	TM (1)
ATIII	Ile	Ala	Gly	Arg	Ser	Leu	Asn	Heparin (2)
HCII	Phe	Met	Pro	Leu	Ser	Thr	Gln	1 and Heparin (2)

Table 2. Cleavage sequences of αT substrates around the scissile peptide bond. PAR, protease activated receptor; PC, protein C; TAFI, thrombin-activable fibrinolysis inhibitor; ATIII, antithrombin; HC, heparin cofactor.

Exosite II or ABE II

On the other side of the catalytic cleft, opposite to exosite I, a prominent C-terminal helix hosts a number of positively charged residues that form the Anion Binding Exosite II (ABE II). At this surface, a small hydrophobic L234-based groove is surrounded (in clockwise order) by the basic residues R93, R101, R165, R233, R126, K236, K235, K240, and H91, with most of their side chain charges not compensated by neighbour residues. This assignment was confirmed with exosite II mutants, by measuring αT inhibition by ATIII, in the presence of heparin [**56**], and crystallographically by the complex between αT and an eight-unit heparin fragment, in which each unit is sandwiched between two molecules of the serine protease.

In effect, αT exosite II is the template for the interaction with poly-anionic ligands, such heparin and glycosaminoglycans. Moreover, exosite II is the region of recognition of platelet receptor GpIbα and of fibrinogen elongated γ'-chain [**57**;**58**].

Since this C-terminal helix packs tightly against the domain supporting D102, it is conceivable that binding to exosite II could influence allosterically the enzymatic activity of αT, by affecting the position of this catalytic residue.

Na^+-binding Site and Allosteric Effect

Sodium is an important allosteric modulator of αT: after its binding, the serine protease converts from a Na^+-free form, referred to as *slow*, to a Na^+-bound form, referred to as *fast*. Since Na^+ affinity for αT (K_d) is 110mM at 37°C, at physiologic ionic strength (150mM) the two forms are significantly populated in a 3:2 ratio, respectively. The two forms display different activity toward the physiological substrates (see **Table 3**). In detail, the *fast* form features procoagulant, pro-thrombotic and pro-signalling properties, cleaving more efficiently PARs and fibrinogen. Conversely, the *slow* form cleaves preferentially protein C, exhibiting remarked anticoagulant properties [**59**].

The Na^+-binding site is centred in the 222-loop, located at 15-20Å from the catalytic triad, and at 5Å from D189, in the S1 specificity site. The ion is octaedrically coordinated by the carbonyl oxygens of R221a and K224, and by four buried water molecules. Ionic salt bridges with D221 and D222 further stabilize the interaction. Di Cera and co-workers identified residues D189, E217, D222, and Y225 clustering around the Na^+ site, being energetically linked and responsible for transducing Na^+ binding into enhanced catalytic activity. In particular, Na^+ binding reorients the R221a carbonyl group to form the R187-D222 salt bridge, reorienting favourably D189, E192, S195 in the catalytic cleft. Moreover, the salt bridge E146-R221a freezes the 148-loop in a more rigid and open conformation [**32**].

	k_{cat}/K_m ($\mu M^{-1} \cdot s^{-1}$)		r
	Fast	**Slow**	
(D)FPR-pNA	88.9 ± 4	3.5 ± 0.5	26
Fibrinopeptide A release	35 ± 4	1.5 ± 0.1	23
Fibrinopeptide B release	17 ± 1	0.73 ± 0.03	23
PAR-1	54 ± 2	1.4 ± 0.1	39
Protein C	0.21 ± 0.001	0.32 ± 0.01	0.7

Table 3 [from Di Cera et al., 2007]. Effect of Na^+ on the catalytic activity of αT towards some relevant physiological substrates. All measures were performed in buffer that stabilized either the fast (0.2M NaCl) or the slow (0.2M ChCl) form.

Crystal structures of human S195A or E217K mutant, suggested to be typical for the slow form of αT, indicated an allosteric switch mechanism due to Na^+ interaction. In detail, Na^+ removal induces flipping of the C168-C182 disulphide bridge, and of the aromatic side chains of F227, W215 and W60d. These small yet significant atomic movements result in the constriction of the active site cleft, limiting the access to the substrates.

Currently available data suggest that Na^+-bound αT form is more stable and exhibits a more accessible and rigid active site cleft, whereas the Na^+-free form possesses a more closed, flexible substrate-binding region. Thus, the *fast* from of αT would be a better template for productive binding of the inherently-flexible cleavage segments of fibrinogen and PAR-1, such that the scissile peptide bonds are optimally presented to the S195 Oγ and to the oxyanion hole. Importantly, thrombin-substrate complexes, in the presence or absence of Na^+, go through transition states that are short-lived, making the structural characterization of these states extremely difficult. Several naturally occurring mutations of the ProT gene, like ProT Frankfurt, Salakta, Greenville, Scranton, Copenhagen and Saint Denis, affect residues linked to Na^+ binding and are often associated with bleeding [**60**].

REFERENCES

[1] Macfarlane RG. An Enzyme Cascade in the Blood Clotting Mechanism, and its Function as a Biochemical Amplifier. Nature 1964 May 2;202:498-499.

[2] Davie EW, Kulman JD. An overview of the structure and function of thrombin. Semin Thromb Hemost 2006 Apr;32 Suppl 1:3-15.

[3] Butenas S, van't Veer C, Mann KG. "Normal" thrombin generation. Blood 1999 Oct 1;94(7):2169-2178.

[4] Pozzi N, Chen Z, Pelc LA, Shropshire DB, Di Cera E. The linker connecting the two kringles plays a key role in prothrombin activation. Proc Natl Acad Sci U S A 2014 May 27;111(21):7630-7635.

[5] Pozzi N, Chen Z, Gohara DW, Niu W, Heyduk T, Di Cera E. Crystal structure of prothrombin reveals conformational flexibility and mechanism of activation. J Biol Chem 2013 Aug 2;288(31):22734-22744.

[6] Sun WY, Witte DP, Degen JL, Colbert MC, Burkart MC, Holmback K, et al. Prothrombin deficiency results in embryonic and neonatal lethality in mice. Proc Natl Acad Sci U S A 1998 Jun 23;95(13):7597-7602.

[7] Xue J, Wu Q, Westfield LA, Tuley EA, Lu D, Zhang Q, et al. Incomplete embryonic lethality and fatal neonatal hemorrhage caused by prothrombin deficiency in mice. Proc Natl Acad Sci U S A 1998 Jun 23;95(13):7603-7607.

[8] Huang YC, Wu YR, Tseng MY, Chen YC, Hsieh SY, Chen CM. Increased prothrombin, apolipoprotein A-IV, and haptoglobin in the cerebrospinal fluid of patients with Huntington's disease. PLoS One 2011 Jan 31;6(1):e15809.

[9] Sciascia S, Bertolaccini ML. Antibodies to phosphatidylserine/prothrombin complex and the antiphospholipid syndrome. Lupus 2014 Oct;23(12):1309-1312.

[10] Rosing J, Tans G, Govers-Riemslag JW, Zwaal RF, Hemker HC. The role of phospholipids and factor Va in the prothrombinase complex. J Biol Chem 1980 Jan 10;255(1):274-283.

[11] Nesheim ME, Taswell JB, Mann KG. The contribution of bovine Factor V and Factor Va to the activity of prothrombinase. J Biol Chem 1979 Nov 10;254(21):10952-10962.

[12] Deguchi H, Takeya H, Gabazza EC, Nishioka J, Suzuki K. Prothrombin kringle 1 domain interacts with factor Va during the assembly of prothrombinase complex. Biochem J 1997 Feb 1;321 (Pt 3)(Pt 3):729-735.

[13] Kotkow KJ, Deitcher SR, Furie B, Furie BC. The second kringle domain of prothrombin promotes factor Va-mediated prothrombin activation by prothrombinase. J Biol Chem 1995 Mar 3;270(9):4551-4557.

[14] Chen L, Yang L, Rezaie AR. Proexosite-1 on prothrombin is a factor Va-dependent recognition site for the prothrombinase complex. J Biol Chem 2003 Jul 25;278(30):27564-27569.

[15] Yegneswaran S, Mesters RM, Fernandez JA, Griffin JH. Prothrombin residues 473-487 contribute to factor Va binding in the prothrombinase complex. J Biol Chem 2004 Nov 19;279(47):49019-49025.

[16] Taneda H, Andoh K, Nishioka J, Takeya H, Suzuki K. Blood coagulation factor Xa interacts with a linear sequence of the kringle 2 domain of prothrombin. J Biochem 1994 Sep;116(3):589-597.

[17] Harlos K, Boys CW, Holland SK, Esnouf MP, Blake CC. Structure and order of the protein and carbohydrate domains of prothrombin fragment 1. FEBS Lett 1987 Nov 16;224(1):97-103.

[18] Yegneswaran S, Mesters RM, Griffin JH. Identification of distinct sequences in human blood coagulation factor Xa and prothrombin essential for substrate and cofactor recognition in the prothrombinase complex. J Biol Chem 2003 Aug 29;278(35):33312-33318.

[19] Srivastava A, Quinn-Allen MA, Kim SW, Kane WH, Lentz BR. Soluble phosphatidylserine binds to a single identified site in the C2 domain of human factor Va. Biochemistry 2001 Jul 27;40(28):8246-8255.

[20] Downing MR, Butkowski RJ, Clark MM, Mann KG. Human prothrombin activation. J Biol Chem 1975 Dec 10;250(23):8897-8906.

[21] Haynes LM, Bouchard BA, Tracy PB, Mann KG. Prothrombin activation by platelet-associated prothrombinase proceeds through the prethrombin-2 pathway via a concerted mechanism. J Biol Chem 2012 Nov 9;287(46):38647-38655.

[22] Tans G, Janssen-Claessen T, Hemker HC, Zwaal RF, Rosing J. Meizothrombin formation during factor Xa-catalyzed prothrombin activation. Formation in a purified system and in plasma. J Biol Chem 1991 Nov 15;266(32):21864-21873.

[23] Bradford HN, Krishnaswamy S. Meizothrombin is an unexpectedly zymogen-like variant of thrombin. J Biol Chem 2012 Aug 31;287(36):30414-30425.

[24] Tracy PB, Nesheim ME, Mann KG. Coordinate binding of factor Va and factor Xa to the unstimulated platelet. J Biol Chem 1981 Jan 25;256(2):743-751.

[25] Tracy PB, Rohrbach MS, Mann KG. Functional prothrombinase complex assembly on isolated monocytes and lymphocytes. J Biol Chem 1983 Jun 25;258(12):7264-7267.

[26] Nesheim ME, Furmaniak-Kazmierczak E, Henin C, Cote G. On the existence of platelet receptors for factor V(a) and factor VIII(a). Thromb Haemost 1993 Jul 1;70(1):80-86.

[27] Boskovic DS, Bajzar LS, Nesheim ME. Channeling during prothrombin activation. J Biol Chem 2001 Aug 3;276(31):28686-28693.

[28] Cote HC, Bajzar L, Stevens WK, Samis JA, Morser J, MacGillivray RT, et al. Functional characterization of recombinant human meizothrombin and Meizothrombin(desF1). Thrombomodulin-dependent activation of protein C and thrombin-activatable fibrinolysis inhibitor (TAFI), platelet aggregation, antithrombin-III inhibition. J Biol Chem 1997 Mar 7;272(10):6194-6200.

[29] Fuster V, Stein B, Ambrose JA, Badimon L, Badimon JJ, Chesebro JH. Atherosclerotic plaque rupture and thrombosis. Evolving concepts. Circulation 1990 Sep;82(3 Suppl):II47-59.

[30] Wood JP, Silveira JR, Maille NM, Haynes LM, Tracy PB. Prothrombin activation on the activated platelet surface optimizes expression of procoagulant activity. Blood 2011 Feb 3;117(5):1710-1718.

[31] Garcia PS, Gulati A, Levy JH. The role of thrombin and protease-activated receptors in pain mechanisms. Thromb Haemost 2010 Jun;103(6):1145-1151.

[32] Di Cera E, Dang QD, Ayala YM. Molecular mechanisms of thrombin function. Cell Mol Life Sci 1997 Sep;53(9):701-730.

[33] Ng AS, Lewis SD, Shafer JA. Quantifying thrombin-catalyzed release of fibrinopeptides from fibrinogen using high-performance liquid chromatography. Methods Enzymol 1993;222:341-358.

[34] Mosesson MW, Hernandez I, Raife TJ, Medved L, Yakovlev S, Simpson-Haidaris PJ, et al. Plasma fibrinogen gamma' chain content in the thrombotic microangiopathy syndrome. J Thromb Haemost 2007 Jan;5(1):62-69.

[35] Vu TK, Hung DT, Wheaton VI, Coughlin SR. Molecular cloning of a functional thrombin receptor reveals a novel proteolytic mechanism of receptor activation. Cell 1991 Mar 22;64(6):1057-1068.

[36] Coughlin SR. Protease-activated receptors in hemostasis, thrombosis and vascular biology. J Thromb Haemost 2005 Aug;3(8):1800-1814.

[37] De Cristofaro R, De Filippis V. Interaction of the 268-282 region of glycoprotein Ibalpha with the heparin-binding site of thrombin inhibits the enzyme activation of factor VIII. Biochem J 2003 Jul 15;373(Pt 2):593-601.

[38] Leung L, Nachman R. Molecular mechanisms of platelet aggregation. Annu Rev Med 1986;37:179-186.

[39] McNicol A, Israels SJ. Platelet dense granules: structure, function and implications for haemostasis. Thromb Res 1999 Jul 1;95(1):1-18.

[40] Harrison P, Cramer EM. Platelet alpha-granules. Blood Rev 1993 Mar;7(1):52-62.

[41] De Candia, E., Hall, S. W., Rutella, S., Landolfi, R., Andrews, R. K. and De Cristofaro, R.(2001) Binding of thrombin to glycoprotein ib accelerates the hydrolysis of par-1 on intact platelets.J. Biol. Chem. 276, 4692-4698. doi:10.1074/jbc.M008160200 [doi]

[42] Esmon CT. The roles of protein C and thrombomodulin in the regulation of blood coagulation. J Biol Chem 1989 Mar 25;264(9):4743-4746.

[43] Johnson DJ, Adams TE, Li W, Huntington JA. Crystal structure of wild-type human thrombin in the Na+-free state. Biochem J 2005 Nov 15;392(Pt 1):21-28.

[44] Arcone R, Chinali A, Pozzi N, Parafati M, Maset F, Pietropaolo C, et al. Conformational and biochemical characterization of a biologically active rat recombinant Protease Nexin-1 expressed in E. coli. Biochim Biophys Acta 2009 Apr;1794(4):602-614.

[45] Bode W, Mayr I, Baumann U, Huber R, Stone SR, Hofsteenge J. The refined 1.9 A crystal structure of human alpha-thrombin: interaction with D-Phe-Pro-Arg chloromethylketone and significance of the Tyr-Pro-Pro-Trp insertion segment. EMBO J 1989 Nov;8(11):3467-3475.

[46] Guinto ER, Vindigni A, Ayala YM, Dang QD, Di Cera E. Identification of residues linked to the slow-->fast transition of thrombin. Proc Natl Acad Sci U S A 1995 Nov 21;92(24):11185-11189.

[47] Stubbs MT, Oschkinat H, Mayr I, Huber R, Angliker H, Stone SR, et al. The interaction of thrombin with fibrinogen. A structural basis for its specificity. Eur J Biochem 1992 May 15;206(1):187-195.

[48] Steen M, Dahlback B. Thrombin-mediated proteolysis of factor V resulting in gradual B-domain release and exposure of the factor Xa-binding site. J Biol Chem 2002 Oct 11;277(41):38424-38430.

[49] Esmon CT, Lollar P. Involvement of thrombin anion-binding exosites 1 and 2 in the activation of factor V and factor VIII. J Biol Chem 1996 Jun 7;271(23):13882-13887.

[50] Sadasivan C, Yee VC. Interaction of the factor XIII activation peptide with alpha -thrombin. Crystal structure of its enzyme-substrate analog complex. J Biol Chem 2000 Nov 24;275(47):36942-36948.

[51] Hall SW, Nagashima M, Zhao L, Morser J, Leung LL. Thrombin interacts with thrombomodulin, protein C, and thrombin-activatable fibrinolysis inhibitor via specific and distinct domains. J Biol Chem 1999 Sep 3;274(36):25510-25516.

[52] Myles T, Le Bonniec BF, Betz A, Stone SR. Electrostatic steering and ionic tethering in the formation of thrombin-hirudin complexes: the role of the thrombin anion-binding exosite-I. Biochemistry 2001 Apr 24;40(16):4972-4979.

[53] Hortin GL, Trimpe BL. Allosteric changes in thrombin's activity produced by peptides corresponding to segments of natural inhibitors and substrates. J Biol Chem 1991 Apr 15;266(11):6866-6871.

[54] Liu L, Freedman J, Hornstein A, Fenton JW,2nd, Ofosu FA. Thrombin binding to platelets and their activation in plasma. Br J Haematol 1994 Nov;88(3):592-600.

[55] Jackman MP, Parry MA, Hofsteenge J, Stone SR. Intrinsic fluorescence changes and rapid kinetics of the reaction of thrombin with hirudin. J Biol Chem 1992 Aug 5;267(22):15375-15383.

[56] Gan ZR, Li Y, Chen Z, Lewis SD, Shafer JA. Identification of basic amino acid residues in thrombin essential for heparin-catalyzed inactivation by antithrombin III. J Biol Chem 1994 Jan 14;269(2):1301-1305.

[57] De Cristofaro R, De Candia E, Landolfi R, Rutella S, Hall SW. Structural and functional mapping of the thrombin domain involved in the binding to the platelet glycoprotein Ib. Biochemistry 2001 Nov 6;40(44):13268-13273.

[58] Lancellotti S, Rutella S, De Filippis V, Pozzi N, Rocca B, De Cristofaro R. Fibrinogen-elongated gamma chain inhibits thrombin-induced platelet response, hindering the interaction with different receptors. J Biol Chem 2008 Oct 31;283(44):30193-30204.

[59] De Filippis V, De Dea E, Lucatello F, Frasson R. Effect of Na+ binding on the conformation, stability and molecular recognition properties of thrombin. Biochem J 2005 Sep 1;390(Pt 2):485-492.

[60] Di Cera E. Thrombin: a paradigm for enzymes allosterically activated by monovalent cations. *C R Biol.* 2004;327:1065-76. Review.

RESULTS

CHAPTER 2.1

Connections between Coagulation and Neurodegenerative Diseases

Neurodegenerative Diseases

Neurodegenerative is a universal term for describing a range of pathologic conditions that primarily affect the neurons in the brain and in the spinal cord. Since neurons do not reproduce, in case of damage or death they cannot be replaced in our body. In detail, we refer to as *synucleinopathies* for a branch of neurodegenerative disorders in which intracellular aggregates of an abundant and conserved presynaptic protein, α-synuclein (αSyn), are the major determinants of the disease [**1**]. These intracellular proteinaceous inclusions can be deposited in both dopaminergic and non-dopaminergic neurons, and in glia. At least five morphologically distinct αSyn-containing inclusions were described: Lewy Bodies (LBs), Lewy neurites, glial cytoplasmic inclusions, neuronal cytoplasmic inclusions and axonal spheroids [**2**]. In particular, LBs are anomalous protein aggregates, histologically described as intracytoplasmic eosinophilic inclusions [**3**]. These spherical masses present two variants: subcortical LBs, in the encephalic trunk, and cortical LBs, in the cerebral cortex. Subcortical LBs feature a dense nucleus, surrounded by a radial fibrillary αSyn halo of about 10nm; cortical LBs are less defined, lacking the halo, yet they are constituted of αSyn fibrils [**4**].

Synucleinopathies include Parkinson's disease (PD), dementia with LBs, diffuse LBs disease, the LBs variant of Alzheimer's disease (AD), multiple system atrophy, and neurodegeneration with brain iron accumulation type I (also known as adult neuroaxonal dystrophy). Particularly, in PD the proteinaceous lesions affect several regions, especially an area called *substantia nigra*, which controls balance and movement. PD can be classified in the autosomal dominant (late-onset) form, if the disease begins after the age of 50, or in the early-onset manifestations [**5**]. Since in solution αSyn is in equilibrium between the monomeric form and the aggregates, the pathological increase of cytoplasmic inclusions may be simply due to abnormal protein expression. Late-onset PD patients often present duplications or eventually triplications of whole αSyn genetic *locus* [**6**;**7**]. On the contrary, early-onset PD is provoked by three point αSyn mutations: A53T [**8**], E46K [**9**] and A30P [**10**]. All these mutants are characterized by an altered kinetic fibrillation constant of αSyn. Moreover, αSyn tendency of aggregation can be triggered by folding impairment or, in the case of AD, by interactions with β-amyloid protein.

Human α-Synuclein

αSyn (140aa, 14.5kDa) belongs to the family of natural unfolded proteins (NUPs), lacking of a well-defined three-dimensional structure. It is a ubiquitous protein in the animal kingdom, presenting a high degree of sequence conservation among different species [**11**]. At least three αSyn isoforms are produced in human by alternative splicing: the full length αSyn-140, αSyn-112 and αSyn-126, due to an in-frame deletion of exon 5 (103-130) or of exon 3 (41-54) respectively [**12**]. The discovery of the αSyn gene dates back to the '90, by many independent laboratories; the name "synuclein" derives from the supposed protein nuclear localization [**13**].

α-Synuclein Structure

Full length αSyn linear sequence can be structurally divided in three regions, depending on their peculiar chemical-physical properties [**2**] (**Fig. 1**).

The N-terminal (1-60) domain is an amphipathic region, including the sites of the three familial PD mutations (A30P, E46K, A53T), which is responsible for αSyn binding to negative membranes [**11**]. This sequence, almost completely composed of imperfect repetitions of the 11aa-pattern X**KTKEGV**XXXX (consensus motif highlighted in bold), folds in a transient α-helix after the binding to synthetic vesicles, in a modality analogous to the interaction between apolipoproteins and lipids [**14**]. Although the helical conformation is favoured in the presence of phospholipids, in the extracellular environment αSyn interconverts from this conformation to random coil and back in a timescale of μs [**15**].

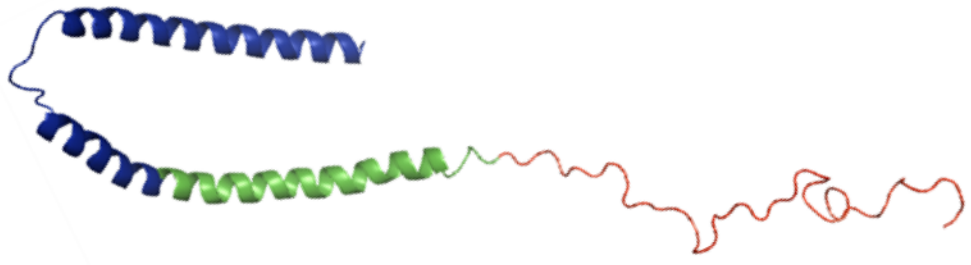

Figure 1. Human micelle-bound αSyn three-dimensional representation (pdb: 1xq8). Human αSyn (140aa, 14.5kDa) is represented in its colour coded architecture domains: N-terminal (1-60), in blue; NAC region (61-95), in green; C-terminal (96-140) in red. The protein can bind to phospholipid membranes by assuming a transient α-helical conformation in its N-terminal domain. In this micelle-bound crystallographic model of αSyn, the sequences V3-V37 and K45-T92 (this segment extends to NAC region) organize in two antiparallel α-helixes, connected by a stretched linker. On the contrary, the C-terminal domain stays free and de-structured even after the binding.

The central portion (61-95) was named NAC (non-amyloid β-component) after its detection in AD amyloid plaques [**16**]. This region is the most hydrophobic section of the protein and it has a crucial importance in the aggregation process, being the major responsible of αSyn conversion from a random coil conformation to a β-sheet structure. Several αSyn molecules can associate at this level, by weak stacking interactions, forming oligomers that deposit in insoluble fibres [**5**]. In this process, critical importance has the sequence (^{71}VTGVTAVAQTTV^{82}), essential for hydrophobic aggregation [**17**]. In physiologic conditions, when αSyn interacts to phospholipids membranes, the NAC portion contributes to the binding, with consequent inhibition of the aggregation pathway, due to competition between α-helix and β-sheet conformations [**18**].

The C-terminal domain (96-140) is rich of acidic amino acids and prolines, conferring an overall negative charge to the protein, and a peculiar secondary structure to this region, that remains always de-structured in solution, even after αSyn binding to the vesicles. Due to the high local concentration of negative charges (E104, E105, E114, E115), this region prevents and contrasts aggregation by electrostatic repulsions between different αSyn molecules [**19**]. As a confirm to this hypothesis, αSyn C-terminus truncated peptides, like fragments (1-89), (1-102) and (1-110) feature an increased tendency of stacking association, with respect to the full length protein [**20**]. This portion is likely to be involved in the regulation of αSyn interactions with other biomolecules, like lipids and proteins [**21**].

The Chameleon Protein

Being part of the NUPs family, αSyn lacks of a well-defined three-dimensional structure, exploring multiple conformations with a great molecular plasticity. This protein presents an intrinsically disordered structure both *in vivo* [**22**] and *in vitro* [**23**;**24**]. In solution, αSyn exists as a dynamic and heterogenic mixture of extremely flexible conformers, which inter-convert in a timescale of μs.

The αSyn fibrillation pathway is extremely complex, and still matter of debate (**Fig. 2**) [**25**]. It is likely that αSyn insoluble aggregates are composed of partially folded or misfolded proteins, in which hydrophobic stacking interactions occur between the β-sheet central portions of the molecules. These connections can result in either dimers or soluble oligomers.

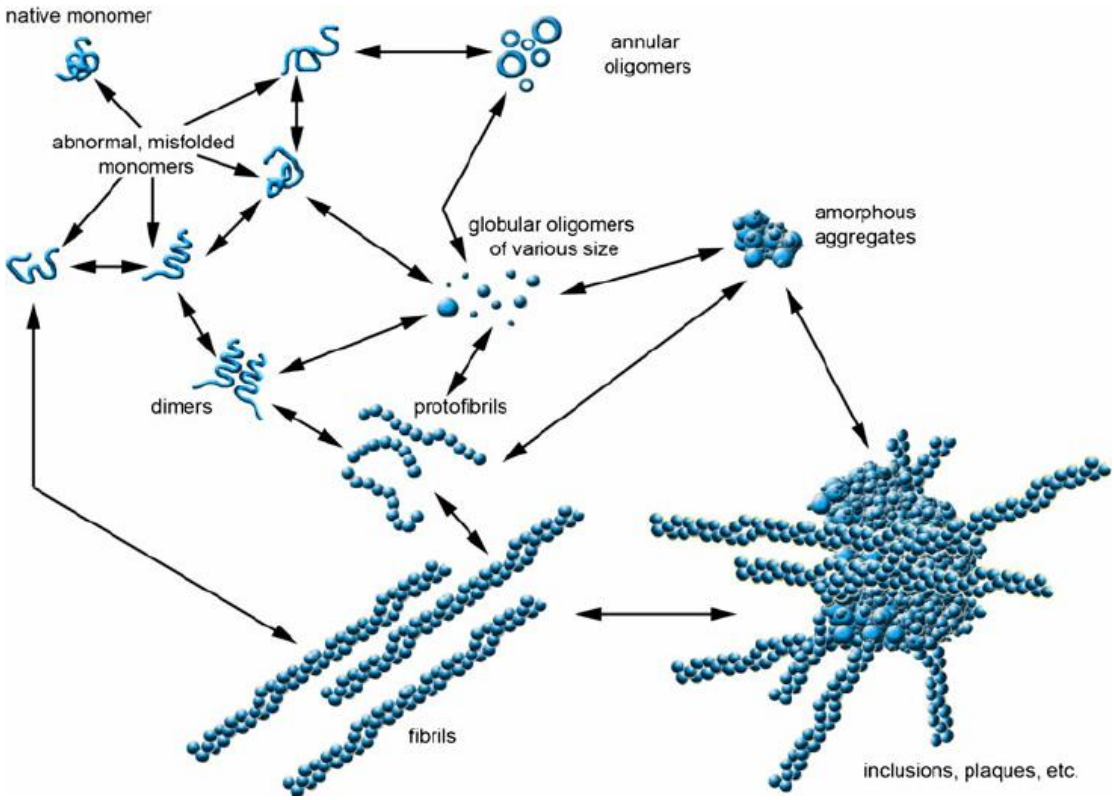

Figure 2 [from Lotz and Legleiter, 2013]. Schematic diagram of αSyn alternative aggregation pathways. Due to its great molecular plasticity, αSyn monomer explores *in vivo* a variety of conformations. In pathological conditions, abnormal or β-sheet misfolded monomers undergo stacking interactions, with the generation of soluble dimers or morphologically different oligomers: chains, rings or spheres. In turn, oligomers can irreversibly associate either in amorphous aggregates or in more organized fibres, depositing as intracellular proteinaceous aggregates.

In detail, oligomers may present different morphological conformations: spheres (2.5-4.2nm), chains (built of several spheres) or rings (annular chains) [**26**]. These three shapes can be obtained by incubating αSyn with different metals, like Cu^{2+}, Fe^{2+}, Ni^{2+}, Co^{2+}, Cd^{2+}, Zn^{2+} and Mg^{2+} [**27**]. It is still unclear whether the soluble oligomers are the transient intermediates of aggregation, dead-ends in the pathway, or even the pathogenic species themselves [**28**]. However, the transient oligomers are likely to irreversibly associate, either in amorphous aggregates or in more organized fibres, depending on the chemical-physical parameters of the solution. The fibrillation pathway, in detail, is characterized by a lag phase, depending on the nucleation mechanism. The fibres, which can display either a straight or a twisted shape [**29**], are well-structured, presenting an ordered cross-linked fibrillation *core* composed of the stacked (36-98) segments [**30**]. The aggregation process is dramatically dependent on the chemical environment, and actually, neurodegenerative diseases are multiple aetiology disorders, affected by several external conditions like temperature, pH and metal ions. In detail, high

temperatures trigger protein folding and aggregation; both acidic pH and high cationic ions concentrations (like metals) hijack αSyn negative charges, promoting stacking interactions [**24**]. Finally, even a crowded macromolecular environment [**31**], alcohols, hydrophobic molecules like herbicides and pesticides endorse protein aggregation [**32**]. Due to its massive structural modulation by surrounding environment, αSyn has been entitled the "chameleon protein".

α-Synuclein Physiologic Functions

Although αSyn is widely characterized as a pathological determinant, its physiological role is still elusive. Owing to its remarkable structural plasticity, αSyn can bind to at least 50 molecular partners, eliciting numerous functions [**33**].

Human αSyn is mainly expressed in the brain, and localizes in the neuron presynaptic terminals. This protein, particularly concentrated in the cerebral cortex and in the hippocampus olfactory area, represents the 1% of the soluble cerebral proteins [**34**]. αSyn can bind to lipid vesicles, both natural and synthetic, made of phospholipids, detergents, fatty acids or lipid rafts [**14**;**35**;**36**]. The protein seems to be involved in the lipids organization in small mono-lamellar vesicles [**37**;**38**] and it is likely to modulate the lipid components of the membranes.

In the presynaptic terminals, αSyn exists in equilibrium between the bound (15%) and the free form (85%). In detail, the N-terminal domain organizes in two transient α-helixes between V3-V37 and K45-T92, connected by an extended flexible linker and aligned in an antiparallel fashion [**18**] (**Fig. 1**). Depending on the micelles morphology and dimensions, the linker can bend or stretch, with the approaching or departing of the helixes. In this scenario, αSyn may regulate vesicular turnover and trafficking in the central nervous system, keeping one helix anchored to the plasma membrane, and the other to the vesicle surface [**16**;**11**;**39**].

Moreover, recent studies demonstrate that this protein may be involved in the release of catecholamines (like adrenalin, noradrenalin and serotonin) from the synaptic vesicles [**40**], and in the inhibition of the membrane fusion processes regulator - phospholipase D2 [**2**]. Finally, αSyn acts in cooperation with the molecular chaperon CSP (Cysteine String Protein α) in the folding of the synaptic NSF (N-ethilmaleimide Sensitive Factor), thus preventing neurodegeneration [**41**].

α-Synuclein Effects on Coagulation

Beyond central nervous system, αSyn is expressed also in the hearth, skeletal muscles, pancreas and placenta [**16**]. Very surprisingly, this presynaptic protein has been detected both in plasma (25.4±9.2 ng/ml) and in the haematopoietic lineage [**42**]. In detail, more than 99% of αSyn is stocked in the erythrocytes, while the remaining is divided between plasma (0.1%), platelets (0.2%) and mononuclear cells (0.05%), like lymphocytes B, lymphocytes T, NK cells, monocytes [**43**]. Actually, the massive αSyn presence in the erythrocytes depends on the fact that these constitute more than 90% of the blood cells. Normalizing αSyn concentration with the respect of the total protein content, platelets contain 246±36 ng/mg αSyn, while red blood cells only 131±23 ng/mg [**42**]. In platelets, αSyn was detected both soluble, and associated to the plasmatic and granules membranes, due to the binding properties of its N-terminal region. Moreover, it has been demonstrated that exogenous αSyn can penetrate platelets and localize in the cytosol, next to the plasmatic membrane [**44**]. Even the fragment (61-140) can enter the plasma membrane, while the truncated segment (96-140) loses this ability [**45**]. These studies suggest that the highly hydrophobic NAC portion may play a role in αSyn translocation inside the platelets. These unexpected experimental evidences suggest that αSyn functions may not be restricted to the central nervous system.

Actually, αSyn is involved in the megakaryocytes differentiation to mature platelets [**44**], and it inhibits the Ca^{2+}-dependent release of α-granules [**46**]. Platelets are the effector cellular targets of the coagulation cascade. Activation is triggered mostly by α-thrombin, through binding to the receptor GpIbα and cleavage of the surface protease activated receptors, PAR-1 and PAR-4 [**47**]. Once activated, platelets expand, expose sticky protuberances named *pseudopods*, express the receptor GpIIb/IIIa in their surface, promiscuous for both fibrinogen and von Willebrand factor, and degranulate. Aggregated platelets organize in a transient clot, localized in the site of the vascular damage. In detail, platelets comprise two kinds of granules: δ-granules contain Ca^{2+}, ADP, ATP and serotonin, while α-granules carry a variety of vasoactive substances, which amplify coagulation with a positive feedback mechanism. In conclusion, the inhibition of the Ca^{2+}-dependent α-granules release impairs platelets aggregation. Actually, PD and AD patients, characterized by higher concentration of αSyn both in the brain and in the blood, present anomalies in platelets degranulation [**48**;**49**]. Moreover, past clinical studies suggest that patients suffering from these neurodegenerative disorders are subjected to lower ischaemic strokes, due to a reduced rate of platelet activation and aggregation [**50**].

Human α-Thrombin and Neurodegenerative Diseases

Human α-thrombin (αT) is the final effector of the coagulation cascade, exerting both procoagulant (fibrin generation, platelets aggregation) and anticoagulant (protein C activation) functions [**51**]. Beyond coagulation, αT acts at the interface between inflammation, cellular proliferation, and the nervous system. In detail, at low concentrations (1-10nM), this serine protease acts as mitogen, modulating glia cells mitosis, neuronal out-growth, astrocytes morphology, and inducing retraction of neurites in neuroblastoma cells [**52**]. Overall, these effects, mediated through activation of protease activated receptors (PARs), exert a protective role towards neurons and astrocytes, defending these cells from death induced by environmental insults [**53**]. Conversely, higher αT concentrations (100nM) determine a general pathologic pro-inflammatory state in the brain [**54**], by inducing apoptosis in motor neurons [**55**], and inhibiting development of neurites outgrowth from the dorsal root ganglion *in vitro* [**56**]. In this scenario, the serpin protease nexin-1 (PN1) plays a vital role in maintaining brain homeostasis, by acting as a suicide αT inhibitor [**57**].

Recent clinical studies suggest that αT is involved in the development of neurodegenerative diseases. In detail, this serine protease accumulates in the brain of AD patients, both in vessel walls and in senile plaques. Immunofluorescent analysis of the cerebral vasculature of AD mice, demonstrate significant increase of αT, interleukin-6 (IL-6), monocyte chemoattractant protein-1 (MCP-1), matrix metalloproteinases (MMPs) and reactive oxygen species (ROS), compared to the controls [**58**]. Moreover, αT induces surface and intracellular secretion of the amyloid precursor protein (APP) from human endothelial cells [**59**], and is able to hydrolyse it, generating fragments of amyloid peptides similar to those found in the fibrils of AD patients [**60**]. On the other side, in PD, αT contributes directly to neuronal degeneration, by exerting a toxic effect on the dopaminergic neurons localized in the *substantia nigra*. In this scenario, αT is both directly noxious to the neurons, but can also potentiate neuronal injury indirectly, *via* activation of neighbouring microglia and astrocytes.

REFERENCES

[1] Bisaglia M, Mammi S, Bubacco L. Structural insights on physiological functions and pathological effects of alpha-synuclein. FASEB J 2009 Feb;23(2):329-340.

[2] Uversky VN. Neuropathology, biochemistry, and biophysics of alpha-synuclein aggregation. J Neurochem 2007 Oct;103(1):17-37.

[3] Forno LS. Neuropathology of Parkinson's disease. J Neuropathol Exp Neurol 1996 Mar;55(3):259-272.

[4] Spillantini MG, Crowther RA, Jakes R, Hasegawa M, Goedert M. alpha-Synuclein in filamentous inclusions of Lewy bodies from Parkinson's disease and dementia with Lewy bodies. Proc Natl Acad Sci U S A 1998 May 26;95(11):6469-6473.

[5] Bisaglia M, Trolio A, Tessari I, Bubacco L, Mammi S, Bergantino E. Cloning, expression, purification, and spectroscopic analysis of the fragment 57-102 of human alpha-synuclein. Protein Expr Purif 2005 Jan;39(1):90-96.

[6] Chartier-Harlin MC, Kachergus J, Roumier C, Mouroux V, Douay X, Lincoln S, et al. Alpha-synuclein locus duplication as a cause of familial Parkinson's disease. Lancet 2004 Sep 25-Oct 1;364(9440):1167-1169.

[7] Singleton AB, Farrer M, Johnson J, Singleton A, Hague S, Kachergus J, et al. alpha-Synuclein locus triplication causes Parkinson's disease. Science 2003 Oct 31;302(5646):841.

[8] Polymeropoulos MH, Lavedan C, Leroy E, Ide SE, Dehejia A, Dutra A, et al. Mutation in the alpha-synuclein gene identified in families with Parkinson's disease. Science 1997 Jun 27;276(5321):2045-2047.

[9] Zarranz JJ, Alegre J, Gomez-Esteban JC, Lezcano E, Ros R, Ampuero I, et al. The new mutation, E46K, of alpha-synuclein causes Parkinson and Lewy body dementia. Ann Neurol 2004 Feb;55(2):164-173.

[10] Kruger R, Kuhn W, Muller T, Woitalla D, Graeber M, Kosel S, et al. Ala30Pro mutation in the gene encoding alpha-synuclein in Parkinson's disease. Nat Genet 1998 Feb;18(2):106-108.

[11] Clayton DF, George JM. The synucleins: a family of proteins involved in synaptic function, plasticity, neurodegeneration and disease. Trends Neurosci 1998 Jun;21(6):249-254.

[12] Beyer K. Alpha-synuclein structure, posttranslational modification and alternative splicing as aggregation enhancers. Acta Neuropathol 2006 Sep;112(3):237-251.

[13] Jakes R, Spillantini MG, Goedert M. Identification of two distinct synucleins from human brain. FEBS Lett 1994 May 23;345(1):27-32.

[14] Davidson WS, Jonas A, Clayton DF, George JM. Stabilization of alpha-synuclein secondary structure upon binding to synthetic membranes. J Biol Chem 1998 Apr 17;273(16):9443-9449.

[15] Dikiy I, Eliezer D. Folding and misfolding of alpha-synuclein on membranes. Biochim Biophys Acta 2012 Apr;1818(4):1013-1018.

[16] Ueda K, Fukushima H, Masliah E, Xia Y, Iwai A, Yoshimoto M, et al. Molecular cloning of cDNA encoding an unrecognized component of amyloid in Alzheimer disease. Proc Natl Acad Sci U S A 1993 Dec 1;90(23):11282-11286.

[17] Lucking CB, Brice A. Alpha-synuclein and Parkinson's disease. Cell Mol Life Sci 2000 Dec;57(13-14):1894-1908.

[18] Ulmer TS, Bax A, Cole NB, Nussbaum RL. Structure and dynamics of micelle-bound human alpha-synuclein. J Biol Chem 2005 Mar 11;280(10):9595-9603.

[19] Dedmon MM, Lindorff-Larsen K, Christodoulou J, Vendruscolo M, Dobson CM. Mapping long-range interactions in alpha-synuclein using spin-label NMR and ensemble molecular dynamics simulations. J Am Chem Soc 2005 Jan 19;127(2):476-477.

[20] Murray IV, Giasson BI, Quinn SM, Koppaka V, Axelsen PH, Ischiropoulos H, et al. Role of alpha-synuclein carboxy-terminus on fibril formation in vitro. Biochemistry 2003 Jul 22;42(28):8530-8540.

[21] Eliezer D, Kutluay E, Bussell R,Jr, Browne G. Conformational properties of alpha-synuclein in its free and lipid-associated states. J Mol Biol 2001 Apr 6;307(4):1061-1073.

[22] McNulty BC, Young GB, Pielak GJ. Macromolecular crowding in the Escherichia coli periplasm maintains alpha-synuclein disorder. J Mol Biol 2006 Feb 3;355(5):893-897.

[23] Weinreb PH, Zhen W, Poon AW, Conway KA, Lansbury PT,Jr. NACP, a protein implicated in Alzheimer's disease and learning, is natively unfolded. Biochemistry 1996 Oct 29;35(43):13709-13715.

[24] Uversky VN, Li J, Fink AL. Evidence for a partially folded intermediate in alpha-synuclein fibril formation. J Biol Chem 2001 Apr 6;276(14):10737-10744.

[25] Lotz GP, Legleiter J. The role of amyloidogenic protein oligomerization in neurodegenerative disease. J Mol Med (Berl) 2013 Jun;91(6):653-664.

[26] Conway KA, Lee SJ, Rochet JC, Ding TT, Williamson RE, Lansbury PT,Jr. Acceleration of oligomerization, not fibrillization, is a shared property of both alpha-synuclein mutations linked to early-onset Parkinson's disease: implications for pathogenesis and therapy. Proc Natl Acad Sci U S A 2000 Jan 18;97(2):571-576.

[27] Lowe R, Pountney DL, Jensen PH, Gai WP, Voelcker NH. Calcium(II) selectively induces alpha-synuclein annular oligomers via interaction with the C-terminal domain. Protein Sci 2004 Dec;13(12):3245-3252.

[28] Rochet JC, Conway KA, Lansbury PT,Jr. Inhibition of fibrillization and accumulation of prefibrillar oligomers in mixtures of human and mouse alpha-synuclein. Biochemistry 2000 Sep 5;39(35):10619-10626.

[29] Vilar M, Chou HT, Luhrs T, Maji SK, Riek-Loher D, Verel R, et al. The fold of alpha-synuclein fibrils. Proc Natl Acad Sci U S A 2008 Jun 24;105(25):8637-8642.

[30] Chen M, Margittai M, Chen J, Langen R. Investigation of alpha-synuclein fibril structure by site-directed spin labeling. J Biol Chem 2007 Aug 24;282(34):24970-24979.

[31] Minton AP. Effect of a concentrated "inert" macromolecular cosolute on the stability of a globular protein with respect to denaturation by heat and by chaotropes: a statistical-thermodynamic model. Biophys J 2000 Jan;78(1):101-109.

[32] Munishkina LA, Phelan C, Uversky VN, Fink AL. Conformational behavior and aggregation of alpha-synuclein in organic solvents: modeling the effects of membranes. Biochemistry 2003 Mar 11;42(9):2720-2730.

[33] Dev KK, Hofele K, Barbieri S, Buchman VL, van der Putten H. Part II: alpha-synuclein and its molecular pathophysiological role in neurodegenerative disease. Neuropharmacology 2003 Jul;45(1):14-44.

[34] Iwai A, Yoshimoto M, Masliah E, Saitoh T. Non-A beta component of Alzheimer's disease amyloid (NAC) is amyloidogenic. Biochemistry 1995 Aug 15;34(32):10139-10145.

[35] McLean PJ, Kawamata H, Ribich S, Hyman BT. Membrane association and protein conformation of alpha-synuclein in intact neurons. Effect of Parkinson's disease-linked mutations. J Biol Chem 2000 Mar 24;275(12):8812-8816.

[36] Fortin DL, Troyer MD, Nakamura K, Kubo S, Anthony MD, Edwards RH. Lipid rafts mediate the synaptic localization of alpha-synuclein. J Neurosci 2004 Jul 28;24(30):6715-6723.

[37] Kamp F, Beyer K. Binding of alpha-synuclein affects the lipid packing in bilayers of small vesicles. J Biol Chem 2006 Apr 7;281(14):9251-9259.

[38] Madine J, Doig AJ, Middleton DA. A study of the regional effects of alpha-synuclein on the organization and stability of phospholipid bilayers. Biochemistry 2006 May 9;45(18):5783-5792.

[39] Lavedan C. The synuclein family. Genome Res 1998 Sep;8(9):871-880.

[40] Larsen KE, Schmitz Y, Troyer MD, Mosharov E, Dietrich P, Quazi AZ, et al. Alpha-synuclein overexpression in PC12 and chromaffin cells impairs catecholamine release by interfering with a late step in exocytosis. J Neurosci 2006 Nov 15;26(46):11915-11922.

[41] Chandra S, Gallardo G, Fernandez-Chacon R, Schluter OM, Sudhof TC. Alpha-synuclein cooperates with CSPalpha in preventing neurodegeneration. Cell 2005 Nov 4;123(3):383-396.

[42] Barbour R, Kling K, Anderson JP, Banducci K, Cole T, Diep L, et al. Red blood cells are the major source of alpha-synuclein in blood. Neurodegener Dis 2008;5(2):55-59.

[43] Shin EC, Cho SE, Lee DK, Hur MW, Paik SR, Park JH, et al. Expression patterns of alpha-synuclein in human hematopoietic cells and in Drosophila at different developmental stages. Mol Cells 2000 Feb 29;10(1):65-70.

[44] Hashimoto M, Yoshimoto M, Sisk A, Hsu LJ, Sundsmo M, Kittel A, et al. NACP, a synaptic protein involved in Alzheimer's disease, is differentially regulated during megakaryocyte differentiation. Biochem Biophys Res Commun 1997 Aug 28;237(3):611-616.

[45] Forloni G, Bertani I, Calella AM, Thaler F, Invernizzi R. Alpha-synuclein and Parkinson's disease: selective neurodegenerative effect of alpha-synuclein fragment on dopaminergic neurons in vitro and in vivo. Ann Neurol 2000 May;47(5):632-640.

[46] Park SM, Jung HY, Kim HO, Rhim H, Paik SR, Chung KC, et al. Evidence that alpha-synuclein functions as a negative regulator of Ca(++)-dependent alpha-granule release from human platelets. Blood 2002 Oct 1;100(7):2506-2514.

[47] De Cristofaro R, De Filippis V. Interaction of the 268-282 region of glycoprotein Ibalpha with the heparin-binding site of thrombin inhibits the enzyme activation of factor VIII. Biochem J 2003 Jul 15;373(Pt 2):593-601.

[48] Zubenko GS, Wusylko M, Cohen BM, Boller F, Teply I. Family study of platelet membrane fluidity in Alzheimer's disease. Science 1987 Oct 23;238(4826):539-542.

[49] Blake CI, Spitz E, Leehey M, Hoffer BJ, Boyson SJ. Platelet mitochondrial respiratory chain function in Parkinson's disease. Mov Disord 1997 Jan;12(1):3-8.

[50] Sharma P, Nag D, Atam V, Seth PK, Khanna VK. Platelet aggregation in patients with Parkinson's disease. Stroke 1991 Dec;22(12):1607-1608.

[51] Di Cera E, Dang QD, Ayala YM. Molecular mechanisms of thrombin function. Cell Mol Life Sci 1997 Sep;53(9):701-730.

[52] Turgeon VL, Milligan CE, Houenou LJ. Activation of the protease-activated thrombin receptor (PAR)-1 induces motoneuron degeneration in the developing avian embryo. J Neuropathol Exp Neurol 1999 May;58(5):499-504.

[53] Vaughan PJ, Pike CJ, Cotman CW, Cunningham DD. Thrombin receptor activation protects neurons and astrocytes from cell death produced by environmental insults. J Neurosci 1995 Jul;15(7 Pt 2):5389-5401.

[54] Nishino A, Suzuki M, Ohtani H, Motohashi O, Umezawa K, Nagura H, et al. Thrombin may contribute to the pathophysiology of central nervous system injury. J Neurotrauma 1993 Summer;10(2):167-179.

[55] Smirnova IV, Zhang SX, Citron BA, Arnold PM, Festoff BW. Thrombin is an extracellular signal that activates intracellular death protease pathways inducing apoptosis in model motor neurons. J Neurobiol 1998 Jul;36(1):64-80.

[56] Faraut B, Ravel-Chapuis A, Bonavaud S, Jandrot-Perrus M, Verdiere-Sahuque M, Schaeffer L, et al. Thrombin reduces MuSK and acetylcholine receptor expression along with neuromuscular contact size in vitro. Eur J Neurosci 2004 Apr;19(8):2099-2108.

[57] Arcone R, Chinali A, Pozzi N, Parafati M, Maset F, Pietropaolo C, et al. Conformational and biochemical characterization of a biologically active rat recombinant Protease Nexin-1 expressed in E. coli. Biochim Biophys Acta 2009 Apr;1794(4):602-614.

[58] Tripathy D, Sanchez A, Yin X, Luo J, Martinez J, Grammas P. Thrombin, a mediator of cerebrovascular inflammation in AD and hypoxia. Front Aging Neurosci 2013 May 9;5:19.

[59] Ciallella JR, Figueiredo H, Smith-Swintosky V, McGillis JP. Thrombin induces surface and intracellular secretion of amyloid precursor protein from human endothelial cells. Thromb Haemost 1999 Apr;81(4):630-637.

[60] Igarashi K, Murai H, Asaka J. Proteolytic processing of amyloid beta protein precursor (APP) by thrombin. Biochem Biophys Res Commun 1992 Jun 30;185(3):1000-1004.

CHAPTER 2.2

Human α-Synuclein Binds to α-Thrombin and Inhibits Platelets Aggregation: Effects on Parkinson's Disease

INTRODUCTION

Human α-Syuclein (αSyn) is a small (140aa, 14.5 kDa) acidic protein from the family of naturally unfolded proteins, involved in several neurodegenerative disorders, such as Parkinson's disease (PD). αSyn is mainly expressed in the brain, particularly in the cerebral cortex and in the olfactory area of the hippocampus, where it primarily localizes in the presynaptic terminals [**1**]. The linear sequence of this protein can be structurally divided in three regions [**2**] (**Fig. 1**). The amino-terminal (1-60) is an amphipathic section almost entirely composed of imperfect repetitions of the string (X**KTKEGV**XXXX), where the amino acids in bold represent the consensus motif, highly conserved. The N-terminus is putative for αSyn binding to negatively charged membranes by assuming a transient α-helix conformation, typical of apolipoproteins lipid-binding domain [**3**]. The portion (61-95), originally referred to as NAC (non-amyloid β-component), was first detected in Alzheimer's disease (AD) amyloid senile plagues [**4**]. This segment is the most hydrophobic portion of the protein. In detail, the region (^{71}VTGVTAVAQKTV^{82}) is required for fibrillation: due to a β-sheet organization at this level, several αSyn molecules can associate and aggregate by stacking interactions [**5**]. On the other hand, the carboxy-terminal (96-140) of the protein is rich of prolines and negatively charged residues (particularly E104, E105, E114, E115), and can thus inhibit aggregation at a physiological pH by electrostatic repulsions [**6**;**7**]. Furthermore, the C-terminus regulates the interaction between the protein and the membrane lipids; yet even after the binding this segment remains always de-structured and free to interact with other species, like phospholipase D2 [**8**].

Although αSyn accounts for as much as 1% of the soluble proteins in the brain, its physiological functions still keep on elusive [**9**]. Being intrinsically disordered, this protein lacks of a well-defined three-dimensional structure: in solution, it explores several random coil flexible conformations [**10**]. Due to its great plasticity, αSyn may bind to and interact with several molecular partners, yielding as many functions [**11**]. Its massive presence in the proximity of the synaptic terminals, supports the hypothesis that this specie may play a key role in the vesicular fusion, trafficking and turnover [**12**;**13**].

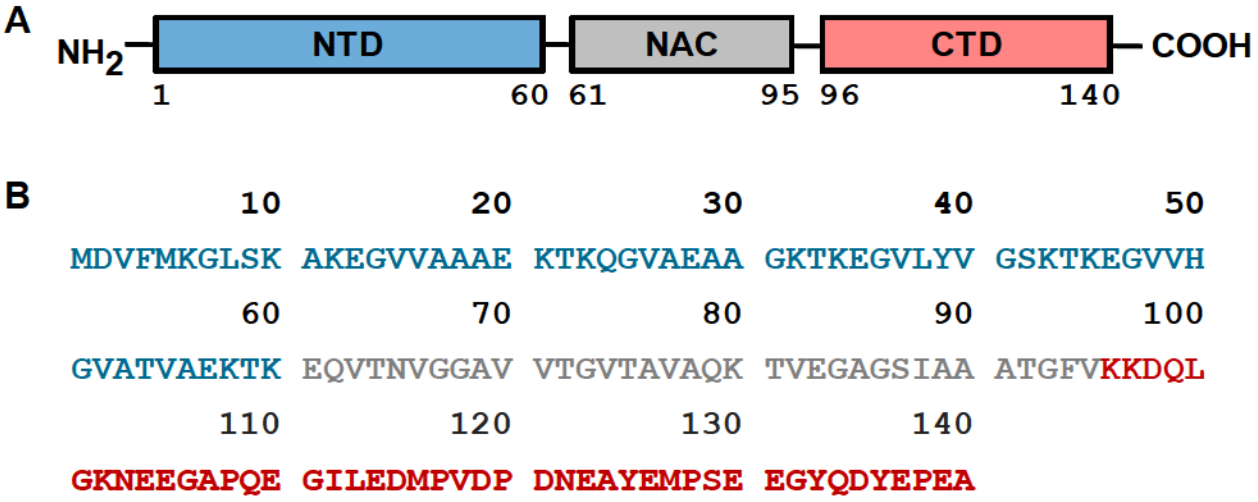

Figure 1. Schematic representation (A) and sequence (B) of full length human αSyn in its colour coded architecture domains. The linear sequence of human αSyn can be divided in three regions. The N-terminal domain (1-60), in blue, is an amphipathic sequence, which can bind to lipid membranes in a transient α-helix conformation. The sequence (61-95), in grey, originally referred to as NAC (non-amyloid β-component) is the most hydrophobic portion of the protein. Due to a β-sheet organization at this level, several molecules of αSyn can associate and aggregate by stacking interactions. The C-terminal domain (96-140), in red, is rich of negatively charged residues, and can thus inhibit aggregation by electrostatic repulsions.

In detail, the N-terminus organizes in two α-helixes between the residues V3-V37 and K45-T92, connected by a flexible linker that aligns the segments in an anti-parallel fashion [**14**]. The protein may thus anchor both to the plasma membrane and to the vesicle, modulating their distance by the linker. Furthermore, a recent study demonstrated that αSyn might regulate catecholamine release from the synaptic vesicles [**15**]. Finally, this protein prevents neurodegeneration by collaborating with cysteine-string protein α, a chaperone involved in the folding of the synaptic proteins N-ethylmaleimide sensitive factors [**16**].

Although its overall protective role toward the neurons, aggregates of αSyn in the brain are highly pathogenic. Being this specie naturally in balance in solution between the monomer and the aggregates, abundance of αSyn is concerned in several neurodegenerative disorders, such as PD, AD, and Lewy Bodies (LBs) dementia. These pathologies can be classified as *synucleinopathies*, due to the typical presence of β-structure αSyn intracellular aggregates in the neurons and glia [**17**;**18**]. Particularly, in PD we can distinguish an autosomal dominant or an early-onset variant. The first presents duplications or triplications of the whole genetic *locus* [**19**;**20**], while the second is due to three missense mutations in the N-terminal region: A53T [**21**], A30P [**22**], E46K [**23**]. All these mutations influence the kinetic constant of αSyn fibrillation, encouraging either oligomerization or

β-sheet conformations, with reduced molecular flexibility [**24**]. The fibrillation pathway from monomers to aggregates is complex and still matter of studies: particularly, a latter hypothesis suggests that the pre-fibrillary soluble oligomers, rather than the insoluble fibres themselves, might be the real pathogenic species [**25**].

Beyond central nervous system, αSyn is present also in the hearth, skeletal muscles, pancreas and placenta. Furthermore, it is expressed in the haematopoietic lineage: more than 99% of the protein is localized in the erythrocytes, while the remaining is subdivided between plasma (0.1%), platelets (0.2%) [**26**], and mononuclear cells (0.05%) [**27**]. This massive presence in the erythrocytes can be explained because red cells alone make up more than 90% of all blood cells. In effect, normalizing the amount of αSyn to the total cellular protein content, platelets yield the highest protein rate (264±36 ng/mg) compared to erythrocytes (131±23 ng/mg) [**28**]. Furthermore, αSyn plasma concentration (25±9 mg/ml) is variable and increases in those subjects who present repetitions of the genetic *locus* [**29**]. Recently it has been established that besides being expressed in the platelets (152 ng/ml), exogenous plasmatic αSyn can penetrate and localize in the cytosol, near the membrane. Due to its N-terminal properties, the protein can weakly associate with plasma membrane and the surface of pro-aggregant α-granules, whose Ca^{2+}-dependent release is inhibited by αSyn [**30**]. Clinical studies assert that PD patients are less susceptible to ischaemic attacks, due to abnormalities in platelets aggregation [**31**]. Several physiologic pathways trigger platelets activation; *in vivo* the main activator is αT.

Human α-thrombin (αT) (FIIa) (295aa, 36.7kDa) is accounted to be the key enzyme of the coagulation cascade. αT is an ellipsoidal protein, composed of a light chain and a heavy chain linked by a disulphide bond [**32**]. Being a serine protease, αT presents a negatively charged active site, in which three conserved residues (S195, H57, D102) catalyse the hydrolysis of peptide bonds [**33**]. Furthermore, this protein bears two positively charged extra regions of binding, called exosite I and exosite II [**34**]. The versatility of αT relies on its molecular mechanism of recognition: this enzyme exerts paradoxically either pro-coagulant (fibrin generation, platelets activation) or anti-coagulant (PC activation) functions, depending on its interactions with different ligands [**35**]. In detail, the pro-aggregant role entails platelet activation through the proteolysis of surface PARs: after the cleavage in the extracellular domain, the fresh-generated N-terminus bends and interacts itself with the receptor, promoting signal transduction [**36**]. Once activated, three events occur, resulting in the formation of the localized clot: platelets degranulate, become sticky and bind fibrin networks [**37**]. First, platelets expand and generate protuberances called pseudopods, thus interacting each other. These cells present two types of granules: δ-granules (Ca^{2+}, ADP, ATP, serotonin) [**38**] and α-

granules (containing several coagulations mediators) [**39**] whose release is driven by Ca^{2+} and determines an overall pro-aggregant effect. Finally, platelets display in their surface the receptor GpIIb/IIIa, promiscuous for fibrinogen and vWF [**40**]. Furthermore, αT promotes the conversion of fibrinogen (FI) to an insoluble fibrin (FIa) clot that anchors platelets to the site of lesion [**41**].

Both experimental and clinical data suggest that αSyn may interfere with coagulation with a down-regulatory effect. The concomitant presence of αSyn and αT on the platelets surface prompted us to investigate the possible binding between these molecular species. This original interaction may represent the meeting point and the interface between coagulation and neurodegenerative diseases, in a pioneer physio-pathologically relevant scenario.

EXPERIMENTALS

Reagents

Natural α-thrombin (αT) and prothrombin (ProT) were purchased from Haematologic Technologies (Essex Junction, VT, USA). Ecarin from *Echis carinatus* venom, fibrinogen from human plasma, PABA (p-aminobenzamidine), all salts, solvents and reagents of analytical grade were purchased from Sigma (St. Louis, MO, USA). The chromogenic substrate S2238 (D-Phe-Pip-Arg-pNA) was from Chromogenix (Milan, Italy), while the N-terminal hirudin domain Hir(1-47) derives from the limited proteolysis of hirudin HM2 from *Hirudinaria manillensis* by bovine pancreas trypsin (Promega Biosciences, CA, USA). Recombinant hirudin HM2 was a generous gift from Dr. G. Orsini (Farmitalia, Italy). Hirugen ^{54}GDFEEIPEEY(PO_3H)LQ^{65} and γ'–peptide ^{408}VRPEHPAETEY (PO_3H)DSLY(PO_3H)PEDDL^{427} were synthesized and purified as previously detailed [**36**;**42**;**43**].

Preparation of Thrombin Samples

The plasmid containing the cDNA of prethrombin-2 (Pre2) was a generous gift of Prof. Huntington (Cambridge University). The recombinant inactive mutant rS195A, obtained by single-point mutagenesis, was expressed in *E. coli*, subjected to *in vitro* disulphide oxidative refolding, activation by ecarin, and characterized as previously detailed [**44**;**45**]. β_T-thrombin (β_TT) was obtained by proteolysis of human αT (7μM) with bovine pancreas trypsin (35nM) for 3 hours at 37°C in HBS, and characterized as previously detailed [**46**;**43**]. The concentrations of thrombin solutions were determined by measuring the absorbance at 280nm, using an absorptivity coefficient of 66390 $M^{-1}\cdot cm^{-1}$. For the concentration of ProT solutions, the absorptivity coefficient of 109790$M^{-1}\cdot cm^{-1}$ was used.

Preparation of α-Synuclein Samples

Human recombinant αSyn wild type and His-tag were expressed in collaboration with Prof. Negro's laboratory (Dept. of Biology – University of Padua). After thermic shock in BL21*(DE3)pLysS *E. coli* strains, the cells containing pRSET-B plasmid were selected on a LB Agar Amp+ (0.1mg/ml) plate overnight, and cultured in LB Broth Amp+ (0.05mg/ml). When the OD of 0.6 was reached, the cells were induced with IPTG (0.1mg/ml) under vigorous shaking. All the cellular growth processes were performed at 37°C. For wild type αSyn, after three hours, bacteria were harvested by centrifugation (6000rpm, 15min, 4°C), and the pellet underwent sonication and ten minutes boiling, being the protein thermostable. The precipitate was discarded, while the supernatant was dialyzed overnight at 4°C against 40mM TRIS-HCl buffer pH 8.0, 0.1M NaCl, 2mM EDTA. Human αSyn wild type was purified by RP-HPLC from JASCO (Tokyo, Japan) on a C18 Vydac (Hesperia, CA, USA) semi-preparative column (10x250mm; 5μM, 300Å), eluted with a linear acetonitrile-0.078% TFA gradient at a flow rate of 1.5ml/min. The material eluted from the major peak was analysed by high resolution MS on a Mariner ESI-TOF instrument from Perseptive Biosystems (Stafford, TX, USA). Lyophilized samples from RP-HPLC were resuspended in four different buffers: (**1**) 5mM TRIS-HCl pH 8.0, 0.2 M NaCl, 0.1% PEG-8000 (w/v); (**2**) 5M Gnd-HCl; (**3**) 7% DMSO (v/v); (**4**) alkaline treatment: 2mM NaOH - 1M NaOH - 100mM TRIS-HCl pH 7.0 [**47**]. The samples were examined by both UV-Vis spectra, at 25°C, and fluorescence measurements, at 37°C. Since αSyn contains four Tyr, the fluorescence intensity at 303nm was compared to the spectroscopic model N^{α}-Acetyl-Tyr-NH_2. A DLS assay was performed on the sample treated with (**4**) alkaline buffer, presenting the lower degree of aggregation.

On the other hand, after bacterial sonication, His-tag αSyn was purified first by IMAC chromatography. About 3ml of IMAC resin were washed with 10ml of 40mM TRIS-HCl pH 8.0, 0.1M NaCl buffer, and added to the bacterial lysis supernatant. The interaction between Ni^{2+} ions and the histidine tag was achieved by slow stirring at 4°C for an hour. After sedimentation, the resin was loaded on a disposable column and conditioned with 60ml of the washing buffer. His-tag αSyn was eluted by 10ml of 40mM TRIS-HCl pH 6.5, 0.1M NaCl, 0.4M imidazole. The collected fractions were pooled, dialyzed overnight versus 500ml of PBS, purified to homogeneity by RP-HPLC on a C18 semi-preparative column (10x250mm; 5μM, 300Å) and analysed by MS. Lyophilized samples were reconstituted in HBS-EP buffer for SPR measurements. The concentration of αSyn solutions was determined by measuring the absorbance at 280nm, using a molar absorptivity of $5960 M^{-1} \cdot cm^{-1}$.

The C-terminal fragments αSyn(103-121), (122-140) and (103-140) were synthesised by standard solid-phase Fmoc chemistry [**48**] using a model PS3 automated synthesizer from Protein

Technologies International (Tucson, AZ, USA), on a ChemMatrix resin (Matrix Innovation, Quebec, Canada). N-Fmoc protected amino acids, solvents and reagents for peptide synthesis were purchased from Applied Biosystems (Forster City, CA, USA) or Bachem AG (Bubendorf, Switzerland). The crude peptides were purified to homogeneity by semi-preparative RP-HPLC on a C18 column (10x250mm; 5μM, 300Å), and the major peaks eluted from RP-HPLC were characterized by MS, as previously detailed. Lyophilized samples were resuspended with HBS buffer. The concentrations of peptide solutions were determined by measuring the absorbance at 280nm, using a molar absorptivity of $4470 M^{-1} \cdot cm^{-1}$ for αSyn(103-140) and (122-140). For peptide (103-121), lacking of chromophores, the concentration was measured by weight.

Platelets Aggregation Assay

The effect of αSyn on αT-induced platelets aggregation was measured in whole blood by multiple electrode aggregometer (MEA) with a multiplate analyser from Dynabyte medical (Munich, Germany). Normal, citrate-treated venous blood samples were taken from three healthy non-smokers donors: all the analysis were performed within three hours from the withdrawn. The donors gave written informed consent for participation in this study, which was approved by the Ethical Committee of the University Hospital of Padua. Monomeric samples of αSyn or fragment (103-140) (0-20μM) were pre-incubated with αT (6nM), in 320μl of HBS buffer at 37°C. After 30min, these solutions were mixed with whole blood (300μl), and analysed. All the measures were accomplished at 37°C, with vigorous stirring, for 10min. The aggregation rate was quantified by measuring the increase of the electric impedance, expressed as relative aggregation units (AU), during time. The extent of platelets aggregation was calculated as the AUC from the mean of two electrodes [**45**;**49**]. Finally, the percent of AUC values was shown as column bars, and plotted against αSyn concentrations.

Release of Fibrinopeptides

Human fibrinogen was desalted on a Sephadex G10 resin from Sigma (St. Louis, MO, USA), manually packed in a (8x125mm) column, eluted with HBS buffer at a flow rate of 0.3ml/min. The release of FpA and FpB by human αT (300pM) from desalted fibrinogen (0.35μM), in the presence or in the absence of 2μM αSyn, was carried out at 37°C in 1ml of HBS buffer. At fixed time points (0, 2, 4, 8, 16, 40, 60min) proteolysis was quenched by 300μl HCOOH 12% (v/v); the sample were centrifuged at 10,000g for 5min to eliminate fibrin and acid-precipitated fibrinogen. The supernatant (1ml) was withdrawn, lyophilized and dissolved in 150μl of 6M Gnd-HCl. Fibrinopeptides were

separated and quantified by RP-HPLC, injecting 100µl of the sample onto a (4.6x250mm; 5µM, 300Å) C18 Vydac analytical column (Hesperia, CA, USA). The column was equilibrated in 40mM ammonium phosphate buffer, pH 3.1, and eluted with a linear acetonitrile gradient at a flow rate of 1.0ml/min, recording the absorbance at 205nm, according to the method previously reported [**50**].

The amount of FpA and FpB released was determined by integrating the AUC, using molar absorptivity at 205nm of $4.4 \cdot 10^4 M^{-1} \cdot cm^{-1}$ or $5.12 \cdot 10^4 M^{-1} \cdot cm^{-1}$, respectively. The specificity constant (k_{catA}/K_{mA}) for the release of FpA was determined by interpolating the data points to the **equation 1**:

$$[FpA]_t = [FpA]_\infty \cdot (1 - e^{-k't}) \qquad \textbf{(Eq. 1)}$$

where $[FpA]_t$ and $[FpA]_\infty$ are the concentrations of FpA at time t and ∞, respectively, and k′ is the observed kinetic constant for FpA release, obtained as a fitting parameter. Under pseudo-first order conditions, i.e. [A-chain]>>[αT], and [fibrinogen]<0.1·[K_{ma}], the specificity constant (k_{catA}/K_{mA}) can be derived according to **equation 2**:

$$\frac{k_{catA}}{K_{mA}} = \frac{k'}{[\alpha T]} \qquad \textbf{(Eq. 2)}$$

where k_{catA} is the real kinetic constant, while K_{mA} is the Michaelis-Menten constant of αT for fibrinogen A-chain. Since in the experimental conditions tested αT concentration is much lower than fibrinogen A-chain, and fibrinogen concentration is lower than K_{mA}=7.2µM at 37°C [**50**], **equation 2** is suitable for deriving the specificity constant.

Analogously, the data points relative to the time-dependent release of FpB were interpolated with **equation 3**:

$$[FpB]_t = [FpB]_\infty \cdot (1 + \alpha \cdot e^{-k't} - \beta \cdot e^{-k''t}) \qquad \textbf{(Eq. 3)}$$

where k′ and k″ are the observed kinetic constants for FpA and FpB release, respectively, and α=k″/(k′-k″), and β=k′/(k′-k″). As for the release of FpA, at αT and fibrinogen concentrations used in this work, the specificity constant (k_{catB}/K_{mB}) can be derived according to **equation 2**.

Fluorescence

Fluorescence binding measurements were carried out at 37°C in HBS (1.5ml), in a 1cm-pathlenght quartz cuvette on a Jasco FP-6500 spectrofluorimeter (Tokyo, Japan). To assert whether the species of interest interact, samples of αT (70nM), αSyn (20µM) and their mixture after pre-incubation for 30min at 37°C were excited at 295nm. The spectra were recorded in the range 305-

500nm, subtracted of the baseline, and compared to the theoretical sum of the proteins profiles.

In a second phase, once established the existence of a complex, to identify αSyn regions involved in the binding, increasing aliquots of full length αSyn or its C-terminal fragments (103-140), (103-121), (122-140) were added to an αT solution (70nM) till reaching saturation. Conversely, αT regions involved in the complex were dissected by probes that selectively bind to different enzyme areas. The titrations of αT (70nM) with specific ligands were performed both in the absence and in the presence of saturating (20μM) αSyn or peptide (103-140) concentrations. In detail, PABA, S2238 and Hir(1-47) were used for the active site; hirugen is specific for exosite I while γ'-peptide for exosite II. In particular, for S2238, the inactive mutant rS195A (50nM) was used. For all the titrations, aliquots (2-20μl) of ligands stock solutions were added, under gentle magnetic stirring (30sec), and the samples were allowed to equilibrate 2min after each addition. Samples were excited at 295nm, and the fluorescence was recorded at 334nm. The spectra were corrected for the dilution factor (that was always lower than 10% at the end of the titration), subtracted of the blank and of raw starting fluorescence. For low affinity binders, like αSyn full length and fragments, PABA, S2238, hirugen and γ'-peptide, the data points were interpolated with **equation 4**, describing a simple one-site binding mechanism R + L ⇔ RL [**51**]:

$$\frac{\Delta F}{\Delta F_{max}} = \frac{[RL]}{[R]} = \frac{[L]}{K_d + [L]} \qquad \textbf{(Eq. 4)}$$

where the fluorescence intensity, F, of the receptor, R, at a given concentration of ligand, L, is linearly related to the concentration of the complex [RL], according to the equation $F=[RL]\cdot F_{bound}+[R]_{free}\cdot F_{free}$. $\Delta F=F-F_0$ is the change in thrombin fluorescence in the absence, F_0, and presence, F, of the ligand; ΔF_{max} is the maximum signal change at infinite concentration of ligand, $[L]_\infty$; K_d is the dissociation constant of the complex, RL. The data were interpolated to obtain the fitting parameters ΔF_{max} and K_d.

Equation 4 assumes the simplification that at equilibrium $[L]_{free} \cong [L]_{tot}$ and thus it is valid only when $K_d >> [R]$. For tight binders, like Hir(1-47), $K_d \cong [R]$ and **equation 4** is no longer valid. In this case, fluorescence data were fitted to the rigorous **equation 5** of tight binding [**52**]:

$$\frac{\Delta F}{\Delta F_{max}} = \frac{[RL]}{[R]} = \frac{[R]+[L]+K_d - \sqrt{\left[[R]+[L]+K_d\right]^2 - 4\cdot[R]\cdot[L]}}{2\cdot[R]} \qquad \textbf{(Eq. 5)}$$

For PABA titration, αT samples (40nM) were excited at 336nm and the fluorescence recorded at 375nm. Raw data were corrected for the inner filter effect (IFE) factor, since fluorescence intensity

is only proportional to the absorbance of the sample up to an optical density of 0.05 units, both at λ_{ex} and λ_{em} [**52**;**53**]. The following **equation 6** was used:

$$IFE = \frac{2.303 \cdot \frac{1}{3}Abs_{PABA}}{10^{-\frac{1}{3}Abs_{PABA}} - 10^{-\frac{2}{3}Abs_{PABA}}} \qquad \textbf{(Eq. 6)}$$

where PABA theoretical absorbance at 336nm was determined using a molar absorptivity of 547.8 $M^{-1} \cdot cm^{-1}$. **Equation 6** is valid only for 1cm-pathlength cuvettes.

Surface plasmon resonance

SPR analyses were carried out in a dual flowcell Biacore-X100 instrument from GE Healthcare (Little Chalfont, UK). His-tag αSyn was immobilized on a nitrilotriacetate (NTA) carboxymethyldestrane sensor chip by chelation with Ni^{2+} in HBS-EP buffer, at a flow rate of 30μl/min and temperature of 25°C. Briefly, after washing the chip with 0.35M EDTA pH 8.3 (700sec), the surface was derivatized by 0.5mM Ni^{2+} (400sec). Excess of Ni^{2+} was removed by 3mM EDTA (350sec), while the non-chelated NTA moieties were irreversibly blocked by ethanolamine (800sec). A solution of His-tag αSyn (200nM) was injected for 400sec, giving a final immobilization degree of 2194.3 response units (RU).

In a first stage, increasing concentrations of inactive rS195A (1nM-1μM) were sequentially injected in the mobile phase, over the His-tag αSyn sensor chip. For each curve, the response value RU_{eq} at steady-state (after reaching equilibrium at each ligand concentration) was plotted against [rS195A] and the K_d and RU_{max} of the complex were obtained fitting the data points to **equation 7**:

$$RU_{eq} = RU_{max} \cdot \frac{[L]}{K_d + [L]} \qquad \textbf{(Eq. 7)}$$

where RU_{max} is the RU value at saturating L concentrations and [L] is the concentration of the free ligand in equilibrium with the receptor-ligand RL complex present on the sensor chip surface. When $[R] << K_d$, then $[L]_{free} \cong [L]_{tot}$, i.e. the total ligand concentration in the mobile phase. Data analysis evaluation was performed using the BIAevaluation software.

In a second stage, rS195A (0.1μM) samples were pre-incubated with increasingly saturating concentrations of either hirugen (0-20μM) or γ'-peptide (0-140μM) one at time, and sequentially injected over the His-tag αSyn sensor chip. In comparison to rS195A alone, the $\%RU_{eq}$ were calculated and plotted against the ligands concentrations. Then, rS195A (0.1μM) samples were pre-

incubated with the same concentrations of hirugen and γ'-peptide together, increasing simultaneously, and injected over the chip. The $\%RU_{eq}$ were plotted for each couple of concentrations, and compared to the values obtained when exosite I and II are masked one in turn.

Finally, solutions of either human ProT, and β_TT were injected in the mobile phase (1nM-1μM). The values of RU_{eq} were interpolated with **equation 7** to obtain K_d and RU_{max} of the complexes as fitting parameters, and compared to the signals given by rS195A. All the analysis were accomplished at 37°C in HBS-EP running buffer.

RESULTS AND DISCUSSION

α-Synuclein Samples Preparation and Characterization

In order to explore αSyn interaction with thrombin, we decided to study the binding with either the full length protein or three C-terminal fragments. The N-terminal domain, likely involved *in vivo* to platelets membrane anchoring, was not investigated. Both wild type and His-tag full length αSyn, lacking of disulphide bridges and of a well-defined folding, were easily expressed in *E. coli* strains. After bacterial expression, αSyn localizes in the cytosolic fraction, in equilibrium between the random coil monomer and the aggregates. For the wild type protein, after sonication, the soluble lysate fraction was diluted and boiled for ten minutes. Being αSyn thermostable, it remains in the supernatant, while mostly of the bacterial proteins in this harsh conditions precipitate. Conversely, His-tag αSyn can be in a first step simply purified by IMAC chromatography. On the other hand, the peptides (103-140), (103-121), (122-140), corresponding to the acidic C-terminal region of the protein, were produced by solid-phase peptide synthesis. The fragments do not correspond to the real C-terminal starting Lys96 for practical synthetic purposes. All the αSyn samples could be purified to homogeneity by RP-HPLC, and lyophilized: in each case, the chromatograms displayed a major peak, corresponding to the desired molecule. The purified species yielded an average experimental MW in accord to their theoretical value, calculated on the amino acidic composition (**Table 1**).

While lyophilized His-tag αSyn and the C-terminal peptides were resuspended in physiological HBS, an extensive investigation was performed on the choice of wild type αSyn proper buffer, in order to contrast its tendency to fibrillation. In detail, lyophilized protein samples were dissolved in four either physiologic, organic, or weakly denaturant buffers. Among all, a treatment adapted from Munishkina and co-workers protocol [**47**] allowed us to maximize αSyn negative charges in a highly alkaline environment, and slowly lower the pH to a physiologic value.

	RP-HPLC Gradient	Experimental MW (a.m.u.)	Theoretical MW (a.m.u.)	Δ MW
Full Length	30-55% in 30min	14458.8	14460.2	1.4
His-tag	30-55% in 30min	16060.8	16060.9	0.1
(103-140)	20-40% in 30min	4289.5	4288.4	1.1
(103-121)	20-45% in 15min	2055.1	2055.1	0.0
(122-140)	5-55% in 40min	2251.2	2251.3	0.1

Table 1. Small library of αSyn samples purification conditions and chemical characterization. Full length and His-tag αSyn were expressed in *E. coli*, while C-terminal peptides were synthesized by solid-phase Fmoc chemistry. Acetonitrile gradient applied for RP-HPLC purification, and comparison between experimental and theoretical MW of the species are highlighted.

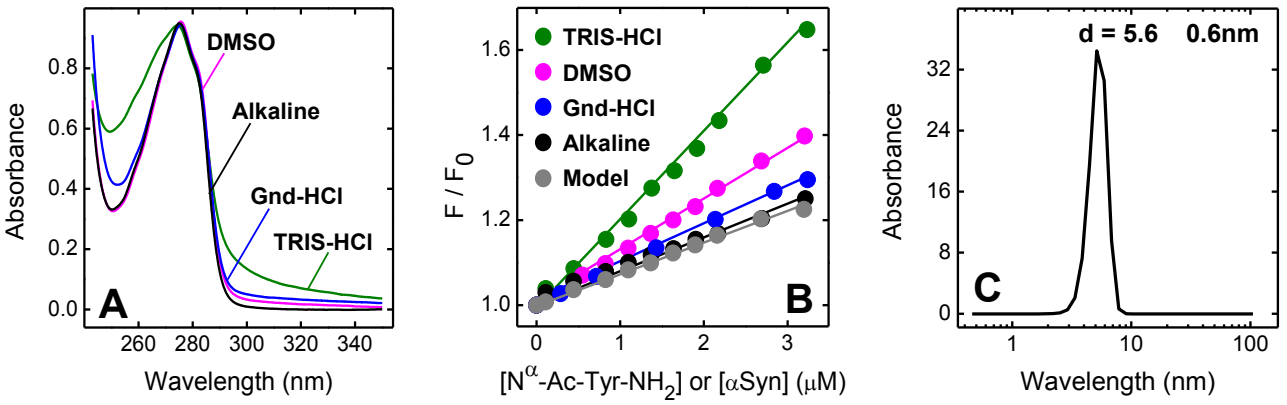

Figure 2. Spectroscopic characterization of αSyn samples resuspended in different buffers. Lyophilized full length αSyn samples from RP-HPLC were dissolved in four different buffers: (—) 5mM TRIS-HCl pH 8.0, 0.2M NaCl, 0.1% PEG-8000 (v/w); (—) 7% DMSO (v/v); (—) 5M Gnd-HCl 7%; (—) alkaline buffer (**see text**). **(A) UV-Vis -** Spectra measurements, performed at 25°C. **(B) Fluorescence -** Fluorescence intensity at 303nm of increasing αSyn concentrations, compared to the model (—) N^{α}-Ac-Tyr-NH_2. The measurements were performed at 37°C. **(C) DLS -** Analysis at 37°C of an αSyn solution (50μM) in alkaline buffer, filtrated at 0.2nm.

In order to determine αSyn aggregation degree, these protein samples were analysed with complementary spectroscopic techniques [**54**]. Since αSyn contains only four Tyr as chromophores, the data could be compared to the spectroscopic model N^{α}-Ac-Tyr-NH_2. Regarding UV-Vis absorption, αSyn samples can be considered monomeric if the ratio Abs_{275nm}/Abs_{250nm} = 2.6±0.2 (characteristic of Tyr), and no appreciable light scattering is detected in the region 300-350nm (**Fig. 2A**). Fluorescence emission intensity of αSyn solutions at 303nm was simply compared to the

spectroscopic model, at increasing sample concentrations (**Fig. 2B**). From the experimental data, it clearly emerged that only αSyn samples subjected to the alkaline treatment display monomeric spectroscopic behaviour, probably due to electrostatic repulsions between different molecules, contrasting aggregation. These solutions were thus analysed by DLS: the data, expressed as a volume distribution, show a major monodisperse peak, representing the 99.99% of the mass, characterized by a diameter of 5.6±0.6nm (**Fig. 2C**). The calculated molecular weight of the protein is 37.0±7.0kDa: this upper-esteem is due to αSyn stretched random coil conformation.

α-Synuclein Inhibits Platelets Aggregation

αT plays a pivotal role in the coagulation cascade, networking with many ligands and substrates. In detail, this serine protease activates platelets through the interaction with receptor GpIbα and subsequent cleavage of surface PARs. *In vivo*, after a vascular damage, platelets aggregation is the very first defence step started, responding even to minimal αT concentrations. In turn, activated platelets amplify the coagulation cascade through the release of vasoactive mediators from the granules. Platelets aggregation was investigated in whole blood, with Multiple Electrode Aggregometer (MEA), using cuvettes equipped with a couple of electrodes. In non-clotted blood, inactive platelets stick to the electrodes, organizing in a monolayer. After the addition of an aggregant exogenous agonist (i.e. αT or ADP), platelets generate pseudopods and adhere to the pre-existing monolayer, thus increasing plasma electric impedance.

To investigate its effect on platelets aggregation, increasing αSyn concentrations were pre-incubated with αT at 37°C, and mixed with whole blood. To mimic a physiologic environment, low (6nM) αT concentrations were used, while a wide range of αSyn concentrations (0-20μM) were explored, since this protein can both penetrate and be secreted from platelets. From the **panel 3A**, it clearly emerges that αSyn inhibits αT-induced platelets aggregation, in a dose-dependent manner, to an extent of 80%. In our hypothesis, αSyn bound to platelets membrane forms a complex with αT, acting as a scavenger for the serine protease enzymatic activity. The C-terminal fragment (103-140) was used as a negative control. Lacking of the N-terminal region, crucial for the membrane interaction, this peptide could not anchor to the platelets surface and preventing the activation with a negative-feedback mechanism.

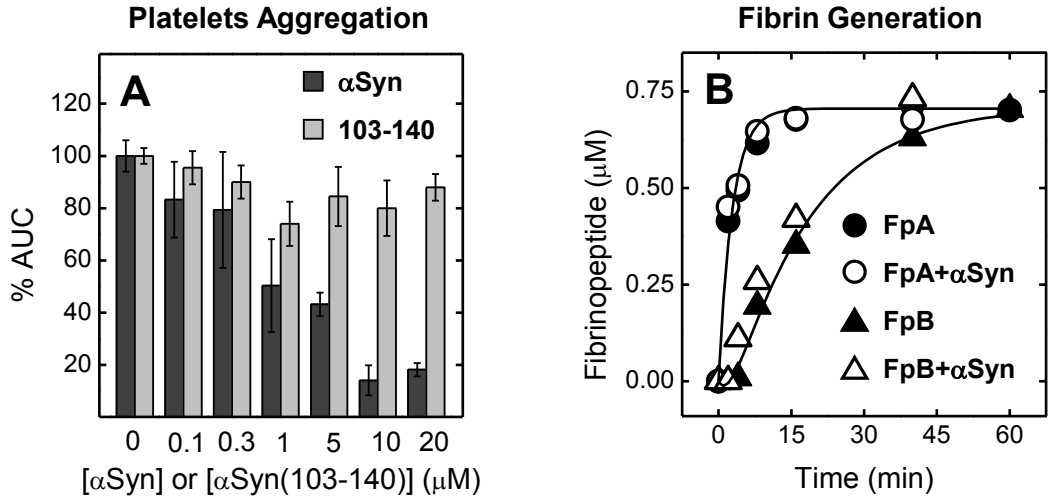

Figure 3. αSyn effects on αT procoagulant functions. (A) Platelets aggregation - Increasing concentrations (0-20μM) of αSyn or fragment (103-140) were pre-incubated with human αT (6nM) in 320μl HBS at 37°C. After 30min, 300μl of whole blood were added, and the degree of platelets aggregation was measured as the increase of electric impedance during the reaction time of 10min, at 37°C. The data are expressed as %AUC, where $AUC_0 = 100\%$ is the area under the aggregation curve at [αSyn]=0. **(B) Fibrin Generation -** The extent of fibrin generation was indirectly measured through the release of FpA and FpB from human fibrinogen (0.35μM) by αT (300pM) either in the absence or in the presence of αSyn (2μM). At fixed time points, the fibrinopeptides were isolated by RP-HPLC and their concentration was derived from the area under the chromatographic peaks. Experimental data points relative to the release of FpA were fitted according to **eq. 1**, while for the release of FpB **eq. 3** was used.

α-Synuclein Does Not Influence Fibrin Generation

αT most specific function in haemostasis is undoubtedly fibrin generation from fibrinogen proteolytic cleavage: the building of the insoluble network is a multi-step process. Fibrinogen is a large plasma glycoprotein circulating as a dimer of three chains $(A\alpha B\beta\gamma)_2$. First, αT cleaves fibrinogen A-chains, with the generation of two FpA (16aa) and fibrin monomer I, which undergoes longitudinal elongation, assembling in double-stranded protofibrils. In a second stage, αT hydrolyses fibrinogen B-chains, with the release of two FpB (14aa), and lateral association of the protofibrils, resulting in the generation of insoluble fibrin fibres. *In vitro*, this Sol→Gel transition can be easily investigated by register the increase of the sample turbidity at 350nm, due to the light scattering. Unfortunately, these spectroscopic assays could not be performed with monomeric αSyn samples, characterized by considerable high ionic strength, due to admixtures of NaOH and TRIS-HCl.

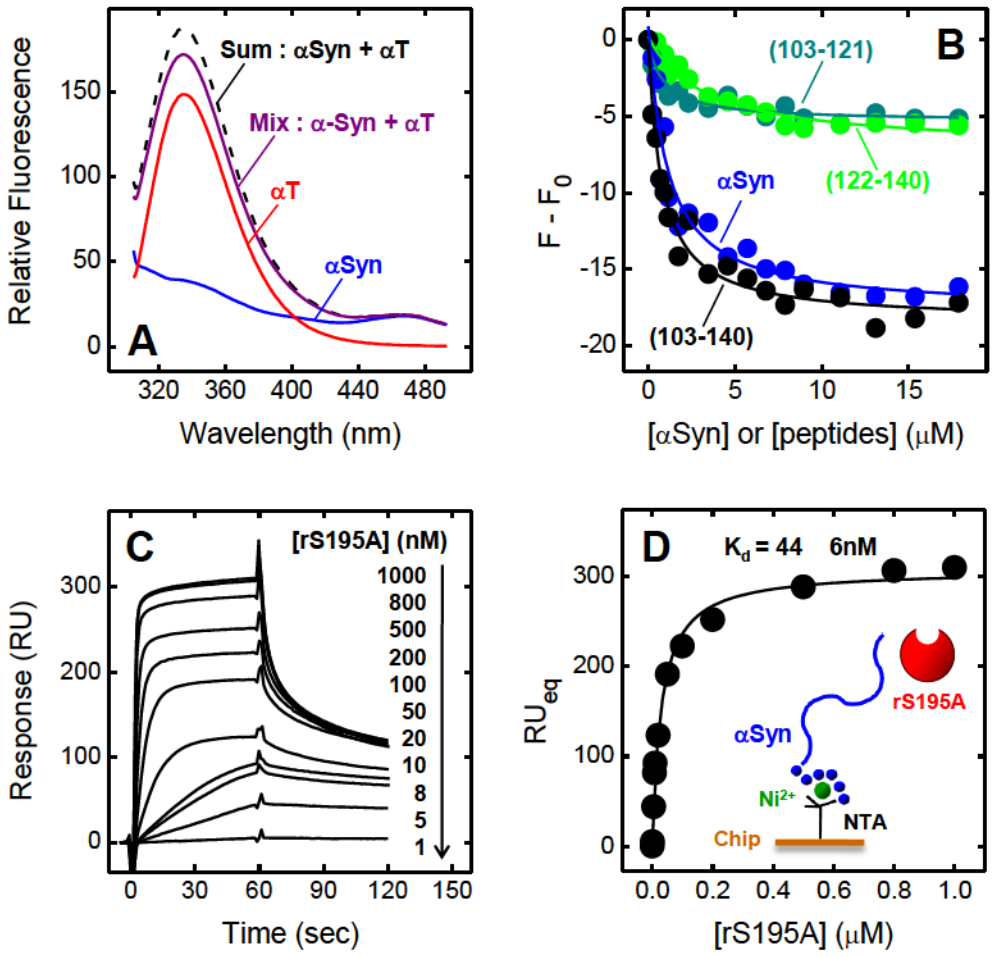

Figure 4. Study of the interaction between αSyn and thrombin. (A) Binding by fluorescence - Fluorescence spectra of solutions of 20μM αSyn (—), 70nM αT (—), and their mixture (—), after excitation at 295nm. The measurements were performed in HBS at 25°C, and compared to the theoretical sum (---) of the species. **(B) Dissecting αSyn regions involved in the binding by fluorescence titrations -** To a solution of αT (70nM) in HBS were added, at 37°C, aliquots (2-20μl) of αSyn full length (—) or fragments (103-140) (—), (103-121) (—), (122-140) (—) stock solutions. The samples were excited at 295, and the emission intensity was recorded at 334nm. The data points were fitted according to **eq. 4**, giving the K_d and ΔF_{max} values displayed in **table 2**. **(C,D) Binding of rS195A to His-tag αSyn immobilized on a NTA sensor chip - (C)** Sensograms relative to rS195A (1-1000nM) binding. **(D)** Plot of RU_{eq} versus rS195A concentrations. Fitting of data points with **eq. 7** yielded a K_d of 44±6nM. All measurements were carried out in HBS-EP at 37°C.

Table 2. Fluorescence titrations fitting parameters relative to Fig. 4B

	K_d(μM)	ΔF_{max}%
αSyn	0.96 ± 0.34	7.10
(103-140)	1.25 ± 0.26	9.39
(103-121)	1.76 ± 0.66	4.35
(122-140)	4.36 ± 1.75	2.84

Actually, an increase in ionic strength dramatically affects the physical parameters of the network: the number of fibres bundles increases, while a decrease in both the average size of fibres diameter, and in the pores between fibres [**55**].

Due to our non-physiological experimental conditions, we investigated αSyn influence on αT-induced fibrin generation only by monitoring the kinetics of the release of fibrinopeptides. The proteolysis was performed in pseudo-first order kinetic conditions, either in the absence or in the presence of 2μM αSyn. The experimental data (**Fig. 3B**) suggest that αSyn does not influence neither the release of FpA from fibrinogen, nor the cleavage of FpB from fibrin I protofibrils. In conclusion, the enzymatic component of the process is not affected, while the physical characteristics of the fibres and on the network organization in the presence of αSyn could not be determined.

α-Synuclein Interacts with α-Thrombin

The generation of a complex between αSyn and thrombin was probed and investigated by two independent biophysical techniques: fluorescence and SPR. A first, qualitative esteem of the proteins affinity was performed by comparing the theoretical sum of the proteins fluorescence spectra with a sample in which αSyn and αT were previously pre-incubated. All the samples were excited at 295nm, to monitor fluorescence of the nine Trp in αT, excluding the contribution of the four Tyr in αSyn. From **panel 4A** it clearly emerged that the admixture of the two proteins presents a fluorescence lower than predicted, maintaining the same λ_{max}, thus indicating the generation of the binary [αSyn-αT] complex. The intensity decrease is probably due to a collisional quenching of αSyn on αT, being the ligand unfolded and extremely hydrophilic. In a second stage, αSyn regions involved in the binding were identified by recording the decrease of natural αT fluorescence intensity at 334nm, after addition of incremental concentrations of either αSyn full length or its C-terminal fragments (**Fig. 4B**). The data points, fitted at saturating concentrations with **equation 4**, yielded the K_d and ΔF_{max}% parameters displayed in **table 2**. Notably, αSyn and peptide (103-140) are perfectly comparable in both affinity (K_d) and αT overlapping (ΔF_{max}), while, as predictable, the shorter fragments (103-121) and (122-140) resulted in only less than half of the percent of coverage. In conclusion, αSyn interacts to αT with a K_d=0.96±0.34μM by its C-terminal region (103-140), in accord with the starting work hypothesis.

SPR measurements were carried on by immobilizing His-tag αSyn through Ni^{2+}/NTA chelation, leaving the C-terminal region free to interact with the analytes (**inset in Fig. 4D**). The more popular immobilization through the amine coupling chemistry at the N-terminus of the protein failed: being the (1-60) fragment rich in Lys, the derivatization resulted non-specific and random.

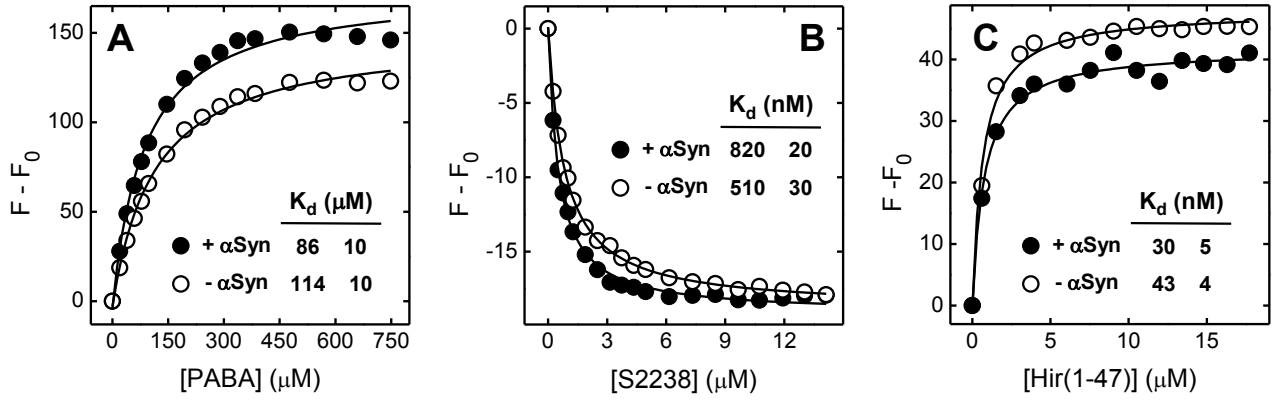

Figure 5. Mapping [αSyn-thrombin] interactions by fluorescence: the active site - To a solution of αT (or rS195A for the chromogenic substrate S2238) in HBS were added, at 37°C, aliquots (2-20μl) of **(A)** PABA; **(B)** S2238; **(C)** Hir(1-47) stock solutions, both in the absence (○) or in the presence (●) of saturating concentrations (20μM) of αSyn. The samples were excited at 295nm, and the emission intensity was recorded at 334nm, except for PABA samples (λ_{ecc}=336nm, λ_{em}=375nm).The data points were fitted according to **eq. 4**, for PABA and S2238, or **eq. 5** for Hir(1-47), giving the K_d and ΔF_{max} values displayed in the panels. For PABA, raw fluorescence data were corrected for the IFE factor, according to **eq. 6**.

Since His-tag αSyn (unless the wild type protein) is hydrolysed by natural αT, inactive mutant rS195A was injected over the sensor chip (**Fig. 4C**). For each sensorgram, the RU_{eq} value at steady state was plotted against rS195A concentration (**Fig. 4D**). Interpolation of data points with the simple one-site binding **equation 7** yielded a K_d=44±6nM, significantly lower than the value calculated with fluorescence titrations. Probably, the immobilization of the N-terminus rigidifies the protein in a conformation more favourable for the interaction, mimicking a physiological scenario in which αSyn is anchored to the platelets membrane.

Mapping [α-Synuclein-Thrombin] Complex Interaction Sites

A deeper understanding of the mechanism of αSyn binding to αT was achieved by studying its influence on the affinity of different probes specific for the serine protease active site, exosite I and exosite II, both by fluorescence and by SRP.

Active Site - Three competitive species, with increasing dimensions and complexity at the enzyme catalytic pocket, were exploited. PABA (p-aminobenzamidine) (**Fig. 5A**) is an aromatic molecule, forming a salt bridge with Asp189 in the bottom of the primary specificity site S1 [**53**]. S2238 (D-Phe-Pip-Arg-pNA) (**Fig. 5B**) is a synthetic peptide mimicking fibrinogen cleavage site.

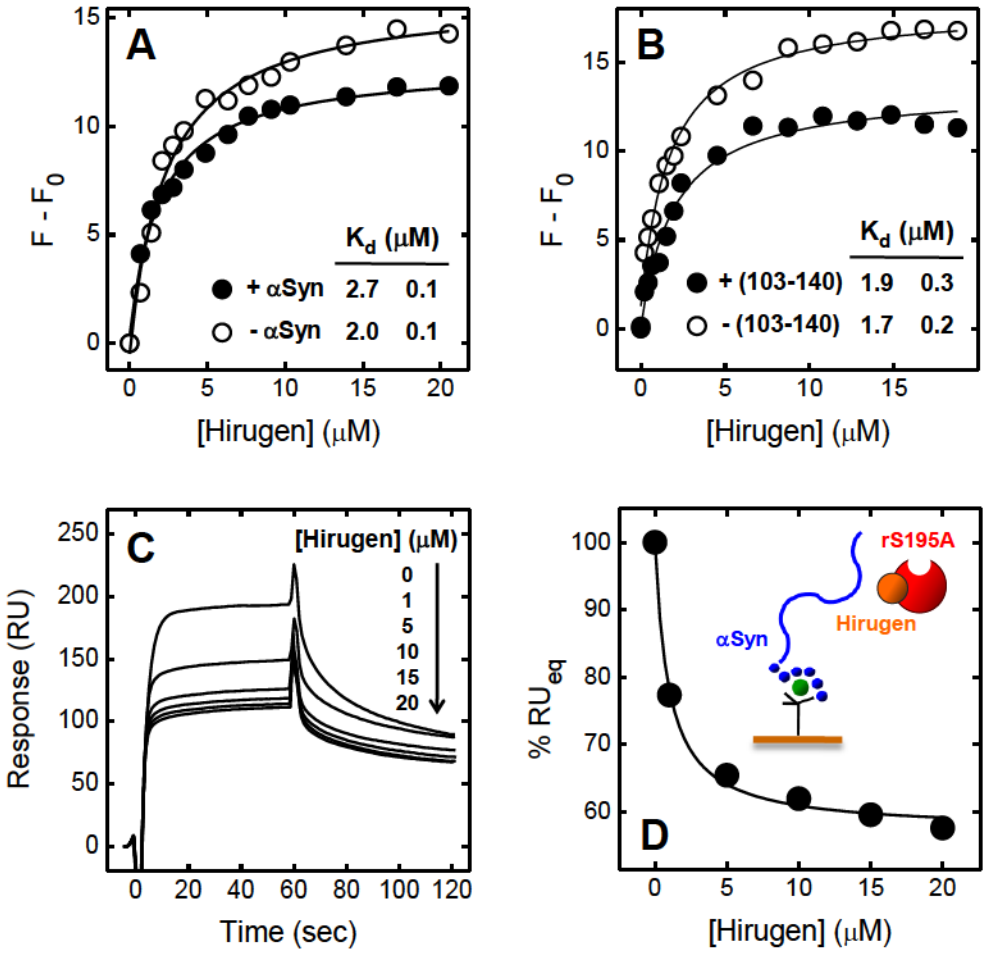

Figure 6. Mapping [αSyn-thrombin] interactions: exosite I. (A,B) Fluorescence titrations - To a solution of αT (70nM) in HBS were added, at 37°C, aliquots (2-20μl) of hirugen stock solution, both in the absence (○) or in the presence (●) of saturating concentrations (20μM) of αSyn or peptide (103-140). The samples were excited at 295nm, and the emission intensity was recorded at 334nm. The data points were fitted according to **eq. 4**, giving K_d values displayed in the panels. **(C,D) Binding of rS195A saturated with hirugen to His-tag αSyn sensor chip - (C)** Sensograms relative to the binding of rS195A (0.1μM) pre-incubated with increasing hirugen (0-20μM) concentrations. **(D)** Plot of $\%RU_{eq}$ versus hirugen concentrations, where $RU_0 = 100\%$ is the response at [hirugen]=0μM. All the measurements were carried out in HBS-EP at 37°C.

This chromogenic substrate orients its bulky residue D-Phe into the aryl binding site S3; Pip (upper Pro homologue) contacts Tyr60a and Trp60d in the S2 site, while Arg harbours Asp189 in the S1 site of the catalytic cleft. Moreover, S2238 also interacts with S1′ site downstream the scissile bond, where the pNA group localizes. Finally, Hir(1-47) is the N-terminal domain of the potent natural inhibitor hirudin HM2 (**Fig. 5C**). This peptide covers αT active site by its β-sheet conformation, and extensively penetrates into the specificity pocket by its first three amino acids. In detail, Val1 points the S2 site; Ser2 shields the S1 site, without entering; Tyr3 fills the apolar cavity of the S3 site [**48**].

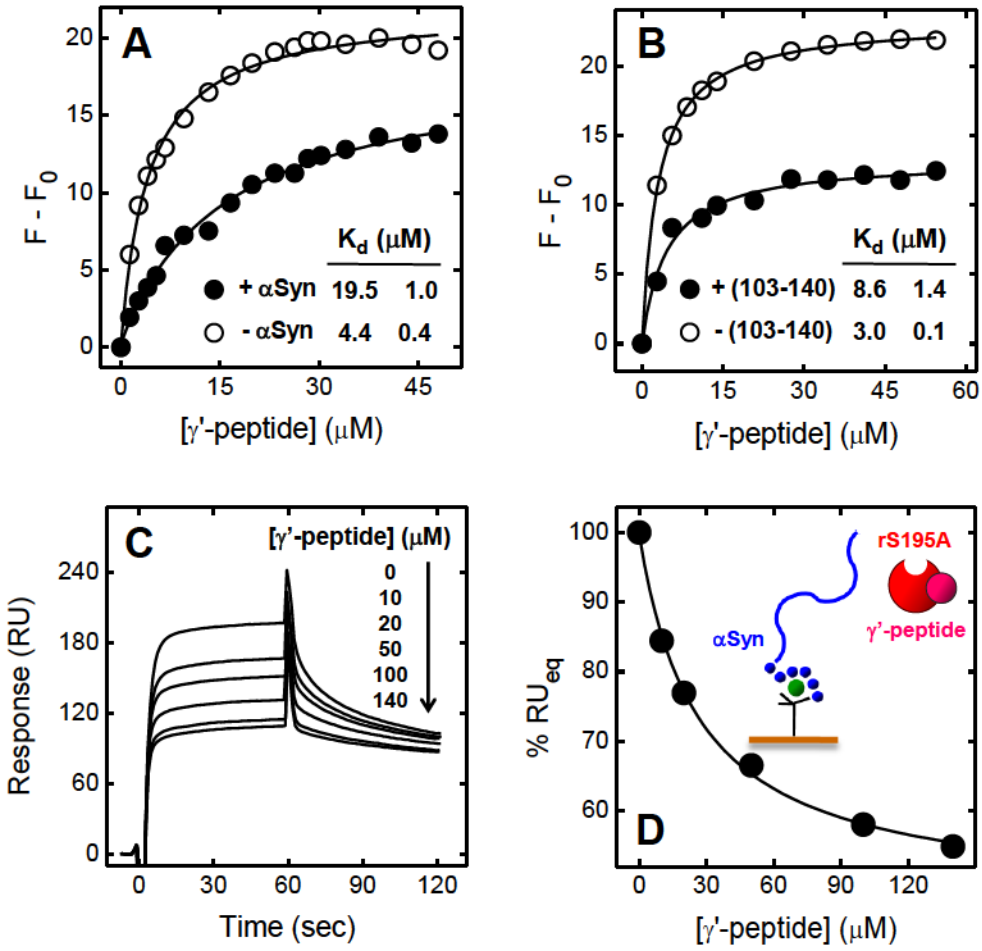

Figure 7. Mapping [αSyn-thrombin] interactions: exosite II. (A,B) Fluorescence titrations - To a solution of αT (70nM) in HBS were added, at 37°C, aliquots (2-20μl) of γ'-peptide stock solution, both in the absence (○) or in the presence (●) of saturating concentrations (20μM) of αSyn or peptide (103-140). The samples were excited at 295nm, and the emission intensity was recorded at 334nm. The data points were fitted according to **eq. 4**, giving K_d values displayed in the panels. **(C,D) Binding of rS195A saturated with γ'-peptide to His-tag αSyn sensor chip - (C)** Sensograms relative to the binding of rS195A (0.1μM) pre-incubated with increasing γ'-peptide (0-140μM) concentrations. **(D)** Plot of $\%RU_{eq}$ versus γ'-peptide concentrations, where RU_0 = 100% is the response at [γ'-peptide]=0μM. All the measurements were carried out in HBS-EP at 37°C.

The eventual interaction of αSyn to the protease catalytic cleft was monitored by recording the variation of natural αT fluorescence, after addition of incremental concentrations of either PABA, S2238 or Hir(1-47). The assays were performed both in the absence and in the presence of saturating concentrations (20μM, determined by the previous fluorescence measurements) of full length αSyn. The data points, fitted with **equation 4** for PABA and S2238, or with **equation 5** for Hir(1-47), demonstrate that αSyn presence do not interfere neither in the K_d nor in the $\Delta F_{max}\%$ parameters typical of the three probes binding. In conclusion, αT active site is not involved in the αSyn complex, but remains free and accessible for natural substrate/binding interfaces.

Exosite I or Exosite II - the involvement of exosite I in [αSyn-αT] complex was evaluated using hirugen, i.e. the C-terminal domain of natural inhibitor hirudin HV1, from *Hirudo medicinalis*. This highly acidic peptide aligns in the fibrinogen binding site, interacting with the serine protease both by ionic and by steric interactions [**56**]. On the other side, γ'-peptide, corresponding to (408-427) sequence of the elongated fibrinogen γ-chain, was tested for exosite II mapping [**57**]. In a first stage, αT fluorescence intensity increase at 334nm, due to incremental additions of hirugen and γ'-peptide stock solutions, was monitored both in the absence and in the presence of saturating concentrations (20μM) of full length αSyn (**Fig. 6A, 7A**) or its C-terminal (103-140) (**Fig. 6B, 7B**). Interpolation of data points with **equation 4**, yielding K_d and ΔF_{max} as fitting parameters, suggests that αSyn slightly interferes with hirugen binding to exosite I. On the other side, γ'-peptide interaction to exosite II is affected both in its affinity (K_d increase of ≈ 2.9-4.4 folds) and in its overlapping (ΔF_{max}% decrease of ≈ 28-43%). The involvement of αT exosites in the complex was qualitatively confirmed with SPR, by injecting samples of rS195A alternatively saturated at exosite I or exosite II. Solutions of rS195A (0.1μM), pre-incubated with increasing concentrations of either hirugen or γ'-peptide, were tested on His-tag αSyn sensor chip (**Fig. 6C, 7C**). The decrease of the SPR signal (%RU_{eq}) was taken as an indication of compromised binding. Saturating concentrations of hirugen (20μM) promoted a 43% decrease of %RU_{eq}, while blockage of exosite II by γ'-peptide (140μM) resulted in a decrease of 46%.

Exosite I and Exosite II - In a late stage, the concurrent influence of exosite I and exosite II was qualitatively determined by SPR, masking both these recognition regions at the same time. The simultaneous blockage of exosite I by hirugen (0-20μM) and of exosite II by γ'-peptide (0-140μM) dramatically abrogates rS195A binding to His-tag immobilized αSyn, resulting in a decrease of 73% of %RU_{eq}, in saturating conditions (**Fig. 8A, 8B**).

Finally, the role of the exosites in the [αSyn-αT] complex was investigated using thrombin precursors or degradation products. In detail, ProT is the inactive αT zymogen, in which exosite II is completely masked by the domain kringle 2, while active site is disorganized and not competent for the catalysis. On the other side, β_TT is a αT degradation product, generated *in vitro* upon prolonged storage (in this case produced by trypsin), which lacks of exosite I (**Fig. 8D**). Solutions (0-1μM) of ProT or β_TT were injected on His-tag αSyn sensor chip. For each sensorgram, the RU_{eq} values at steady-state were plotted against ligands concentrations, and compared to rS195A values. Fitting of data points with **equation 7** yielded values of K_d=45±8nM and RU_{max}=96.9 for β_TT, and K_d=1090±198nM and

RU_{max}=38.5 for ProT, compared to K_d=44±6nM and RU_{max}=310.4 for rS195A (**Fig. 8C**). Once again, the predominant role of exosite II in the binding was confirmed.

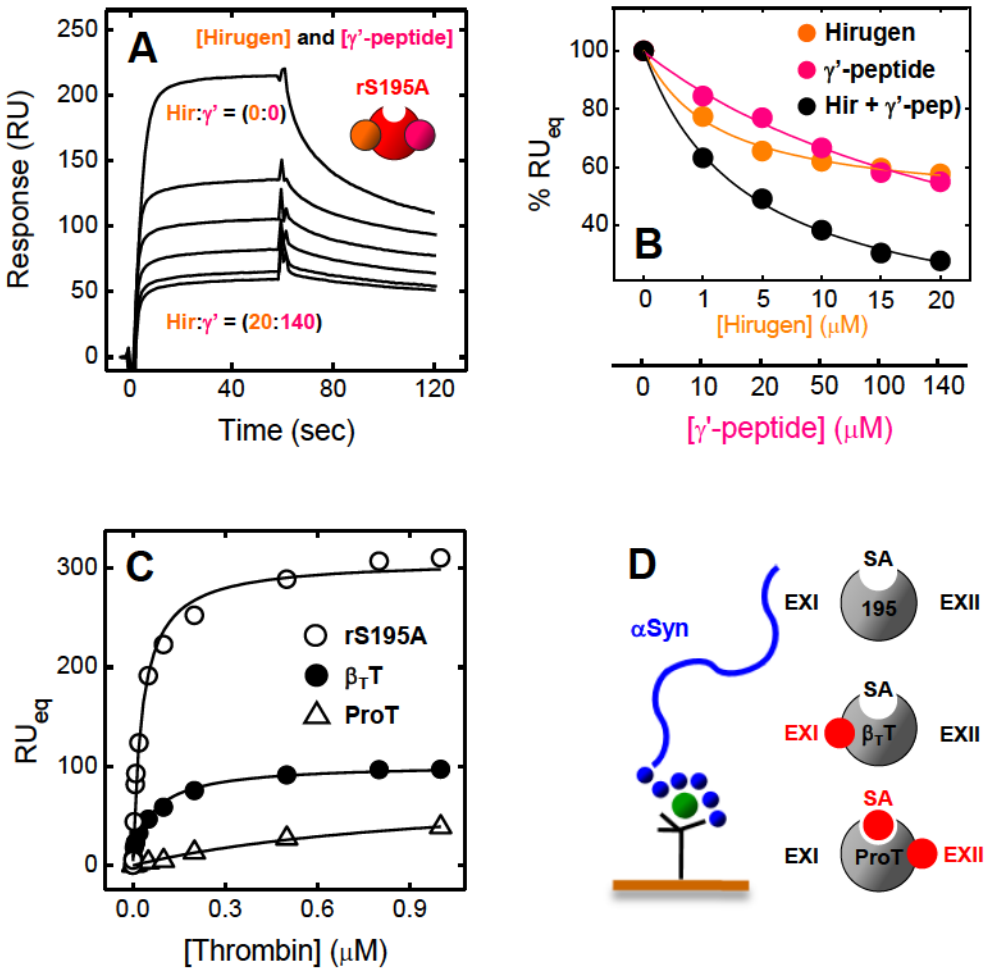

Figure 8. Probing the simultaneous influence of exosite I and exosite II in [αSyn-thrombin] interaction: (A) Sensograms relative to the binding of rS195A (0.1μM) pre-incubated with increasing hirugen (0-20 μM) and γ'-peptide (0-140 μM) concentrations at the same time. **(B)** Plot of $\%RU_{eq}$ versus both the probes concentrations (●), compared to the decrease of $\%RU_{eq}$ induced by hirugen (●) or γ'-peptide (●) one in turn. **(C)** Plot of RU_{eq} and **(D)** schematic representation of rS195A (○), β_TT (●) or ProT (Δ) binding over the His-tag αSyn sensor chip. The regions that are not competent for the binding are highlighted by red circles. The data points were fitted according to **eq. 7**, giving K_d and RU_{max} values as fitting parameters. All the measurements were carried out in HBS-EP at 37°C.

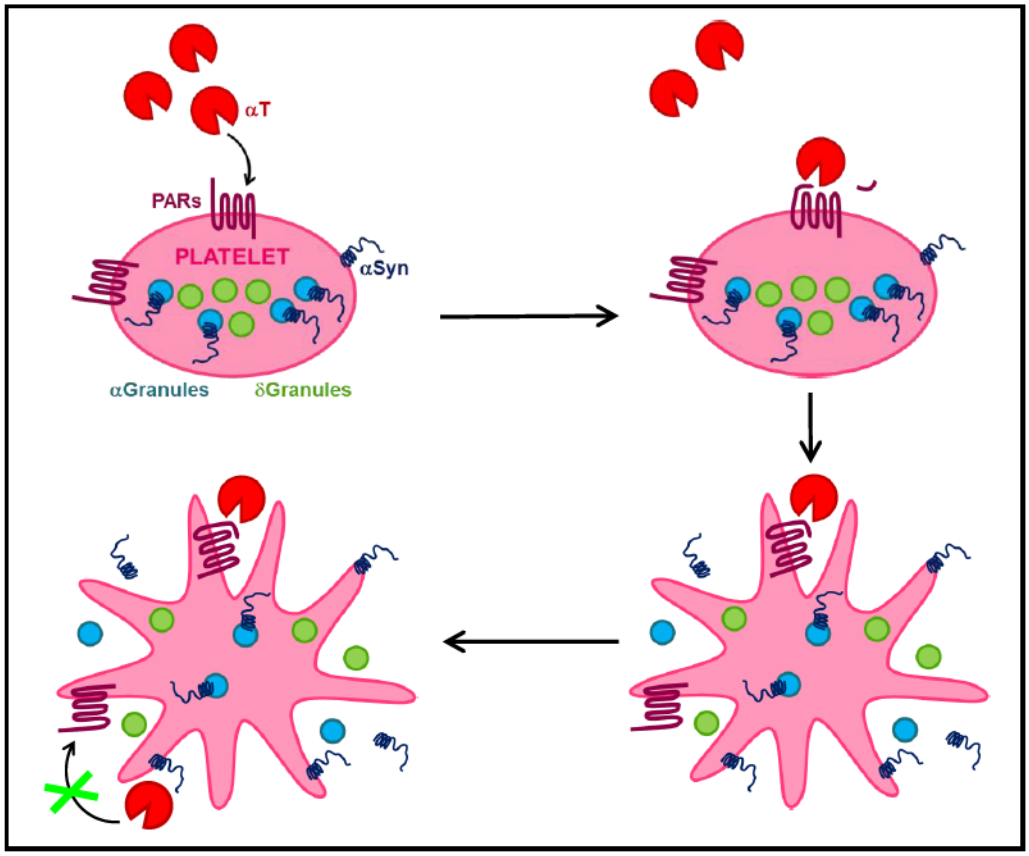

Figure 9. Theoretical model of αT pro-aggregant effects downregulation by αSyn on the platelets surface - In platelets, αSyn can both localize in the cytosol, be anchored to the plasma membrane, or be associated to the pro-aggregant α-granules, highlighted by blue circles. After αT-cleavage of surface PARs, platelets activate and degranulate, concentrating αSyn contained in the granules in the microenvironment surrounding their surface. In this context αSyn can interact both with the cellular membrane by its N-terminus, and with αT by its C-terminal domain, downregulating the serine protease pro-aggregant effects. This theoretical model of interaction may explain, and is in accord to clinical evidences that suggest that patients suffering from neurodegenerative disorders, characterized by high αSyn levels, present a lower degree of ischaemic attacks, due to impaired platelets aggregation.

CONCLUSIONS

αT is the key enzyme of the coagulation cascade, acting at the interface between coagulation, inflammation and cellular proliferation [**32**]. On the other side, human αSyn is a cerebral protein, mainly localized in the presynaptic terminals. Abnormal accumulation of cytoplasmic αSyn aggregates, both in neurons, glia, and LBs, is the major determinant for the insurgence and progression of neurodegenerative disorders such AD, PD, or dementia with LBs [**2**]. While αT physiological functions are well-established and characterized, αSyn role is still matter of debate [**4**]. These two divergent proteins share an unexpected meeting point: they are both localized on the platelets surface. In primary haemostasis, platelets activation is mainly triggered by αT, even at

extremely low concentrations, by binding to the receptor GpIbα and cleavage of surface PARs. Conversely, αSyn is expressed in the platelets, and involved in megakaryocytes differentiation [**26**]. Due to its N-terminal domain properties, this protein can localize in the cytosol, associate to the plasmatic membrane, or be contained in the pro-aggregant α-granules, thus inhibiting their Ca^{2+}-mediated release [**30**]. Past clinical studies demonstrated that the patients suffering from neurodegenerative disorders are less subjected to ischaemic attacks, due to platelets abnormalities and impaired degranulation [**31**].

These intriguing evidences prompted us to investigate the interaction between αT and αSyn. In a first step, the influence of αSyn was tested on αT procoagulant functions. While fibrin generation (through fibrinopeptides release) is not affected, platelets aggregation, measured in whole blood, is dose-dependently decreased by αSyn to an extent of 80%. On the other side, the C-terminal peptide (103-140) had no effect in impairing the aggregation. Therefore, the possible generation of a [αSyn-αT] complex was monitored by two complementary techniques. Fluorescence measurements yielded a dissociation constant K_d=0.96±0.34μM, suggesting the segment (103-140) as the region involved in the interaction. Conversely, SPR assays on His-tag αSyn NTA chip, resulted in a K_d determination of 44±6nM. This discrepancy is probably due to the fact that αSyn, immobilized through its N-terminus to the sensor surface, rigidifies in an optimal conformation for the binding, exposing only the competent C-terminal. This data, altogether with the functional assays, suggest that *in vivo* αSyn, either exogenous or released from the α-granules after pro-aggregant stimuli, may anchor to platelets membrane by its N-terminus, while binding to αT by its C-terminal domain.

The αT regions involved in the binding were assessed both quantitatively and qualitatively by fluorescence titrations and SPR competitions. Predictably, our results indicate that αSyn entails a promiscuous binding with both thrombin exosites, with preference with exosite II, characterized by a higher positive charge density. αT active site is not involved in the binary [αSyn-αT] complex. Notably, by SPR assays, when exosite II and I are masked one in turn, the RU_{eq} signal (diagnostic for the compromised binding) decreases of 43-47%, but when the exosites are both covered, the interaction is dramatically impaired, with a drop of 73%. These results were confirmed by binding of inactive ProT (K_d=1090±198nM) and β_TT (K_d=45±8nM) to the His-tag αSyn chip.

These unanticipated results shed new light on the coagulation/neurodegeneration interface, in a pioneering scenario in which αSyn scavengers αT pro-aggregant action through a negative feedback mechanism. Notably, [αSyn-αT] interaction maintains a physiologic relevance only in the concentrated microenvironment surrounding the platelets surfaces.

REFERENCES

[1] Clayton DF, George JM. The synucleins: a family of proteins involved in synaptic function, plasticity, neurodegeneration and disease. Trends Neurosci 1998 Jun;21(6):249-254.

[2] Uversky VN. Neuropathology, biochemistry, and biophysics of alpha-synuclein aggregation. J Neurochem 2007 Oct;103(1):17-37.

[3] Davidson WS, Jonas A, Clayton DF, George JM. Stabilization of alpha-synuclein secondary structure upon binding to synthetic membranes. J Biol Chem 1998 Apr 17;273(16):9443-9449.

[4] Ueda K, Fukushima H, Masliah E, Xia Y, Iwai A, Yoshimoto M, et al. Molecular cloning of cDNA encoding an unrecognized component of amyloid in Alzheimer disease. Proc Natl Acad Sci U S A 1993 Dec 1;90(23):11282-11286.

[5] Lucking CB, Brice A. Alpha-synuclein and Parkinson's disease. Cell Mol Life Sci 2000 Dec;57(13-14):1894-1908.

[6] Dedmon MM, Lindorff-Larsen K, Christodoulou J, Vendruscolo M, Dobson CM. Mapping long-range interactions in alpha-synuclein using spin-label NMR and ensemble molecular dynamics simulations. J Am Chem Soc 2005 Jan 19;127(2):476-477.

[7] Murray IV, Giasson BI, Quinn SM, Koppaka V, Axelsen PH, Ischiropoulos H, et al. Role of alpha-synuclein carboxy-terminus on fibril formation in vitro. Biochemistry 2003 Jul 22;42(28):8530-8540.

[8] Eliezer D, Kutluay E, Bussell R,Jr, Browne G. Conformational properties of alpha-synuclein in its free and lipid-associated states. J Mol Biol 2001 Apr 6;307(4):1061-1073.

[9] Iwai A, Yoshimoto M, Masliah E, Saitoh T. Non-A beta component of Alzheimer's disease amyloid (NAC) is amyloidogenic. Biochemistry 1995 Aug 15;34(32):10139-10145.

[10] Sandal M, Valle F, Tessari I, Mammi S, Bergantino E, Musiani F, et al. Conformational equilibria in monomeric alpha-synuclein at the single-molecule level. PLoS Biol 2008 Jan;6(1):e6.

[11] Dev KK, Hofele K, Barbieri S, Buchman VL, van der Putten H. Part II: alpha-synuclein and its molecular pathophysiological role in neurodegenerative disease. Neuropharmacology 2003 Jul;45(1):14-44.

[12] Clayton DF, George JM. The synucleins: a family of proteins involved in synaptic function, plasticity, neurodegeneration and disease. Trends Neurosci 1998 Jun;21(6):249-254. (1) Clayton DF, George JM. Synucleins in synaptic plasticity and neurodegenerative disorders. J Neurosci Res 1999 Oct 1;58(1):120-129.

[13] Lavedan C. The synuclein family. Genome Res 1998 Sep;8(9):871-880.

[14] Ulmer TS, Bax A, Cole NB, Nussbaum RL. Structure and dynamics of micelle-bound human alpha-synuclein. J Biol Chem 2005 Mar 11;280(10):9595-9603.

[15] Larsen KE, Schmitz Y, Troyer MD, Mosharov E, Dietrich P, Quazi AZ, et al. Alpha-synuclein overexpression in PC12 and chromaffin cells impairs catecholamine release by interfering with a late step in exocytosis. J Neurosci 2006 Nov 15;26(46):11915-11922.

[16] Chandra S, Gallardo G, Fernandez-Chacon R, Schluter OM, Sudhof TC. Alpha-synuclein cooperates with CSPalpha in preventing neurodegeneration. Cell 2005 Nov 4;123(3):383-396.

[17] Bisaglia M, Mammi S, Bubacco L. Structural insights on physiological functions and pathological effects of alpha-synuclein. FASEB J 2009 Feb;23(2):329-340.

[18] Forno LS. Neuropathology of Parkinson's disease. J Neuropathol Exp Neurol 1996 Mar;55(3):259-272.

[19] Chartier-Harlin MC, Kachergus J, Roumier C, Mouroux V, Douay X, Lincoln S, et al. Alpha-synuclein locus duplication as a cause of familial Parkinson's disease. Lancet 2004 Sep 25-Oct 1;364(9440):1167-1169.

[20] Singleton AB, Farrer M, Johnson J, Singleton A, Hague S, Kachergus J, et al. alpha-Synuclein locus triplication causes Parkinson's disease. Science 2003 Oct 31;302(5646):841.

[21] Polymeropoulos MH, Lavedan C, Leroy E, Ide SE, Dehejia A, Dutra A, et al. Mutation in the alpha-synuclein gene identified in families with Parkinson's disease. Science 1997 Jun 27;276(5321):2045-2047.

[22] Kruger R, Kuhn W, Muller T, Woitalla D, Graeber M, Kosel S, et al. Ala30Pro mutation in the gene encoding alpha-synuclein in Parkinson's disease. Nat Genet 1998 Feb;18(2):106-108.

[23] Zarranz JJ, Alegre J, Gomez-Esteban JC, Lezcano E, Ros R, Ampuero I, et al. The new mutation, E46K, of alpha-synuclein causes Parkinson and Lewy body dementia. Ann Neurol 2004 Feb;55(2):164-173.

[24] McLean PJ, Kawamata H, Ribich S, Hyman BT. Membrane association and protein conformation of alpha-synuclein in intact neurons. Effect of Parkinson's disease-linked mutations. J Biol Chem 2000 Mar 24;275(12):8812-8816.

[25] Conway KA, Lee SJ, Rochet JC, Ding TT, Williamson RE, Lansbury PT,Jr. Acceleration of oligomerization, not fibrillization, is a shared property of both alpha-synuclein mutations linked to early-onset Parkinson's disease: implications for pathogenesis and therapy. Proc Natl Acad Sci U S A 2000 Jan 18;97(2):571-576.

[26] Hashimoto M, Yoshimoto M, Sisk A, Hsu LJ, Sundsmo M, Kittel A, et al. NACP, a synaptic protein involved in Alzheimer's disease, is differentially regulated during megakaryocyte differentiation. Biochem Biophys Res Commun 1997 Aug 28;237(3):611-616.

[27] Shin EC, Cho SE, Lee DK, Hur MW, Paik SR, Park JH, et al. Expression patterns of alpha-synuclein in human hematopoietic cells and in Drosophila at different developmental stages. Mol Cells 2000 Feb 29;10(1):65-70.

[28] Barbour R, Kling K, Anderson JP, Banducci K, Cole T, Diep L, et al. Red blood cells are the major source of alpha-synuclein in blood. Neurodegener Dis 2008;5(2):55-59.

[29] Miller DW, Hague SM, Clarimon J, Baptista M, Gwinn-Hardy K, Cookson MR, et al. Alpha-synuclein in blood and brain from familial Parkinson disease with SNCA locus triplication. Neurology 2004 May 25;62(10):1835-1838.

[30] Park SM, Jung HY, Kim HO, Rhim H, Paik SR, Chung KC, et al. Evidence that alpha-synuclein functions as a negative regulator of Ca(++)-dependent alpha-granule release from human platelets. Blood 2002 Oct 1;100(7):2506-2514.

[31] Sharma P, Nag D, Atam V, Seth PK, Khanna VK. Platelet aggregation in patients with Parkinson's disease. Stroke 1991 Dec;22(12):1607-1608.

[32] Di Cera E, Dang QD, Ayala YM. Molecular mechanisms of thrombin function. Cell Mol Life Sci 1997 Sep;53(9):701-730.

[33] Bode W, Mayr I, Baumann U, Huber R, Stone SR, Hofsteenge J. The refined 1.9 A crystal structure of human alpha-thrombin: interaction with D-Phe-Pro-Arg chloromethylketone and significance of the Tyr-Pro-Pro-Trp insertion segment. EMBO J 1989 Nov;8(11):3467-3475.

[34] Bing DH, Cory M, Fenton JW,2nd. Exo-site affinity labeling of human thrombins. Similar labeling on the A chain and B chain/fragments of clotting alpha- and nonclotting gamma/beta-thrombins. J Biol Chem 1977 Nov 25;252(22):8027-8034.

[35] Di Cera E. Thrombin as procoagulant and anticoagulant. J Thromb Haemost 2007 Jul;5 Suppl 1:196-202.

[36] De Cristofaro R, De Filippis V. Interaction of the 268-282 region of glycoprotein Ibalpha with the heparin-binding site of thrombin inhibits the enzyme activation of factor VIII. Biochem J 2003 Jul 15;373(Pt 2):593-601.

[37] Holmsen H. Signal transducing mechanisms in platelets. Proc Natl Sci Counc Repub China B 1991 Jul;15(3):147-152.

[38] McNicol A, Israels SJ. Platelet dense granules: structure, function and implications for haemostasis. Thromb Res 1999 Jul 1;95(1):1-18.

[39] Harrison P, Cramer EM. Platelet alpha-granules. Blood Rev 1993 Mar;7(1):52-62.

[40] Leung L, Nachman R. Molecular mechanisms of platelet aggregation. Annu Rev Med 1986;37:179-186.

[41] Vermylen J, Verstraete M, Fuster V. Role of platelet activation and fibrin formation in thrombogenesis. J Am Coll Cardiol 1986 Dec;8(6 Suppl B):2B-9B.

[42] De Filippis V, Colombo G, Russo I, Spadari B, Fontana A. Probing the hirudin-thrombin interaction by incorporation of noncoded amino acids and molecular dynamics simulation. Biochemistry 2002 Nov 19;41(46):13556-13569.

[43] Sokolov AV, Acquasaliente L, Kostevich VA, Frasson R, Zakharova ET, Pontarollo G, et al. Thrombin inhibits the anti-myeloperoxidase and ferroxidase functions of ceruloplasmin: relevance in rheumatoid arthritis. Free Radic Biol Med 2015 Sep;86:279-294.

[44] Li W, Johnson DJ, Adams TE, Pozzi N, De Filippis V, Huntington JA. Thrombin inhibition by serpins disrupts exosite II. J Biol Chem 2010 Dec 3;285(49):38621-38629.

[45] Pozzi N, Acquasaliente L, Frasson R, Cristiani A, Moro S, Banzato A, et al. beta2 -Glycoprotein I binds to thrombin and selectively inhibits the enzyme procoagulant functions. J Thromb Haemost 2013 Jun;11(6):1093-1102.

[46] Hofsteenge J, Braun PJ, Stone SR. Enzymatic properties of proteolytic derivatives of human alpha-thrombin. Biochemistry 1988 Mar 22;27(6):2144-2151.

[47] Munishkina LA, Phelan C, Uversky VN, Fink AL. Conformational behavior and aggregation of alpha-synuclein in organic solvents: modeling the effects of membranes. Biochemistry 2003 Mar 11;42(9):2720-2730.

[48] De Filippis V, Vindigni A, Altichieri L, Fontana A. Core domain of hirudin from the leech Hirudinaria manillensis: chemical synthesis, purification, and characterization of a Trp3 analog of fragment 1-47. Biochemistry 1995 Jul 25;34(29):9552-9564.

[49] Toth O, Calatzis A, Penz S, Losonczy H, Siess W. Multiple electrode aggregometry: a new device to measure platelet aggregation in whole blood. Thromb Haemost 2006 Dec;96(6):781-788.

[50] Ng AS, Lewis SD, Shafer JA. Quantifying thrombin-catalyzed release of fibrinopeptides from fibrinogen using high-performance liquid chromatography. Methods Enzymol 1993;222:341-358.

[51] Lakowicz, J.R. (1999) Principles of Fluorescence Spectroscopy 2nd ed., Kluwer Academic/Plenum, New York.

[52] Copeland, R. A. (2000) Kinetics of Single-Substrate Enzyme Reactions. In Enzymes, pp. 109-145, Wiley-VHC Inc., New York

[53] Evans SA, Olson ST, Shore JD. p-Aminobenzamidine as a fluorescent probe for the active site of serine proteases. J Biol Chem 1982 Mar 25;257(6):3014-3017.

[54] Mahler HC, Friess W, Grauschopf U, Kiese S. Protein aggregation: pathways, induction factors and analysis. J Pharm Sci 2009 Sep;98(9):2909-2934.

[55] Weisel JW, Nagaswami C. Computer modeling of fibrin polymerization kinetics correlated with electron microscope and turbidity observations: clot structure and assembly are kinetically controlled. Biophys J 1992 Jul;63(1):111-128.

[56] Naski MC, Fenton JW,2nd, Maraganore JM, Olson ST, Shafer JA. The COOH-terminal domain of hirudin. An exosite-directed competitive inhibitor of the action of alpha-thrombin on fibrinogen. J Biol Chem 1990 Aug 15;265(23):13484-13489.

[57] Lancellotti S, Rutella S, De Filippis V, Pozzi N, Rocca B, De Cristofaro R. Fibrinogen-elongated gamma chain inhibits thrombin-induced platelet response, hindering the interaction with different receptors. J Biol Chem 2008 Oct 31;283(44):30193-30204.

CHAPTER 3.1

Crosslinks between Coagulation and Inflammation

The Network Connecting Coagulation to Inflammation

Coagulation and inflammation, traditionally regarded as two independent physio-pathologic systems, are actually tightly connected, and enhance each other in a vicious circle [**1**]. α-thrombin (αT) itself, the key enzyme of the coagulation cascade, plays a pivotal role at the interface between inflammation and cellular proliferation.

The most striking example of this interplay is represented by the interaction between activated platelets and leukocytes, through a ligand-receptor recognition mechanism. After vascular damage in the vessel walls, platelets adhere to the sub-endothelial collagen, and are activated by even minimal αT concentrations. Beyond amplifying the coagulation cascade through the release of vasoactive substances from the granules, activated platelets express P-selectin, a leukocyte chemoattractant molecule. On the other hand, monocytes stimulated by endotoxins or cytokines, like tumour necrosis factor-α (TNF-α) and cluster of differentiation 40 (CD40), synthetize tissue factor (TF) and release active microparticles [**2**;**3**].

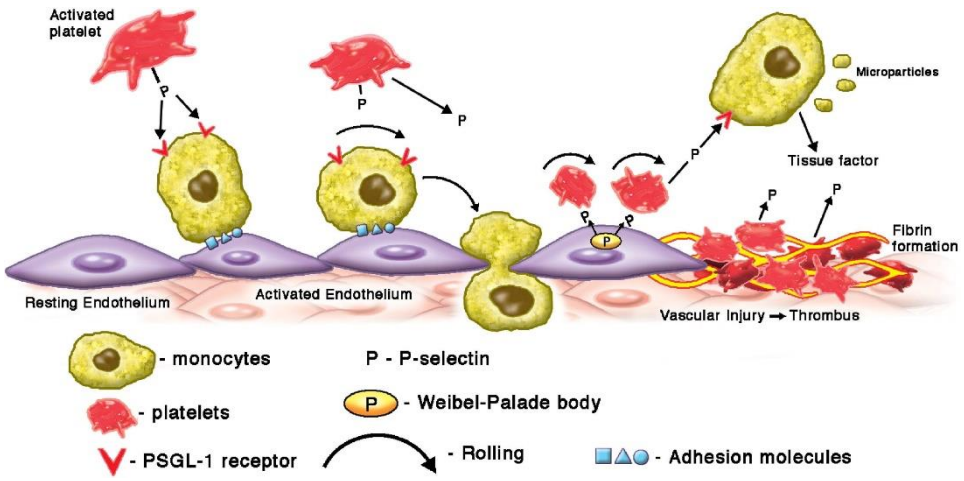

Figure 1 [from Alfonso & Angiolillo, 2013]. Interactions between activated platelets at the site of injury and microparticles released from monocytes. After vessel damage, platelets adhere to the sub-endothelial collagen and activate, thus expressing P-selectin (a chemoattractant agent) on their surface. In inflammatory contexts, monocytes release highly negative-charged microparticles, which express TF on their surface. Activated platelets recruit the monocyte microparticles, which in turn initiate clotting cascade through their exposed TF.

Circulating microparticles, beyond TF, bear P-selectin glycoprotein ligand-1 (PSGL-1) on their highly negative charged surface [**4**]. Highly reactive microparticles concentrate at the wound site by the (P-selectin)-(PSGL-1) interaction, and initiate clotting by TF and negatively charged phospholipids (**Fig. 1**). This mechanism has been confirmed both *in vivo* [**5**] and on the wound site of artificial surfaces [**6**].

The shared nature of the inflammation and coagulation systems is reflected by common structural protein motifs. For instance, the endothelial protein C receptor (EPCR) features structural similarities, both in its primary sequence [**7**] and in its three-dimensional structure [**8**] with the major histocompatibility class 1/CD1 family. Moreover, TF shares similarities with the cytokine receptors [**9**]. The motif resemblances among these proteins suggest their parallel evolution from common ancestors. This hypothesis is supported by the observation that highly conserved animals, like *Limulus polyphemus*, unvaried for 400 million years, are characterized by an innate immune system that recognizes exogenous bacterial endotoxins, and, after cascade reactions, traps them in a protective gel matrix, repairing the generated wound at the same time.

The intimate connection between coagulation and inflammation is confirmed by the evidence that the natural anticoagulant pathways dampen not only the procoagulant mechanisms, but also dowregulate inflammatory manifestations. When the coagulation/inflammation interface overwhelms these natural defence systems, catastrophic events, like systemic sepsis, occur.

Effects of Inflammation on Coagulation

Inflammatory states initiate clotting, leading to pathological manifestations like thrombosis or eventually disseminated intravascular coagulation (DIC), through multiple pathways.

Inflammatory mediators and cytokines may act directly on the agents involved in primary and secondary haemostasis. In detail, histamine, TNF-α, and interleukins (IL-6, IL-8) endorse the release of von Willebrand Factor ultra large multimers (UL-vWF), promoting platelets thrombi generation at high shear rates [**10**]. During inflammation, platelets count increases, and, under IL-6 effect, these cells become more thrombogenic, i.e. activate at lower αT concentrations [**11**]. Even the acute-phase reactant fibrinogen is upregulated in inflammatory situations, while the fibrinolytic system is impaired [**1**]. Moreover, several cytokines induce the expression of both protease activated receptors (PARs) [**12**], and TF [**13**] on the endothelium, and facilitate monocyte-endothelial cells interactions through increased concentrations of the C reactive protein in the blood [**14**]. The complement system activation, on the other hand, provides key available procoagulant surfaces, contributing to the hyper-coaguable state [**15**]. Finally, during inflammatory manifestations, natural anticoagulant pathways are largely downregulated. In acute inflammation (sepsis), antithrombin (ATIII) is consumed and/or

inactivated, retaining less than 50% of its physiological activity [**16**]. In association, the activation and release of neutrophil products lowers the concentration of heparin-like molecules [**17**]. Even protein C (PC) pathway is highly affected in this context: both thrombomodulin (TM) and the endothelial PC receptor (EPCR) are downregulated by cytokines. In addition, TM is cleaved by neutrophil elastase [**18**]. Due to these dramatically effects, in septic patients the complete disappearance of TM on the endothelial cell surface has been described [**19**]. Furthermore, it is generally though that the reduction of PC concentration is correlated to a negative prognosis in septic patients [**20**].

Effects of Coagulation on Inflammation

Upregulation of inflammatory mediators from the coagulation system is endorsed by the TF-FVIIa complex, activated platelets and fibrin(ogen). The TF-FVIIa procoagulant complex activates PARs on both platelets and endothelial cells [**21**], with the subsequent expression of several adhesion molecules. In addition, it induces the expression of the major histocompatibility complex class II (MHCII) on the surface of monocytes and macrophages, along with the production of reactive oxygen species (ROS) [**22**;**23**]. Activated platelets contain and release high concentrations of the pro-inflammatory CD40, which in turn triggers TF [**24**;**25**] and IL-6, IL-8 synthesis [**26**]. Finally, both fibrinogen and fibrin stimulate the production of pro-inflammatory cytokines, like TNF-α, IL-β and macrophage chemiotactic protein-1 [**27**]. Fibrin binds tightly to neutrophils, thus impairing leukocytes migration [**28**].

Inhibition of Inflammation by Natural Anticoagulant Pathways

Three major anticoagulant mechanisms, beyond the fibrinolytic system, regulate haemostatic equilibrium. Tissue factor pathway inhibitor (TFPI) neutralizes FVIIa bound to TF by a unique mechanism, *via* two Kunitz domains (one of which involved in the binding to FXa) [**29**]. ATIII, whose effects are incremented by heparin, inhibits FIIa, FVIIa, FIXa and FXa [**30**]. On the other hand, when PC zymogen is converted to aPC (active protein C) by TM-bound αT on the endothelium surface, it inactivates FVa and FVIIIa, with a subsequent downregulation of the entire coagulation cascade. aPC action is increased when this protein (from starting PC) is bound to EPCR. While implications of TFPI during inflammatory manifestations are still matter of debate, ATIII-heparin and PC pathways efficiently dampen these pathologic disorders through a plethora of effects. ATIII downregulates the expression *in vitro* of CD11b/CD18 on leukocytes [**31**] and of TF and IL-6 in monocytes and endothelial cells. Moreover, it inhibits cellular NF-κB signalling [**32**] and chemokine-induced

neutrophil migration [**33**;**34**]. *In vivo*, the administration of ATIII to septic experimental animals has been proven to decrease leukocyte recruitment [**35**].

Regarding PC anticoagulant pathway, all the involved molecular actors exert anti-inflammatory effects. When it is bound to αT, TM prevents the serine protease from activating cellular PARs, simply through physical occupancy of exosite I [**36**;**37**]. TM-αT complex triggers the thrombin-activatable fibrinolysis inhibitor (TAFI) which, beyond making the fibrin clot more resistant to plasmin attack, it is a strong inhibitor of complement anaphylotoxin C5a [**38**;**39**]. In addition, TM exhibits direct anti-inflammatory activity through its N-terminal lectin-like domain. Is has been observed that *in vivo*, transgenic mice carrying a deleted mutant TM gene recruit leukocytes much more aggressively than the wild type animals. This effect can be reverted by the administration of the isolated lectin-like domain [**40**]. Both PC and aPC bound to EPCR reduce leukocyte chemotaxis and endothelial cells apoptosis [**41**]. aPC impairs neutrophils adhesion to endothelium and TF expression on leukocyte cell lines in a EPCR-dependent fashion [**42**]. Isolated aPC, on the other side, inhibits NF-κB signalling in monocytes [**43**].

Since increased inflammation can upregulate coagulation, which in turn enhances inflammation, the failure of the anticoagulant mechanisms in controlling the clotting progression would naturally increase the inflammatory processes. This suggest that, in acute inflammation disorders, like sepsis, administration of anti-coagulants might provide an effective treatment. Actually, ATIII [**44**], aPC [**45**] and even TFPI [**46**] have been demonstrated to prevent death from lethal *E. coli* levels in a baboon model of sepsis.

Activation of Coagulation during Sepsis

Sepsis is a life-threatening condition caused by a detrimental response to an invading pathogen. The systematically activated immune response to an infection results in an exaggerated inflammation, leading to damage to the host's own tissues and organs failure. These pathological complications and injuries are associated with high morbidity and mortality. During the early stages of infection, the coagulation system is stimulated as well. The local activation of coagulation contributes to host's defence, in the attempt to trap and kill the pathogen. Since bleeding sites are potential accesses to microorganisms, the coagulation system may act as one of the first humoral regulatory effectors. Conversely, uncontrolled procoagulant response results in disseminated intravascular coagulation (DIC), a syndrome in which the generation of scattered thrombi is coupled to an imbalanced haemorrhagic state in the rest of the body [**47**;**48**;**49**;**50**].

In this scenario, invading pathogens may be harmful not only for the triggering of the inflammation, but also in case of direct activation of the coagulation system.

Snake Venom Proteases

The most strikingly example in nature of exogenous agents affecting the host blood haemostasis is undoubtedly provided by snake venom toxins. These molecules can trigger platelets aggregation [**51**] or directly interfere in the coagulation cascade [**52**;**53**;**54**;**55**]. The majority of these toxins are proteases that specifically activate FX, prothrombin (ProT) or fibrinogen. In addition, oscutarin from *Oxyuranus scutellatus* has been described to selectively activate FVII. On the other hand, thrombocytin from *Bothrops atrox*, and Russell's viper venom from *Daboia russelli* activate FV [**56**].

In particular, several ProT activators are found in massive amounts in snake venoms: these toxins can be classified into four groups based on their structure and cofactors requirement [**57**] (**Table 1** and **Fig.2**).

Table 1. Classification of prothrombin activators from snake venom proteases.

Class	Cofactor requirement	Type of protease	Product	Examples
Group A	None	Metalloproteinase	Meizothrombin	Ecarin
Group B	Ca^{2+}	Metalloproteinase	Meizothrombin	Carinactivase Multactivase
Group C	Ca^{2+}, phospholipids	Serine protease	Thrombin	Oscutarin, Pseutarin C
Group D	Ca^{2+}, phospholipids, FVa	Serine protease	Thrombin	Notecarin Trocarin D Hopsarin D

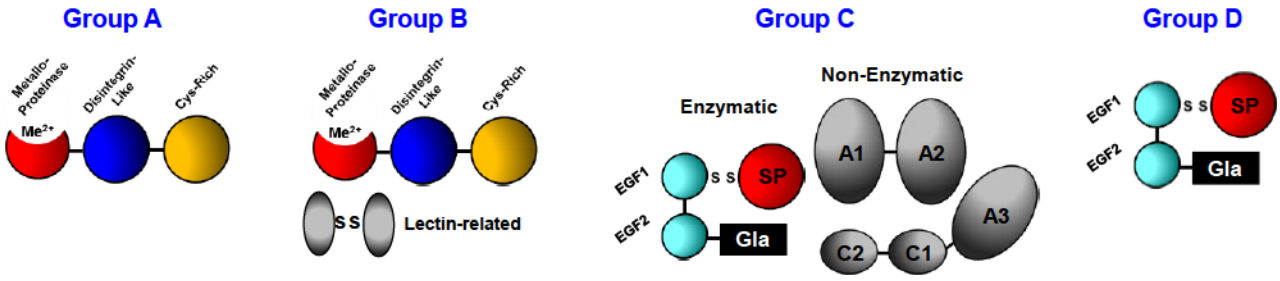

Figure 2 [adapted from Kini, 2005]. Schematic structures of snake venom prothrombin activators. Group A activators are composed of a metalloproteinase, a disintegrin-like and a Cys-rich domain. **Group B** toxins are structurally analogue to group A, but in addition they are characterized by the presence of a lectin-related domain. **Group C** activators are the most complex, featuring a FXa-like enzymatic component (Gla-EGF1-EGF2-SP domains) and a FVa-like non-enzymatic one (A1-A2-A3-C1-C2 domains). **Group D** toxins, on the other hand, are comprised only of the enzymatic component, structurally and functionally similar to mammalian FXa.

Group A and ***B*** activators, from viperids venom, are composed by a metalloproteinase, a disintegrin-like and a Cys-rich domain. ProT activation is accomplished through the metalloproteinase domain, with the cleavage at Arg320-Ile321, resulting in meizothrombin generation. In turn, active meizothrombin converts to mature αT by auto proteolysis. While group A toxins does not require any cofactors for their catalytic activity [**58**;**59**], group B proteases, which are characterized by an additional C-type lectin-like disulphide linked dimer, require Ca^{2+} up to mM concentrations for their functioning. The most famous and well-characterized toxin from group A is ecarin, from *Echis carinatus* venom [**60**]. Ecarin metalloproteinase domain contains the consensus sequence **HE**XX**H**XX**G**XX**H** (where X is any amino acid), corresponding to the zinc-chelating active site. In the disintegrin-like domain, the Arg-Gly-Asp sequence, pivotal for cell-cell adhesion, is replaced by Arg-Asp-Asp. For this reason, ecarin has no effect on platelets aggregation. On the other side, ProT proteolysis is extremely efficient and fast. Regarding group B activators, two proteases have been characterized: carinactivase-1 from *Echis carinatus* [**61**] and multiactivase from *Echis multiquamatus* venom [**62**].

Conversely, ***group C*** and ***D*** toxins are extracted exclusively from the venom of some Australian elapids [**58**;**59**]. These activators are serine proteases, largely similar to mammalian coagulation factors. For these classes ProT activation is achieved through the same two physiologic cleavages performed by FXa, at Arg271 and Arg320, with the release of mature αT. In detail, group C activators are composed by a non- and a enzymatic subunit, and need Ca^{2+} and phospholipids as cofactors. The enzymatic component is functionally and structurally similar to mammalian FXa, featuring a light chain, composed of a γ-carboxyglutamic acid (Gla) domain, two epidermal growth factor-like (EGF1, EGF2) domains, and a heavy chain serine protease (SP) domain, linked by a disulphide bridge. The non-enzymatic component shares 50% similarity with mammalian coagulation FV [**63**], presenting the same A1-A2-B-A3-C1-C2 architecture domain [**64**]. The activation cleavage sites Arg709 and Arg1545 (bovine FV numbering) are conserved in this component: this subunit, in the venom, is found in its active form (A1-A2-A3-C1-C2) as a complex with the FXa-like component. *In vivo*, anticoagulant aPC neutralizes FVa by hydrolysis at Arg306, Arg506 and Arg679 [**65**]. Notably, in the snake venom protease, two of these cleavage sites (Arg306 and Arg679) are not conserved. This unique feature, together with the observation that this component is protected in the complex with the FXa-like subunit, prevents the domain inactivation by the host's aPC. Group C activators have been extracted from the venom of *Oxyuranus scutellatus* [**66**;**67**] and of *Pseudonaja texilis* [**68**] and, remarkably, they represent the 20-30% of the venom proteins. On the other hand, group D toxins are constituted only by the enzymatic FXa-like component, but unlike the mammalian FXa, these proteases are glycoproteins [**69**]. In the presence of Ca^{2+}, negative phospholipids and FVa

as cofactors, the catalysis rate of the serine protease domain is enhanced of about four orders of magnitude [**70**]. These activators constitute the 3-6% of the total protein content in the venom [**64**]; trocarin D, purified from *Trophidechis carinatus* venom, is the most well-studied group D activator.

In vivo, after the snakebite, all these activators induce thrombotic events in the victim/prey, with cyanosis and DIC manifestations [**70**]. This hyper-coaguable state in the site of injury, is connected to massive depletion of coagulation factors levels in the plasma, with an imbalanced haemorrhagic state in the other districts of the body. Due to their massive levels, these toxins play a vital role in the toxicity of the venom. Another huge advantage as toxins is represented by the observation that they are always detected in the active form in the venom, and that they are not easily inactivated. In particular, while group A and B are not inactivated by plasma serpins [**61**], regarding group C and D not clearly laboratory data have been collected yet.

Microbial Proteases Triggering non-Canonical Prothrombin Activation

During microbial infections, surface or secreted bacterial proteases may activate blood coagulation zymogens, in particular ProT, either in a proteolytic or non-proteolytic manner.

The first class comprises metalloproteases from *Bacillus megaterium*, and cysteine proteases from *Porphyromonas gingivalis*, which activate the zymogen at the physiologic cleavage sites. Bacillolysin from *B. megaterium* is a neutral metalloproteinase that hydrolyses plasminogen in angiostatin-like fragments, and activates prourokinase, ProT, FX and PC to their active forms, with simultaneous clot formation and dissolution [**71**]. *P. gingivalis* is a periodontal-pathogenic bacterium, which has also been detected immobilized to carotid atherosclerotic plaques. This microorganism contains two gingipain R Arg-specific proteases of 95 and 50kDa, which release αT from ProT, with subsequent fibrin clotting [**72**].

Conversely, staphylocoagulase secreted from *Staphylococcus aureus* is regarded as the prototype of a new kind of ProT non-proteolytical activation, by inducing a conformational change in the ligand. Staphylocoagulase N-terminal (1-325) fragment (SC) is a boomerang-shaped protein, composed of two three-helix bundle domains. Domain 1 (1-146) binds to the 148-loop and south rim of the catalytic site of prethrombin-2 (Pre2) and αT. On the other side, Domain 2 (147-325) binds to (pro)exosite I in ProT, Pre2 and αT. The crystal structure of the SC(1-325) bound to the Pre2 protease domain of human ProT, accomplished by Friedrick and co-workers [**73**] provided the first structural proof of Bode's "molecular sexuality" theory for zymogen activation [**74**]. In detail, segment Ile1-Val2 of SC enters the Ile16 pocket in ProT (chymotrypsinogen numbering), resulting in the formation of a salt bridge with the carboxyl of Asp194, necessary and sufficient for the moulding of the catalytic site. The overall affinity (K_d) of SC(1-325)·(pro)thrombin binary complex ranges from 12 to 72pM.

In canonical ProT activation, FXa-cleavage at Arg15 frees a new Ile16-Val17 N-terminal, which inserts into the preformed "Ile16 pocket" of the inactive zymogen and engages itself the salt bridge with Asp194. In conclusion, SC Ile1-Val2 segment substitutes the fresh-generated Ile16-Val17 N-terminal during ProT activation.

This complex is able to recognize and cleave fibrinogen, thus bypassing the canonical coagulation cascade. Since exosite I, putative for fibrinogen binding, is immature in ProT, a novel molecular mechanism for the fibrinogen interaction to SC(1-325)·(pro)thrombin complex has been supposed. In particular, the C-terminal staphylocoagulase domain, containing multiple 27-residue repeat sequences interacting with fibrinogen [**75**], may help for the correct substrate orientation. The subsequent fibrin generation may contribute to the pathology of *Staphylococcus aureus* in disorders such as pulmonary infections and acute bacterial endocarditis. The specificity of this binary complex is highly restricted, since this novel enzyme does not cleave other αT substrates, like FV, FVIII or PARs [**76**].

Microbial Proteases Role during Sepsis: a Word to Unravel

In the early stages of infections, extracellular microbial proteases, either on the membrane or secreted, may play a pivotal role on the evolution of sepsis. Unfortunately, these enzymes are mostly uncharacterized, and little is known about several detrimental mechanisms. An abundant and well-characterized class of microbial extracellular proteases is subtilases, the superfamily of serine-like proteases, featured by a well-conserved catalytic triad and a broad specificity of cleavage. Several microorganisms express and secrete subtilisin-like proteases that may contribute to their pathogenicity.

Neisseria meningitidis expresses a 112kDa auto-transporter serine protease A (AspA), which shares N-terminal homology with the subtilase superfamily. AspA is transported to the outer membrane and remains surface exposed, while 68-70kDa fragments are secreted and found in the meningococcus-cultured supernatant. In addition, *Neisseria gonorrhoea* contains an AspA homologue pseudogene [**77**].

Plasmodium falciparum is the malaria parasite, which invades vertebrate hosts and replicates asexually within circulating erythrocytes. DIC, eventually coupled to peripheral gangrene, has been reported in less of 5% severe malaria patients, particularly in cerebral cases [**78**]. During erythrocyte invasion, proteolytic enzymes play an essential but poorly understood role. Blackman and co-workers identified a gene, named PfSUB-1, encoding a member of the subtilases family, expressed in the asexual blood stages of *Plasmodium falciparum*. In the invasive stages, the mature subtilisin-like

protease (p47) is stocked in dense secretory granules. p47 is then secreted in a truncated, soluble form, probably playing a role during erythrocyte invasion [**79**].

Pseudomonas aeruginosa is a ubiquitous, opportunistic bacterium, entailing severe infections and sepsis in the man. This microorganisms express several proteolytic enzymes, which are determinant as virulence factors. Among these, only two belong to the subtilisin-like family. In detail. Subtilase SprP is an auto-catalytically activated protease, which is probably involved in several harmful processes, like heat shock responses [**80**;**81**].

Shiga toxin *Escherichia coli* express a subtilase cytotoxin (SubAB), comprised of subunits A and B. A-subunit is a subtilisin-like serine protease that hydrolyses an endoplasmic reticulum chaperone, while B-subunits binds to a surface receptor. Intraperitoneal injection of purified SubAB in mice induces leukocytes redistribution and apoptosis, organs failure, fatal haemorrhage and thrombocytopenia through IL-6 induced expression, in a time-dependent manner [**82**;**83**].

Among streptococci, several cases of secreted harmful serine proteases have been identified. *Streptococcus suis* is an emerging human pathogen, whose infection is due to the exposure to contaminated pigs or pig meat. Due to change in feed habits, in the past few years the number of reported cases is increasing exponentially, particularly in southern Asia. Clinical manifestations of microbial infections are mainly arthritis, endocarditis, meningitis and sepsis. This streptococcus expresses a surface-associated SspA subtilisin-like protease playing a role as a virulence factor. In detail, Bonifait and Grenier reported that SspA induces cytokine (i.e. IL-1β, IL-6, TNF-α) secretion from macrophages in a dose-dependent manner. Since this effect in animal models has been described even for the heat-inactivated enzyme, these clinical manifestations may be accomplished through a non-proteolytical mechanism. Moreover, SspA, sharing remarked homologies with subtilases produced by other pathogenic streptococci, hydrolyses fibrinogen Aα chain, impairing αT-induced fibrin network generation [**84**;**85**]. On the other side, Group B streptococcus expresses a cell-surface associated subtilisin-like protease (cspA) which cleaves fibrinogen Aα chain, resulting in a product characterized by strongly adhesive properties, which may be somehow similar to fibrin network [**86**]. *Streptococcus pneumoniae* synthesizes five subtilisin-like serine proteases, of which two are secreted or surface exposed. Serine protease HtrA (high-temperature requirement A) is accountable for the microbial virulence, while PtrA (cell wall-associated serine protease A) entails lung damages in high dose pneumonia [**87**]. Finally, *Streptococcus pyogenes* [**88**] expresses and secretes subtilisin-like serine proteases.

REFERENCES

[1] Esmon CT. The interactions between inflammation and coagulation. Br J Haematol 2005 Nov;131(4):417-430.

[2] Lindmark E, Tenno T, Siegbahn A. Role of platelet P-selectin and CD40 ligand in the induction of monocytic tissue factor expression. Arterioscler Thromb Vasc Biol 2000 Oct;20(10):2322-2328.

[3] Parry GC, Mackman N. NF-kappaB Mediated Transcription in Human Monocytic Cells and Endothelial Cells. Trends Cardiovasc Med 1998 Apr;8(3):138-142.

[4] Day SM, Reeve JL, Pedersen B, Farris DM, Myers DD, Im M, et al. Macrovascular thrombosis is driven by tissue factor derived primarily from the blood vessel wall. Blood 2005 Jan 1;105(1):192-198.

[5] Falati S, Liu Q, Gross P, Merrill-Skoloff G, Chou J, Vandendries E, et al. Accumulation of tissue factor into developing thrombi in vivo is dependent upon microparticle P-selectin glycoprotein ligand 1 and platelet P-selectin. J Exp Med 2003 Jun 2;197(11):1585-1598.

[6] Giesen PL, Rauch U, Bohrmann B, Kling D, Roque M, Fallon JT, et al. Blood-borne tissue factor: another view of thrombosis. Proc Natl Acad Sci U S A 1999 Mar 2;96(5):2311-2315.

[7] Fukudome K, Esmon CT. Identification, cloning, and regulation of a novel endothelial cell protein C/activated protein C receptor. J Biol Chem 1994 Oct 21;269(42):26486-26491.

[8] Oganesyan V, Oganesyan N, Terzyan S, Qu D, Dauter Z, Esmon NL, et al. The crystal structure of the endothelial protein C receptor and a bound phospholipid. J Biol Chem 2002 Jul 12;277(28):24851-24854.

[9] Edgington TS, Ruf W, Rehemtulla A, Mackman N. The molecular biology of initiation of coagulation by tissue factor. Curr Stud Hematol Blood Transfus 1991;(58)(58):15-21.

[10] Bernardo A, Ball C, Nolasco L, Moake JF, Dong JF. Effects of inflammatory cytokines on the release and cleavage of the endothelial cell-derived ultralarge von Willebrand factor multimers under flow. Blood 2004 Jul 1;104(1):100-106.

[11] Burstein SA. Cytokines, platelet production and hemostasis. Platelets 1997;8(2-3):93-104.

[12] Nystedt S, Ramakrishnan V, Sundelin J. The proteinase-activated receptor 2 is induced by inflammatory mediators in human endothelial cells. Comparison with the thrombin receptor. J Biol Chem 1996 Jun 21;271(25):14910-14915.

[13] Devaraj S, Xu DY, Jialal I. C-reactive protein increases plasminogen activator inhibitor-1 expression and activity in human aortic endothelial cells: implications for the metabolic syndrome and atherothrombosis. Circulation 2003 Jan 28;107(3):398-404.

[14] Han KH, Hong KH, Park JH, Ko J, Kang DH, Choi KJ, et al. C-reactive protein promotes monocyte chemoattractant protein-1--mediated chemotaxis through upregulating CC chemokine receptor 2 expression in human monocytes. Circulation 2004 Jun 1;109(21):2566-2571.

[15] Wolbink GJ, Bossink AW, Groeneveld AB, de Groot MC, Thijs LG, Hack CE. Complement activation in patients with sepsis is in part mediated by C-reactive protein. J Infect Dis 1998 Jan;177(1):81-87.

[16] Opal SM. Therapeutic rationale for antithrombin III in sepsis. Crit Care Med 2000 Sep;28(9 Suppl):S34-7.

[17] Klein NJ, Ison CA, Peakman M, Levin M, Hammerschmidt S, Frosch M, et al. The influence of capsulation and lipooligosaccharide structure on neutrophil adhesion molecule expression and endothelial injury by Neisseria meningitidis. J Infect Dis 1996 Jan;173(1):172-179.

[18] Takano S, Kimura S, Ohdama S, Aoki N. Plasma thrombomodulin in health and diseases. Blood 1990 Nov 15;76(10):2024-2029.

[19] Faust SN, Levin M, Harrison OB, Goldin RD, Lockhart MS, Kondaveeti S, et al. Dysfunction of endothelial protein C activation in severe meningococcal sepsis. N Engl J Med 2001 Aug 9;345(6):408-416.

[20] Fisher CJ,Jr, Yan SB. Protein C levels as a prognostic indicator of outcome in sepsis and related diseases. Crit Care Med 2000 Sep;28(9 Suppl):S49-56.

[21] Camerer E, Rottingen JA, Gjernes E, Larsen K, Skartlien AH, Iversen JG, et al. Coagulation factors VIIa and Xa induce cell signaling leading to up-regulation of the egr-1 gene. J Biol Chem 1999 Nov 5;274(45):32225-32233.

[22] Cunningham MA, Romas P, Hutchinson P, Holdsworth SR, Tipping PG. Tissue factor and factor VIIa receptor/ligand interactions induce proinflammatory effects in macrophages. Blood 1999 Nov 15;94(10):3413-3420.

[23] Pendurthi UR, Alok D, Rao LV. Binding of factor VIIa to tissue factor induces alterations in gene expression in human fibroblast cells: up-regulation of poly(A) polymerase. Proc Natl Acad Sci U S A 1997 Nov 11;94(23):12598-12603.

[24] Miller DL, Yaron R, Yellin MJ. CD40L-CD40 interactions regulate endothelial cell surface tissue factor and thrombomodulin expression. J Leukoc Biol 1998 Mar;63(3):373-379.

[25] Henn V, Slupsky JR, Grafe M, Anagnostopoulos I, Forster R, Muller-Berghaus G, et al. CD40 ligand on activated platelets triggers an inflammatory reaction of endothelial cells. Nature 1998 Feb 5;391(6667):591-594.

[26] Andre P, Prasad KS, Denis CV, He M, Papalia JM, Hynes RO, et al. CD40L stabilizes arterial thrombi by a beta3 integrin--dependent mechanism. Nat Med 2002 Mar;8(3):247-252.

[27] Szaba FM, Smiley ST. Roles for thrombin and fibrin(ogen) in cytokine/chemokine production and macrophage adhesion in vivo. Blood 2002 Feb 1;99(3):1053-1059.

[28] Loike JD, el Khoury J, Cao L, Richards CP, Rascoff H, Mandeville JT, et al. Fibrin regulates neutrophil migration in response to interleukin 8, leukotriene B4, tumor necrosis factor, and formyl-methionyl-leucyl-phenylalanine. J Exp Med 1995 May 1;181(5):1763-1772.

[29] Broze GJ,Jr, Warren LA, Novotny WF, Higuchi DA, Girard JJ, Miletich JP. The lipoprotein-associated coagulation inhibitor that inhibits the factor VII-tissue factor complex also inhibits factor Xa: insight into its possible mechanism of action. Blood 1988 Feb;71(2):335-343.

[30] Okajima K. Regulation of inflammatory responses by natural anticoagulants. Immunol Rev 2001 Dec;184:258-274.

[31] Kaneider NC, Egger P, Dunzendorfer S, Wiedermann CJ. Syndecan-4 as antithrombin receptor of human neutrophils. Biochem Biophys Res Commun 2001 Sep 14;287(1):42-46.

[32] Oelschlager C, Romisch J, Staubitz A, Stauss H, Leithauser B, Tillmanns H, et al. Antithrombin III inhibits nuclear factor kappaB activation in human monocytes and vascular endothelial cells. Blood 2002 Jun 1;99(11):4015-4020.

[33] Souter PJ, Thomas S, Hubbard AR, Poole S, Romisch J, Gray E. Antithrombin inhibits lipopolysaccharide-induced tissue factor and interleukin-6 production by mononuclear cells,

human umbilical vein endothelial cells, and whole blood. Crit Care Med 2001 Jan;29(1):134-139.

[34] Ostrovsky L, Woodman RC, Payne D, Teoh D, Kubes P. Antithrombin III prevents and rapidly reverses leukocyte recruitment in ischemia/reperfusion. Circulation 1997 Oct 7;96(7):2302-2310.

[35] Liu LW, Vu TK, Esmon CT, Coughlin SR. The region of the thrombin receptor resembling hirudin binds to thrombin and alters enzyme specificity. J Biol Chem 1991 Sep 15;266(26):16977-16980.

[36] Ye X, Fukudome K, Tsuneyoshi N, Satoh T, Tokunaga O, Sugawara K, et al. The endothelial cell protein C receptor (EPCR) functions as a primary receptor for protein C activation on endothelial cells in arteries, veins, and capillaries. Biochem Biophys Res Commun 1999 Jun 16;259(3):671-677.

[37] Campbell W, Okada N, Okada H. Carboxypeptidase R is an inactivator of complement-derived inflammatory peptides and an inhibitor of fibrinolysis. Immunol Rev 2001 Apr;180:162-167.

[38] Myles T, Nishimura T, Yun TH, Nagashima M, Morser J, Patterson AJ, et al. Thrombin activatable fibrinolysis inhibitor, a potential regulator of vascular inflammation. J Biol Chem 2003 Dec 19;278(51):51059-51067.

[39] Pixley RA, De La Cadena R, Page JD, Kaufman N, Wyshock EG, Chang A, et al. The contact system contributes to hypotension but not disseminated intravascular coagulation in lethal bacteremia. In vivo use of a monoclonal anti-factor XII antibody to block contact activation in baboons. J Clin Invest 1993 Jan;91(1):61-68.

[40] Isermann B, Hendrickson SB, Hutley K, Wing M, Weiler H. Tissue-restricted expression of thrombomodulin in the placenta rescues thrombomodulin-deficient mice from early lethality and reveals a secondary developmental block. Development 2001 Mar;128(6):827-838.

[41] Sturn DH, Kaneider NC, Feistritzer C, Djanani A, Fukudome K, Wiedermann CJ. Expression and function of the endothelial protein C receptor in human neutrophils. Blood 2003 Aug 15;102(4):1499-1505.

[42] Joyce DE, Gelbert L, Ciaccia A, DeHoff B, Grinnell BW. Gene expression profile of antithrombotic protein c defines new mechanisms modulating inflammation and apoptosis. J Biol Chem 2001 Apr 6;276(14):11199-11203.

[43] Hancock WW, Grey ST, Hau L, Akalin E, Orthner C, Sayegh MH, et al. Binding of activated protein C to a specific receptor on human mononuclear phagocytes inhibits intracellular calcium signaling and monocyte-dependent proliferative responses. Transplantation 1995 Dec 27;60(12):1525-1532.

[44] Emerson TE,Jr, Fournel MA, Redens TB, Taylor FB,Jr. Efficacy of antithrombin III supplementation in animal models of fulminant Escherichia coli endotoxemia or bacteremia. Am J Med 1989 Sep 11;87(3B):27S-33S.

[45] Taylor FB,Jr, Chang A, Esmon CT, D'Angelo A, Vigano-D'Angelo S, Blick KE. Protein C prevents the coagulopathic and lethal effects of Escherichia coli infusion in the baboon. J Clin Invest 1987 Mar;79(3):918-925.

[46] Creasey AA, Chang AC, Feigen L, Wun TC, Taylor FB,Jr, Hinshaw LB. Tissue factor pathway inhibitor reduces mortality from Escherichia coli septic shock. J Clin Invest 1993 Jun;91(6):2850-2860.

[47] Levi M, van der Poll T. Inflammation and coagulation. Crit Care Med 2010 Feb;38(2 Suppl):S26-34.

[48] Angus DC, van der Poll T. Severe sepsis and septic shock. N Engl J Med 2013 Nov 21;369(21):2063.

[49] Hotchkiss RS, Monneret G, Payen D. Immunosuppression in sepsis: a novel understanding of the disorder and a new therapeutic approach. Lancet Infect Dis 2013 Mar;13(3):260-268.

[50] de Stoppelaar SF, van 't Veer C, van der Poll T. The role of platelets in sepsis. Thromb Haemost 2014 Oct;112(4):666-677.

[51] Kini RM, Chow G, Registry of Exogenous Hemostatic Factors of the Scientific and Standardization Committee of the International Society on Thrombosis and Haemostasis. Exogenous inhibitors of platelet aggregation from animal sources. Thromb Haemost 2001 Jan;85(1):179-181.

[52] Hutton RA, Warrell DA. Action of snake venom components on the haemostatic system. Blood Rev 1993 Sep;7(3):176-189.

[53] Markland FS,Jr. Snake venoms. Drugs 1997;54 Suppl 3:1-10

[54] Markland FS. Snake venoms and the hemostatic system. Toxicon 1998 Dec;36(12):1749-1800.

[55] Braud S, Bon C, Wisner A. Snake venom proteins acting on hemostasis. Biochimie 2000 Sep-Oct;82(9-10):851-859.

[56] Nakagaki T, Lin P, Kisiel W. Activation of human factor VII by the prothrombin activator from the venom of Oxyuranus scutellatus (Taipan snake). Thromb Res 1992 Jan 1;65(1):105-116.

[57] Kini RM. The intriguing world of prothrombin activators from snake venom. Toxicon 2005 Jun 15;45(8):1133-1145.

[58] Rosing J, Tans G. Inventory of exogenous prothrombin activators. For the Subcommittee on Nomenclature of Exogenous Hemostatic Factors of the Scientific and Standardization Committee of the International Society on Thrombosis and Haemostasis. Thromb Haemost 1991 May 6;65(5):627-630.

[59] Rosing J, Tans G. Structural and functional properties of snake venom prothrombin activators. Toxicon 1992 Dec;30(12):1515-1527.

[60] Kornalik F, Blomback B. Prothrombin activation induced by Ecarin - a prothrombin converting enzyme from Echis carinatus venom. Thromb Res 1975 Jan;6(1):57-63.

[61] Yamada D, Sekiya F, Morita T. Isolation and characterization of carinactivase, a novel prothrombin activator in Echis carinatus venom with a unique catalytic mechanism. J Biol Chem 1996 Mar 1;271(9):5200-5207.

[62] Yamada D, Morita T. Purification and characterization of a Ca2+ -dependent prothrombin activator, multactivase, from the venom of Echis multisquamatus. J Biochem 1997 Nov;122(5):991-997.

[63] Kane WH, Davie EW. Blood coagulation factors V and VIII: structural and functional similarities and their relationship to hemorrhagic and thrombotic disorders. Blood 1988 Mar;71(3):539-555.

[64] Rao VS, Joseph JS, Kini RM. Group D prothrombin activators from snake venom are structural homologues of mammalian blood coagulation factor Xa. Biochem J 2003 Feb 1;369(Pt 3):635-642.

[65] Mann KG, Hockin MF, Begin KJ, Kalafatis M. Activated protein C cleavage of factor Va leads to dissociation of the A2 domain. J Biol Chem 1997 Aug 15;272(33):20678-20683.

[66] Walker FJ, Owen WG, Esmon CT. Characterization of the prothrombin activator from the venom of Oxyuranus scutellatus scutellatus (taipan venom). Biochemistry 1980 Mar 4;19(5):1020-1023.

[67] Speijer H, Govers-Riemslag JW, Zwaal RF, Rosing J. Prothrombin activation by an activator from the venom of Oxyuranus scutellatus (Taipan snake). J Biol Chem 1986 Oct 5;261(28):13258-13267.

[68] Rao VS, Kini RM. Pseutarin C, a prothrombin activator from Pseudonaja textilis venom: its structural and functional similarity to mammalian coagulation factor Xa-Va complex. Thromb Haemost 2002 Oct;88(4):611-619.

[69] Rao VS, Swarup S, Kini RM. The nonenzymatic subunit of pseutarin C, a prothrombin activator from eastern brown snake (Pseudonaja textilis) venom, shows structural similarity to mammalian coagulation factor V. Blood 2003 Aug 15;102(4):1347-1354.

[70] Joseph JS, Chung MC, Jeyaseelan K, Kini RM. Amino acid sequence of trocarin, a prothrombin activator from Tropidechis carinatus venom: its structural similarity to coagulation factor Xa. Blood 1999 Jul 15;94(2):621-631.

[71] Narasaki R, Kuribayashi H, Shimizu K, Imamura D, Sato T, Hasumi K. Bacillolysin MA, a novel bacterial metalloproteinase that produces angiostatin-like fragments from plasminogen and activates protease zymogens in the coagulation and fibrinolysis systems. J Biol Chem 2005 Apr 8;280(14):14278-14287.

[72] Imamura T, Banbula A, Pereira PJ, Travis J, Potempa J. Activation of human prothrombin by arginine-specific cysteine proteinases (Gingipains R) from porphyromonas gingivalis. J Biol Chem 2001 Jun 1;276(22):18984-18991.

[73] Friedrich R, Panizzi P, Fuentes-Prior P, Richter K, Verhamme I, Anderson PJ, et al. Staphylocoagulase is a prototype for the mechanism of cofactor-induced zymogen activation. Nature 2003 Oct 2;425(6957):535-539.

[74] Bode W, Huber R. Induction of the bovine trypsinogen-trypsin transition by peptides sequentially similar to the N-terminus of trypsin. FEBS Lett 1976 Oct 1;68(2):231-236.

[75] Heilmann C, Herrmann M, Kehrel BE, Peters G. Platelet-binding domains in 2 fibrinogen-binding proteins of Staphylococcus aureus identified by phage display. J Infect Dis 2002 Jul 1;186(1):32-39.

[76] Panizzi P, Friedrich R, Fuentes-Prior P, Kroh HK, Briggs J, Tans G, et al. Novel fluorescent prothrombin analogs as probes of staphylocoagulase-prothrombin interactions. J Biol Chem 2006 Jan 13;281(2):1169-1178.

[77] Turner DP, Wooldridge KG, Ala'Aldeen DA. Autotransported serine protease A of Neisseria meningitidis: an immunogenic, surface-exposed outer membrane, and secreted protein. Infect Immun 2002 Aug;70(8):4447-4461.

[78] Tessier-Marteau A, Cruguel S, Grand F, Asfar P, Zandecki M, Macchi L. DIC and peripheral gangrene in a severe Plasmodium falciparum malaria: the coagulation-inflammation cycle with Plasmodium falciparum as a model. Ann Biol Clin (Paris) 2009 Sep-Oct;67(5):569-572.

[79] Blackman MJ, Fujioka H, Stafford WH, Sajid M, Clough B, Fleck SL, et al. A subtilisin-like protein in secretory organelles of Plasmodium falciparum merozoites. J Biol Chem 1998 Sep 4;273(36):23398-23409.

[80] Pelzer A, Polen T, Funken H, Rosenau F, Wilhelm S, Bott M, et al. Subtilase SprP exerts pleiotropic effects in Pseudomonas aeruginosa. Microbiologyopen 2014 Feb;3(1):89-103.

[81] Pelzer A, Schwarz C, Knapp A, Wirtz A, Wilhelm S, Smits S, et al. Functional expression, purification, and biochemical properties of subtilase SprP from Pseudomonas aeruginosa. Microbiologyopen 2015 Oct;4(5):743-752.

[82] Wang H, Rogers TJ, Paton JC, Paton AW. Differential effects of Escherichia coli subtilase cytotoxin and Shiga toxin 2 on chemokine and proinflammatory cytokine expression in human macrophage, colonic epithelial, and brain microvascular endothelial cell lines. Infect Immun 2014 Sep;82(9):3567-3579.

[83] Furukawa T, Yahiro K, Tsuji AB, Terasaki Y, Morinaga N, Miyazaki M, et al. Fatal hemorrhage induced by subtilase cytotoxin from Shiga-toxigenic Escherichia coli. Microb Pathog 2011 Mar-Apr;50(3-4):159-167.

[84] Bonifait L, Vaillancourt K, Gottschalk M, Frenette M, Grenier D. Purification and characterization of the subtilisin-like protease of Streptococcus suis that contributes to its virulence. Vet Microbiol 2011 Mar 24;148(2-4):333-340.

[85] Bonifait L, Grenier D. The SspA subtilisin-like protease of Streptococcus suis triggers a pro-inflammatory response in macrophages through a non-proteolytic mechanism. BMC Microbiol 2011 Mar 1;11:47-2180-11-47.

[86] Harris TO, Shelver DW, Bohnsack JF, Rubens CE. A novel streptococcal surface protease promotes virulence, resistance to opsonophagocytosis, and cleavage of human fibrinogen. J Clin Invest 2003 Jan;111(1):61-70.

[87] de Stoppelaar SF, Bootsma HJ, Zomer A, Roelofs JJ, Hermans PW, van 't Veer C, et al. Streptococcus pneumoniae serine protease HtrA, but not SFP or PrtA, is a major virulence factor in pneumonia. PLoS One 2013 Nov 11;8(11):e80062.

[88] Abate F, Malito E, Falugi F, Margarit Y Ros I, Bottomley MJ. Cloning, expression, purification, crystallization and preliminary X-ray diffraction analysis of SpyCEP, a candidate antigen for a vaccine against Streptococcus pyogenes. Acta Crystallogr Sect F Struct Biol Cryst Commun 2013 Oct;69(Pt 10):1103-1106.

CHAPTER 3.2

Non-Canonical Proteolytic Activation of the Zymogen Prethrombin-2 by Subtilisin Carlsberg

INTRODUCTION

Haemostasis is an important defence system involving both cellular processes and enzymatic reactions performed by blood zymogens sequentially activated by limited proteolysis: the coagulation factors (FI - FXIII). In the penultimate step of the coagulation cascade, both the intrinsic and the extrinsic pathways converge to the activation of prothrombin (ProT) [**1**]. This glycosylated protein (579aa, 72.3kDa) can be structurally divided in three regions: fragment 1 (1-155), containing Gla domain and kringle-1; fragment 2 (156-271), containing kringle-2; and the protease domain (272-579). The inactive ProT, circulating in the plasma as a single chain, is proteolitically converted to active α-thrombin (αT), by FXa at two sites. This reaction is greatly increased (>3000-fold) when catalysed by the prothrombinase complex, in which FXa works along with cofactors FVa and Ca^{2+} on a negatively charged phospholipidic surface [**2**;**3**]. Two mutually exclusive activation pathways can be accomplished *in vivo*, producing two different intermediates: prethrombin-2 (cleavage at Arg271 first) or meizothrombin (cleavage at Arg320 first). Once the catalytic site is moulded, an auto-proteolysis at Arg284 releases the mature protease [**4**;**5**].

αT (295aa, 36.7kDa) is an ellipsoidal glycosylated protein, composed of a light and a heavy chain linked by a disulphide bridge between Cys1 and Cys122 (chymotrypsinogen numbering). αT is accounted to be the key enzyme of coagulation because it can paradoxically exert both pro- and anticoagulant functions, depending on its interaction with different ligands. The functional versatility of this serine protease relies on its molecular mechanisms of recognition: besides a negatively charged active site, it bears two positive extra regions of binding, named exosite I and exosite II [**6**;**7**]. In detail, the procoagulant roles entail platelets aggregation and fibrin generation, with the production of a transient clot localized at the site of vessel injury. On the other side, αT anticoagulant function is represented by protein C (PC) activation: active aPC, in turn, neutralizes FVa and FVIIIa, with a massive downregulation of the clotting cascade [**8**;**9**]. αT acts at the interface between different physio-pathologic systems: beside coagulation, this protein plays a pivotal role in inflammatory processes.

Actually, inflammation and coagulation are intimately connected, and enhance each other in a vicious circle [**10**]. In detail, inflammation initiates clotting providing key available procoagulant surfaces [**11**], increases fibrinogen concentration, impairs the fibrinolytic system and downregulates the natural anticoagulant pathways [**10**]. During inflammation, platelets count increases, and, under IL-6 effect, these cells become more thrombogenic, i.e. activate at lower αT concentrations [**12**]. In addition, inflammatory mediators like cytokines endorse the release of ultra-large von Willebrand Factor multimers [**13**] and boost the expression of protease activated receptors (PARs) and tissue factor (TF) [**14**] on the endothelium. On the other side, the coagulation actors triggering inflammation are the TF-FVIIa complex [**15**;**16**], fibrin(ogen) [**17**;**18**] and active platelets [**19**]. In detail, once activated, these cells express P-selectin, an adhesion leukocyte chemoattractant molecule, with the recruitment of monocytes on the thrombus surface. On the other side, active microparticles released from cytokine-stimulated monocytes carry on their surface TF, initiating in turn the coagulation cascade [**20**]. Furthermore, anticoagulant mechanisms not only neutralize coagulation, but also dampen the inflammatory manifestations [**10**]. In the early response to infections, local coagulation may contribute to the host defence in the attempt to trap and kill the invading pathogen. Since bleeding sites are potential entries for microorganisms, in this scenario, the coagulation system would act as an innate immunity regulatory effector [**21**]. This model suggests a common evolution of the two systems [**22**;**23**;**24**], and it is supported by the fact that in ancient highly conserved animals, like the horseshoe crab (*Limulus polyphemus*) the two pathways are fused in one. These organisms feature an innate immune system that recognizes exogenous bacterial endotoxins, and, after a cascade reaction, traps them in a protective gel matrix, repairing the generated wound at the same time [**25**].

When the coagulation/inflammation interface overwhelms the natural defence systems, catastrophic events burst in severe pathologic manifestations, first of all sepsis. Sepsis is a potentially lethal condition caused by an exaggerated and destructive body response to an invalidating pathogen. Concomitant and often agonistic processes contribute to damage the host's own tissues and organs, in the attempt to fight the infection. Both this systematically activation of the immune response and the triggering of the coagulation system are associated with high morbidity and mortality [**26**;**27**;**28**]. In detail, the unstopped procoagulant response leads to the disseminated intravascular coagulation (DIC). In this clinical syndrome, scattered microvascular thrombi generation is coupled to depletion of the coagulation factors and a haemorrhagic state in the rest of the body [**29**]. In this scenario, proteases from foreign sources are thought to be harmful in inflammatory episodes not only for the immune system stimulation, but also for the eventual direct activation of procoagulant mechanisms. The most strikingly example in nature is provided by several snake venom proteases, which activate ProT [**30**]. Regarding microbial enzymes, only a few proteins have been investigated:

metalloproteinases from *Staphylococcus aureus* and *Bacillus megaterium*, and cysteine proteases from *Phorphyromonas gingivalis* [**31**;**32**;**33**]. A recent study reports that two subtilisin-like proteases from the fungus *Acremonium sp.* proteolitically activate human ProT [**34**]. This intriguing scenario prompted us to investigate alternative activation pathways of αT zymogens.

Subtilisin Carlsberg (27.3kDa, 274 aa) is a serine protease secreted from *Bacillus subtilis* and *B. licheniformis*. These bacterial strains are obligate aerobe gram-positive, living in the soil and in the gastrointestinal tract of humans and ruminants. Before the introduction of antibiotics, *B. subtilis* was usually employed as a broad range probiotic for the treatment of gastrointestinal and urinary tract diseases. On the other hand, this bacterium may be pathogenic in extremely immunocompromised patients, leading to septicaemia [**35**]. The subtilisins are an extensive class of extracellular, alkaline bacterial proteases, first identified in the 40's by Linderstrøm-Lang and Ottesen, and purified by Güntelberg and Ottesen [**36**;**37**]. According to their amino acidic composition, the subtilisins can be classified in two families: class A comprises subtilisin Carlsberg and the enzymes from *B. pumilis*, whereas group B includes subtilisins Novo, BPN′ and Amylosacchariticus [**38**]. Being a serine protease, subtilisin Carlsberg is characterized by a negative active site, in which three amino acids (Ser221, His64, Asp32, i.e. the catalytic triad) work in synergism for the hydrolysis of peptide bonds [**39**]. This enzyme manifests a very broad specificity, preferring aromatic or apolar residues [**40**]. Furthermore, subtilisin is characterized by two Ca^{2+} binding sites: one strong, with a binding constant of 10^8M, and one weak, with a binding constant of 10^2M. The interaction with Ca^{2+} ions is crucial both for activity and for stability [**41**]. In this work, after a screening of the most common bacterial proteases, from preliminary data it emerged that subtilisin Carlsberg interacts with and activates the zymogens Pre2 and ProT. In a first stage we focused our efforts on the study of the intermediate Pre2 (313aa, 35.9kDa,), recombinantly produced in our Laboratory.

EXPERIMENTALS

Reagents

Natural human αT, PC and rabbit thrombomodulin (TM) were purchased from Haematologic Technologies (Essex Junction, VT, USA). Subtilisin Carlsberg (Subtilopeptidase A) from *Bacillus subtilis*, ecarin from *Echis carinatus* venom, fibrinogen from human plasma, PABA (p-aminobenzamidine), all salts, solvents and reagents of analytical grade were purchased from Sigma (St. Louis, MO, USA). The chromogenic substrates S2238 (D-Phe-Pip-Arg-pNA) and S2366 (pyroGlu-Pro-Arg-pNA) were from Chromogenix (Milan, Italy), while the N-terminal hirudin domain Hir(1-47) derives from the limited proteolysis of hirudin HM2 from *Hirudinaria manillensis* by bovine pancreas trypsin (Promega Biosciences, CA, USA). Recombinant hirudin HM2 was a generous gift from Dr. G. Orsini (Farmitalia, Italy). The small substrate D-Phe-Pip-Arg was manually synthetized by using standard Fmoc-chemistry. Hirugen ^{54}GDFEEIPEEY(PO$_3$H)LQ^{65} , GpIbα peptide ^{268}GDEGDTDLY(PO$_3$H) DY(PO$_3$H)Y(PO$_3$H)PEE^{282}, and PAR1 ^{38}LDPR↓SFLLRNPNDK YEPFWEDDE^{60} were synthetized by the solid phase strategy on a PS3 automated synthesizer (Protein Technologies, AZ, USA) using the Fmoc-chemistry, as described [**42**;**43**;**44**]. N-Fmoc protected amino acids, solvents and reagents for peptide synthesis were purchased from Applied Biosystems (Forster City, CA, USA) or Bachem AG (Bubendorf, Switzerland). The synthetic peptides were purified by semi-preparative RP-HPLC and characterized by high-resolution MS on a Xevo G2-S Q-TOF instrument from Waters (Milford, MA, USA), yielding experimental mass values in agreement with the expected amino acid composition within 1-2 ppm.

Production and Characterization of Recombinant Prethrombin-2

The plasmid containing the cDNA of Pre2 was a generous gift of Prof. Huntington (Cambridge University). Recombinant wild type Pre2 was expressed in *E. coli*, subjected to *in vitro* disulphide oxidative refolding, and characterized by RP-HPLC and high-resolution MS. The recombinant protein is 18aa longer than αT at N-terminus: 13aa are typical of the wild type intermediate, while 5aa ($^{-18}$AIEGR^{-14}) were added for the plasmid construction. A portion of Pre2 was activated to mature recombinant αT (rT) by ecarin, and characterized as previously detailed. [**45**;**4**].

The concentrations of thrombin solutions were determined by measuring the absorbance at 280nm, using an absorptivity coefficient of 1.892mg^{-1}·cm^2 for Pre2, and of 1.964mg^{-1}·cm^2 for rT and αT.

Proteolysis of Prethrombin-2 by Subtilisin

A solution of Pre2 (0.1mg/ml) was subjected to proteolysis by subtilisin (0.05µg/ml) in HBS-$CaCl_2$ buffer, at decreasing temperatures: 37°C, 25°C, 10°C, 5°C. At fixed time points (0, 1, 10, 30, 90, 180, 300min - and 390min for 5°C) an aliquot (50µl) of the reaction mixture was quenched by 1.25µl H_2O-TFA 4% (v/v) and cold precipitated in TCA. The samples were analysed by SDS-PAGE (4-14% acrylamide) under non-reducing conditions, and Coomassie stained. The bands corresponding to the starting Pre2 were quantified according to a densitometric analysis, performed by the free software ImageJ. The concentrations of the residual Pre2 were plotted against the reaction times, and the experimental data points were fitted according to **equation 1**:

$$[Pre2]_t = [Pre2]_0 \cdot e^{-k_{obs} \cdot t} \qquad \textbf{(Eq. 1)}$$

where $[Pre2]_t$ is the concentration of the residual Pre2 at time t, $[Pre2]_0$ is the starting concentration of Pre2 and k_{obs} is the kinetic constant observed for the reaction. Under pseudo-first order conditions, i.e. [Pre2]>>[subtilisin], and assuming [Pre2]<0.1·K_m, the specificity constant (k_{cat}/K_m) of subtilisin for Pre2 can be derived according to **equation 2**:

$$\frac{k_{cat}}{K_m} = \frac{k_{obs}}{[enzyme]} \qquad \textbf{(Eq. 2)}$$

where k_{cat} is the real kinetic constant, while K_m is the Michaelis-Menten constant of subtilisin for Pre2. Since in the experimental conditions tested subtilisin concentration (0.05µg/ml) is much lower than Pre2 (0.1mg/ml), **equation 2** is suitable for deriving the specificity constant.

After performing the proteolysis in the same conditions detailed above, the reaction mixture was analysed by RP-HPLC from Jasco (Tokyo, Japan). At fixed time points, an aliquot (200µl) of the solution was quenched by 5µl H_2O-TFA 4% (v/v) and loaded onto a (4.6x150mm, 5µM, 300Å) C4 Vydac analytical column (Hesperia, CA, USA). The samples were eluted with a linear acetonitrile-0.078% TFA biphasic gradient of 5-35% in 15min and 35-55% in 35min, at a flow rate of 0.8ml/min. For the reaction accomplished at 37°C, the concentrations of the residual Pre2 were quantified at 226nm, according to the area under the chromatographic peak, and plotted against the reaction times. The experimental data points were fitted with **equation 1** and **equation 2** to obtain the specificity constant (k_{cat}/K_m) of subtilisin for Pre2 with another technique.

To characterize subtilisin proteolysis products, different stages of the reaction were explored by coupled LC-MS on an Agilent 1290 Infinity Binary UHPLC (Santa Clara, CA, USA) connected to a Xevo G2-S Q-TOF apparatus from Waters (Milford, MA, USA). The proteolysis was accomplished in the same enzyme:substrate ratio of 1:2000 (w/w), but in HBS-$CaCl_2$ without PEG-

8000. After 1min at 37°C or 90min at 10°C, an aliquot of 20µl of the solution was quenched by 0.5µl H_2O-TFA 4% (v/v) and loaded on a (1.0x50mm, 5µM, 300Å) C4 Vydac Microbore analytical column (Hesperia, CA, USA) eluted with a linear acetonitrile-0.1% HCOOH gradient of 15-65% in 30min, at a flow rate of 0.05ml/min. The mass versus charge signals, visualized as BPI (base peak intensity) by the program MassLynx V4.1, were deconvoluted by the software MaxEnt1 to achieve the peaks average masses.

Chromogenic Substrate S2238 Hydrolysis by Subtilisin-nicked Prethrombin-2 (σPre2)

A solution of Pre2 (0.1mg/ml) was subjected to proteolysis by subtilisin (0.05µg/ml) in HBS-$CaCl_2$ buffer at 37°C. At fixed time points (0, 1, 10, 20, 30, 40, 50, 60, 90, 120, 180, 240, 300, 420min) an aliquot (15µl) of the reaction mixture was added to a solution of S2238 (20µM) in a final volume of 800µl of HBS buffer. The time-course release of pNA was monitored by recording the absorbance at 405nm for 5min at 37°C on a Jasco (Tokyo, Japan) V-630 spectrophotometer, equipped with a PAC-743 Peltier thermostat. The slope of the straight lines, taken as the initial velocity v_0 of the hydrolysis, was correlated to the released pNA concentration using the molar absorptivity coefficient of $9920 M^{-1} \cdot cm^{-1}$, and plotted versus the reaction times. The experimental data points were compared to the hydrolysis rates achieved by performing the same experiment in the absence of starting Pre2.

Purification of Subtilisin-nicked Prethrombin-2 (σPre2)

For micro-purification purposes, a solution of Pre2 (200µg, 0.1mg/ml) was treated with subtilisin (0.05µg/ml) in HBS-$CaCl_2$ buffer for 15h at 5°C. This aliquot was loaded on a 1ml HiTrap (7.0x25mm) heparin sepharose column connected to an ÄKTA purifier system, both from GE Healthcare (Little Chalfont, UK). The column was equilibrated with 25mM TRIS-HCl pH 7.4, 0.25M NaCl, and the sample was eluted by applying an on/off gradient of 65% 25mM TRIS-HCl pH 7.4, 1M NaCl, at a flow rate of 0.5ml/min. Three fractions (0.4-1.0ml) collected from the chromatographic course were cold precipitated in TCA, analysed by SDS-PAGE (4-14% acrylamide) under non-reducing conditions, and Silver stained.

The solution of the purified αT-like active specie, named σPre2, was stored at 20°C. At fixed time points (0, 2, 5, 7, 24h) an aliquot (8µg) was cold precipitated in TCA. The samples were analysed by SDS-PAGE (4-14% acrylamide) under non-reducing conditions, and Coomassie stained. In a second stage, the activity of fresh purified σPre2 was compared to different storage solutions: 20°C for 7h; 4°C for 24h; -20°C for 24h and slow thawing on ice. After the declared times, aliquots of the samples were added to a solution of S2238 (20µM) to a final concentration of 10nM σPre2 in 800µl

of HBS buffer. The time-course release of pNA was monitored by recording the absorbance at 405nm for 4min at 37°C on a Jasco (Tokyo, Japan) V-630 spectrophotometer, equipped with a PAC-743 thermostat.

Circular Dichroism in the Far-UV

CD measurements were performed on a Jasco (Tokyo, Japan) model J-810 spectropolarimeter, equipped with a thermostated cell holder connected to a model RTE-111 (NesLab) water-circulating bath. Far-UV spectra were recorded for recombinant Pre2, σPre2 and rT (2μM) in a 2mm-pathlength quartz cuvette, at scan speed of 10nm/min, using a response time of 16sec, as the average of four accumulations. The CD signals, monitored in the region 198-250nm, and subtracted for the baseline, were expressed as the mean residue ellipticity [θ], according to **equation 3**:

$$[\theta] = \frac{\theta_{obs} \cdot MRW}{10 \cdot l \cdot c} \qquad \textbf{(Eq. 3)}$$

where θ_{obs} is the observed ellipticity in degrees, MRW is the mean molecular weight per residue, l is the optical pathlength in cm, and c is the protein concentration expressed in g/ml.

Fluorescence

Fluorescence binding measurements were carried out at 37°C in HBS (1.5ml), in a 1cm-pathlength quartz cuvette on a Jasco FP-6500 spectrofluorimeter (Tokyo, Japan). To compare Pre2, σPre2 and rT fluorescence, samples (30nM) of the proteins of interest in TBS containing 0.2M ChCl were analysed at 25°C. The samples were excited at 280nm, and the fluorescence spectra was recorded in the range 295-500nm and corrected for the baseline.

In a second stage, solutions of σPre2 were confronted to human αT in the binding of probes that selectively interact to specific thrombin areas, at 37°C in HBS. In detail, PABA, D-Phe-Pip-Arg (FPR) and Hir(1-47) were used for the active site; hirugen is specific for exosite I, while recombinant wild type HM2 binds both to active site and to exosite I. For all the titrations, aliquots (2-20μl) of ligands stock solutions were added under gentle magnetic stirring (30sec), and the samples were allowed to equilibrate 2min after each addition. Solutions were excited at 280nm for FPR and hirugen, and at 295nm for Hir(1-47) and HM2. The fluorescence was recorded at the emission λ_{max}, i.e., 334nm for αT and 340nm for σPre2. The spectra were corrected for the dilution factor (that was always lower than 10% at the end of the titration), subtracted of the blank and of raw starting fluorescence. For low affinity binders, like PABA, FPR and hirugen, the data points were interpolated with **equation 4**, describing a simple one-site binding mechanism R + L ⇔ RL [**46**]:

$$\frac{\Delta F}{\Delta F_{max}} = \frac{[RL]}{[R]} = \frac{[L]}{K_d+[L]} \qquad \textbf{(Eq. 4)}$$

where the fluorescence intensity, F, of the receptor, R (σPre2, αT), at a given concentration of ligand, [L], is linearly related to the concentration of the complex [RL], according to the equation $F=[RL]\cdot F_{bound}+[R]_{free}\cdot F_{free}$. $\Delta F=F-F_0$ is the change in receptor fluorescence in the absence, F_0, and presence, F, of the ligand; ΔF_{max} is the maximum signal change at infinite concentration of ligand, $[L]_\infty$; K_d is the dissociation constant of the complex, RL. The data were interpolated to obtain K_d and ΔF_{max} as fitting parameters.

Equation 4 assumes the simplification that at equilibrium $[L]_{free} \cong [L]_{tot}$ and thus it is valid only when $K_d >> [R]$. For tight binders, like Hir(1-47) and HM2, since $K_d \cong [R]$ **equation 4** is no longer valid. In these cases, fluorescence data were fitted to the rigorous **equation 5** of tight binding [**47**]:

$$\frac{\Delta F}{\Delta F_{max}} = \frac{[RL]}{[R]} = \frac{[R]+[L]+K_d-\sqrt{\left[[R]+[L]+K_d\right]^2-4\cdot[R]\cdot[L]}}{2\cdot[R]} \qquad \textbf{(Eq. 5)}$$

For PABA titration, samples were excited at 336nm and the fluorescence was recorded at 375nm. Raw fluorescence data were corrected for the inner filter effect (IFE) factor, since fluorescence intensity is only proportional to the absorbance of the sample up to an optical density of 0.05 units, both at λ_{ex} and λ_{em} [**47**;**48**]. The following **equation 6** was used:

$$IFE = \frac{2.303 \cdot \frac{1}{3}Abs_{PABA}}{10^{-\frac{1}{3}Abs_{PABA}} - 10^{-\frac{2}{3}Abs_{PABA}}} \qquad \textbf{(Eq. 6)}$$

where PABA theoretical absorbance at 336nm was determined using a molar absorptivity coefficient of $547.8 M^{-1}\cdot cm^{-1}$. **Equation 6** is valid only for 1cm-pathlength cuvettes.

For Na^+ binding, σPre2 was compared to both recombinant Pre2 and recombinant rT at 25°C. A solution of 30nM protein in TBS containing 1M NaCl was incremented substituted (aliquots 2-20μl) to a solution of 30nM protein in TBS containing 1M ChCl. Ionic strength and protein concentration were held constant, while the Na^+ concentration was varied. Samples were excited at 280nm, and the fluorescence was recorded at λ_{max} of 334nm for Pre2 and rT, and of 340nm for σPre2. After subtracting the values for the initial fluorescence F_0, the experimental data were fitted according to **equation 4**.

Surface plasmon resonance

SPR analyses were carried out at 25°C on a C1 sensor chip in a dual flowcell Biacore-X100 instrument from GE Healthcare (Little Chalfont, UK). A biotinyl-PEG-GpIbα solution (100µl, 0.4µM) was loaded for 700sec on a NeutrAvidin-coated C1 chip at a flow rate of 10µl/min.

Aliquots of recombinant Pre2, σPre2 or human αT at increasing concentrations (0-600nM) were sequentially injected in the mobile phase, over the immobilized GpIbα sensor chip, in HBS-EP buffer. For each curve, the response value RU_{eq} at steady state was plotted against the protein concentrations, and K_d of the complex was obtained fitting the data points to **equation 7**:

$$RU_{eq} = RU_{max} \cdot \frac{[L]}{K_d + [L]} \qquad \textbf{(Eq. 7)}$$

where RU_{max} is the RU value at saturating L concentrations and [L] is the concentration of the free ligand in equilibrium with the receptor-ligand RL complex present on the sensor chip surface. When $[R] << K_d$, then $[L]_{free} \cong [L]_{tot}$, i.e. the total ligand concentration in the mobile phase. Data analysis was performed using the BIAevaluation software.

Proteolysis of Thrombin Substrates by σPre2

S2238 Hydrolysis **-** Steady-state kinetic of hydrolytic reaction of S2238 (D-Phe-Pip-Arg-pNA) substrate was investigated at 37°C on a Victor3 plate reader from PerkinElmer (Waltham, MA, USA) on a 96-well polystyrene plate from Sigma (St. Louis, MO, USA). To a solution of σPre2 (40nM) or αT (50pM) were added decreasing (60-0µM, by 1:2 dilutions) concentrations of S2238 in a final volume of 200µl HBS. The time-course release of pNA was monitored by recording the absorbance at 405nm for 5min at 37°C. The slope of the straight lines, taken as the initial velocity v_0 of the hydrolysis, was correlated to the released pNA concentration using molar absorptivity coefficient of $9920 M^{-1} \cdot cm^{-1}$. The hydrolysis rates (v), plotted versus the starting substrate concentrations were interpolated by the Michaelis-Menten **equation 8**, obtaining k_{cat} and K_m as fitting parameters.

$$v = \frac{V_{max} \cdot [S]}{K_m + [S]} \qquad \textbf{(Eq. 8)}$$

where $V_{max} = k_{cat} \cdot [E]$ is the maximum rate of the reaction at fixed enzyme concentration, and [S] is S2238 concentration.

Release of Fibrinopeptides - Human fibrinogen was desalted on a Sephadex G10 resin from Sigma (St. Louis, MO, USA), manually packed in a (8x125mm) column, eluted with HBS buffer at a flow rate of 0.3ml/min. The release of FpA and FpB by σPre2 (30nM) or human αT (0.3nM) from desalted fibrinogen (0.35μM), was carried out at 37°C in 1ml of HBS buffer. At fixed time points (0, 2, 4, 8, 16, 40, 60min) proteolysis was quenched by 300μl HCOOH 12% (v/v); the samples were centrifuged at 10,000g for 5min to eliminate fibrin and acid-precipitated fibrinogen. The supernatant (1ml) was withdrawn, lyophilized and dissolved in 150μl of 6M Gnd-HCl. Fibrinopeptides were separated and quantified by RP-HPLC, injecting 100μl of the sample onto a (4.6x250mm; 5μM, 300Å) C18 Vydac analytical column (Hesperia, CA, USA). The column was equilibrated in 40mM ammonium phosphate buffer, pH 3.1, and eluted with a linear acetonitrile gradient at a flow rate of 1.0ml/min, recording the absorbance at 205nm, according to the method previously reported [**49**].

The amount of FpA and FpB released was determined by integrating the AUC, using molar absorptivity at 205nm of $4.4 \cdot 10^4 M^{-1} \cdot cm^{-1}$ or $5.12 \cdot 10^4 M^{-1} \cdot cm^{-1}$, respectively. The specificity constant (k_{catA}/K_{mA}) for the release of FpA was determined by interpolating the data points to the **equation 9**:

$$[FpA]_t = [FpA]_\infty \cdot (1 - e^{-k't}) \qquad \textbf{(Eq. 9)}$$

where $[FpA]_t$ and $[FpA]_\infty$ are the concentrations of FpA at time t and ∞, respectively, and k′ is the observed kinetic constant for FpA release, obtained as a fitting parameter. Under pseudo-first order conditions, i.e. [A-chain]>>[enzyme], and [fibrinogen]<0.1·[K_{ma}], the specificity constant (k_{catA}/K_{mA}) of αT or σPre2 for fibrinogen A-chain can be derived according to **equation 2**. Since in the experimental conditions tested the enzymatic concentrations are much lower than fibrinogen A-chain, and, in case of αT fibrinogen concentration is lower than K_{mA}=7.2μM at 37°C [**49**], **equation 2** is suitable for deriving the specificity constant. Regarding σPre2 K_{mA}, we made the raw assumption, due to its homology to αT, to be in pseudo-first order conditions as well.

Analogously, the data points relative to the time-dependent release of FpB were interpolated with **equation 10**:

$$[FpB]_t = [FpB]_\infty \cdot (1 + \alpha \cdot e^{-k't} - \beta \cdot e^{-k''t}) \qquad \textbf{(Eq. 10)}$$

where k′ and k″ are the observed kinetic constants for FpA and FpB release, respectively, α = k″/(k′-k″), and β = k′/(k′-k″). As for the release of FpA, at enzyme and substrate concentrations used in this work, the specificity constant (k_{catB}/K_{mB}) can be derived according to **equation 2**.

PAR-1 Hydrolysis - The hydrolysis of synthetic PAR-1(38-60) peptide was carried out at 25°C and investigated by RP-HPLC analysis. To a solution of PAR-1 (1μM) in HBS were added either σPre2 or αT, to a final concentration of 10nM or 0.1nM, respectively. At fixed time points (0, 5, 10, 20, 30, 40, 60, 90min for σPre2; 0, 0.5, 1, 1.5, 2, 3, 5, 8, 15min for αT) an aliquot (360μl) of the reaction mixture was quenched by 9μl H_2O-TFA 4% (v/v) and loaded onto a (4.6x250mm, 5μM, 300Å) C18 Vydac analytical column (Hesperia, CA, USA). The samples were eluted with a linear acetonitrile-0.078% TFA biphasic gradient of 10-45% in 40min, at a flow rate of 0.8ml/min. The release of the C-terminal PAR-1(42-60) fragment was determined by integrating the AUC at 226nm, and plotted against the reaction time. The observed kinetic constant k_{obs} for the release of PAR-1(42-60) was determined by interpolating the data points to the **equation 11**:

$$[PAR-1(42-60)]_t = [PAR-1(42-60)]_\infty \cdot (1 - e^{-k_{obs} \cdot t}) \qquad \textbf{(Eq. 11)}$$

where $[PAR\text{-}1(42\text{-}60)]_t$ and $[PAR\text{-}1(42\text{-}60)]_\infty$ are the concentrations of the C-terminal peptide at time t and ∞, respectively, and k_{obs} is the observed kinetic constant for its release, obtained as a fitting parameter. Under pseudo-first order conditions, i.e. [PAR-1(38-60)]>>[enzyme] and [PAR-1(38-60)]<0.1·K_m, the specificity constant (k_{cat}/K_m) can be derived according to **equation 2**. Since in the experimental conditions tested the enzymatic concentrations are much lower than PAR-1(38-60), and, in case of αT the substrate concentration is lower than K_m>10μM at 25°C [**50**], **equation 2** is suitable for deriving the specificity constant. Regarding σPre2 K_m, we made the raw assumption, due to its homology to αT, to be in pseudo-first order conditions as well.

Protein C Activation - PC activation in the absence of TM was measured at 37°C on a Victor3 plate reader from PerkinElmer (Waltham, MA, USA) on a 96-well polystyrene plate from Sigma (St. Louis, MO, USA). According to the quenching method described elsewhere [**51**], to a solution of PC (200nM) in HBS were added either σPre2 or αT, to a final concentration of 40nM. At fixed time points (0, 5, 20min, 1, 2.5, 3.5, 5, 7, 10, 13, 16, 20h) aliquots (10μl) of the reaction mixture were diluted with 150μl of a solution containing 1μM HM2 and 200μM S2366. While HM2 stops σPre2/αT activity, the chromogenic substrate hydrolysis by the generated aPC was quantified by monitoring the absorbance at 405nm for 5min at 37°C. The slope of the straight lines was taken as the initial velocity v_0 of the hydrolysis of S2366 and was correlated to pNA concentrations by using the molar absorptivity coefficient of 9920$M^{-1} \cdot cm^{-1}$. In turn, the concentrations of pNA released were converted to [aPC] from a standard titration curve, achieved with known PC concentrations fully

activated to aPC in the presence of TM. The so calculated aPC concentrations were plotted against the reaction times, and the data points were interpolated according to **equation 12**:

$$[aPC]_t=[aPC]_\infty \cdot (1 - e^{-k_{obs} \cdot t}) \qquad \textbf{(Eq. 12)}$$

where $[aPC]_t$ and $[aPC]_\infty$ are the concentrations of the newly generated aPC at time t and ∞, respectively, and k_{obs} is the observed kinetic constant for the activation, obtained as a fitting parameter. Under pseudo-first order conditions, i.e. [PC]>>[enzyme], and [PC]<0.1·K_m, the specificity constant (k_{cat}/K_m) of αT or σPre2 for PC can be derived according to **equation 2** [**52**]. Since in the experimental conditions tested the enzymatic concentrations (40nM) are lower than the starting PC (200nM), **equation 2** is suitable for deriving the specificity constant. Regarding σPre2 K_m, we made the raw assumption, due to its homology to αT, to be in pseudo-first order conditions as well.

Fibrin Generation

Turbidimetric analysis of fibrin generation were performed at 37°C on a Jasco (Tokyo, Japan) V-630 spectrophotometer, equipped with a PAC-743 thermostat. Human fibrinogen was desalted on a Sephadex G10 resin from Sigma (St. Louis, MO, USA), manually packed in a (8x125mm) column, eluted with HBS buffer at a flow rate of 0.3ml/min. To a solution of desalted fibrinogen (440nM, 800µl) were added either σPre2 or αT to a final concentration of 50nM. The Sol→Gel transition was measured at 350nm for a time-course interval of 180min for σPre2, or 3min for αT. The so obtained sigmoidal clotting curves were dissected to extrapolate t_c, S_m, t_m and ΔA_{max} as clotting parameters [**53**].

Platelets Aggregation Assay

The effect of σPre2 on platelets aggregation was measured in whole blood by multiple electrode aggregometer (MEA) with a multiplate analyser from Dynabyte medical (Munich, Germany), and compared to the response induced by αT. Normal, citrate-treated venous blood samples were taken from two healthy non-smokers donors: all the analysis were performed within three hours from the withdrawn. The donors gave written informed consent for participation in this study, which was approved by the Ethical Committee of the University Hospital of Padua. Whole blood (300µl) was diluted with a solution of either σPre2 or αT in HBS (320µl) to a final concentration of 50nM and 0.5nM, respectively. All the measures were accomplished at 37°C, with vigorous stirring, for 10min. The aggregation rate was quantified by measuring the increase of the

electric impedance, expressed as relative aggregation units (AU), during time. The extent of platelets aggregation was calculated as the AUC from the mean of two electrodes [**54**;**55**]. Finally, the ratio between AUC values and the relative enzymatic concentrations was shown as column bars.

RESULTS AND DISCUSSION

Limited Proteolysis of Prethrombin-2 by Subtilisin and Generation of an Active Specie

The proteolysis between recombinant Pre2 and subtilisin Carlsberg was accomplished in a 1:2000 (w/w) ratio, using a starting reagent concentration (0.1mg/ml) correspondent to the physiologic value of circulating ProT. The reaction was performed at decreasing temperatures (37°C, 25°C, 10°C, 5°C) and described by two complementary techniques. As highlighted from the electrophoretic analysis in **panel 1A**, after 1-min reaction at physiologically relevant temperature (37°C) two major bands, generated from intact Pre2 (313aa, 35872.9Da) appear, migrating at an apparent molecular weight of about 20kDa and 15kDa. This result is confirmed by RP-HPLC analysis displayed in **panel 1F** (**—**), in which the two fragments are eluted at 40.0% and 40.4% of acetonitrile. At longer times, the disappearance of the starting Pre2 is coupled to the generation and digestion of many species from the two first cleavage products, reflecting subtilisin broad specificity. In about 3h (**Fig. 1A**) the complete digestion of the protein species in small peptides can be observed.

At lower temperatures, as shown in **Fig. 1B**, **C**, **D**, **1F** (**—**), Pre2 proteolysis is reasonably slowed down, and subtilisin specificity is greatly increased, with the generation of only three main species, identified by coupled LC-MS analysis. The two first fragments result from the subtilisin-catalysed hydrolysis of Pre2 at the peptide bond Ala149a-Asn149b (according to chymotrypsinogen numbering). In detail, the 20kDa band corresponds to the N-terminal sequence (NT) Ala(-18)-Ala149a (204aa, 23542.9Da); the 15kDa band, on the other hand, corresponds to the C-terminal sequence (CT) Asn149b-Glu247 (109aa, 12348.1Da). Notably the two fragments are not linked by disulphide bridges. At longer reaction times, the NT specie is excised of the segment ($^{-18}$AIEGR^{-14}) and it is further hydrolysed at the peptide bond Tyr14j-Ile14k, slowing converting to the specie we identified as NT* (199aa, 23034.3Da). Remarkably, NT* migrates with an apparent molecular weight higher than NT, consisted with the more relaxed structure, since the two internal peptides generated after the cleavage are linked by the disulphide bridge Cys1-Cys122. All main subtilisin cleavage sites are localized in highly flexible regions: the exposed γ-loop, Pre2 N-terminal sequence, thrombin light chain.

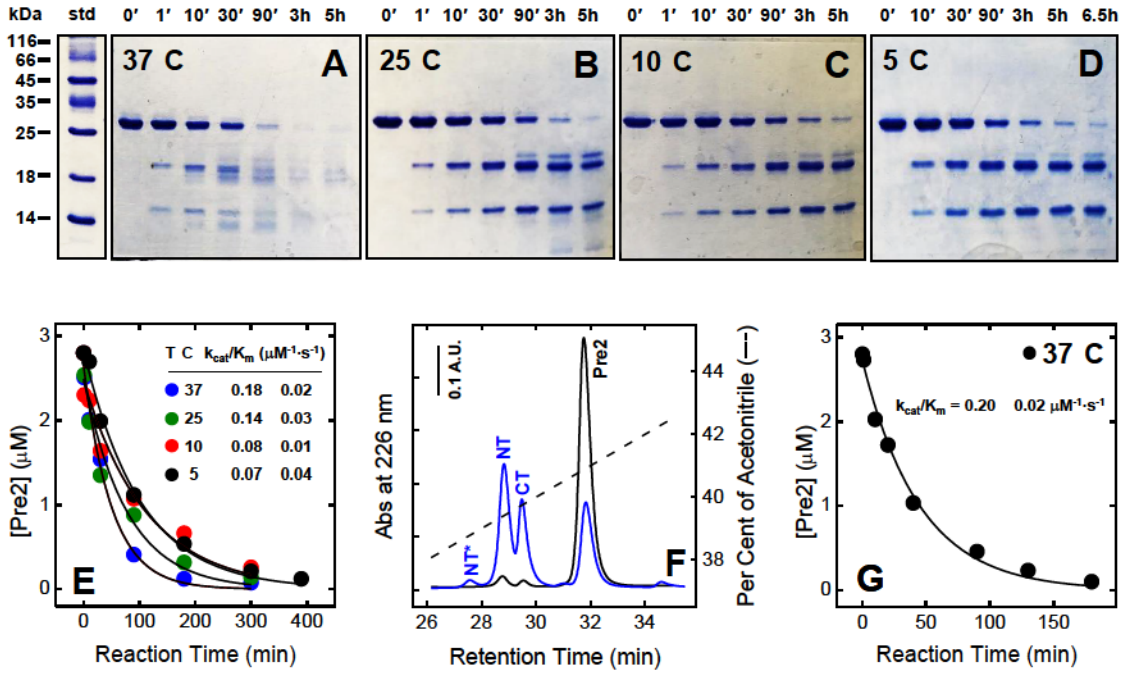

Figure 1. Limited proteolysis of Pre2 with subtilisin. (A-D) Electrophoretic analysis of the time-course reaction of Pre2 with subtilisin. In all the experiments, Pre2 (2.8μM) was reacted at the indicated temperatures in HBS-$CaCl_2$ with subtilisin (1.8nM), at an ezyme:Pre2 ratio of 1:2000 (w/w). At fixed time points, aliquots (50μl) of the proteolysis mixtures were analysed by SDS-PAGE (4-14% acrylamide) under non-reducing conditions, and Coomassie stained. Molecular weight protein standards (std*) was loaded in the left-handed lane. (**E**) **Kinetics of the electrophoretic analysis of subtilisin-catalysed proteolysis of Pre2.** The concentration of residual intact Pre2 at different reaction times was estimated by a densitometric analysis of the gels in panels **A-D**. The data points were fitted with pseudo first order **eq. 1** and **2**, yielding the k_{cat}/K_m values indicated. (**F**) **RP-HPLC analysis of Pre2 proteolysis with subtilisin after 1min at 37°C (—) and after 90min at 10°C (—).** Aliquots (200μl) of the reaction mixtures were loaded onto a C4 analytical column. The protein material eluted from the column was analysed by high-resolution MS: the signs (NT*, NT, CT) near the major chromatographic peaks identify the main proteolytic fragments. (**G**) **Kinetics of the RP-HPLC analysis of subtilisin-catalysed proteolysis of Pre2 at 37°C.** The concentration of intact Pre2 at different reaction times was estimated by integrating the area under the chromatographic peaks of Pre2, as in **panel F**. After data fitting with **eq. 1** and **2**, the k_{cat}/K_m value was calculated as reported.

Kinetic of Pre2 digestion by subtilisin in pseudo-first order conditions was quantified both by SDS-PAGE, for all the temperatures explored, and by RP-HPLC analysis at 37°C, yielding specificity constants comparable for the two techniques (**Fig. 1E**, **G**). The data in **Fig. 2A** indicate that addition of an aliquot of the proteolysis mixture of Pre2 with subtilisin at 37°C to a solution of the αT-specific chromogenic substrate S2238 (D-Phe-Pip-Arg-pNA) results in the release of pNA, as documented by the absorbance increase at 405nm.

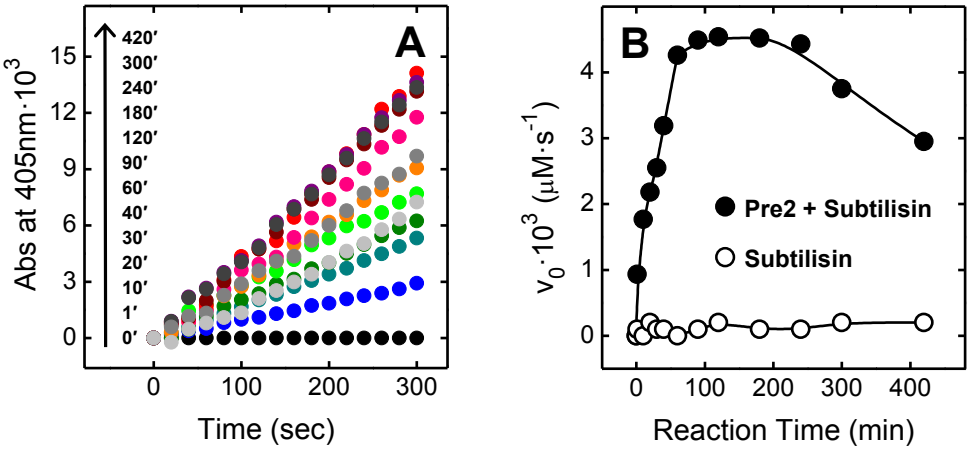

Figure 2. Time-course generation of thrombin-like enzymatic activity during proteolysis of Pre2 by subtilisin (**A**) Pre2 (0.1mg/ml) was treated in HBS-$CaCl_2$ at 37°C with subtilisin (0.05μg/ml). At increasing time points, an aliquot (15μl) of the proteolysis mixture was added to a solution of the chromogenic substrate S2238 (20μM) in HBS. The time-course release of pNA was monitored at 37°C by recording for 300sec the absorbance increase at 405nm. The slope of the straight lines was taken as the initial velocity, v_0, of S2238 hydrolysis by the active αT-like species which were being generated during limited proteolysis of Pre2 with subtilisin. (**B**) (●) Plot of v_0 as a function of the reaction time of Pre2 incubation with subtilisin at 37°C. (○) Blank experiment, performed by incubating S2238 (20μM) with subtilisin (0.05μg/ml) in the absence of Pre2, demonstrates that subtilisin does not cleave the chromogenic substrate.

The plot of the initial rate v_0 of S2238 hydrolysis against the reaction time strongly increases within 90min, reaching a plateau stable until 240min. At longer times (300-420min), the activity of the proteolysis mixture slowly decreases (**Fig. 2B**). Since from the blank experiment it emerges that subtilisin does not cleave S2238, as expected from the protease specificity [**40**], these results provide clear evidence that during the proteolysis of Pre2, a αT-like active specie is generated, able to hydrolyse thrombin chromogenic substrate. We named this new enzyme, displaying significant catalytic activity, σPre2.

Interestingly, from the comparison of the time-course increase of hydrolytic activity (**Fig. 2B**) with the progression of proteolysis reaction at 37°C (**Fig. 1A**), it is conceivable to conclude that σPre2 is the non-covalent complex between NT and CT, containing two stabilizing SS bonds each. The two main fragments NT Ala(-18)-Ala149a and CT Asn149b-Glu247 are generated from subtilisin first cut on recombinant Pre2. Most likely, also NT*, characterized by a more relaxed structure, is still able to contribute to the enzymatic activity. When these active fragments are further degraded by subtilisin in smaller peptides (not detectable by SDS-PAGE in the experimental conditions performed), the non-covalent complex, hold toghether by steric and electrostatic interactions, completely breaks up.

Purification of the Active Thrombin-like Specie (σPre2) derived from Prethrombin-2 Proteolysis by Subtilisin

Since in σPre2 complex non-covalent interactions drive the formation of a stable fragment-complementing system, we focused our efforts on the isolation of this active specie, for further characterization. To maximise the yields of σPre2 production, we performed the proteolysis in the same experimental conditions detailed above, but at 5°C for 15h. Taking advantage of heparin affinity for exosite II, present not only in active αT, but also in its intermediate Pre2, the proteolysis mixture was fractionated on a Heparin Sepharose column, applying an on/off gradient of 0.75M NaCl (**Fig. 3A**). Three samples were collected: one corresponding to the a-specific peak (**1**), at the beginning of the chromatographic course; one during the purification (**2**), and the main peak eluted during the NaCl gradient (**3**).

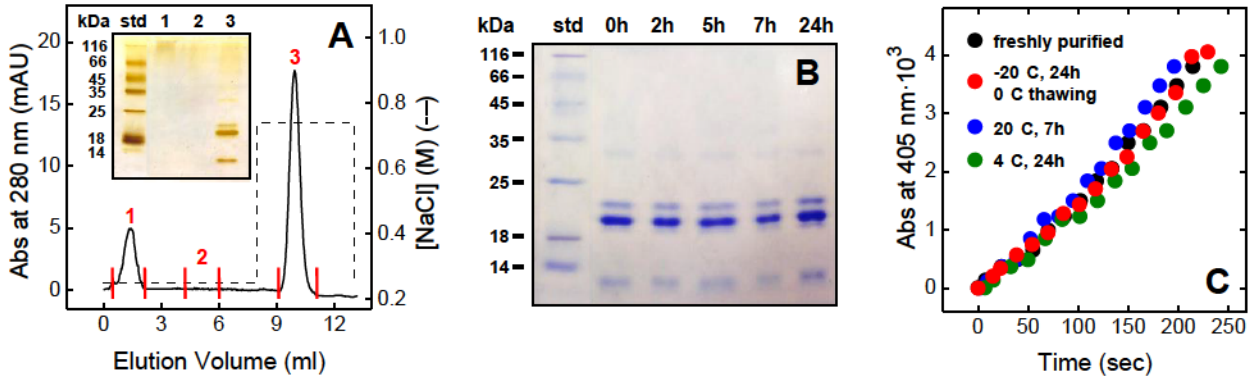

Figure 3. (A) Purification of subtilisin-nicked prethrombin-2 (σPre2). To maximize the yields of σPre2 production, a Pre2 solution (200µg, 0.1mg/ml) was treated for 15h at 5°C with subtilisin (0.05µg/ml) in HBS-$CaCl_2$. The sample was loaded onto a HiTrap Heparin Sepharose affinity column, which was equilibrated with 25mM TRIS-HCl pH 7.4, 0.25M NaCl, and then eluted with the same buffer, containing 1M NaCl. The material eluted in correspondence of fractions 1-3 (0.4-1.0ml) was cold precipitated with TCA for subsequent electrophoretic analysis. (**Inset**) SDS-PAGE (4-14% acrylamide) under non-reducing conditions of the fractions eluted from the affinity column, Silver stained. **(B) Chemical stability of σPre2 upon storage.** Purified σPre2 (1µM) was stored at 20°C for up to 24h. Aliquots (8µg) of aged σPre2 solution were analysed by SDS-PAGE (4-14% acrylamide) under non-reducing conditions and Coomassie stained. **(C) Functional stability of σPre2 upon different storage conditions.** For all the measurements, the time course release of pNA from S2238 (20µM) by σPre2 (10nM) was monitored in HBS at 37°C by recording the absorbance increase at 405nm.

The samples were analysed by SDS-PAGE and subjected to silver staining treatment, to increase the sensitivity (**Fig. 3A, Inset**). The material corresponding to the single chromatographic peak at 0.75M NaCl split in three bands at 22, 20 and 12kDa, identified as the NT*, NT and CT fragments of σPre2. Conversely, the unretained material, eluted with the void volume, did not show the presence of any large polypeptide, and it is likely composed by very small peptides, not detected in the electrophoretic analysis. Moreover, the absence of material in fraction 2 confirms that, in spite of σPre2 non-covalent complex, no material is lost during the flow.

Purified σPre2 was stored for 24h at room temperature, and analysed by SDS-PAGE to check its chemical stability (**Fig. 3B**). Since no further proteolysis is observed during this time, we can conclude that subtilisin is completely removed after the affinity chromatography, and the proteolysis can be stopped without quenching the reaction. Strikingly, material eluted from fraction 3, but not that eluting from fractions 1-2, was able to hydrolyse S2238 and release pNA, retaining stable functional activity in the different storage conditions indicated in **panel 3C**. These evidences altogether confirm that active σPre2 non-covalent complex remains stable and active during time.

Conformational Characterization of Purified σPre2

Conformational characterization of isolated σPre2 was investigated both by circular dichroism in the far-UV and by fluorescence. At a first glance, the shape of the far-UV CD rT spectra suggests the presence of a significant α-helical content (**Fig. 4A**, ─). However, a deeper inspection reveals that the two minima centred at 210 and 225nm are red-shifted of 2-5nm compared to the bands typical of a α-helix conformation, arising at 208nm and 220-222nm. Moreover, the intensity of these bands is unrealistically low for a polypeptide chain characterized by a predominant helical secondary structure. These observations are supported by the experimental evidence that αT crystallographic structure (pdb: 1ppb) is characterized by 14% α-helix and 27% β-sheet contributions.

Human αT is actually a globular protein composed of two asymmetrical β-barrels that comprise the narrow catalytic cleft. The CD signal is therefore highly affected by the contribution of both the aromatic amino acids (9 Trp) and by the four disulphide bridges. Such effects are most prominent in proteins displaying low CD signal intensity and aromatic groups clustered in asymmetric rigid environments [**56**], as in the case of αT. Recombinant Pre2 displays an analogue far-UV CD signal, characterized by quite the same two minima, and by an even lower intensity, due to the overall less rigid structure. Strikingly, σPre2 CD spectra in the far-UV region stands exactly between αT and Pre2 signals, and this protein is likely to be characterized by intermediate features between the zymogen and the wild type enzyme.

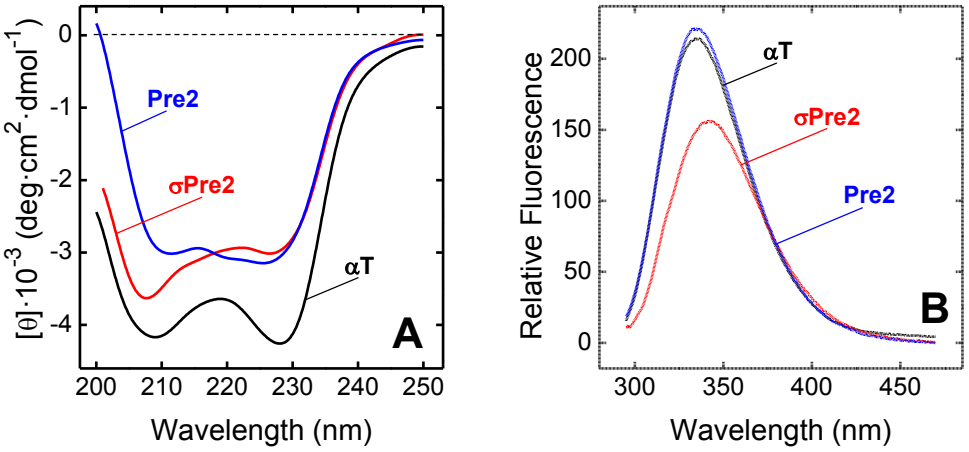

Figure 4. Conformational properties of σPre2, Pre2, and αT. (A) Far-UV CD and (B) fluorescence spectra of purified σPre2 (—), Pre2 (—), and rT (—). CD spectra were recorded at a protein concentration of 2μM in PBS. Fluorescence spectra were taken at a protein concentration of 30nM in TBS, containing 0.2M ChCl, after exciting the protein samples at 280nm. All the measurements were carried out at 25°C and the resulting spectra were corrected for the corresponding baselines.

Interestingly, the lowering of the signal in the region 198-208nm suggests the presence of a random coil contribution in σPre2 signal, likely to be attributable to the amino acids near the hydrolysed Ala149a-Asn149b bond, in the highly flexible and exposed γ-loop.

Since αT, conversely to recombinant Pre2, is an allosteric enzyme modulated by the binding of the Na^+ ion, we accomplished fluorescent measurements in 0.2M ChCl. This ion keeps the physiologic ionic strength, without entering the Na^+ binding site [**57**], thus preventing αT activation and conformation modulation. Overall fluorescence spectra is dominated and derives from the contribution of the nine Trp, localized in the protein in heterogeneous environments [**58**]. In particular, rT and Pre2 display a λ_{max} value at short wavelengths (i.e. 334nm), consistent with the crystallographic structure of human αT, presenting average Trp-residues embedded in chemical environments of medium polarity. Although the three proteins of interest are characterized by a nearly identical amino acid sequence, σPre2 presents a less intense signal compared to recombinant Pre2 and rT, characterized by a maximum centred at 340nm. Both the red shift and the decrease of intensity are likely determined by the change in environment of Trp148. This residue, localized next to the non-canonical hydrolysed bond, becomes more exposed to the solvent and able to explore different conformations in the molecule.

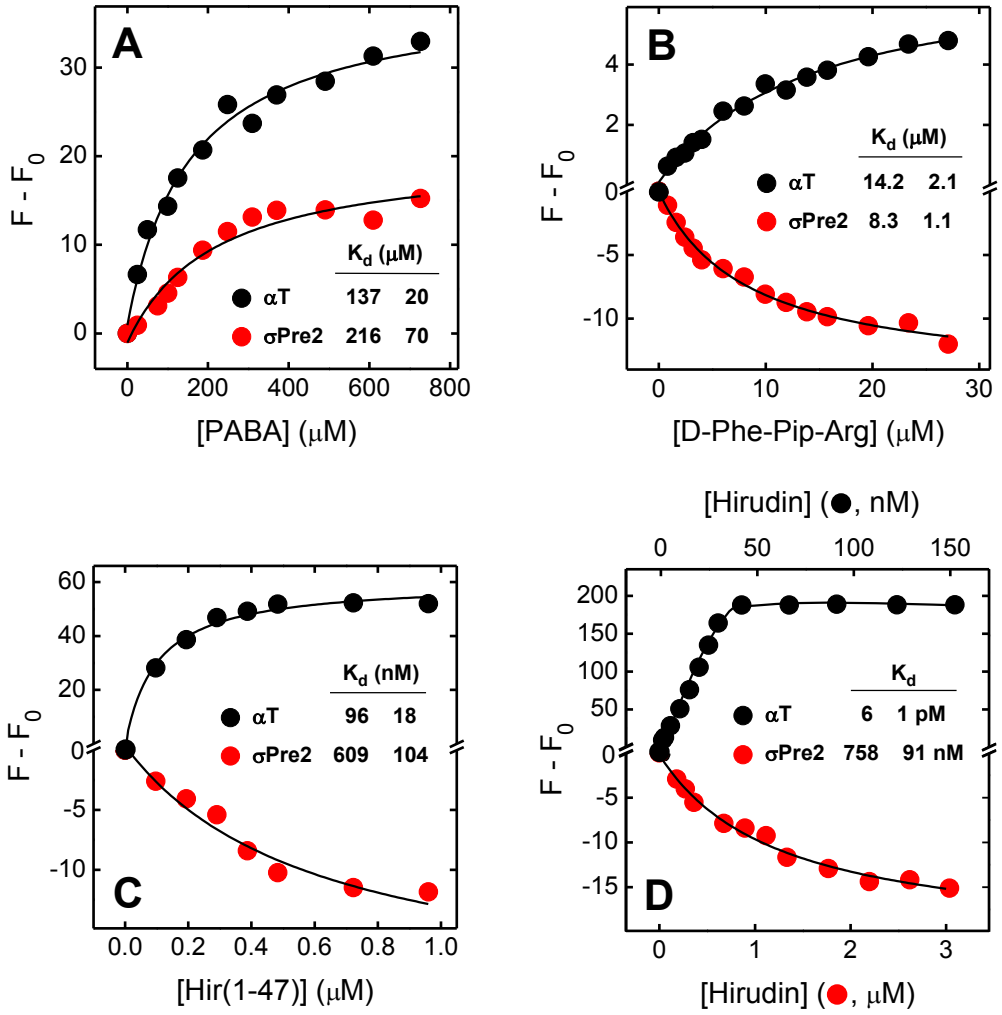

Figure 5. Probing the substrate recognition sites of σPre2 (●) and αT (●) by PABA, FPR, Hir(1-47), and HM2. (**A**) **Binding of PABA.** Protein samples (200nM, 1.5ml) were added with increasing concentrations of PABA and excited at 336nm, while the fluorescence intensity was recorded at 375nm and subtracted of the baseline. After correcting raw fluorescence data for the IFE coefficient, according to **eq. 6**, the data points were fitted with eq. **eq. 4**, describing the one-site binding model, to extract the corresponding K_d values. (**B**) **Binding of FPR.** To a solution of αT or σPre2 (100nM, 1.5ml) were added increasing concentrations of FPR. Protein samples were excited at 280nm, and the fluorescence intensity was recorded at the emission λ_{max} of αT (334nm) or σPre2 (340nm). The data points relative to the binding, subtracted to the corresponding baseline, were interpolated with **eq. 4**. (**C,D**) **Binding of Hir(1-47) and of HM2.** Protein samples of 1.5ml (100nM for Hir(1-47), or 50nm for HM2) were added with increasing concentrations of either Hir(1-47) or HM2, and excited at 295nm. The fluorescence intensity was recorded at the emission λ_{max} of αT (334nm) or σPre2 (340nm). The data points relative to the binding were fitted to **eq. 5**, describing the tight binding model. In all cases, the data were expressed as $F-F_0$, where F_0 is the fluorescence intensity in the absence of ligand. All the measurements were carried out in HBS at 37°C, adding aliquots (2-20μl) of ligands under gentle magnetic stirring.

Mapping σPre2 Three-Dimensional Structure by Fluorescence and Surface Plasmon Resonance

A deeper understanding of σPre2 structure was provided by complementary investigations, performed either with fluorescence titrations or with SPR measurements. The novel active specie was compared to αT or, in few cases, to recombinant Pre2, in the binding of ligands that interact selectively with different recognition areas.

Active Site - Four different species, with increasing dimensions and complexity at the enzyme catalytic pocket, were exploited.

PABA is an aromatic molecule forming a salt bridge with Asp189, deep in the bottom of the primary specificity site S1 [**48**]. As highlighted in **panel 5A**, αT and σPre2 bind PABA with a comparable dissociation constant K_d: 137±20μM and 216±70μM, respectively. Unsurprisingly, increase in ΔF_{max}, due to the hydrophobicity of the environment after PABA interaction with the active cleft is lower in σPre2. Due to its non-canonical activation, σPre2 might organize in a more relaxed and de-structured catalytic cleft, in which PABA could bounce.

FPR is a synthetic peptide mimicking fibrinogen cleavage site. In human αT this ligand orients its bulky residue D-Phe into the aryl binding site S3; Pip (upper Pro homologue) contacts Tyr60a and Trp60d in the S2 site, while Arg harbours Asp189 in the S1 site. Analogously to PABA, αT and σPre2 bind FPR with a comparable dissociation constant K_d: 14.2±2.1μM and 8.3±1.1μM, respectively. Surprisingly, despite their equivalent affinity, the two proteins present an opposite fluorescence trend. FPR interaction with αT induces an increase of the signal, while binding to σPre2 results in a fluorescence decrease (**Fig. 5B**). Also in this case, it is probable that the imperfect complementarity between σPre2 catalytic cleft and FPR moieties results in a deficient binding in which the ligand may produce a collisional quenching.

Hir(1-47) is the N-terminal domain of the potent natural αT inhibitor HM2, produced by limited digestion. This peptide covers αT active site by its β-sheet conformation, and extensively penetrates into the catalytic pocket by its first three amino acids. In detail, Val1 points the S2 site; Ser2 shields the S1 site, without entering; Tyr3 fills the apolar cavity of the S3 site [**59**]. Being this probe bigger than both PABA and FPR, the difference in its affinity with the serine proteases is definitively bigger. Hir(1-47) binds to αT with a K_d of 96±18nM , but interacts to σPre2 with an affinity 6-fold lower: 609±104nM. Like FPR, the inexact binding may result in a collisional quenching effect, supported by the decrease in fluorescence (**Fig. 5C**).

Finally, hirudin HM2 from *Hirudinaria manillensis* is the most potent and specific αT natural inhibitor [**60**]. It is a small polypeptide chain, composed by a compact N-terminal (1-47) core, crosslinked by three disulphide bridges, and by a highly de-structured C-terminal tail. While the N-terminal region interacts with the serine protease active site, especially with the starting tripeptide as detailed above, the C-terminal segment binds to fibrinogen binding site, both by steric and ionic interactions. As displayed in **panel 5D**, binding to this multivalent ligand is dramatically impaired for σPre2. HM2 binds to αT with a K_d of 6±1pM, but interacts to σPre2 with an affinity of 758±91nM. This great discrepancy, in addition to the decreasing fluorescence trend, support once again the collisional quenching effect due to un-matched interactions.

Exosite II and Exosite II- Presence of exosite II in the novel specie σPre2 was determined by the binding to the fragment (268-282) of platelet GpIbα [**61**]. This protein is a receptor to which αT anchors by its exosite II, before triggering platelet aggregation by PARs hydrolysis. Biotinyl-PEG-GpIbα was immobilized to a NeutrAvidin C1 coated sensor chip (**cartoon Fig. 6B**), and solutions of either Pre2, σPre2 or αT were injected in the mobile phase. As displayed in **panel 6A**, **B**, the three investigated proteins bind to the ligand with the same affinity (K_d = 206±4nM for αT; K_d = 120±21nM for Pre2; K_d = 131±42nM for σPre2) and RU_{max}. These results are consistent with the observation that not only αT, but also Pre2 is characterized by a formed exosite II fully competent for the binding [**4**]. Moreover since σPre2 was purified by affinity chromatography in a Heparin Sepharose column, this result absolutely agrees with our expectations.

On the other hand, state of exosite I in σPre2 was investigated through hirugen titration by fluorescence. Hirugen is a synthetic phosphorylated peptide [**43**], corresponding to the C-terminal tail of hirudin HV1 from *Hirudo medicinalis*. As previously anticipated, this probe binds selectively to exosite I by both ionic and steric interactions [**62**]. As highlighted in **panel 6C**, hirugen binds to αT with a K_d of 1.5±0.1μM, but interacts to σPre2 with an affinity about 9-fold lower: 12.8±2.4μM. Even in this experiment, the opposite decreasing fluorescence trend is confirmed. From these evidences, we can deduce that exosite I in σPre2 is not 100% competent for the binding, as in starting Pre2.

Na^+ Loop - Sodium is an important allosteric modulator of αT activity, since its interaction induces a conformational transition from a Na^+-free form, called *slow*, to a Na^+-bound form, called *fast*. While the *fast* form exhibits remarked procoagulant properties, hydrolysing fibrinogen and PARs more efficiently, the *slow* form, more competent for PC activation, features anticoagulant properties [**57**].

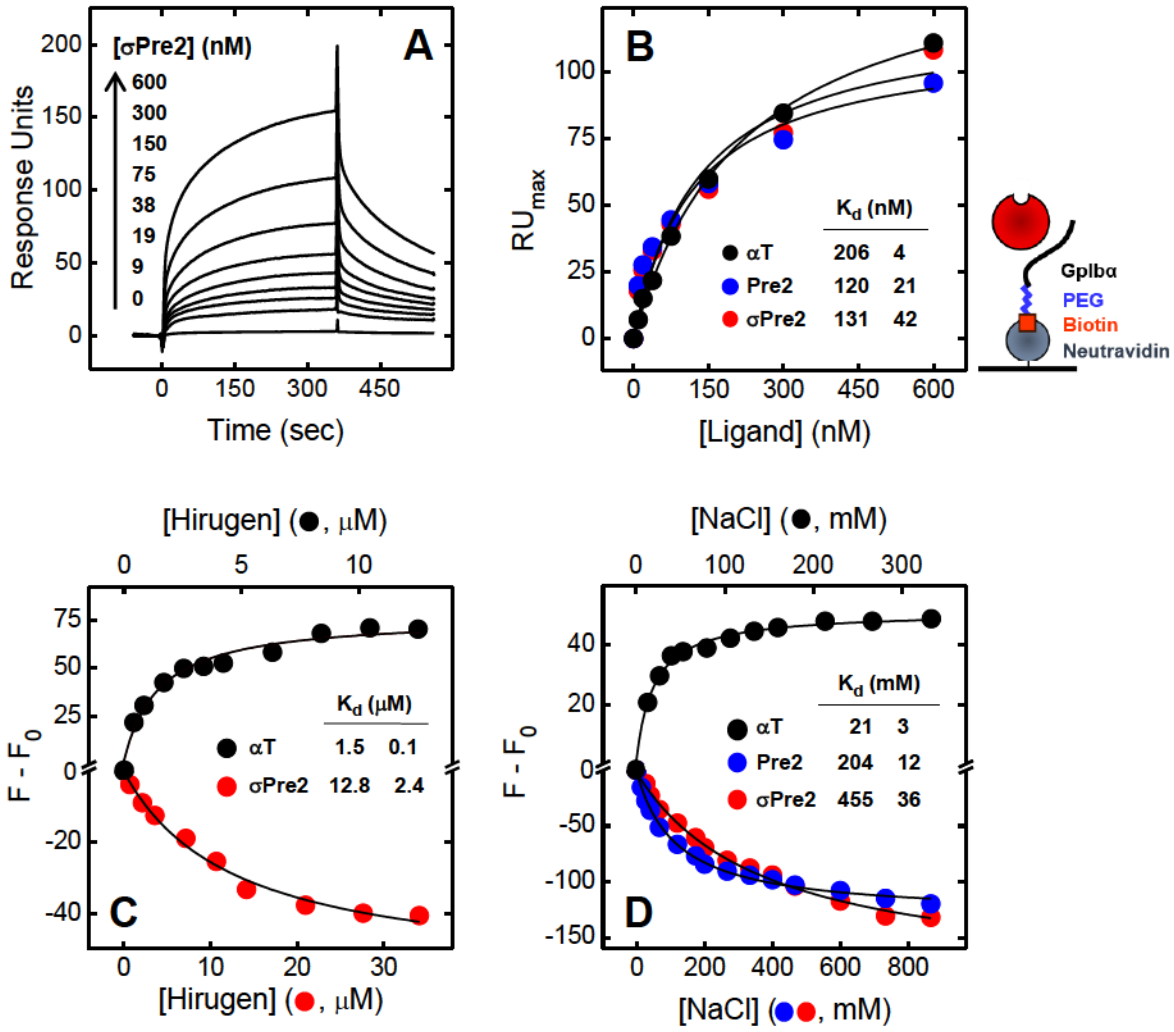

Figure 6. Probing the structure of exosites and of Na^+ binding site of σPre2 (●),Pre2 (●) and αT (●) by fluorescence and SPR. (A,B) SPR analysis of binding to GpIbα(268-282) sensor chip. **(A)** Sensograms relative to the binding of σPre2, Pre2 and αT to biotinyl-PEG-GpIbα(268-282) which was anchored to a Neutravidin-coated C1 chip. **(B)** Plot of RU_{eq} versus the protein concentrations. The data points were interpolated with **eq. 7** to yield K_d values displayed in the panel. **(C) Fluorescence binding of hirugen to σPre2 and αT.** Protein samples of 1.5ml (50nM for αT, 150nM for σPre2) were added with increasing hirugen concentrations at 37°C in HBS **(D) Fluorescence binding of sodium to σPre2, Pre2, and αT.** Samples (15nM, 1.5ml) were added with increasing NaCl concentrations at 25°C in TBS. The ionic strength was kept constant with ChCl. For all the fluorescence measurements **(C,D)**, the samples were excited at 280nm and the fluorescence emission was recorded at 334nm for αT and Pre2, and at 340nm for σPre2. The data are presented as $F - F_0$, where F_0 is the fluorescence intensity in the absence of ligand. The K_d values for hirugen or Na^+ binding were determined by interpolating the data points with **eq. 4**, as indicated.

In mature αT, Na^+-binding site is located 15-20Å away from the catalytic cleft, in a solvent-filled cavity behind S1 specificity pocket, next to Asp189 (5Å). For its binding, Na^+ ion is coordinated octaedrically by the oxygens of the carbonyl groups of Arg221a and Lys224, and by four buried water molecules. In turn, these residues are stabilized by ionic pairs with Glu217, Asp221, Asp222 and Tyr225. In particular, the salt bridge Glu146-Arg221a freezes the 148-loop in a more rigid and open conformation [**8**].

In σPre2, due to cleavage between Ala149a and Asn149b, the highly flexible 148-loop is reasonably totally exposed to the solvent (as suggested from the protein fluorescence spectra). In this scenario, Glu146, next to the scissile bond, should overcome a huge entropic barrier to be engaged in the salt bridge with Arg221a. Lacking this stabilizing interaction, in σPre2 Na^+-binding site is likely to be destroyed. These structural observations totally agree with the fluorescence Na^+ titration experiment performed with Pre2, σPre2 and αT. As displayed in **panel 6D**, while Na^+ binds to αT with a K_d of 21±3mM , it interacts to both Pre2 and σPre2 with an affinity about 10- and 20-fold lower respectively: 204±12mM and 455±36mM, as expected.

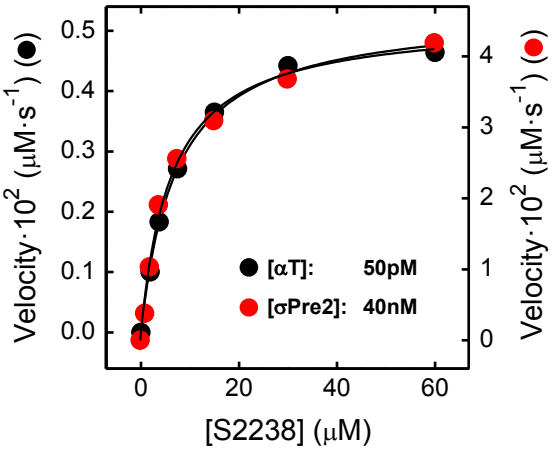

	k_{cat} (s^{-1})	K_m (μM)	k_{cat}/K_m ($\mu M^{-1} \cdot s^{-1}$)
αT	106.6 ± 2.2	7.2 ± 0.5	14.8 ± 0.1
σPre2	1.2 ± 0.1	6.6 ± 1.2	0.17 ± 0.01

Figure 7 and Table 1. Determination of the enzyme kinetic constants, k_{cat} and K_m, of σPre2 (●) and αT (●) for the hydrolysis of chromogenic substrate S2238. The initial rate of pNA release from S2238 by purified σPre2 (40nM) and αT (50pM) was measured at 405nm in HBS (200μl final volume) at 37°C. Form the interpolation of the data points with the Michaelis-Menten equation, k_{cat} and K_m values were obtained as best-fit parameters.

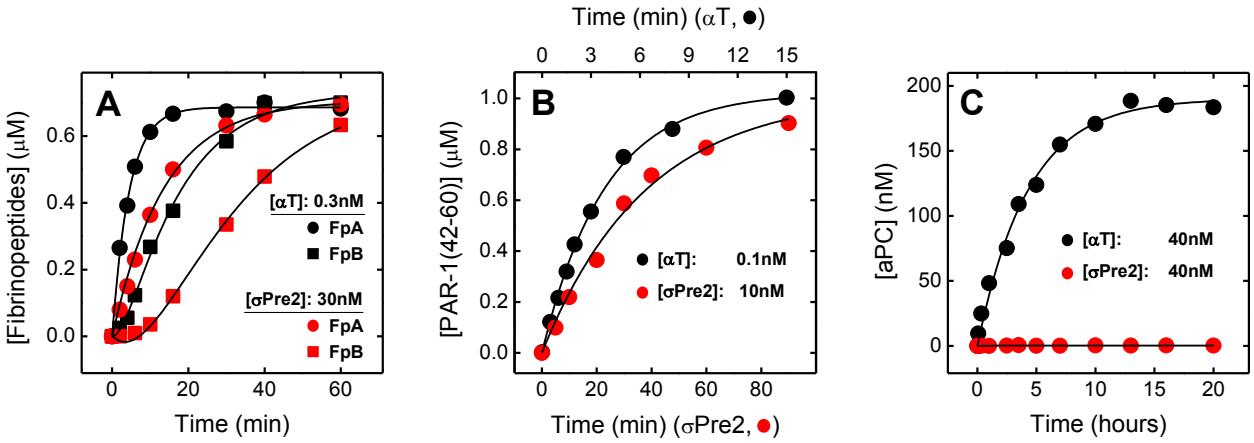

Figure 8. Cleavage of physiological thrombin substrates by σPre2. (A) Release of the fibrinopeptides from human fibrinogen. The release of FpA (●, ●) and FpB (■, ■) from human fibrinogen (0.35μM) by purified σPre2 (30nM) (●, ■) or αT (0.3nM) (●,■) was carried out at 37°C in HBS, and quantified by RP-HPLC at 205nm (**see Experimentals**). For σPre2, interpolation of the data points with **eq. 9** or **10**, yielded the specificity constants k_{catA}/K_{mA} = 0.042±0.001$s^{-1}\cdot\mu M^{-1}$ and k_{catB}/K_{mB} = 0.036±0.008$s^{-1}\cdot\mu M^{-1}$ for FpA and FpB release, respectively. For comparison, the specificity constants of αT were determined as: k_{catA}/K_{mA} = 12.5±0.6$s^{-1}\cdot\mu M^{-1}$ and k_{catB}/K_{mB} = 3.7±0.8$s^{-1}\cdot\mu M^{-1}$. **(B) Cleavage of PAR1(38-60).** The cleavage of PAR1(38-60) peptide (1μM) by σPre2 (10nM) (●) or αT (0.1nM) (●) was carried out at 25°C in HBS. The time course of PAR1(42-60) fragment release was quantified by RP-HPLC and the data points were fitted with **eq. 11**. The following k_{cat}/K_m values were estimated as best-fit parameters: σPre2, k_{cat}/K_m = 0.044±0.005$s^{-1}\cdot\mu M^{-1}$; αT, k_{cat}/K_m = 43.3±1.5$s^{-1}\cdot\mu M^{-1}$. **(C) Activation of PC zymogen in the absence of TM.** σPre2 (40nM) (●) or human αT (40nM) (●) were added to a solution of PC (200nM) at 37°C in HBS. At fixed time points, an aliquot (10μl) of the proteolysis mixture was added to a solution (150μl) of the chromogenic substrate S2366 (200μM), containing 1μM HM2 to selectively block σPre2/αT. The concentration of the newly generated aPC was determined at 37°C by measuring the rate of the aPC-specific substrate S2366 hydrolysis at 405nm, after comparison with a standard curve. For αT, the apparent specificity constant of PC hydrolysis was estimated as k_{cat}/K_m = 1.6±0.1$s^{-1}\cdot mM^{-1}$, while the maximum concentration of aPC at t→∞, $[aPC]_\infty$, was extrapolated as 190±4nM, in agreement with the starting PC concentration. For σPre2, instead, no significant aPC generation could be detected.

Active σPre2 Hydrolyses Thrombin Procoagulant Substrates

To investigate σPre2 catalytic efficiency, its kinetic constants k_{cat} and K_m, relative to S2238 hydrolysis, were determined by standard Michaelis-Menten treatment. Analysis of the data in **Fig. 7** revealed that σPre2 hydrolyses S2238 with a specificity constant (k_{cat}/K_m) about ≈90-fold lower than αT, mainly due to a selective decrease (by 89-fold) of the catalytic constant (k_{cat}), whereas the Michaelis-Menten constant (K_m) was slightly decreased (by 1.1-fold) (**see Table 1**). The invariance of K_m strongly suggests that the substrate specificity sites S1, S2 and S3 are fully formed in σPre2, as

confirmed from FPR binding by fluorescence (K_d = 8.3±1.1μM). On the other hand, the marked decrease of k_{cat} indicates that that the catalytic machinery leading to peptide bond hydrolysis through the transition state is somewhat altered. However, this is not surprising, since the amino acids forming the catalytic triad are located on distinct fragments in σPre2 non-covalent complex. In particular, His57 and Asp102 are located in the NT fragment, whereas Ser195 is on the CT fragment (**Fig. 10C**): this might perturb the optimal stereochemistry and efficient coupling of the residues in the catalytic pocket.

Once determined the order of magnitude (roughly 1:100) of σPre2 catalytic activity compared to mature αT, we investigated the novel protease efficiency in the proteolysis of thrombin procoagulant (fibrinogen), proaggregant (PAR-1) and anticoagulant (PC) substrates. All the assays were performed in a 1:100 (M/M) ratio, except for PC activation (equivalent σPre2 and αT concentrations of 40nM), to work in pseudo-first order kinetic conditions (**see Experimentals**).

αT most important procoagulant function is undoubtedly fibrin generation from fibrinogen, circulating in the plasma as a dimer of three chains $(A\alpha B\beta\gamma)_2$. First, the serine protease binds to the macromolecule by its exosite I, and hydrolyses fibrinogen A-chains, with the rapid release of two FpA (16aa) and fibrin monomer I. The latters undergoes longitudinal elongation, assembling in double-stranded protofibrils. In a second stage, αT cleaves fibrinogen B-chains, with the slower generation of two FpB (14aa) and lateral association of the protofibrils, resulting in the generation of insoluble fibrin fibers. The kinetic data relative to fibrinopeptides generation were analyzed according to Shafer's model [**49**]. For σPre2, the specificity constants (k_{cat}/K_m) extracted from the data in **panel 8A** are of 0.042±0.001$s^{-1}\cdot\mu M^{-1}$, and of 0.036±0.008$s^{-1}\cdot\mu M^{-1}$ for FpA and FpB release, respectively. For comparison, the specificity constants of αT were determined as k_{catA}/K_{mA} = 12.5±0.6$s^{-1}\cdot\mu M^{-1}$ and k_{catB}/K_{mB} = 3.7±0.8$s^{-1}\cdot\mu M^{-1}$, identical to those reported earlier. These values indicate that in the same experimental conditions the release of FpA and of FpB triggered by σPre2 are respectively ≈300-fold and ≈100-fold slower. The discrepancy between these values suggest that fibrin I monomer release is the rate limiting step of the process, and when several molecules organize in the double-stranded protofibrils, FpB is easily released.

As for fibrinogen, even PAR-1 receptor proteolysis is mediated by exosite I binding, for properly orientating the substrate in the protease active site for efficient cleavage [**63**]. Notably, PAR-1(38-60) peptide reproduces the substrate binding properties of the extracellular receptor domain, as it contains both the exosite-I binding sequence and the scissile bond Arg41-Ser42 for αT. Unexpectedly, the (k_{cat}/K_m) value of PAR-1(38-60) hydrolysis by σPre2 is of 0.044±0.005$s^{-1}\cdot\mu M^{-1}$, about ≈1000-fold lower than the value calculated for αT (43.3±1.5$s^{-1}\cdot\mu M^{-1}$) (**Fig. 8B**), identical to

that previously estimated [**64**]. This surprisingly low value may be caused by an anti-cooperative effect between exosite I and active site, due to an imperfect PAR-1 binding.

Finally, regarding PC activation in the absence of TM, no significant effect could be detected for σPre2, while αT assay confirmed the values calculated before [**54**], yielding k_{cat}/K_m = 1.6±0.1 $s^{-1}\cdot mM^{-1}$, and aPC concentration at t→∞ as 190±4nM, in agreement with the starting PC concentration. The absence of proteolysis is likely to be due not to an altered specificity of σPre2, but rather to the experimental conditions accomplished.

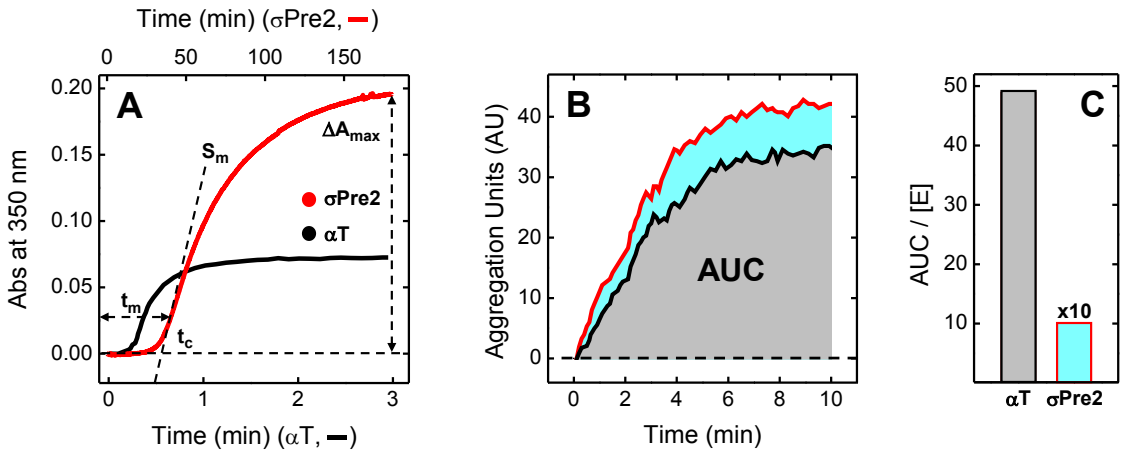

Figure 9. Fibrin generation and platelets aggregation. (A) Turbidimetric analysis of fibrin generation induced by σPre2 (—) or αT (—). To a human fibrinogen solution (440nM, 800µl) in HBS, was added σPre2 (50nM) or αT (50nM), and the time course increase of turbidity was detected by monitoring the absorbance at 350nm and 37°C. For clarity, the lower time scale (0-3min) refers to the experiment run with αT (—), while the upper scale (0-180min) refers to the experiment run with σPre2 (—). The absorbance scale for both experiments is the same (0-0.2 AU). From each clotting curve, the values of S_m, t_m, t_c, and ΔA_{max} were extracted (**see text**). σPre2: $S_m = 2.6\times10^{-3}$ AU·min^{-1}; t_m = 44min; t_c = 32min; ΔA_{max} = 0.196 AU; αT: $S_m = 3.4\times10^{-3}$ AU·s^{-1}; t_m = 18s; t_c = 14s; ΔA_{max} = 0.072AU. **(B) Impedance aggregometry analysis of platelet aggregation induced by σPre2 (—) or αT (—) in whole blood.** The aggregation curves represent the time-dependent change of the plasma impedance, expressed as relative aggregation units (AU). Integration of AU over time (10min) gives the AUC value for σPre2 (cyan) and αT (grey). Whole blood from healthy donors (300µl) was diluted with HBS (320µl), containing αT or σPre2 to a final concentration of 0.5nM and 50nM, respectively. (**C**) Histograms of the AUC/[E] ratio for σPre2 (cyan bar) and αT (black bar), where [E] is the enzyme concentration. Each value is the average of single determinations on a blood sample from two healthy donors.

σPre2 Exerts α-Thrombin Procoagulant Functions

Once established that this novel enzyme is able to hydrolyse αT physiologic procoagulant substrates, σPre2-induced fibrin generation and platelets aggregation were analysed.

The multi-step process leading to the generation of the insoluble fibrin network results in a Sol→Gel transition of the solution, that can be easily studied by a turbidimetric assay. By adding the same concentrations of σPre2 or αT to a human fibrinogen solution, the plot of turbidity (i.e. absorbance at 350nm) versus time results in the characteristic sigmoidal clotting curves (**Fig. 9A**). Four parameters were extracted from each clotting curve: 1) S_m, the maximum slope (increase in turbidity-per-unit time) at the inflection point of the clotting curve; 2) t_m, the time needed to reach S_m; 3) t_c, the clotting time, obtained as the intercept of the tangent line at S_m with the time axis (zero absorbance baseline); 4) ΔA_{max}, the maximum difference of absorbance recorded between t=0 and t→∞ [**53**]. With respect to αT ($S_m = 3.4x10^{-3} AU \cdot s^{-1}$; $t_m = 18s$; $t_c = 14s$; $\Delta A_{max} = 0.072AU$), the clotting curve generated by σPre2 is characterized by a longer lag phase ($t_m = 44min$; $t_c = 32min$) a lower slope at the inflexion point ($S_m = 2.6x10^{-3} AU \cdot min^{-1}$) and by a higher final turbidity ($\Delta A_{max} = 0.196AU$). In other words, compared to the same αT concentration, the σPre2-induced fibrin clot is a network delayed in time, in which double strand protofibrils assemble slower. The resulting fibers are less in number, but thicker in bundle size, resulting in a higher turbidity. The increased lag phase is in accord with the observation that σPre2 releases FpA and FpB with a specificity constant about 300- and 100-fold less, as previously described (**Fig. 8A**). These experimental results reflect the physical features of a fibrin network generated by a low αT concentration [**65**]. Since σPre2 catalytic efficiency is about 100-fold less than mature αT, it is reasonable that, in order to achieve the same clot structure, a bigger enzymatic concentration is required.

αT activates platelets through the interaction with receptor GpIbα and subsequent cleavage of surface PARs [**66**]. *In vivo*, after a vascular damage, platelets aggregation is the very first defence step boosted, responding even to minimal αT concentrations. Platelets aggregation was investigated in whole blood, with Multiple Electrode Aggregometer (MEA), using cuvettes equipped with a couple of electrodes. In non-clotted blood, inactive platelets stick to the electrodes, organizing in a monolayer. After the addition of an aggregant exogenous agonist (i.e. αT or ADP), platelets generate pseudopods and adhere to the pre-existing monolayer, thus increasing plasma electric impedance, which is measured by the relative aggregation units (AU) in a time-course of 10min. Integration of area under the curve (AUC) during the analysis time represents the aggregation response, given as a mean of the impedance between a couple of electrodes [**55**]. Diluting a sample of whole blood with a solution of σPre2 (50nM) or αT (0.5nM) yielded AUC values of 55 and 62, respectively (**Fig. 9B**).

In conclusion, a 100-fold more concentrated σPre2 solution, used as aggregant agonist, elicits the same effect of αT-induced platelets aggregation.

From the previous mapping experiments it resulted that σPre2 binds with its exosite II to GpIbα with an affinity analogue to αT and Pre2 (**Fig. 6B**), while it loses 1000-fold catalytic efficiency in in the hydrolysis of PAR-1 (**Fig. 8B**). On the platelet surface, anchoring to GpIbα is propedeutical to the subsequent cleavage of PAR-1, and the two favourable interactions act in a cooperative way to trigger platelets activation [**66**]. This molecular mechanism explains and is in accord to the kinetic data of receptor proteolysis and macroscopic platelets activation.

CONCLUSIONS

Coagulation and inflammation are two tightly connected systems, enhancing each other in a physio-pathological context [**10**]. In particular, coagulation triggering during the early stages of the infections could act as an innate immunity effector, since bleeding sites are potential accesses to microbial pathogens [**21**]. If natural anticoagulant mechanisms fail to control this vicious circle, pathological manifestations, like sepsis, can occur. Sepsis is a life-threatening condition in which a detrimental and exaggerated immune response outcomes in host's tissue damages and organ failures. In addition, systematically activated coagulation can lead to DIC [**27**]. In this scenario, exogenous pathogens may be harmful not only for inflammatory manifestations, but also by directly activating the coagulation cascade.

The central reaction of the coagulation cascade is the conversion of ProT (579aa, 72.3kDa) to mature αT (295aa, 36.7kDa) [**4**]. The active enzyme, in turn, plays a pivotal role in the haemostatic equilibrium, entailing both procoagulant and anticoagulant functions [**8**]. *In vivo*, ProT is activated by FXa at two consequent sites (Arg271/Arg320) producing two mutually exclusive intermediates, of which Pre2 (cleavage at Arg271 first) is the most physiologically relevant. Conversely, proteases from foreign sources can trigger ProT alternative activation pathways. Among these, snake venom proteases [**30**] have been extensively described, while little is known about microbial proteases.

In this work, we present a novel alternative activation of recombinant Pre2 (313aa, 35.8kDa), by subtilisin Carlsberg from *Bacillus subtilis*, to a new active enzyme, we named σPre2. The specie derives from subtilisin-catalysed non-physiologic cleavage of Ala149a-Asn149b peptide bond, in the highly flexible γ-loop (**Fig. 10B**).

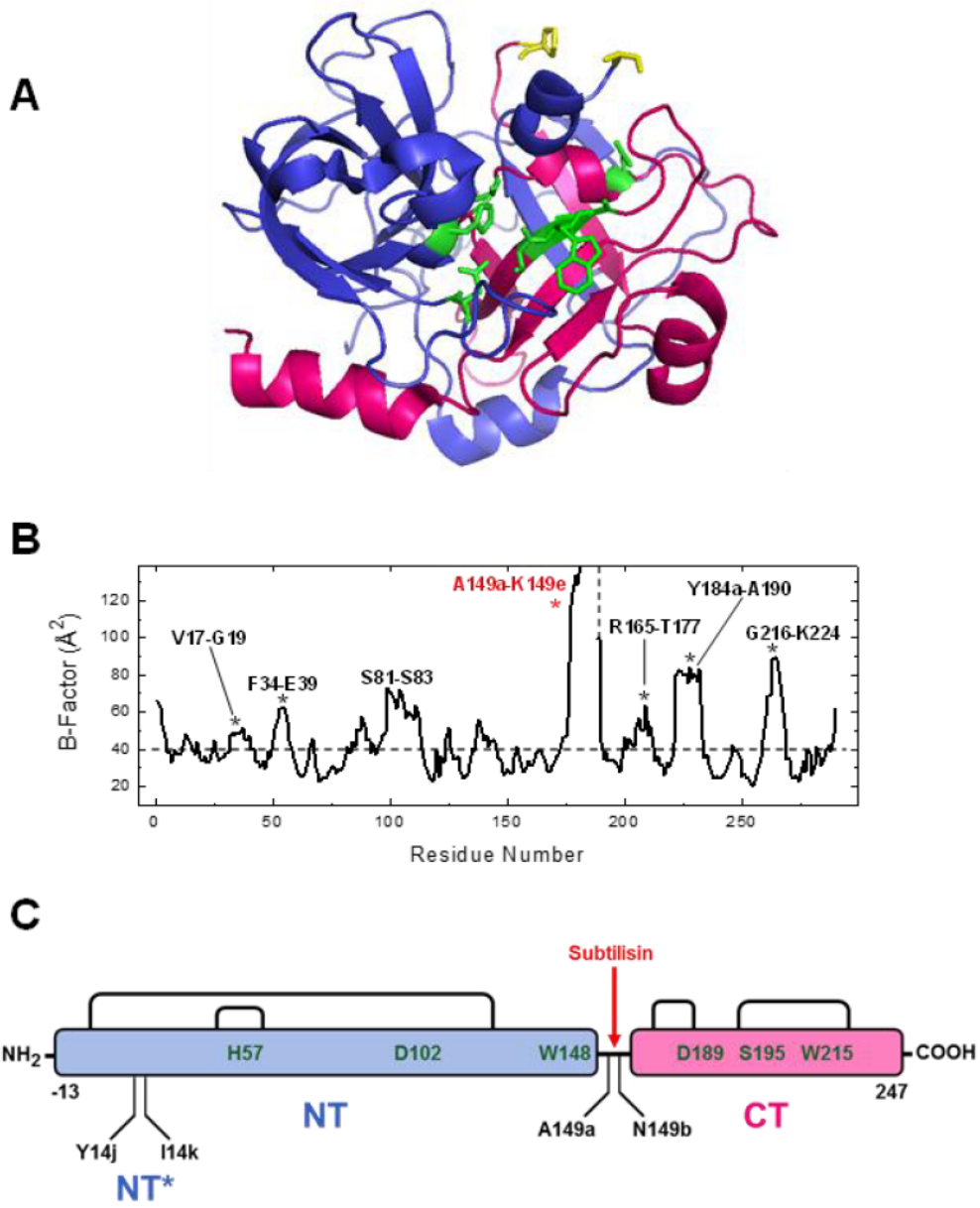

Figure 10. Schematic representations of subtilisin cleavages on wild type Pre2. (A) Three-dimensional S195A Pre2 mutant in the open conformation structure (pdb: 3sqh), displayed in σPre2 colour-coded architecture domains. NT domain Thr(-13)-Ala149a is showed in blue, while CT domain Asn149b-Glu247 is displayed in pink. The amino acids of the catalytic triad (His57, Asp102, Ala195), the oxyanion hole (Asp189, Gly193) and the highly hydrophobic 214-216 segment are represented by green sticks. In this open conformation, highly flexible γ-loop (^{149b}NVGKGQ^{151}) could not be crystallized; Ala149a and Pro152 are displayed by yellow sticks. **(B) Average B-Factor plot of Pre2 in open conformation.** The most flexible Pre2 regions, according to the B-factor plot, are highlighted; γ-loop is stressed in red. **(C) Subtilisin-catalysed cleavages on Pre2 wild type.** Schematic representation of subtilisin-catalysed cleavages on Pre2, giving rise to σPre2 non-covalent complex. Once again, NT and CT, both characterized by two internal SS bonds, are displayed in blue and pink, respectively; the amino acids composing the catalytic cleft are stressed in green. Subtilisin first cleavage site, between Ala149a and Asn149b, is highlighted by a red arrow. NT* derives from an additional cleavage performed at the bond Tyr14j-Ile14k: the two generated internal fragments are held together by a SS bond between Cys1 and Cys122.

The resulting protease is a non-covalent complex between the NT domain Ala(-18)-Ala149a, and the CT domain Asn149b-Glu247, displayed respectively in blue and pink in **panel 10A**. Moreover, a second internal cleavage between Tyr14j and Ile14k, performed in NT fragment after the excision of ($^{-18}$AIEGR^{-14}), gives rise to the fragment NT*, in which the two internal peptides are held together by a disulphide bridge (**Fig. 10C**). Beside subtilisin broad specificity, at a physiologically relevant temperature (37°C) in a 1:2000 (w/w) enzyme:substrate ratio, the thrombin-like activity of the newly generated σPre2 lasts for at least 7h, reaching a plateau at 4h. We maximised the yield of σPre2 production by performing the proteolysis at 5°C for 15h; after that, the specie of interest was purified by affinity chromatography on a Heparin Sepharose column.

Active σPre2 is characterized by a less rigid catalytic cleft in which the specificity sites S1, S2, S3 are moulded; exosite II is fully competent for the binding, while exosite I features an imperfect conformation. The novel specie does not carry the Na^+-binding site, so it is likely to lack allosteric modulation. Steady-states kinetics revealed that σPre2 hydrolyses αT-substrate S2238 with the same affinity (K_m), but with an impaired conversion to the final product release (k_{cat}), resulting in 100-fold decrease in catalytic efficiency. In accord with these results, σPre2 cleaves αT procoagulant substrates fibrinogen and PAR-1(38-60) with a decreased (from100- to 1000-fold) specificity constant (k_{cat}/K_m). No activity has been detected toward the anticoagulant PC in the absence of TM. Finally, σPre2 is able to accomplish fibrin generation and platelets aggregation in whole blood, with a catalytic efficiency comparable to the previous kinetic measurements.

This intriguing discovery sheds new light to the intricate coagulation/inflammation network triggered during microbial infections. Moreover, this non-canonical σPre2 proteolysis study can be used as model for the poorly characterized extracellular subtilisin-like proteases secreted by pathogen microorganisms. Future perspectives will be the study of the molecular mechanisms of σPre2 activation through the non-canonical subtilisin-catalysed cleavage, and the investigation of ProT eventual activation.

REFERENCES

[1] Macfarlane RG. An Enzyme Cascade in the Blood Clotting Mechanism, and its Function as a Biochemical Amplifier. Nature 1964 May 2;202:498-499.

[2] Rosing J, Tans G, Govers-Riemslag JW, Zwaal RF, Hemker HC. The role of phospholipids and factor Va in the prothrombinase complex. J Biol Chem 1980 Jan 10;255(1):274-283.

[3] Nesheim ME, Taswell JB, Mann KG. The contribution of bovine Factor V and Factor Va to the activity of prothrombinase. J Biol Chem 1979 Nov 10;254(21):10952-10962.

[4] Pozzi N, Chen Z, Pelc LA, Shropshire DB, Di Cera E. The linker connecting the two kringles plays a key role in prothrombin activation. Proc Natl Acad Sci U S A 2014 May 27;111(21):7630-7635.

[5] Bradford HN, Krishnaswamy S. Meizothrombin is an unexpectedly zymogen-like variant of thrombin. J Biol Chem 2012 Aug 31;287(36):30414-30425.

[6] Bode W, Mayr I, Baumann U, Huber R, Stone SR, Hofsteenge J. The refined 1.9 A crystal structure of human alpha-thrombin: interaction with D-Phe-Pro-Arg chloromethylketone and significance of the Tyr-Pro-Pro-Trp insertion segment. EMBO J 1989 Nov;8(11):3467-3475.

[7] Bing DH, Cory M, Fenton JW,2nd. Exo-site affinity labeling of human thrombins. Similar labeling on the A chain and B chain/fragments of clotting alpha- and nonclotting gamma/beta-thrombins. J Biol Chem 1977 Nov 25;252(22):8027-8034.

[8] Di Cera E. Thrombin as procoagulant and anticoagulant. J Thromb Haemost 2007 Jul;5 Suppl 1:196-202.

[9] Esmon CT. The protein C pathway. Chest 2003 Sep;124(3 Suppl):26S-32S.

[10] Esmon CT. The interactions between inflammation and coagulation. Br J Haematol 2005 Nov;131(4):417-430.

[11] Wolbink GJ, Bossink AW, Groeneveld AB, de Groot MC, Thijs LG, Hack CE. Complement activation in patients with sepsis is in part mediated by C-reactive protein. J Infect Dis 1998 Jan;177(1):81-87.

[12] Nystedt S, Ramakrishnan V, Sundelin J. The proteinase-activated receptor 2 is induced by inflammatory mediators in human endothelial cells. Comparison with the thrombin receptor. J Biol Chem 1996 Jun 21;271(25):14910-14915.

[13] Bernardo A, Ball C, Nolasco L, Moake JF, Dong JF. Effects of inflammatory cytokines on the release and cleavage of the endothelial cell-derived ultralarge von Willebrand factor multimers under flow. Blood 2004 Jul 1;104(1):100-106.

[14] Devaraj S, Xu DY, Jialal I. C-reactive protein increases plasminogen activator inhibitor-1 expression and activity in human aortic endothelial cells: implications for the metabolic syndrome and atherothrombosis. Circulation 2003 Jan 28;107(3):398-404.

[15] Camerer E, Rottingen JA, Gjernes E, Larsen K, Skartlien AH, Iversen JG, et al. Coagulation factors VIIa and Xa induce cell signaling leading to up-regulation of the egr-1 gene. J Biol Chem 1999 Nov 5;274(45):32225-32233.

[16] Cunningham MA, Romas P, Hutchinson P, Holdsworth SR, Tipping PG. Tissue factor and factor VIIa receptor/ligand interactions induce proinflammatory effects in macrophages. Blood 1999 Nov 15;94(10):3413-3420.

[17] Szaba FM, Smiley ST. Roles for thrombin and fibrin(ogen) in cytokine/chemokine production and macrophage adhesion in vivo. Blood 2002 Feb 1;99(3):1053-1059.

[18] Loike JD, el Khoury J, Cao L, Richards CP, Rascoff H, Mandeville JT, et al. Fibrin regulates neutrophil migration in response to interleukin 8, leukotriene B4, tumor necrosis factor, and formyl-methionyl-leucyl-phenylalanine. J Exp Med 1995 May 1;181(5):1763-1772.

[19] Henn V, Slupsky JR, Grafe M, Anagnostopoulos I, Forster R, Muller-Berghaus G, et al. CD40 ligand on activated platelets triggers an inflammatory reaction of endothelial cells. Nature 1998 Feb 5;391(6667):591-594.

[20] Day SM, Reeve JL, Pedersen B, Farris DM, Myers DD, Im M, et al. Macrovascular thrombosis is driven by tissue factor derived primarily from the blood vessel wall. Blood 2005 Jan 1;105(1):192-198.

[21] Engelmann B, Massberg S. Thrombosis as an intravascular effector of innate immunity. Nat Rev Immunol 2013 Jan;13(1):34-45.

[22] Fukudome K, Esmon CT. Identification, cloning, and regulation of a novel endothelial cell protein C/activated protein C receptor. J Biol Chem 1994 Oct 21;269(42):26486-26491.

[23] Oganesyan V, Oganesyan N, Terzyan S, Qu D, Dauter Z, Esmon NL, et al. The crystal structure of the endothelial protein C receptor and a bound phospholipid. J Biol Chem 2002 Jul 12;277(28):24851-24854.

[24] Edgington TS, Ruf W, Rehemtulla A, Mackman N. The molecular biology of initiation of coagulation by tissue factor. Curr Stud Hematol Blood Transfus 1991;(58)(58):15-21.

[25] Levin J. The horseshoe crab: a model for gram-negative sepsis in marine organisms and humans. Prog Clin Biol Res 1988;272:3-15.

[26] Levi M, van der Poll T. Inflammation and coagulation. Crit Care Med 2010 Feb;38(2 Suppl):S26-34.

[27] Angus DC, van der Poll T. Severe sepsis and septic shock. N Engl J Med 2013 Nov 21;369(21):2063.

[28] Hotchkiss RS, Monneret G, Payen D. Immunosuppression in sepsis: a novel understanding of the disorder and a new therapeutic approach. Lancet Infect Dis 2013 Mar;13(3):260-268.

[29] de Stoppelaar SF, van 't Veer C, van der Poll T. The role of platelets in sepsis. Thromb Haemost 2014 Oct;112(4):666-677.

[30] Kini RM. The intriguing world of prothrombin activators from snake venom. Toxicon 2005 Jun 15;45(8):1133-1145.

[31] Wegrzynowicz Z, Heczko PB, Drapeau GR, Jeljaszewicz J, Pulverer G. Prothrombin activation by a metalloprotease from Staphylococcus aureus. J Clin Microbiol 1980 Aug;12(2):138-139.

[32] Narasaki R, Kuribayashi H, Shimizu K, Imamura D, Sato T, Hasumi K. Bacillolysin MA, a novel bacterial metalloproteinase that produces angiostatin-like fragments from plasminogen and activates protease zymogens in the coagulation and fibrinolysis systems. J Biol Chem 2005 Apr 8;280(14):14278-14287.

[33] Imamura T, Banbula A, Pereira PJ, Travis J, Potempa J. Activation of human prothrombin by arginine-specific cysteine proteinases (Gingipains R) from porphyromonas gingivalis. J Biol Chem 2001 Jun 1;276(22):18984-18991.

[34] Liu C, Matsushita Y, Shimizu K, Makimura K, Hasumi K. Activation of prothrombin by two subtilisin-like serine proteases from Acremonium sp. Biochem Biophys Res Commun 2007 Jun 22;358(1):356-362.

[35] Oggioni MR, Pozzi G, Valensin PE, Galieni P, Bigazzi C. Recurrent septicemia in an immunocompromised patient due to probiotic strains of Bacillus subtilis. J Clin Microbiol 1998 Jan;36(1):325-326.

[36] Linderstrøm-Lang K, Ottesen M. Nature 1947; 159(807).

[37] Guntelberg AV, ottesen M. Purification of the proteolytic enzyme from Bacillus subtilis. C R Trav Lab Carlsberg Chim 1954;29(3-4):36-48.

[38] Smith EL, DeLange RJ, Evans WH, Landon M, Markland FS. Subtilisin Carlsberg. J Biol Chem 1968 May10;243(9):2184-2191.

[39] Bode W, Papakamos E, Musil D. The high-resolution X-ray crystal structure of the complex formed between subtilisin Carlsberg and eglin c, an elastase inhibitor from the leech *Hirudo medicinalis*. Eur J Biochem 1987 Jan;166:673-692.

[40] Bratovanova EK, Petkov DD. Glycine flanked by hydrophobic bulky amino acid residues as minimal sequence for effective subtilisin catalysis. Biochem J 1987 Dec;15(248):957-960.

[41] Lee S, Jang DJ. Progressive rearrangement of subtilisin Carlsberg into orderly and inflexible conformation with Ca2+ binding. Bioph J 2001 Nov;81:2972-2978.

[42] De Cristofaro R, De Filippis V. Interaction of the 268-282 region of glycoprotein Ibalpha with the heparin-binding site of thrombin inhibits the enzyme activation of factor VIII. Biochem J 2003 Jul 15;373(Pt 2):593-601.

[43] De Filippis V, Colombo G, Russo I, Spadari B, Fontana A. Probing the hirudin-thrombin interaction by incorporation of noncoded amino acids and molecular dynamics simulation. Biochemistry 2002 Nov 19;41(46):13556-13569.

[44] Sokolov AV, Acquasaliente L, Kostevich VA, Frasson R, Zakharova ET, Pontarollo G, et al. Thrombin inhibits the anti-myeloperoxidase and ferroxidase functions of ceruloplasmin: relevance in rheumatoid arthritis. Free Radic Biol Med 2015 Sep;86:279-294.

[45] DiBella EE, Maurer MC, Scheraga HA. Expression and folding of recombinant bovine prethrombin-2 and its activation to thrombin. J Biol Chem 1995 Jan 6;270(1):163-169.

[46] Lakowicz, J.R. (1999) Principles of Fluorescence Spectroscopy 2nd ed., Kluwer Academic/Plenum, New York

[47] Copeland, R. A. (2000) Kinetics of Single-Substrate Enzyme Reactions. In Enzymes, pp. 109-145, Wiley-VHC Inc., New York

[48] Evans SA, Olson ST, Shore JD. p-Aminobenzamidine as a fluorescent probe for the active site of serine proteases. J Biol Chem 1982 Mar 25;257(6):3014-3017.

[49] Ng AS, Lewis SD, Shafer JA. Quantifying thrombin-catalyzed release of fibrinopeptides from fibrinogen using high-performance liquid chromatography. Methods Enzymol 1993;222:341-358.

[50] Arosio D, Ayala YM, Di Cera E. Mutation of W215 compromises thrombin cleavage of fibrinogen, but not of PAR-1 or protein C. Biochemistry 2000 Jul 11;39(27):8095-8101.

[51] Pozzi N, Barranco-Medina S, Chen Z, Di Cera E. Exposure of R169 controls protein C activation and autoactivation. Blood 2012 Jul 19;120(3):664-670.

[52] Di Cera E, Dang QD, Ayala YM. Molecular mechanisms of thrombin function. Cell Mol Life Sci 1997 Sep;53(9):701-730.

[53] De Cristofaro R, Di Cera E. Phenomenological analysis of the clotting curve. J Protein Chem 1991 Oct;10(5):455-468.

[54] Pozzi N, Acquasaliente L, Frasson R, Cristiani A, Moro S, Banzato A, et al. beta2 -Glycoprotein I binds to thrombin and selectively inhibits the enzyme procoagulant functions. J Thromb Haemost 2013 Jun;11(6):1093-1102.

[55] Toth O, Calatzis A, Penz S, Losonczy H, Siess W. Multiple electrode aggregometry: a new device to measure platelet aggregation in whole blood. Thromb Haemost 2006 Dec;96(6):781-788.

[56] Brahms S, Brahms J. Determination of protein secondary structure in solution by vacuum ultraviolet circular dichroism. J Mol Biol 1980 Apr;138(2):149-178.

[57] De Filippis V, De Dea E, Lucatello F, Frasson R. Effect of Na+ binding on the conformation, stability and molecular recognition properties of thrombin. Biochem J 2005 Sep 1;390(Pt 2):485-492.

[58] Bell R, Stevens WK, Jia Z, Samis J, Cote HC, MacGillivray RT, et al. Fluorescence properties and functional roles of tryptophan residues 60d, 96, 148, 207, and 215 of thrombin. J Biol Chem 2000 Sep 22;275(38):29513-29520.

[59] De Filippis V, Vindigni A, Altichieri L, Fontana A. Core domain of hirudin from the leech Hirudinaria manillensis: chemical synthesis, purification, and characterization of a Trp3 analog of fragment 1-47. Biochemistry 1995 Jul 25;34(29):9552-9564.

[60] Scacheri E, Nitti G, Valsasina B, Orsini G, Visco C, Ferrera M, et al. Novel hirudin variants from the leech Hirudinaria manillensis. Amino acid sequence, cDNA cloning and genomic organization. Eur J Biochem 1993 May 15;214(1):295-304.

[61] Lancellotti S, Rutella S, De Filippis V, Pozzi N, Rocca B, De Cristofaro R. Fibrinogen-elongated gamma chain inhibits thrombin-induced platelet response, hindering the interaction with different receptors. J Biol Chem 2008 Oct 31;283(44):30193-30204.

[62] Naski MC, Fenton JW,2nd, Maraganore JM, Olson ST, Shafer JA. The COOH-terminal domain of hirudin. An exosite-directed competitive inhibitor of the action of alpha-thrombin on fibrinogen. J Biol Chem 1990 Aug 15;265(23):13484-13489.

[63] Bock, P. E., Panizzi, P. and Verhamme, I. M. (2007) Exosites in the substrate specificity of blood coagulation reactions. J. Thromb. Haemost. 5 Suppl 1, 81-94. doi:JTH2496 [pii]

[64] Ayala, Y. M., Cantwell, A. M., Rose, T., Bush, L. A., Arosio, D. and Di Cera, E. (2001) Molecular mapping of thrombin-receptor interactions. Proteins. 45, 107-116. doi:10.1002/prot.1130 [pii]

[65] Weisel, J. W. and Nagaswami, C. (1992) Computer modeling of fibrin polymerization kinetics correlated with electron microscope and turbidity observations: Clot structure and assembly are kinetically controlled. Biophys. J. 63, 111-128. doi:S0006-3495(92)81594-1 [pii]

[66] De Candia, E., Hall, S. W., Rutella, S., Landolfi, R., Andrews, R. K. and De Cristofaro, R.(2001) Binding of thrombin to glycoprotein ib accelerates the hydrolysis of par-1 on intact platelets.J. Biol. Chem. 276, 4692-4698. doi:10.1074/jbc.M008160200 [doi]

CHAPTER 3.3

Alternative Proteolytic Activation of Human Prothrombin by a Bacterial Protease: A Link between Sepsis and Thrombosis

---

INTRODUCTION

Inflammation and haemostasis, traditionally regarded as two distinct defence systems, are intimately connected, enhancing each other in a vicious circle [**1**]. In detail, inflammatory mediators increase platelets count and reactivity [**2**], while stimulating the production of ultra-large von Willebrand Factor multimers [**3**] and of fibrinogen. Moreover, they impair the natural fibrinolytic and anticoagulant systems. In acute inflammation antithrombin (ATIII) is consumed and/or inactivated [**4**], heparin is diminished by neutrophil products [**5**], and protein C (PC) pathway is affected in all its components. In detail, both thrombomodulin (TM) and endothelial protein C receptor (EPCR) are downregulated by cytokines, and TM is further hydrolysed by neutrophil elastase [**6**]. In addition, several cytokines induce the expression of both protease activated receptors (PARs) [**7**] and tissue factor (TF) [**8**] on endothelial cells, facilitating their interaction with monocytes. Activation of the complement system provides key available surfaces on which clotting can start [**9**]. Since injuries in the vessel walls are potential access sites for microorganisms, the generation of a blood clot may trap and kill the invading pathogen. In this scenario, local activation of coagulation represents a first-line regulator of immune response [**10**].

On the other hand, coagulation factors and platelets endorse inflammation. In detail, both TF-FVIIa complex [**11**] and fibrin(ogen) [**12**] trigger cytokine expression and release. Moreover, activated platelets express on their surface P-selectin, a leukocyte chemoattractant molecule. In turn, stimulated monocytes release microparticles carrying on their surface P-selectin glycoprotein ligand-1 (PSGL-1) and TF. Beyond releasing vasoactive substances from the granules, platelets amplify coagulation by recruiting the monocyte microparticles through the (P-selectin)-(PSGL-1) interaction. Once concentrated on the site of vessel injury, microparticles trigger the coagulation cascade by their surface TF [**13**;**14**;**15**].

The interplay between these two systems, along with the hypothesis that the involved molecular actors derive from common ancestors, is supported by the evidence that anticoagulant pathways, beyond coagulation, dampen inflammatory manifestations. While TF inhibitory pathway

role is still matter of debate, ATIII-heparin and PC pathways down-regulatory functions are well characterized. Both the pathways decrease the expression of cytokines and TF in leukocytes and endothelial cells [**16**;**17**], inhibit NF-κB signalling in monocytes [**18**;**19**], and impair chemokine-induced neutrophils migration and adhesion to endothelium [**20**;**21**]. In addition, TM alone exhibits an anti-inflammatory effect through its lectin-like domain [**22**], and when bound to αT it physically abrogates cleavage of surface PARs.

Since inflammation enhances coagulation, which in turn upregulates inflammation, if the natural anticoagulant mechanisms fail to control the coagulation/inflammation interface, severe pathologic manifestations, like sepsis, occur. Sepsis is a life-threatening condition, in which hyper-stimulated immune system, systematically activated in order to fight an invading pathogen, is detrimental for the host itself. This exaggerated acute inflammatory response results in tissue damages and organ failures, with high morbidity and mortality [**23**;**24**]. Along with inflammation, uncontrolled coagulation may lead to disseminated intravascular coagulation (DIC), a clinical syndrome in which the generation of scattered thrombi is coupled to sequestration of the coagulation factors, with a general unbalanced haemorrhagic state [**10**]. In this context, the exogenous proteases secreted during infections may be harmful not only for the stimulation of inflammatory responses, but also for the direct activation of coagulation, thus bypassing the natural regulatory mechanisms.

The key reaction of the coagulation cascade, at the meeting between the intrinsic and the extrinsic pathway, is prothrombin (ProT) activation to mature α-thrombin (αT) [**25**]. Human ProT (579aa, 72.3kDa), carrying three N-glycosylations at N78, N100 and N373, can be structurally divided in three regions. Fragment 1 (1-155) containing Gla domain and kringle-1 (K1); fragment 2 (156-271) encompassing kringle-2 (K2); and the protease domain (272-579). Three highly flexible linkers connect the domains: Lnk1 (47-64), between Gla and K1; Lnk2 (144-169), between K1 and K2; Lnk3 (249-284), between K2 and the protease domain. The inactive ProT, circulating in the plasma (0.1mg/ml) as a single chain, is proteolytically converted to mature αT, by FXa, at two sites (Arg271 and Arg320) [**26**]. The reaction is greatly increased (k_{cat}>3000-fold) when catalysed by the prothrombinase complex, in which FXa works along with cofactors FVa and Ca^{2+} on a negatively charged surface [**27**;**28**]. Depending on which cleavage is performed first, two physiologic intermediates can be generated *in vivo*. If the first cleavage occurs at Arg271, fragment 1·2 is released, with the generation of inactive prethrombin-2 (Pre2). Pre2 (308aa, 38.2kDa) is the most relevant physiologic intermediate, since this pathway is preferred on the surface of activated platelets [**29**]. Conversely, if the first cleavage occurs at Arg320, active site is moulded, with the generation of meizothrombin (579aa, 72.3kDa), held together by a disulphide bridge [**30**]. Active αT is released after the accomplishment of the missing cleavage and an auto-proteolysis at R284.

The proteolysis at Arg320(15)-Ile321(16) bond (chymotrypsinogen numbering) generates a novel N-terminal strand, ending with the apolar Ile16-Val17 segment. According to the "molecular sexuality" theory suggested by Bode and Huber [**31**], this segment penetrates the preformed Ile16 pocket, forming a critical salt bridge between the ammonium group of Ile16 and the carboxylate group of Asp524(194). Since this salt bridge is buried in the protein core, the energy released upon electrostatic coupling triggers a dramatic conformational change, with the formation of the substrate-binding site and of the oxyanionic hole, both required for catalysis. Mature αT (295aa, 36.7kDa) is an ellipsoidal protein, glycosylated at N60g (former N373), composed of a light and a heavy chain, linked together by a disulphide bridge. This serine protease plays a pivotal role in haemostasis, exerting both pro- and anticoagulant functions. In detail, procoagulant actions entail platelets aggregation (primary haemostasis) and fibrin generation (secondary haemostasis).

Exogenous proteases can activate ProT both by proteolytic or non-proteolytic mechanisms. The most strikingly example is undoubted provided by snake venom proteases. These toxins are either metalloproteinases or enzymes structurally similar to mammalian FXa and FVa, able to cleave inactive ProT, releasing meizothrombin or wild type mature αT [**32**]. Moreover, metalloproteinases from *Bacillus megaterium* [**33**], and cysteine proteases from *Porphyromonas gingivalis* [**34**], activate the zymogen at the physiologic sites. On the other side, the prototype of non-proteolytic ProT activation is staphylocoagulase (SC) from *Staphylococcus aureus*. In the SC(1-325)·(pro)thrombin complex, unravelled by Friedrich and co-workers, SC N-terminal Ile1-Val2 enters the Ile16 pocket, mimicking the newly generated N-terminal Ile16-Val17 segment after FXa cleavage [**35**;**36**].

Regarding other microbial proteases involved in sepsis, little is known, due to difficulties in their biochemical characterization. In the early infection stages, both surface and secreted proteases are likely to play a detrimental role in inflammatory manifestations. In particular, several microorganisms express and release subtilases, i.e. subtilisin-like serine proteases. The subtilisins are an extensive class of extracellular, alkaline bacterial proteases, first identified in the 40's by Linderstrøm-Lang and Ottesen, and purified by Güntelberg and Ottesen [**37**;**38**]. In detail, subtilisin Carlsberg (274aa, 27.3kDa) is a serine protease secreted from *Bacillus subtilis* and *B. licheniformis* [**39**]. This enzyme features two Ca^{2+} binding sites [**40**], crucial for both its stability and activity, and a broad specificity of cleavage, preferring aromatic or apolar residues [**41**]. Although bacteria expressing subtilisin Carlsberg are not dramatically pathogenic [**42**], this well-characterized and commercially available enzyme can be used as a model for the whole class of subtilases. A recent study demonstrates that two subtilisin-like proteases from the fungus *Acremonium sp.* proteolitically activate ProT at a non-canonical cleavage site [**43**].

Moreover, preliminary experiments performed in our Laboratory revealed that subtilisin activates recombinant Pre2, to a novel specie we named σPre2. Hence, we decided to investigate the possible role of subtilisin in ProT activation during infections, exploring the effect on fibrin generation and platelets activation after bacterial invasion.

EXPERIMENTALS

Reagents

Natural human αT and ProT were purchased from Haematologic Technologies (Essex Junction, VT, USA). The concentrations the solutions were determined by measuring the absorbance at 280nm, using an absorptivity coefficient of 1.964$mg^{-1}\cdot cm^2$ for αT, and of 1.681$mg^{-1}\cdot cm^2$ for ProT. Subtilisin Carlsberg (Subtilopeptidase A) from *Bacillus subtilis*, fibrinogen from human plasma, BSA, KNCO, all salts, solvents and reagents of analytical grade were purchased from Sigma (St. Louis, MO, USA). The chromogenic substrates S2238 (D-Phe-Pip-Arg-pNA), S2366 (pyroGlu-Pro-Arg-pNA) and S2765 (Arg-Gly-Arg-pNA) were from Chromogenix (Milan, Italy).

Chromogenic Substrate S2238 Hydrolysis by Subtilisin-nicked Prothrombin

A solution of ProT (0.1mg/ml) was added to subtilisin (0.05μg/ml) in HBS-$CaCl_2$ buffer at 37°C. At fixed time points (0, 1, 10, 20, 30, 40, 50, 80, 120, 180, 240, 360, 420min) an aliquot (28μl) of the reaction mixture was added to a solution of S2238 (20μM) in a final volume of 800μl of HBS buffer. The time-course release of pNA was monitored by recording the absorbance at 405nm for 7min at 37°C on a Jasco (Tokyo, Japan) V-630 spectrophotometer, equipped with a PAC-743 Peltier thermostat. The slope of the straight lines, taken as the initial velocity v_0 of the hydrolysis, was correlated to the released pNA concentration using the molar absorptivity coefficient of 9920$M^{-1}\cdot cm^{-1}$, and plotted versus reaction times. The experimental data points were compared to the hydrolysis rates achieved by performing the same experiment in the absence of starting ProT.

Proteolysis of Prothrombin by Subtilisin

A solution of ProT (0.1mg/ml) was subjected to proteolysis by subtilisin (0.05µg/ml) in HBS-$CaCl_2$ buffer, at decreasing temperatures: 37°C, 20°C, and 10°C. At fixed time points, an aliquot (100µl) of the reaction mixture was quenched by 2.5µl H_2O-TFA 4% (v/v) and cold precipitated in TCA. The analysed times were: 0, 1, 10, 30, 90min, 3, 5h for the reaction at 37°C; 0, 10min, 1, 2, 6, 9, 14h for the reaction at 20°C; 0, 10min, 1, 5, 8, 15, 24h for the reaction at 10°C. The samples were analysed by SDS-PAGE (4-14% acrylamide) under non-reducing conditions, and Coomassie stained.

After performing the proteolysis at 37°C in the same conditions detailed above, the reaction mixture was analysed by RP-HPLC from Jasco (Tokyo, Japan). At fixed time points, an aliquot (200µl) of the solution was quenched by 5µl H_2O-TFA 4% (v/v) and loaded onto a (4.6x150mm, 5µM, 300Å) C4 Vydac analytical column (Hesperia, CA, USA). The samples were eluted with a linear acetonitrile-0.078% TFA biphasic gradient of 5-35% in 15min and 35-55% in 35min, at a flow rate of 0.8ml/min.

Identification of the Subtilisin-Catalysed Proteolysis Fragments

To characterize subtilisin proteolysis products, different stages of the reaction were explored by coupled LC-MS on an Agilent 1290 Infinity Binary UHPLC (Santa Clara, CA, USA) connected to a Xevo G2-S Q-TOF apparatus from Waters (Milford, MA, USA). The proteolysis was accomplished at 10°C in the same enzyme:substrate ratio of 1:2000 (w/w), but in HBS-$CaCl_2$ without PEG-8000. At the fixed time points detailed above (0, 10min, 1, 5, 8, 15, 24h), an aliquot of 20µl of the solution was quenched by 0.5µl H_2O-TFA 4% (v/v) and loaded on a (1.0x50mm, 5µM, 300Å) C4 Vydac Microbore analytical column (Hesperia, CA, USA), eluted with a linear acetonitrile-0.1% HCOOH gradient of 15-65% in 30min, at a flow rate of 0.05ml/min. The effluent from the column was on-line analysed in the positive ion mode. Typical experimental conditions were: capillary potential, 1.5kV; sampling cone, 40; source temperature, 100°C; desolvation gas temperature, 350°C. The mass versus charge signals, visualized as BPI (base peak intensity) by the program MassLynx V4.1, were deconvoluted by the software MaxEnt1 to achieve the peaks average masses. Subtilisin cleavage sites on ProT sequence were identified by comparing the so obtained experimental values with the theoretical assigned fragments molecular weight, calculated on the amino acidic composition, disulphide bridges, Gla residues and carbohydrate moieties.

Purification of Subtilisin-nicked Prothrombin (σPre2)

For micro-purification purposes, a solution of ProT (300μg, 0.1mg/ml) was treated with subtilisin (0.05μg/ml) in HBS-$CaCl_2$ buffer for 24h at 10°C. This aliquot was loaded on a 1ml HiTrap (7.0x25mm) Heparin Sepharose column connected to an ÄKTA purifier system, both from GE Healthcare (Little Chalfont, UK). The column was equilibrated with 25mM TRIS-HCl pH 7.4, 0.25M NaCl, and the sample was eluted by applying an on/off gradient of 65% 25mM TRIS-HCl pH 7.4, 1M NaCl, at a flow rate of 0.5ml/min. 200μl-aliquots of the three fractions (F1, F2, and F3) collected from the chromatographic course were cold precipitated in TCA, analysed by SDS-PAGE (4-14% acrylamide) under non-reducing conditions, and Coomassie stained.

On the other hand, an aliquot of 60μl from each fraction was immediately added to a solution of 20μM S2238 in HBS, in a final volume of 800μl. The time-course release of pNA was monitored by recording the absorbance at 405nm for 10min at 37°C on a Jasco (Tokyo, Japan) V-630 spectrophotometer, equipped with a PAC-743 thermostat. F3 sample, the only one active towards the chromogenic substrate, was stored for 24h at 4°C, and after that, an aliquot (60μl) was functionally analysed as detailed above. The active specie, deriving from ProT proteolysis by subtilisin, was named σPre2.

Proteolysis of Chromogenic Substrates by σPre2

The specificity of Heparin Sepharose-purified σPre2 was checked against three different substrates. Aliquots of σPre2 or commercial αT were added to a solution (20μM) either of S2238, S2366 or S2765 in 800μl HBS, to a final concentration of 30nM or 100pM, respectively. In all the experiments, the time-course release of pNA was monitored by recording the absorbance at 405nm for 30min at 37°C on a Jasco (Tokyo, Japan) V-630 spectrophotometer, equipped with a PAC-743 thermostat.

Steady-state kinetics of S2238 substrate hydrolysis were investigated at 37°C on a Victor3 plate reader from PerkinElmer (Waltham, MA, USA) on a 96-well polystyrene plate from Sigma (St. Louis, MO, USA). To a solution of σPre2 (30nM) or αT (50pM) were added decreasing (60-0μM, by 1:2 dilutions) concentrations of S2238 in a final volume of 200μl HBS. The time-course release of pNA was monitored by recording the absorbance at 405nm for 5min at 37°C. The slope of the straight lines, taken as the initial velocity v_0 of the hydrolysis, was correlated to the respective released pNA concentration using molar absorptivity coefficient of $9920 M^{-1} \cdot cm^{-1}$. The hydrolysis rates (v), plotted versus the starting substrate concentrations, were interpolated by the Michaelis-Menten **equation 1**, obtaining k_{cat} and K_m as fitting parameters.

$$v = \frac{V_{max} \cdot [S]}{K_m + [S]} \qquad \textbf{(Eq. 1)}$$

where $V_{max} = k_{cat} \cdot [E]$ is the maximum rate of the reaction at fixed enzyme concentration, and [S] is S2238 concentration.

Fibrin Generation

Turbidimetric analysis of fibrin generation were performed at 37°C on a Jasco (Tokyo, Japan) V-630 spectrophotometer, equipped with a PAC-743 thermostat. Human fibrinogen was desalted on a Sephadex G10 resin from Sigma (St. Louis, MO, USA), manually packed in a (8x125mm) column, eluted with HBS buffer at a flow rate of 0.3ml/min. To a solution of desalted fibrinogen (440nM, 800µl) were added either σPre2 or αT to a final concentration of 50nM. The Sol→Gel transition was measured at 350nm for a time course interval of 100min for σPre2, or 3min for αT. The so obtained sigmoidal clotting curves were dissected to extrapolate t_c, S_m, t_m and ΔA_{max} as clotting parameters [**44**].

Platelets Aggregation Assay

The effect of σPre2 on platelets aggregation was quantified in whole blood (WB) and gel-filtered platelets (GFP), and compared to the response induced by αT. The measurements were accomplished by multiple electrode aggregometer (MEA) with a multiplate analyser from Dynabyte medical (Munich, Germany). Normal, citrate-treated venous blood samples were taken from two healthy non-smokers donors: all the analysis were performed within three hours from the withdrawn. The donors gave written informed consent for participation in this study, which was approved by the Ethical Committee of the University Hospital of Padua. An aliquot of WB was centrifuged (800rpm, 15min) to obtain platelets-rich plasma (PRP). In turn, GFP were purified by filtering PRP on a Sepharose 2B resin (40000000-70000 MW) from Sigma (St. Louis, MO, USA), manually packed in a (10x250mm) column, equilibrated with Tyrode buffer: 20mM HEPES pH 7.4, 135mM NaCl, 5mM KCl, 5.5mM glucose, 0.2% BSA. Aliquots (300µl) of WB or GFP (platelets count ≈200000/µl) were diluted with solutions of either σPre2 or αT in HBS (320µl) to a final concentration of 50nM and 0.5nM, respectively. All the measures were accomplished at 37°C, with vigorous stirring, for 10min. The aggregation rate was quantified by measuring the increase of the electric impedance, expressed as relative aggregation units (AU), during time. The extent of platelets aggregation was calculated as the AUC from the mean of two electrodes [**45**;**46**]. Finally, the ratio between AUC values and the relative enzymatic concentrations was shown as column bars.

Carbamylation of σPre2 and αT N-terminals by KNCO

Carbamylation of σPre2 or αT amino-terminals was accomplished by reacting the proteins of interest with KNCO. To simplify the derivatization detection, active σPre2 was produced from recombinant Pre2, expressed in our Laboratory in *E. coli* strains. The plasmid containing the cDNA of Pre2 was a generous gift of Prof. Huntington (Cambridge University). The recombinant protein is 18aa longer than αT at N-terminal: 13aa are typical of the natural intermediate, while 5aa ($^{-18}$AIEGR^{-14}) were added for the plasmid construction. Recombinant wild type Pre2 was subjected to *in vitro* disulphide oxidative refolding, and characterized by RP-HPLC and high resolution MS. [**47**;**48**]. The concentrations of Pre2 solutions were determined by measuring the absorbance at 280nm, using an absorptivity coefficient of 1.892$mg^{-1}\cdot cm^2$. Recombinant Pre2 (0.1mg/ml) was treated with subtilisin (0.05μg/ml) for 15h at 5°C in HBS-$CaCl_2$. The fresh-generated active specie was purified by Heparin Sepharose affinity chromatography, as previously detailed.

The derivatization was achieved by adding KNCO to either a σPre2 or a αT sample (1μM) to a final concentration of 0.2M in 250μl of 50mM HEPES pH 6.8, 0.15M NaCl, 0.1% PEG-8000 (w/v) at 37°C. At fixed time points (0, 0.5, 1, 2, 3h) aliquots of the reaction mixtures were added to 20μM S2238 in 800μl HBS, to a final concentration of 50nM for σPre2 or 100pM for αT, and the time-course increase of the absorbance at 405nm was measured for 10min at 37°C. The rate of pNA release at carbamylation time t_i (v_i), compared to the initial rate (v_0) at time t_0, was taken as an indicator of the residual catalytic efficiency of the proteolysis mixture. The experimental data were displayed as percentages of residual activity and plotted against the reaction time.

To evaluate the sites of carbamylation, the derivatized proteins were analysed by RP-HPLC. A solution of 1μM σPre2 was reacted with 0.2M KNCO in 600μl of 50mM HEPES pH 6.8, 0.15M NaCl, 0.1% PEG-8000 (w/v) at 37°C. After 30min, the derivatization was quenched by adding 15μl H_2O-TFA 4% (v/v), and the reaction mixture was loaded onto a (4.6x150mm, 5μM, 300Å) C4 Vydac analytical column (Hesperia, CA, USA). The samples were eluted with a linear acetonitrile-0.078% TFA biphasic gradient of 5-35% in 15min and 35-55% in 35min, at a flow rate of 0.8ml/min. The material eluted from the major peaks was analyzed in the positive-ion mode by high resolution MS on a Xevo G2-S Q-TOF apparatus from Waters (Milford, MA, USA). Regarding αT, carbamylation was achieved in the same experimental conditions reported above, for 1h at 37°C. The quenched reaction mixture was desalted on a Sephadex G10 resin from Sigma (St. Louis, MO, USA), manually packed in a (8x125mm) column, and reduced by adding 1ml of 100mM TRIS-HCl pH 7.4, 6M Gnd-HCl, 1mM EDTA, 125mM DTT for 1h at 25°C, and the treated sample was analysed by RP-HPLC and MS as detailed above.

RESULTS AND DISCUSSION

Proteolysis of Prothrombin by Subtilisin and Generation of Thrombin-like Activity

Proteolysis of ProT by subtilisin Carlsberg was accomplished in an enzyme:substrate ratio of 1:2000 (w/w) at 37°C, from a starting reagent concentration (0.1mg/ml) correspondent to the physiologic value of plasma circulating ProT. Data in **Fig. 1A** clearly display that addition of an aliquot of this proteolysis mixture to a solution of the αT-specific chromogenic substrate S2238 (D-Phe-Pip-Arg-pNA) results in the release of pNA, absorbing UV-Vis light at 405nm. As highlighted in **panel 1B**, the initial rate (v_0) of substrate hydrolysis, given by the slope of the plot of ΔA_{405nm} versus time, increases with the ProT-subtilisin incubation time, reaching a maximum after 180-360min. At longer times (i.e. see 420min) the activity of the proteolysis mixture slightly decreases. Since from the blank experiment it clearly emerges that subtilisin is not able to cleave S2238 (**Fig. 1B**), the release of pNA strikingly derives from the generation of αT-like active species after subtilisin proteolysis on inactive ProT.

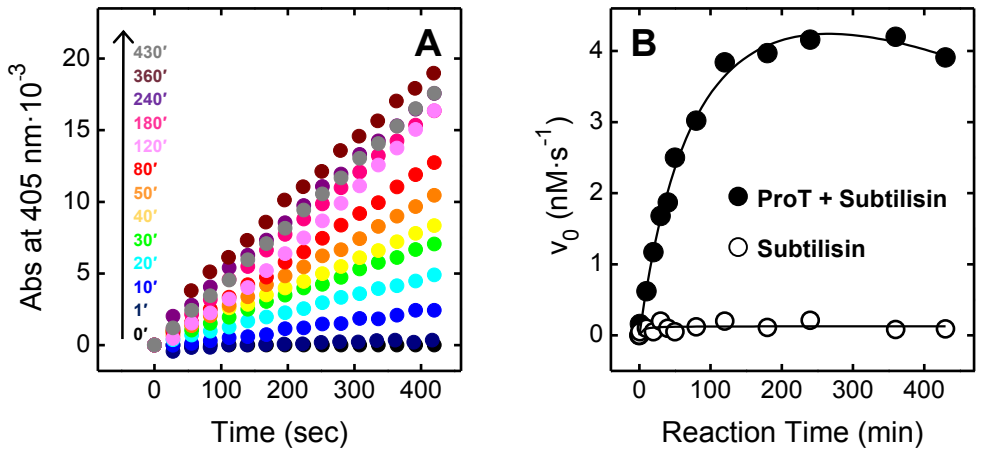

Figure 1. Time-course generation of thrombin-like enzymatic activity during proteolysis of ProT by subtilisin. (**A**) ProT (0.1mg/ml, 350µl) was treated in HBS-$CaCl_2$ at 37°C with subtilisin (0.05µg/ml) at an enzyme:ProT ratio of 1:2000 (w/w). At increasing time points, an aliquot (28µl) of the proteolysis mixture was added to a solution of the chromogenic substrate S2238 (20µM) in 800µl HBS. The time-course release of pNA was monitored at 37°C by recording the absorbance increase at 405nm. The slope of the straight lines was taken as the initial velocity, v_0, of S2238 hydrolysis by the active thrombin-like species that were being generated during limited proteolysis of ProT with subtilisin. (**B**) (●) Plot of v_0 as a function of the reaction time of ProT proteolysis by subtilisin at 37°C. (○) Blank experiment, performed by incubating S2238 (20µM) with subtilisin (0.05µg/ml) in the absence of ProT, demonstrates that subtilisin does not cleave the chromogenic substrate.

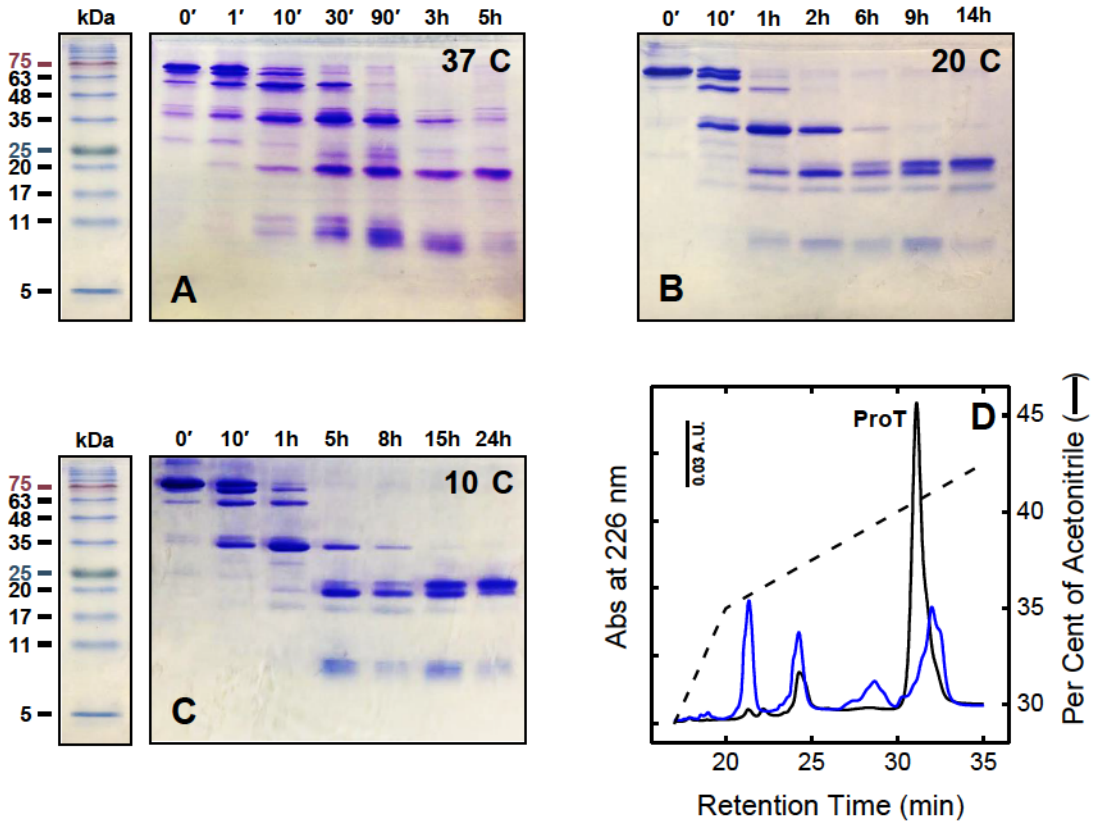

Figure 2. Time-course analysis of the proteolysis reaction of ProT by subtilisin. (A-C) Non-reducing electrophoretic analysis of the time-course reaction between ProT (1.4µM) with subtilisin (1.8nM) at different temperatures. In all the experiments, ProT (0.1mg/ml) was reacted at the indicated temperature in HBS-$CaCl_2$ with subtilisin at an ezyme:substrate ratio of 1:2000 (w/w). At fixed time points, aliquots (100µl, 10µg) of the proteolysis mixtures were cold precipitated with TCA, analysed by SDS-PAGE (4-14% acrylamide) under non-reducing conditions, and Coomassie stained. Molecular weight protein standards (std*) was loaded in the left-handed lane. **(D) RP-HPLC analysis of the proteolysis reaction of ProT with subtilisin after 1min (—) and 30min (—) at 37°C.** Aliquots (200µl, 20µg) of the reaction mixtures were loaded onto a C4 Vydac analytical column, eluted with a biphasic aqueous acetonitrile-0.078% TFA gradient (---) of 5-35% in 15min and 35-55% in 35min.

To explore subtilisin proteolysis sites on ProT, the reaction, performed at 37°C as detailed above, was quenched at fixed reaction times (from 0 to 5h) and analysed by SDS-PAGE in non-reducing conditions (**Fig. 2A**) and by RP-HPLC (**Fig. 2D**). From both the techniques, it emerged that starting commercial ProT is already partially degraded. As displayed in **panel 2A**, as the proteolysis proceeds, in the 5h time-course reaction, ProT disappearance is coupled to the generation and digestion of several species, with the presence of some major bands.

Identification of Subtilisin Cleavage Sites on Prothrombin Sequence

In a second stage, the proteolysis of ProT by subtilisin was accomplished with the same enzyme:substrate ratio, at decreased temperatures, i.e. 20°C and 10°C. At fixed time points (0-14h for 20°C and 0-24h for 10°C) the reaction mixtures were analysed by SDS-PAGE in non-reducing conditions. At lower temperatures, as expected, ProT proteolysis was slowed down, maintaining a cleavage pathway qualitatively similar to that observed at 37°C (**Fig. 2B, C**).

Subtilisin proteolysis pathway on ProT was unravelled at 10°C, in the same experimental conditions performed in **panel 2C**. At the declared reaction times, aliquots of the reaction mixture were on-line analysed by coupled LC-MS, in the positive ion mode. The assignment of subtilisin cleavage sites was accomplished by comparing the experimental molecular weight of the generated fragments to theoretical predictions, based on amino acidic composition, disulphide bridges, the presence of ten Gla residues, and the nature of the carbohydrate moieties (**Table 1**). In detail, ProT features three Asn-linked sugar chains at N78, N100 and N373, presenting the typical complex double-branched structure. The three identical moieties are composed of four N-acetylglucosamines (GlnAc), three mannoses (Man), two galactoses (Gal) and two terminal sialic acids (NeuAc, N-acetylneuraminic acid), for an overall molecular weight of 2206.18Da [**49**;**50**].

As displayed in **panel 2C**, after 10-min reaction at 10°C (i.e. 1min at 37°C) three first cleavages are performed, generating three major bands of comparable intensity, migrating at an apparent molecular weight of about 60, 50 and 37kDa. The 60-kDa band corresponds to fragment Ala1-Ala470(149a), resulting from the subtilisin-catalysed cleavage at Ala470(149a)-Asn471(149b), referred to as cleavage site-1 (CS-1). On note, the numbers in parenthesis refer to the chymotrypsinogen numbering. This fragment contains Gla domain, K1, K2, and the N-terminal (NT) region of Pre2. The 50-kDa band corresponds to fragment Met152-Glu579(247), deriving from the hydrolysis of Ala151-Met152 peptide bond, denoted as cleavage site-2 (CS-2). This fragment contains K2 and Pre2 domains, and it is equivalent to physiological prethrombin-1 Ser156-Glu579(247), a minor intermediate in ProT activation pathway, resulting from FXa cleavage after Arg155 and release of fragment F1 [**51**]. At last, the 37-kDa band originates from the cleavage at Arg271-Thr272 bond, i.e. the cleavage site-3 (CS-3). This fragment Thr272-Glu579(247) corresponds to wild type Pre2, the key physiologic intermediate of ProT activation by FXa [**29**].

At longer reaction times, the parent fragments deriving from CS-1, CS-2 or CS-3 may in turn be digested at the remaining hydrolytic sites still available along their sequences, with the generation of smaller fragments along preferred cleavage pathways.

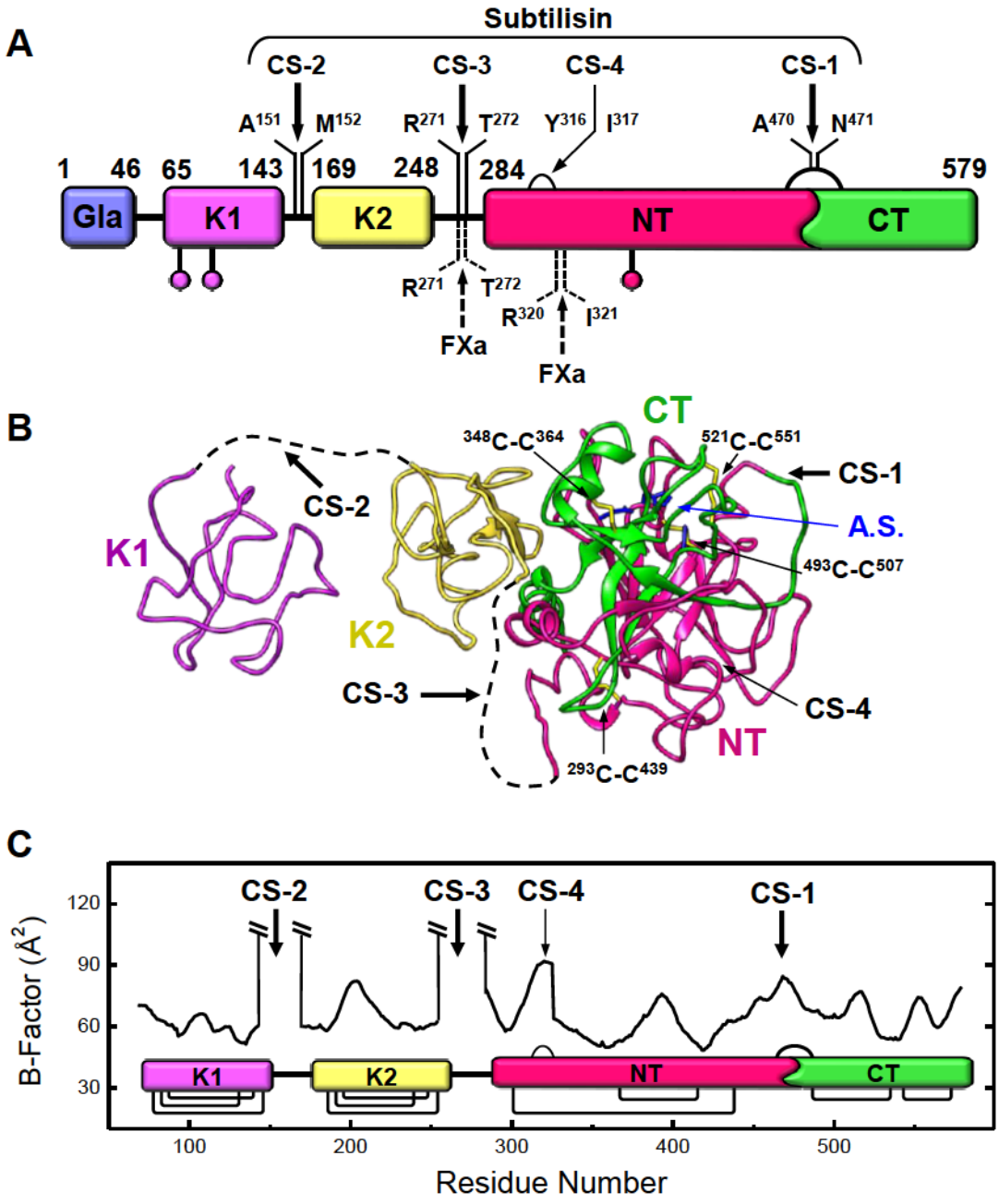

Figure 3. Identification of the subtilisin cleavage sites (CS) on ProT. (A) Schematic representation of the colour-coded architecture domains of ProT. The numbers identify the zymogen domains, displayed with different colours, according to the ProT sequence numbering: Gla domain, in light blue; K1, in purple; K2, in yellow; NT, in magenta, and CT, in green, are the N- and C-terminal fragments of Pre2 deriving from subtilisin cleavage. Non-physiological cleavage sites by subtilisin are highlighted by black arrows on the top side of ProT sequence; physiological cleavage sites by factor Xa are indicated as dashed arrows on the bottom side. **(B) Ribbon drawing of Gla-domainless ProT structure (pdb: 4hzh).** Dashed lines represent the unresolved linker regions connecting K1 to K2 (Lnk2) and K2 to Pre2 (Lnk3). Subtilisin cleavage sites are indicated by arrows, while the four SS bonds in the Pre2 domain are displayed as yellow segments. The amino acids forming the active site (A.S.) are showed as cyan sticks. **(C) B-factor plot of Gla-domainless ProT structure (pdb: 4hzh).** ProT is schematically represented under the average B-factor plot, with the twelve disulphide bridges. The subtilisin cleavage sites perfectly match with the regions of highest segmental flexibility.

Table 1: Mass Values of the protein fragments generated by limited proteolysis of ProT with Subtilisin*

Fragment	Mass (a.m.u.)	Fragment	Mass (a.m.u.)
A1 Gla K1 K2 NT CT E579	**72347.0** 72339.7	A1 Gla K1 K2 NT A470	**60016.6** 60009.7
M152 K2 NT CT E579	**50628.9** 50626.8	A1 Gla K1 A151	**21732.6** 21731.0
T272 NT CT E579	**37553.0** 37551.5	A1 Gla K1 K2 R271	**34808.0** 34806.2
M152 K2 NT A470	**38298.4** 38296.7	M152 K2 R271	**13093.5** 13093.3
T272 NT A470	**25222.6** 25221.5	N471 CT E579	**12348.4** 12348.1
T272 NT A470	**25240.8** 25239.5		

Table 1. Experimental and theoretical mass values of the fragments generated by limited proteolysis of ProT by subtilisin. The proteolysis reaction was performed at 10°C, under the experimental conditions reported in **Fig. 2C**. The experimental average molecular masses of proteolytic fragments, calculated by the software MaxEnt1, are reported in bold, together with the theoretical mass values, as deduced from the known amino acid and carbohydrate (○) composition of ProT, disulphide bonds and Gla residues. The error on mass determination was always <50 ppm.

In particular, after 1h-reaction (i.e. 10-90min at 37°C), the 50-kDa band is cleaved at CS-3, with the transient accumulation of the 37-kDa band, as displayed in all the electrophoretic analysis (**Fig. 2A, B, C**). Pre2, in turn, is slowly but quantitatively hydrolysed at CS-1, with the release of an N-terminal (NT) and a C-terminal (CT) domains. The 25-kDa NT domain corresponds to the fragment Thr272-Ala470(149a), while the 12-kDa CT domain matches the sequence Asn471(149b)-Glu579(247).

From the comparison of the time-course hydrolysis of αT-specific substrate S2238 (**Fig. 1B**), with the progression of the proteolysis reaction at 37°C (**Fig. 2A**) it is conceivable to conclude that cleavage of Pre2 at CS-1 is required for the onset and the increase of αT-like activity. Actually, after 3-h reactions, at the maximum rate of pNA release, Pre2 band is almost disappeared, while the 25-kDa and 12-kDa fragments are the most abundant species in the proteolysis mixture. Since the catalytic triad is split between these Pre2 non-canonical fragments (i.e. His57, Asp102 in NT; Ser195 in CT) the active specie is likely to be the complex between the two domains. Notably, both the fragments contain two stabilizing intra-chain SS bonds, but they are not linked by disulphide bridges.

Nevertheless, this novel non-covalent specie, we named σPre2, generated in physiologically relevant conditions, is stable and active during time. Notably, as deduced from preliminary experiments performed in our Laboratory, σPre2 can also be obtained by subtilisin-catalysed single cleavage on recombinant Pre2.

At low temperatures and higher reaction times, an additional specie, migrating with an apparent molecular weight slightly bigger than NT fragment, is generated. From LC-MS analysis performed in non-reducing and reducing conditions, the fragment was identified as deriving from internal NT cleavage at the Tyr316(14j)-Ile317(14k) peptide bond (CS-4). The new specie, denoted as NT*, features fragments Thr272-Tyr316(14j) and Ile317(14k)-Ala470(149a) held together by the SS bond Cys293(1)-Cys439(122) (**Table 1**). Hereafter, the higher apparent molecular weight displayed in the electrophoretic analysis is consistent with NT* more relaxed structure. It is feasible that NT* may be part, in alternative to NT, of the active complex.

Notably, while CS-1, CS-2 and CS-4 are performed after apolar or aromatic residues, CS-3 occurs after a positively charged Arg (**Fig. 3A**). Albeit unusual, this cleavage should not be surprising, due to subtilisin broad hydrolysis specificity [**41**]. Despite the large number of potential cleavage sites along ProT sequence, even at 37°C the protease quantitatively attacks the zymogen only at three cleavage sites, i.e. CS-1, CS-2 and CS-3 (**Fig. 3A, B**). This unexpected evidence can be explained on the zymogen structure, considering both the accessibility and the flexibility of the different sequences. Strikingly, the subtilisin cleavage sites perfectly match the regions of highest segmental flexibility, as highlighted from the average B-factor plot (**Fig. 3C**). CS-1 is embedded in the highly exposed γ-loop, while CS-2 and CS-3 are centred in Lnk2, connecting K1 to K2, and in Lnk3, at physiologic Pre2 start, respectively. Notably, the two linkers are so dynamic that could not be resolved in ProT crystallographic structure (**Fig. 3B**).

Purification of the Active Thrombin-like Specie (σPre2) derived from Prothrombin Proteolysis by Subtilisin

The key aspect emerging from the proteolysis and kinetics data reported above, is that a non-physiological cleavage, at Ala470(149a)-Asn471(149b) is instrumental for the generation of αT-like enzymatic activity. In particular, the end-point of subtilisin proteolytic pathway is the generation of NT e CT domains from wild type Pre2, composing σPre2. Since in the σPre2 complex non-covalent interactions drive the formation of a stable fragment-complementing system, we focused our efforts on the isolation of this active specie, for further characterization.

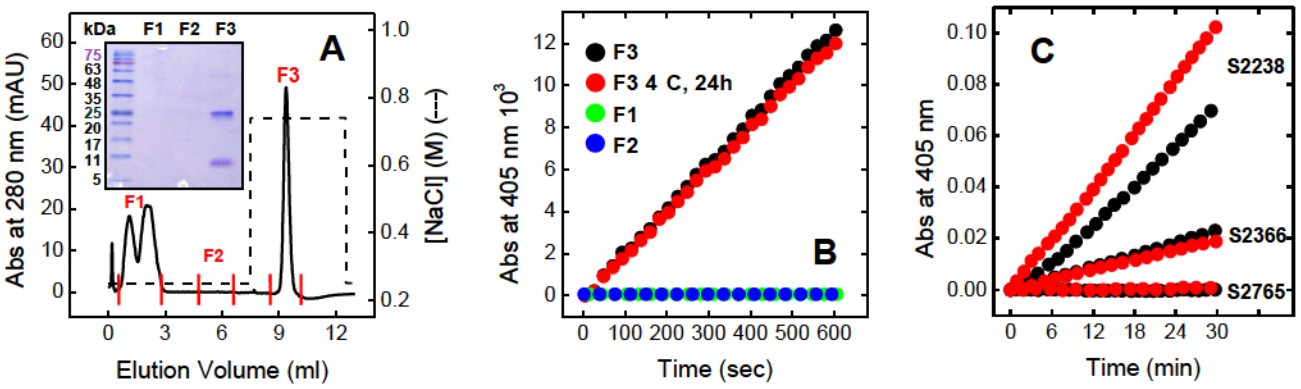

Figure 4. Purification, storage stability, and substrate specificity of σPre2. (A) Purification of σPre2 by Heparin Sepharose affinity chromatography. For micro-preparative purposes, a ProT solution (300µg, 0.1mg/ml) was treated for 24h at 10°C with subtilisin (0.05µg/ml) in HBS-$CaCl_2$. The reaction mixture was loaded onto a HiTrap Heparin Sepharose column, which was equilibrated with 25mM TRIS-HCl pH 7.4, 0.25M NaCl and eluted at 0.75M NaCl (---). Aliquots of the material collected in correspondence of fractions F1 to F3 (200µl) were cold precipitated with TCA for subsequent electrophoretic analyses. (**Inset**) SDS-PAGE (4-14% acrylamide) of F1, F2 F3, under non-reducing conditions and Coomassie staining. **(B) Hydrolytic activity of the fractions eluted from the Heparin Sepharose column.** After elution from the column, aliquots (60µl) of F1 (●), F2 (●), and F3 (●), were immediately added to a S2238 solution (20µM) in 800µl HBS. The time-course release of pNA was monitored by recording the absorbance at 405nm at 37°C, for 10min. For F3 (σPre2), the only active towards the chromogenic substrate, storage stability was checked on its functional activity after incubation at 4°C for 24h (●). **(C) Evaluation of substrate specificity of σPre2.** Aliquots of purified σPre2 (●) were added to solutions (20µM) of three chromogenic substrates specific for αT (S2238), aPC (S2366) or FXa (S2765) in 800µl HBS, to a final concentration of 30nM. The initial rates (v_0) of pNA release were monitored by recording the absorbance at 405nm for 30min, and compared to the curves generated by 100pM commercial αT (●) in the same experimental conditions.

To maximise the yields of σPre2 production, a ProT solution was treated with subtilisin in a 1:2000 (w/w) ratio, for 24h at 10°C. Since the novel active specie is basically the complex of non-canonical NT and CT domain of wild type Pre2, we adopted a purification strategy based on heparin affinity chromatography. Taking advantage of heparin affinity for exosite II, present both in αT and in its inactive precursor Pre2, the proteolysis mixture was fractionated on Heparin Sepharose column, applying an on/off gradient of 0.75M NaCl (**Fig. 3A**). Three samples were collected: one corresponding to the a-specific peak (F1), at the beginning of the chromatographic course; one during the purification (F2), and the main peak eluted during the NaCl gradient (F3).

An aliquot from the three fractions was analysed by SDS-PAGE under non-reducing conditions. From the inset panel in **Fig. 4A** it clearly emerges that the material corresponding to the

single chromatographic peak in fraction F3 splits in NT, NT* and CT domains, composing active σPre2. Conversely, the unretained protein material, eluted with the void volume, is likely to be composed by small peptides, not detectable by electrophoretic analysis, deriving from F1·2 digestion. Evidences in **Fig. 2C** confirm this hypothesis: while the 25- and 12-kDa species are quite resistant to time-course proteolysis, the other fragments are all extensively degraded. Finally, absence of protein bands in fraction F2 confirms that there is no leakage of material during the chromatographic course.

Strikingly, the material eluted from F3, but not from F1 and F2, was able to hydrolyse S2238 and to release pNA, retaining functional stability even after storage at 4°C for 24h (**Fig. 4B**). These data provide strong evidences that, after isolation by Heparin Sepharose, subtilisin is completely removed from the mixture, and no σPre2 auto-proteolysis reaction occurs. To better characterize σPre2 enzymatic specificity, its activity was tested against chromogenic substrates specific for αT (S2238), aPC (S2366) or FXa (S2765), and compared to mature αT. The data in **panel 4C** clearly demonstrate that σPre2 features the same specificity of αT, cleaving S2238 with the highest rate, whereas S2366 and S2765 were only poorly (or even not) cleaved.

Characterization of σPre2 Catalytic Efficiency and Procoagulant Functions

S2238 Hydrolysis **-** Steady-state kinetics of S2238 hydrolysis allow us to obtain the catalytic constants k_{cat} and K_m, according to the Michaelis-Menten treatment. Analysis of the data in **panel 5A** reveal that σPre2 hydrolyses S2238 with a specificity constant (k_{cat}/K_m) = 0.09±0.01$\mu M^{-1} \cdot s^{-1}$, about 165-fold less than αT. Notably, this loss in enzymatic efficiency is due to the selective decrease (by 124-fold) of the catalytic constant (k_{cat}), whereas the Michaelis-Menten constant (K_m) slightly increases (by 1.4-fold). These experimental data suggest that σPre2 active site is moulded in its S1, S2 and S3 specificity sites, binding the substrate with αT-comparable affinity. Conversely, the molecular machinery leading to the peptide bond hydrolysis and subsequent product release is somewhere impaired. However, these results are not surprising, since the three amino acids composing the catalytic triad, as detailed above, are distributed in both σPre2 fragments. This peculiar localization may result in a less rigid catalytic cleft, characterized by a sub-optimal stereochemistry, in which the conversion through the transition state may require a higher energetic cost (**Fig. 3A, B**).

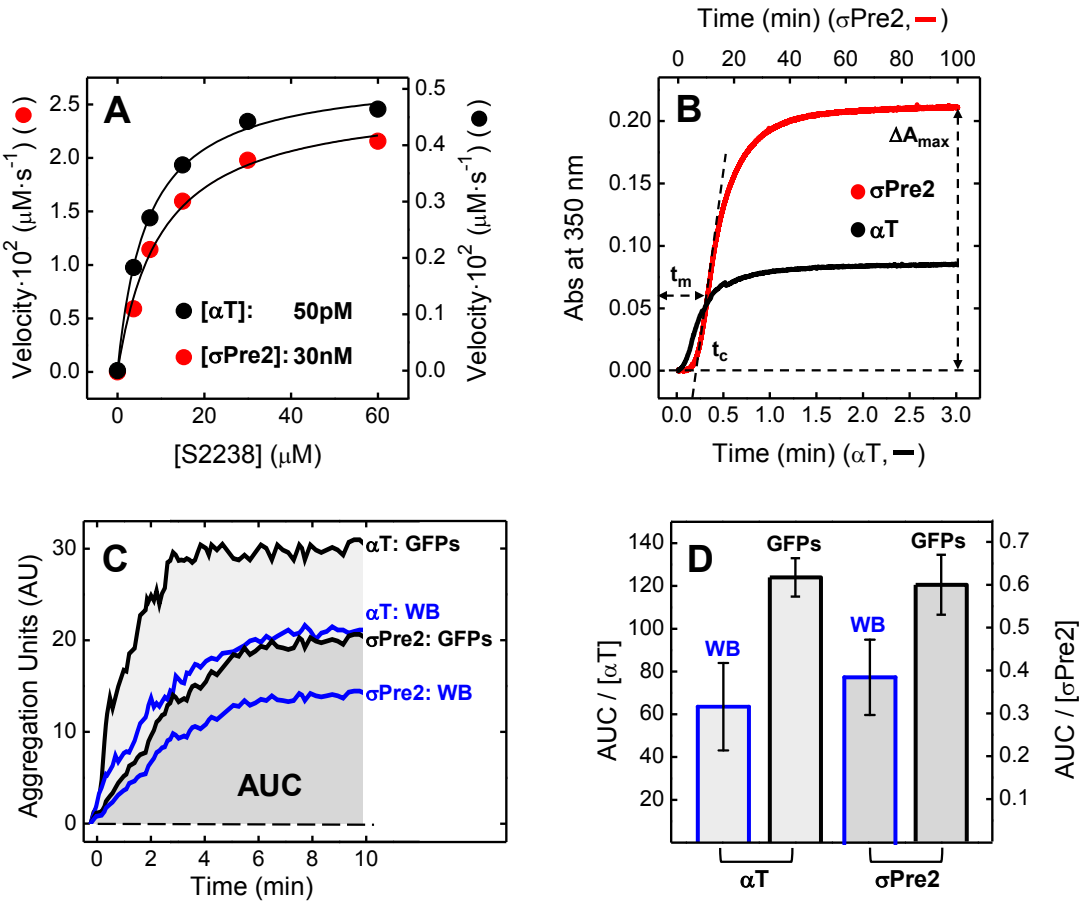

Figure 5. σPre2 efficiency on S2238 hydrolysis and αT procoagulant functions. (A) Steady-state hydrolysis of the chromogenic substrate S2238. A solution of 30nM σPre2 (●) or 50pM αT (●) was added to decreasing concentrations (60-0μM) of S2238 in 200μl HBS. The initial rate of pNA release was monitored by recording the absorbance at 405nm at 37°C for 5min. From the interpolation of data points with the Michaelis-Menten equation **eq. 1**, k_{cat} and K_m values were obtained as best fit-parameters. σPre2: k_{cat}=0.86±0.04s^{-1}; K_m=10.0±1.3μM; k_{cat}/K_m=0.09±0.01$\mu M^{-1}\cdot s^{-1}$. αT: k_{cat}=106.6±2.2s^{-1}; K_m=7.2±0.5μM; k_{cat}/K_m=14.8±0.03$\mu M^{-1}\cdot s^{-1}$. **(B) Turbidimetric analysis of fibrin generation.** To a solution of desalted human fibrinogen (440nM) in HBS were added either αT (—) or σPre2 (—) to a final concentration of 50nM in 800μl. The Sol→Gel transition was monitored by recording the time-course absorbance at 350nm. For clarity, the upper (0-100min) time scale refers to σPre2, while the lower (0-3min) time scale refers to αT. The absorbance scale for all the experiments (0-0.25 A.U.) is the same. From each clotting curve, the values of S_m, t_m, t_c, and ΔA_{max} were extracted (**see text**). σPre2: S_m = 15.8x10^{-3}AU·min^{-1}; t_m = 10.6min; t_c = 6.7min; ΔA_{max} = 0.21AU; αT: S_m = 5.3x10^{-3}AU·s^{-1}; t_m = 10.2s; t_c = 3.7s; ΔA_{max} = 0.08AU. **(C) Impedance aggregometry analysis of platelets aggregation in whole blood (—) or gel-filtered platelets (—).** A solution of WB or GFP (300μl) was diluted with 320μl HBS containing either σPre2 or αT, to a final concentration of 50nM and 0.5nM, respectively. Platelets aggregation was measured as the time-course increase of plasma impedance, expressed as relative Aggregation Units (AU). Integration of AU over time (10min) gives the AUC values for σPre2 or αT. **(D) Normalized αT- or σPre2-induced platelets aggregation.** For all the assays, the obtained AUC value was normalized to σPre2 or αT concentrations. Final data are the average of single determination on two healthy donors samples. The errors bars correspond to the standard deviation.

Fibrin Generation - Fibrinogen (FI), circulating in the plasma (2.6mg/ml) as a dimer of three chains $(A\alpha B\beta\gamma)_2$, presents an overall stretched conformation, featuring a central *E* nodule and two distal *D* knobs. The multi-step process leading to fibrin network starts from αT-hydrolysis of Aα chains, with the release of two fibrinopeptides A (FpA, 16aa) and the generation of fibrin I monomer. Fibrin I monomers, in turn, undergo longitudinal elongation by staggered *E-D* interactions, organizing in double-stranded protofibrils. After αT-hydrolysis of Bβ chains, and fibrinopeptides B (FpB, 14aa) release, protofibrils of a certain length can associate laterally, with the rise of the insoluble fibrin network [**52**]. *In vivo*, fibrin clot is further stabilized by crosslinking interactions performed by FXIIIa.

In vitro, the Sol→Gel transition deriving from the fibrin clot can be easily investigated by a turbidimetric assay. The plot of turbidity (i.e. absorbance at 350nm) versus time results in the onset of the characteristic sigmoidal clotting curves (**Fig. 5B**), presenting a lag phase, a linear rise and a plateau. According to the kinetic model of fibrin generation, the lag phase corresponds to FpA/B release and protofibrils elongation; the rapid onset of absorbance is due to lateral association of those protofibrils that feature a certain length threshold to aggregate; the plateau is reached when most of protofibrils have been transformed to fibrils, able to scatter visible light.

After triggering σPre2- or αT-induced fibrin generation from a fibrinogen solution, four parameters were extracted from the clotting curve: 1) S_m, the maximum slope (increase in turbidity-per-unit time) at the inflection point of the clotting curve; 2) t_m, the time needed to reach S_m; 3) t_c, the clotting time, obtained as the intercept of the tangent line at S_m with the time axis (zero absorbance baseline); 4) ΔA_{max}, the maximum difference of absorbance recorded between t=0 and t→∞, proportional to the square of the average diameter of the fibres [**53**]. With respect to αT (S_m = 5.3x $10^{-3}AU\cdot s^{-1}$; t_m = 10.2s; t_c = 3.7s; ΔA_{max} = 0.08AU), the clotting curve generated by the same concentration (50nM) of σPre2 is characterized by a ≈100-fold longer lag phase (t_m = 10.6min; t_c = 6.7min) a lower slope in the inflexion point ($S_m = 15.8x10^{-3}AU\cdot min^{-1}$) and by a ≈3-fold higher final turbidity (ΔA_{max} = 0.21AU). These discrepancies are fully consistent with the 165-fold decrease of the catalytic constant k_{cat} towards S2238 (**Fig. 5A**). In the kinetic model of fibrin generation predicted by Weisel and co-workers, at constant fibrinogen concentration, a decrease of enzymatic concentration results in a slower release of FpA/B (prolonged t_c), reflecting in a smaller number of protofibrils, which however, associate in thicker fibres yielding a more intense turbidimetric signal [**54**]. Considered that the k_{cat} of S2238 hydrolysis by σPre2 is selectively reduced by about 124-fold compared to αT, from a purely kinetic standpoint ($V_{max}=k_{cat}\cdot[E]$) a solution of σPre2 at a given concentration can be treated as a αT solution 124-fold less concentrated.

Platelets Aggregation **-** αT activates platelets through the interaction with receptor GpIbα and subsequent cleavage of surface PARs [**55**;**56**]. *In vivo*, after a vascular damage, platelets aggregation is the very first defence step boosted, responding even to minimal αT concentrations. Platelets aggregation was investigated in both whole blood and gel-filtered platelets, with Multiple Electrode Aggregometer (MEA), using cuvettes equipped with a couple of electrodes. In non-clotted solutions, inactive platelets stick to the electrodes, organizing in a monolayer. After the addition of an aggregant exogenous agonist (i.e. αT or ADP), platelets generate pseudopods and adhere to the pre-existing monolayer, thus increasing plasma electric impedance, which is measured by the relative aggregation units (AU) as a mean between the electrodes. Integration of area under the curve (AUC) during the time-course analysis of 10min quantifies the aggregation response [**46**]. Diluting a sample (300μl) of whole blood with a solution of σPre2 (50nM) or αT (0.5nM) yielded AUC values of 19 and 31, respectively. From the gel-filtered platelets (300μl), instead, the resulting AUC values were 30 from 50nM σPre2 and 62 for 0.5nM αT (**Fig. 5C**). Increase in aggregation rate for GFP is consistent with the fact that this purification concentrates the platelets. Normalizing the data for the relative enzymatic concentrations, the absolute aggregation potency are displayed in the histograms in **panel 5D**. σPre2 elicits a 159-fold and 207-fold less efficiency as an aggregant agonist in whole blood, or gel-filtered platelets, respectively. This data are in accord with the 165-fold loss in S2238 hydrolysis and ≈100-fold lag phase increase during fibrin generation.

Molecular Mechanism of Prothrombin Activation by Subtilisin

Our experimental data clearly demonstrate that after proteolytic attack of ProT by subtilisin, the generation of αT-like catalytic activity is triggered only by the cleavage at the peptide bond Ala470(149a)-Asn471(149b). The molecular mechanism of alternative zymogen activation remains unknown. To unravel the biochemical pathways leading to the formation of the active site, both σPre2 and αT were subjected to carbamylation of their N-terminals by potassium cyanate (KNCO). This reagent, at a physiologic pH, displays a derivatization preference for α-amino groups of N-terminal, rather than ε-amino groups of Lys. The selective N-terminal derivatization is accomplished by forming a neutral ureido-group, according to the scheme: $R\text{-}NH_2 + HNCO \leftrightarrow R\text{-}NHCONH_2$, where HNCO is the reactive isocyanic acid, in equilibrium with cyanate (NCO^-). Notably, the carbamylation rate is positively correlated with the availability and accessibility of the unprotonated N-terminal α-amino groups.

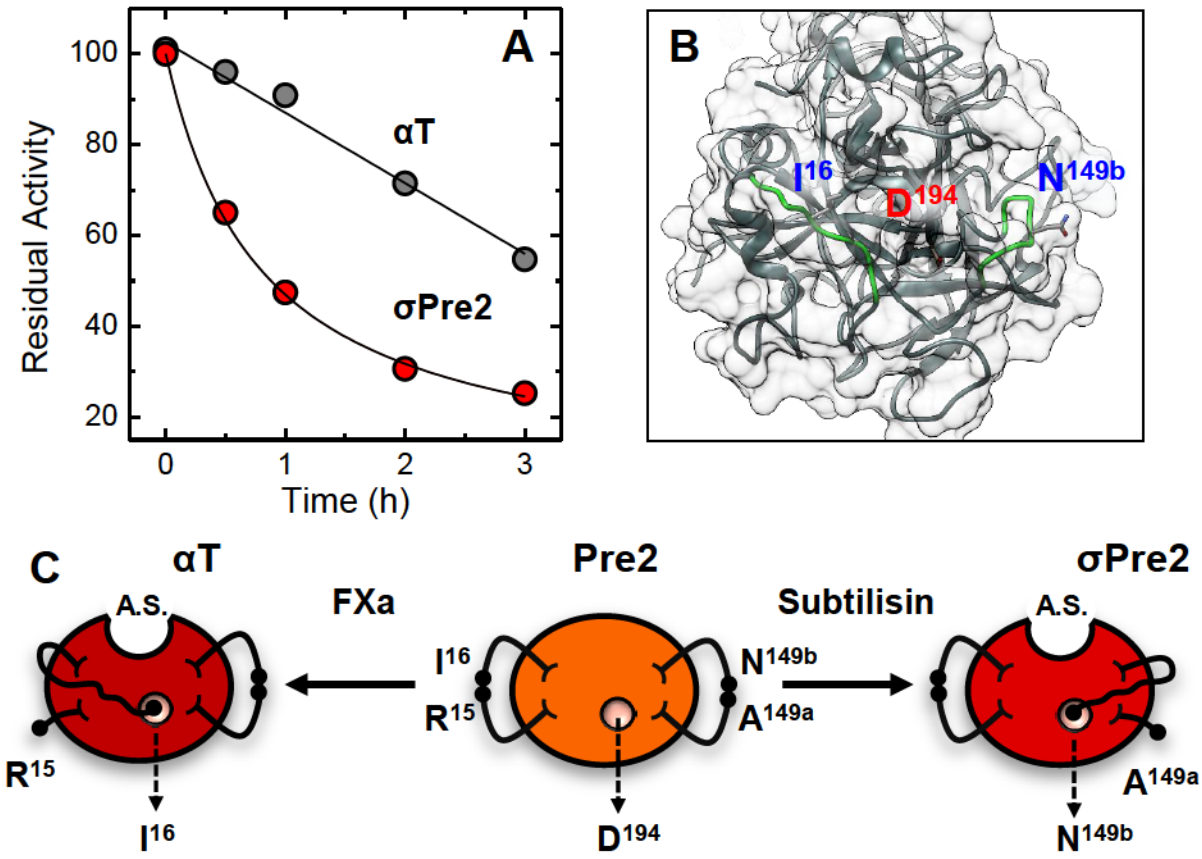

Figure 6. Mechanism of zymogen activation in σPre2. (A) Effect of time-course carbamylation of σPre2 (•) and αT (•) on the rate of substrate hydrolysis. σPre2 or αT solutions (1μM) in 50mM HEPES pH 6.8, 0.15M NaCl, 0.1% PEG-8000 (w/v) were incubated at 37°C in the presence of 0.2M KNCO. At the indicated time points, aliquots (final concentration 50nM σPre2 or 100pM αT) were taken and the initial rate (v_i) of S2238 (20μM) hydrolysis was determined in HBS at 37°C. The data are expressed as the percentage relative rate of substrate hydrolysis, (v_i/v_0), where v_i and v_0 are the rate of hydrolysis determined at time t_i and 0, respectively. **(B) Surface representation (ribbon drawing) of the Pre2 domain of ProT (pdb: 4hzh).** The panel displays Asp194, positioned at the bottom of a deep cleft shaped by the two β-barrels of Pre2, and the two scissile bonds: physiologic Arg15-Ile16 and alternative Ala149a-Asn149b, represented as green sticks. **(C) Schematic representation of the physiological and non-physiological Pre2 zymogen activation by FXa or bacterial subtilisin, respectively.** After physiological cleavage of the peptide bond Arg15-Ile16 by FXa in Pre2, the newly generated dipeptide Ile16-Val17 swings into the 194-cleft and triggers the formation of substrate binding sites and oxyanion hole, required for catalysis. Likewise, after non-physiological cleavage by subtilisin at Ala149a-Asn149b in the exposed γ-loop of Pre2, the new N-terminal dipeptide Asn149b-Val149c can enter the 194-cleft and evoke zymogen activation.

To achieve N-termini carbamylation, solutions of σPre2 or αT were simply incubated with KNCO (0.2M) in a physiological buffer at pH 6.8. At increasing time points, the catalytic efficiency of the derivatized proteins was tested against the chromogenic substrate S2238. As displayed in **panel 6A**, after 3h-reaction, αT sample retains 53% residual activity (being almost insensitive to cyanate in the 0-60min time range), while σPre2 displays only 26% of the starting catalytic efficiency.

To identify the carbamylation sites on the proteins of interest, the reaction mixtures were fractionated on RP-HPLC, analysed by MS and compared to the experimental molecular weight of the non-derivatized species. Regarding αT, the derivatization was performed for 60min at 37°C, and the sample was desalted on a G-10 filtration column to eliminate excess of KNCO. The eluted sample was treated with a reducing buffer to separate light chain (Thr1h-Arg15) from heavy chain (Ile16-Glu247), physiologically linked by the disulphide bridge Cys1-Cys122. The molecular mass of the light chain was increased by 42.80a.m.u. (4133.60 vs 4090.80a.m.u.), while the molecular mass of the heavy chain was unchanged (31945.35a.m.u.). For this assay, σPre2 was produced by treating recombinant Pre2 Ala(-18)-Glu247 with subtilisin, at 1:2000 (w/w) ratio for 15h at 5°C. In these experimental conditions the resulting σPre2 is composed by NT* domain Thr(-13)-Ala149a, presenting an internal nicking at Tyr14j-Ile14k, and by CT domain (Asn149b-Glu247). After the derivatization, performed for 0.5h at 37°C, the reaction mixture was directly analysed by RP-HPLC and MS, being NT* and CT not linked by disulphide bridges. NT* was carbamylated at its both N-terminals, presenting an experimental mass (22947.45a.m.u.) 84.95a.m.u. bigger than the non-derivatized domain (22862.50a.m.u.). The CT domain was derivatized at its amino-terminal, yielding a 42.70a.m.u-increased experimental mass (12390.90 vs 12348.20a.m.u.).

Strikingly, σPre2 Asn149b in CT domain was carbamylated, while αT Ile16 in heavy chain was protected from reaction with cyanate. These results suggest that, while αT FXa-generated N-terminal dipeptide Ile16-Val17 is well protected from the reaction, being buried in Ile16 pocket, σPre2 subtilisin-generated N-terminal dipeptide Asn149b-Val149c is more accessible. On the other side, both σPre2 NT* and αT light chain were carbamylated. Since αT retains most of its residual activity after 1h-reaction (**Fig. 6A**), derivatization at Pre2 N-terminal is likely not to interfere with enzymes hydrolytic properties. On the other hand, if we compare the carbamylation data with the 0.5h-decrease in σPre2 hydrolytic activity, we can conclude that neutralization of the Asn149b N-terminal positive charge, even with a small carbamyl-group, inhibits amidolytic activity of σPre2 (**Fig. 6A**). These results suggest that the raising of catalytic competence in σPre2 is not the fortuitous result of γ-loop flexibilization, but of a precise conformational change clearly associated to the new Asn149b-Val149c N-terminal sequence.

Here we propose that raising of catalytic activity in σPre2 is triggered by an analogous mechanism driving to the physiologic ProT activation by FXa. Briefly, after FXa-cleavage at Arg15-Ile16, the newly generated N-terminal Ile16-Val17 penetrates the preformed Ile16 pocket, deep in the Asp194 cleft. The amino group of Ile16 forms a salt bridge with the carboxylate of the well-buried Asp194, which in turn triggers, by conformational changes, the moulding of the active site and the oxyanionic hole, both necessary for catalysis [**45**;**46**]. In an analogue way, the subtilisin-generated N-terminal Asn149b-Val149c may enter the Ile16 pocket and electrostatically couple to Asp194 (**Fig. 6C**). As a confirm of this hypothesis, visual inspection of ProT structure, in **panel 6B**, displays that both the positively charged N-terminal segments in σPre2 (Asn149b-Val149c) and αT (Ile16-Val17) are located in unconstrained loop regions, which may become even more flexible after the nicking. In addition, the two segments stand and at a comparable distance (≈23Å in αT and ≈14Å in σPre2) from the crucial negative Asp194 side chain.

This model accounts also for the higher reactivity to carbamylation of σPre2 Asn149b, and for its 165-fold lower catalytic efficiency. While in αT Ile16 is tightly bound to Asp194, in σPre2 the interaction may be weaker, likely due to the 10-fold lower basicity of the α-amino group [pKa(Asn) = 8.72; pKa(Ile) = 9.76], and lower polarity of the Asn side chain compared to Ile. This chemical features, added to the non-covalent nature of σPre2 complex, suggest that the N-terminal segment Asn149b-Val149 may explore two interconverting conformations in dynamic equilibrium, i.e. in and out the Ile16 pocket. When buried, the salt bridge triggers the onset of catalytic activity, with the generation of a less rigid and competent catalytic cleft. When exposed, the unprotonated form of Asn149b can react with cyanate, thus losing its ability to enter the pocket again, with a decrease of residual activity. In conclusion, two different peptide bond hydrolysis mediate Pre2 activation with a comparable molecular mechanism, although resulting in a different overall catalytic activity.

CONCLUSIONS

Inflammation and coagulation are two tightly connected defence responses, enhancing each other in a vicious circle [**1**]. Since vessel injuries may be potential access sites for microorganisms, activation of local coagulation, with trapping of the invading pathogen, may act as a first-line innate response regulator [**10**]. The interplay between these systems is confirmed by the evidence that anticoagulant mechanisms dampen inflammatory manifestations. If the physiologic anticoagulant pathways fail to control the inflammation/coagulation interface, severe pathologic manifestations, like sepsis, can occur. Sepsis is a life-threatening condition, in which the systematically activated immune system, in response to a pathogen agent, is eventually detrimental for the host. In particular, exaggerated inflammatory manifestations result in tissue damages and organ failures. In addition, uncontrolled coagulation may lead to DIC, a clinical syndrome in which the presence of scattered thrombi is coupled to an unbalanced haemorrhagic state [**23**].

In this scenario, exogenous agents penetrating during infection may be harmful not only for the triggering of inflammation, but also for the direct activation of coagulation, thus bypassing physiologic regulatory systems. In particular, the key reaction of coagulation cascade is ProT (579aa, 72.3kDa) conversion to active αT (295aa, 36.7kDa), preferentially through inactive Pre2 (308aa, 38.2kDa) intermediate. However, most bacterial proteases, which may play a role in sepsis progression, are largely uncharacterized. Several microbial pathogens express and secrete subtilisin-like serine proteases (subtilases). Subtilases are a large class of extracellular proteases, characterized by a broad specificity of cleavage. In this work, we investigated ProT activation by subtilisin Carlsberg, a well-characterized and commercially available enzyme, which we took as an extensible model for the subtilase family.

Our data clearly demonstrate that proteolysis of inactive ProT with subtilisin in physiological conditions (pH 7.4, 37°C), leads to the generation of active species, able to cleave αT-specific substrate S2238. Although the abundance of potential nicking sites, subtilisin attacks ProT at three main cleavage sites, referred to as CS-1, CS-2 and CS-3, which perfectly match the substrate most flexible regions. CS-1 is localized at the peptide bond Ala470(149a)-Asn471(149b), in the highly exposed γ-loop; CS-2 refers to the peptide bond Ala151-Met152, in Lnk2, connecting K1 to K2; CS3 is centred at the peptide bond Arg271-Thr272, in Lnk3, connecting K2 to the protease domain. Both Lnk2 and Lnk3 are so dynamical that could not be resolved in ProT crystallographic structure (pdb: 4hzh). The three main species deriving from the first cleavage may in turn be attacked at the other available sites along the fragment sequence. In particular, proteolysis at CS-2 and CS-3 lead to the transient accumulation of wild type Pre2 Thr272-Glu579(247). In turn, Pre2 is attacked at CS-1 to yield NT domain Thr272-Ala470(149a) and CT domain Asn471(149b)-Glu579(247), not linked by

disulphide bridges. Comparing the S2238 hydrolysis assay and the proteolysis trend, we can deduce that generation of these non-canonical NT and CT domains from Pre2 is instrumental for the onset of αT-like proteolytic activity. Since the catalytic triad is split between the two fragments (i.e. His57, Asp102 in NT, Ser195 in CT), it is feasible that the active specie, we named σPre2, is the non-covalent complex of both the domains, stabilized by electrostatic and steric interactions. At longer times, an additional cleavage (CS-4) is performed between Tyr316(14j)-Ile317(14k) peptide bond in NT, yielding to the more relaxed NT*, in which the two internal fragments are linked by a SS bridge. NT* is likely to participate to the complementing-fragment system, in alternative to NT, of active σPre2. To maximize σPre2 yield of production, ProT was incubated with subtilisin in a 1:2000 (w/w) ratio for 24h at 10°C. The novel active specie was purified by fractionating the proteolysis mixture on a Heparin Sepharose column, taking advantage of heparin affinity for exosite II.

From kinetics assays it emerged that σPre2 features the same specificity of αT, cleaving efficiently S2238, whereas aPC (S2366) and FXa (S2765) specific substrates were only poorly (or even not) hydrolysed. In a second stage, steady-state kinetics of S2238 hydrolysis allowed us to extract kinetic k_{cat} and K_m parameters according to Michaelis-Menten treatment. In detail, σPre2 features a 165-fold reduced specificity constant (k_{cat}/K_m) towards S2238, due to a selective decrease (124-fold) in k_{cat}. The reduced catalytic efficiency is reflected in thrombin procoagulant functions: fibrin generation and platelets aggregation. The non-canonical active specie triggers the Sol→Gel transition in a human fibrinogen solution, with a clotting curve featuring a ≈100-fold longer lag phase. Regarding platelets aggregation, σPre2 elicits a 159-fold and 207-fold less efficiency as an aggregant agonist compared to αT in whole blood and gel-filtered platelets, respectively.

From carbamylation assays performed with KNCO it emerged that the newly generated N-terminal Asn149b is time-dependently derivatized, with a parallel reduction in σPre2 activity. Due to these experimental evidences, we supposed that formation of σPre2 active site may proceed in a way analogue to FXa-catalysed ProT activation [**45**;**46**]. In mature αT, FXa-generated Ile16-Val17 N-terminal fragment penetrates the preformed Ile16 pocket, forming a salt bridge with Asp194. This well-buried electrostatic interaction, in turn, moulds the catalytic cleft and the oxyanionic hole, both required for catalysis. In σPre2, the process may be triggered by subtilisin-generated Asn149b-Val149c. This hypothesis is supported by the comparable distance (≈23Å in αT and ≈14Å in σPre2) of the two fragments from the crucial negative Asp194 side chain. Due both to the non-covalent nature of σPre2, and to the lower basicity and polarity of Asn compared to Ile, in σPre2 the salt bridge is reasonably less stable, leading to an impaired catalytic efficiency. This model is in accord to, and explains, all the catalytic assays detailed above.

REFERENCES

[1] Esmon CT. The interactions between inflammation and coagulation. Br J Haematol 2005 Nov;131(4):417-430.

[2] Burstein SA. Cytokines, platelet production and hemostasis. Platelets 1997;8(2-3):93-104.

[3] Bernardo A, Ball C, Nolasco L, Moake JF, Dong JF. Effects of inflammatory cytokines on the release and cleavage of the endothelial cell-derived ultralarge von Willebrand factor multimers under flow. Blood 2004 Jul 1;104(1):100-106.

[4] Opal SM. Therapeutic rationale for antithrombin III in sepsis. Crit Care Med 2000 Sep;28(9 Suppl):S34-7.

[5] Klein NJ, Ison CA, Peakman M, Levin M, Hammerschmidt S, Frosch M, et al. The influence of capsulation and lipooligosaccharide structure on neutrophil adhesion molecule expression and endothelial injury by Neisseria meningitidis. J Infect Dis 1996 Jan;173(1):172-179.

[6] Takano S, Kimura S, Ohdama S, Aoki N. Plasma thrombomodulin in health and diseases. Blood 1990 Nov 15;76(10):2024-2029.

[7] Nystedt S, Ramakrishnan V, Sundelin J. The proteinase-activated receptor 2 is induced by inflammatory mediators in human endothelial cells. Comparison with the thrombin receptor. J Biol Chem 1996 Jun 21;271(25):14910-14915.

[8] Devaraj S, Xu DY, Jialal I. C-reactive protein increases plasminogen activator inhibitor-1 expression and activity in human aortic endothelial cells: implications for the metabolic syndrome and atherothrombosis. Circulation 2003 Jan 28;107(3):398-404.

[9] Wolbink GJ, Bossink AW, Groeneveld AB, de Groot MC, Thijs LG, Hack CE. Complement activation in patients with sepsis is in part mediated by C-reactive protein. J Infect Dis 1998 Jan;177(1):81-87.

[10] Levi M, van der Poll T. Inflammation and coagulation. Crit Care Med 2010 Feb;38(2 Suppl):S26-34.

[11] Cunningham MA, Romas P, Hutchinson P, Holdsworth SR, Tipping PG. Tissue factor and factor VIIa receptor/ligand interactions induce proinflammatory effects in macrophages. Blood 1999 Nov 15;94(10):3413-3420.

[12] Szaba FM, Smiley ST. Roles for thrombin and fibrin(ogen) in cytokine/chemokine production and macrophage adhesion in vivo. Blood 2002 Feb 1;99(3):1053-1059.

[13] Lindmark E, Tenno T, Siegbahn A. Role of platelet P-selectin and CD40 ligand in the induction of monocytic tissue factor expression. Arterioscler Thromb Vasc Biol 2000 Oct;20(10):2322-2328.

[14] Day SM, Reeve JL, Pedersen B, Farris DM, Myers DD, Im M, et al. Macrovascular thrombosis is driven by tissue factor derived primarily from the blood vessel wall. Blood 2005 Jan 1;105(1):192-198.

[15] Falati S, Liu Q, Gross P, Merrill-Skoloff G, Chou J, Vandendries E, et al. Accumulation of tissue factor into developing thrombi in vivo is dependent upon microparticle P-selectin glycoprotein ligand 1 and platelet P-selectin. J Exp Med 2003 Jun 2;197(11):1585-1598.

[16] Souter PJ, Thomas S, Hubbard AR, Poole S, Romisch J, Gray E. Antithrombin inhibits lipopolysaccharide-induced tissue factor and interleukin-6 production by mononuclear cells, human umbilical vein endothelial cells, and whole blood. Crit Care Med 2001 Jan;29(1):134-139.

[17] Joyce DE, Gelbert L, Ciaccia A, DeHoff B, Grinnell BW. Gene expression profile of antithrombotic protein c defines new mechanisms modulating inflammation and apoptosis. J Biol Chem 2001 Apr 6;276(14):11199-11203.

[18] Oelschlager C, Romisch J, Staubitz A, Stauss H, Leithauser B, Tillmanns H, et al. Antithrombin III inhibits nuclear factor kappaB activation in human monocytes and vascular endothelial cells. Blood 2002 Jun 1;99(11):4015-4020.

[19] Hancock WW, Grey ST, Hau L, Akalin E, Orthner C, Sayegh MH, et al. Binding of activated protein C to a specific receptor on human mononuclear phagocytes inhibits intracellular calcium signaling and monocyte-dependent proliferative responses. Transplantation 1995 Dec 27;60(12):1525-1532.

[20] Ostrovsky L, Woodman RC, Payne D, Teoh D, Kubes P. Antithrombin III prevents and rapidly reverses leukocyte recruitment in ischemia/reperfusion. Circulation 1997 Oct 7;96(7):2302-2310.

[21] Sturn DH, Kaneider NC, Feistritzer C, Djanani A, Fukudome K, Wiedermann CJ. Expression and function of the endothelial protein C receptor in human neutrophils. Blood 2003 Aug 15;102(4):1499-1505.

[22] Isermann B, Hendrickson SB, Hutley K, Wing M, Weiler H. Tissue-restricted expression of thrombomodulin in the placenta rescues thrombomodulin-deficient mice from early lethality and reveals a secondary developmental block. Development 2001 Mar;128(6):827-838.

[23] Angus DC, van der Poll T. Severe sepsis and septic shock. N Engl J Med 2013 Nov 21;369(21):2063.

[24] de Stoppelaar SF, van 't Veer C, van der Poll T. The role of platelets in sepsis. Thromb Haemost 2014 Oct;112(4):666-677.

[25] Macfarlane RG. An Enzyme Cascade in the Blood Clotting Mechanism, and its Function as a Biochemical Amplifier. Nature 1964 May 2;202:498-499.

[26] Pozzi N, Chen Z, Pelc LA, Shropshire DB, Di Cera E. The linker connecting the two kringles plays a key role in prothrombin activation. Proc Natl Acad Sci U S A 2014 May 27;111(21):7630-7635.

[27] Rosing J, Tans G, Govers-Riemslag JW, Zwaal RF, Hemker HC. The role of phospholipids and factor Va in the prothrombinase complex. J Biol Chem 1980 Jan 10;255(1):274-283.

[28] Nesheim ME, Taswell JB, Mann KG. The contribution of bovine Factor V and Factor Va to the activity of prothrombinase. J Biol Chem 1979 Nov 10;254(21):10952-10962.

[29] Haynes LM, Bouchard BA, Tracy PB, Mann KG. Prothrombin activation by platelet-associated prothrombinase proceeds through the prethrombin-2 pathway via a concerted mechanism. J Biol Chem 2012 Nov 9;287(46):38647-38655.

[30] Tans G, Janssen-Claessen T, Hemker HC, Zwaal RF, Rosing J. Meizothrombin formation during factor Xa-catalyzed prothrombin activation. Formation in a purified system and in plasma. J Biol Chem 1991 Nov 15;266(32):21864-21873.

[31] Bode W, Huber R. Induction of the bovine trypsinogen-trypsin transition by peptides sequentially similar to the N-terminus of trypsin. FEBS Lett 1976 Oct 1;68(2):231-236.

[32] Kini RM. The intriguing world of prothrombin activators from snake venom. Toxicon 2005 Jun 15;45(8):1133-1145.

[33] Narasaki R, Kuribayashi H, Shimizu K, Imamura D, Sato T, Hasumi K. Bacillolysin MA, a novel bacterial metalloproteinase that produces angiostatin-like fragments from plasminogen and

activates protease zymogens in the coagulation and fibrinolysis systems. J Biol Chem 2005 Apr 8;280(14):14278-14287.

[34] Imamura T, Banbula A, Pereira PJ, Travis J, Potempa J. Activation of human prothrombin by arginine-specific cysteine proteinases (Gingipains R) from porphyromonas gingivalis. J Biol Chem 2001 Jun 1;276(22):18984-18991.

[35] Friedrich R, Panizzi P, Fuentes-Prior P, Richter K, Verhamme I, Anderson PJ, et al. Staphylocoagulase is a prototype for the mechanism of cofactor-induced zymogen activation. Nature 2003 Oct 2;425(6957):535-539.

[36] Panizzi P, Friedrich R, Fuentes-Prior P, Kroh HK, Briggs J, Tans G, et al. Novel fluorescent prothrombin analogs as probes of staphylocoagulase-prothrombin interactions. J Biol Chem 2006 Jan 13;281(2):1169-1178.

[37] Linderstrøm-Lang K, Ottesen M. Nature 1947; 159(807).

[38] Guntelberg AV, Ottesen M. Purification of the proteolytic enzyme from Bacillus subtilis. C R Trav Lab Carlsberg Chim 1954;29(3-4):36-48.

[39] Smith EL, DeLange RJ, Evans WH, Landon M, Markland FS. Subtilisin Carlsberg. J Biol Chem 1968 May10;243(9):2184-2191.

[40] Lee S, Jang DJ. Progressive rearrangement of subtilisin Carlsberg into orderly and inflexible conformation with Ca2+ binding. Bioph J 2001 Nov;81:2972-2978.

[41] Bratovanova EK, Petkov DD. Glycine flanked by hydrophobic bulky amino acid residues as minimal sequence for effective subtilisin catalysis. Biochem J 1987 Dec;15(248):957-960.

[42] Oggioni MR, Pozzi G, Valensin PE, Galieni P, Bigazzi C. Recurrent septicemia in an immunocompromised patient due to probiotic strains of Bacillus subtilis. J Clin Microbiol 1998 Jan;36(1):325-326.

[43] Liu C, Matsushita Y, Shimizu K, Makimura K, Hasumi K. Activation of prothrombin by two subtilisin-like serine proteases from Acremonium sp. Biochem Biophys Res Commun 2007 Jun 22;358(1):356-362.

[44] De Cristofaro R, Di Cera E. Phenomenological analysis of the clotting curve. J Protein Chem 1991 Oct;10(5):455-468.

[45] Pozzi N, Acquasaliente L, Frasson R, Cristiani A, Moro S, Banzato A, et al. beta2 -Glycoprotein I binds to thrombin and selectively inhibits the enzyme procoagulant functions. J Thromb Haemost 2013 Jun;11(6):1093-1102.

[46] Toth O, Calatzis A, Penz S, Losonczy H, Siess W. Multiple electrode aggregometry: a new device to measure platelet aggregation in whole blood. Thromb Haemost 2006 Dec;96(6):781-788.

[47] DiBella EE, Maurer MC, Scheraga HA. Expression and folding of recombinant bovine prethrombin-2 and its activation to thrombin. J Biol Chem 1995 Jan 6;270(1):163-169.

[48] Pozzi N, Acquasaliente L, Frasson R, Cristiani A, Moro S, Banzato A, et al. beta2 -Glycoprotein I binds to thrombin and selectively inhibits the enzyme procoagulant functions. J Thromb Haemost 2013 Jun;11(6):1093-1102.

[49] Mizuochi T, Fujii J, Kisiel W, Kobata A. Studies on the structures of the carbohydrate moiety of human prothrombin. J Biochem 1981 Oct;90(4):1023-1031.

[50] Harlos K, Boys CW, Holland SK, Esnouf MP, Blake CC. Structure and order of the protein and carbohydrate domains of prothrombin fragment 1. FEBS Lett 1987 Nov 16;224(1):97-103.

[51] Chen Z, Pelc LA, Di Cera E. Crystal structure of prethrombin-1. Proc Natl Acad Sci U S A 2010 Nov 9;107(45):19278-19283.

[52] Ng AS, Lewis SD, Shafer JA. Quantifying thrombin-catalyzed release of fibrinopeptides from fibrinogen using high-performance liquid chromatography. Methods Enzymol 1993;222:341-358.

[53] De Cristofaro R, Di Cera E. Phenomenological analysis of the clotting curve. J Protein Chem 1991 Oct;10(5):455-468.

[54] Weisel, J. W. and Nagaswami, C. (1992) Computer modeling of fibrin polymerization kinetics correlated with electron microscope and turbidity observations: Clot structure and assembly are kinetically controlled. Biophys. J. 63, 111-128. doi:S0006-3495(92)81594-1 [pii]

[55] De Candia, E., Hall, S. W., Rutella, S., Landolfi, R., Andrews, R. K. and De Cristofaro, R.(2001) Binding of thrombin to glycoprotein ib accelerates the hydrolysis of par-1 on intact platelets.J. Biol. Chem. 276, 4692-4698. doi:10.1074/jbc.M008160200 [doi]

[56] De Cristofaro R, De Filippis V. Interaction of the 268-282 region of glycoprotein Ibalpha with the heparin-binding site of thrombin inhibits the enzyme activation of factor VIII. Biochem J 2003 Jul 15;373(Pt 2):593-601.

CHAPTER 4.1

Natural Anticoagulants

Alterations in Coagulation: Thrombotic Disorders

Haemostasis is an extremely complex procoagulant biochemical response, which triggers after vascular damage and exposure of the sub-endothelial collagen. This system is finely regulated by both physiologic anticoagulants and by the fibrinolytic system [**1**]. In healthy conditions, the homeostasis is slightly un-balanced towards a haemorrhagic state, to keep blood fluid in the intact vessels, while generating a clot in the site of injury. If this equilibrium disrupts, pathological manifestations can lead both to impaired or to abnormal coagulation. Briefly, in case of loss of functioning, a haemorrhagic state occurs, attributable either to *thrombocytopenia* (platelets count < $150 \cdot 10^3$/μl plasma), haemophilia type A or B, von Willebrand disease, or deficits in vitamin K.

On the other side, pathologies due to an increase in functioning are widely classified as *thrombotic* diseases, causing high levels of morbidity and mortality. If the abnormalities affect the primary haemostasis (platelets count > $450 \cdot 10^3$/μl plasma) we refer to as *thrombocytosis*; in case the disorders involve secondary haemostasis, they are classified as *thrombophilia*. Both arterial and venous thrombosis may occur in the thrombophilic state; however the latter is surely more frequent [**2**]. One key concept involved in either haemostasis or thrombosis is that, in healthy conditions, the processes are localized. The simply increase of coagulation factors concentrations, with or without adding negative phospholipid vesicles, leads to extensive α-thrombin (αT) generation [**3**]. This widespread uncontrolled activation can eventually lead to disseminated intravascular coagulation (DIC), a pathological condition typical of sepsis [**4**].

Recently, a combination of genetically manipulated mouse models, and a broad study in human epidemiology has revealed the variety of genetic factors contributing to the onset of thrombosis [**5**]. This disorder is eventually generated by abnormally high concentrations or functioning of some coagulation factors, with defects of the natural anticoagulant mechanisms. Particularly von Willebrand factor (vWF), FVII, FVIII and prothrombin (ProT) are associated with increased risk of thrombosis. In detail, the hazard connected to FVIII may due to its inherent instability following activation; on the other hand, ProT is both the inactive precursor of αT and an effective inhibitor of active protein C (aPC) [**6**]. Moreover, Leiden mutation of FV results in the generation of FVa resistant to proteolytic degradation by aPC. Among all, this genetic alteration is the most frequent, since approximately 5% of the Caucasian population carry this mutation. In

thrombophilic families, FV Leiden occurs in 40-60% of cases [**7**]. On the other hand, deficiencies of the anticoagulant pathways may involve the heparin-antithrombin (ATIII) pathway, the protein C (PC) pathway and the tissue factor (TF) inhibitory pathway (TFPI). Defects in ATIII and in each component of the PC pathway, i.e. PC [**8**], cofactor protein S (PS) [**9**], thrombomodulin (TM) [**10**], and protein C endothelial receptor (EPCR) [**11**] are all associated with increased risk of thrombotic disease. The role of TF is still matter of debate, since the majority of the protein is associated with the endothelium [**12**].

These genetically controlled variants in coagulation factors work in concert with other risks factors, with strong synergy between multiple aspects. Hypoxic and inflammatory states modulate the pro- and anticoagulant properties of the endothelium, by downregulating anticoagulant pathways and upregulating TF [**13**;**14**;**15**]. Moreover, hypoxia increases the expression of the chemoattractant P-selectin on the endothelium, with the recruitment of leukocytes and monocyte microparticles. Exposing TF on their surface, these cellular components can serve as the nidus for the initiation of blood clot [**16**;**17**;**18**]. The risk of thrombosis rises dramatically with aging. The molecular basis of this clinical evidence remains uncertain, but the disorder may be provoked by increase in body mass, decrease in physical activity, immobilization due to illness, acute infections and co-morbidities. Moreover, in old individuals, an increase of procoagulant factors levels, as ProT fragment 1·2, results in a persistent hypercoagulable state [**19**]. Obesity >30 kg/m^2 enhances the risk of two-fold [**20**], oral contraceptives of four-fold [**21**]. Pregnancy, in all trimesters and in the postpartum period, is another consistent risk condition, due to disturbed blood flow and hormonal changes [**22**]. Cancer increases the thrombotic risk of about 6/10-fold, due to the release, from the tumour, of membrane particles that display procoagulant activities, and membrane lipids that propagate coagulation [**23**]. Finally, also the antiphospholipid syndrome [**24**] and postoperative thrombosis participate to these pathological manifestations. In this scenario, the development and design of safer antithrombotics is of crucial importance.

Anticoagulants

Nowadays, thrombotic disorders have become a serious cause of morbidity and mortality. Globally, with the change of food habits and lifestyle, atherosclerosis and thromboembolic disorders are becoming dramatically common [**25**;**26**;**27**]. Heparin [**28**] and vitamin K antagonists such as warfarin [**29**] are the cornerstones of the anticoagulant drugs. The fibrinolytic agents complete the picture of the classical anticoagulant therapy. Unfortunately, these classes of drugs are characterized by well-documented limitations, which drive the continuous and intense efforts to develop new, safer anticoagulants, especially those targeting specific coagulation factors [**30**]. Some of the leaders in this market are FXa inhibitors (apixaban, rivaroxaban) [**31**] and αT direct inhibitors, like hirudin [**32**], bivalirudin [**33**], argatroban [**34**] and dabigatran [**35**], both synthetic or from hematophagous organisms. Nevertheless, the complicated nature and wide clinical manifestations of thrombosis continue to call for more new and safe anticoagulants, with different pharmacological and pharmacokinetic proprieties. Researches are still studying for the establishment of a new leader compound.

Classical Therapy

Classical therapy anticoagulants can be sub-divided in drugs acting on the coagulation cascade, both injectable (heparin) or oral (warfarin), or in thrombolytic agents.

Heparin is a highly sulphated glycosaminoglycan polymer of varying length, accounted to carry the highest negative charge density of any known biological molecule. Unfractioned heparin (UFH) binds to ATIII and induces a conformational change in FXa, thus inhibiting the latter and FIIa in a 1:1 ratio. On the other hand, smaller low molecular weight heparins (LMWH) have a higher proportional impact on FXa, versus FIIa, in a 3:1 or 2:1 ratio. UHF is indicated for the treatment and prophylaxis of venous thromboembolism, atrial fibrillation, and in case of DIC. This drug is administered parenterally, both subcutaneous for the prophylaxis use (efficacy within 20-60min), and as continuous venous infusion when used therapeutically (immediate effect) [**36**]. Common side effects, like bleeding, can be reversed by the administration of protamine sulphate (1mg will reverse 100 units of UFH). Another severe adverse outcome of UFH is the onset of heparin-induced thrombocytopenia (HIT), with the generation of abnormal antibodies that activate platelets. In case of HIT, therapy with UHF must be stopped immediately. LMWH (i.e. dalteparin, enoxaparin, tinzaparin) are subcutaneously administered (efficacy within 2-4h), but, since they have a controlled molecular weight, they exhibit a more predictable dose-response curve [**37**], and can be administered at fixed dose, without regulation or monitoring. When used prophylactically, major bleeding occurs seldom; the incidence increases during the treatment of acute coronary syndrome [**38**]. Bleeding can

be reversed with the administration of protamine sulphate (reversibility ≈ 60%), anti-FXa, cryoprecipitate or fresh frozen plasma.

Vitamin K antagonists (VKAs), such as oral warfarin, function by blocking the vitamin K-epoxide reductase, thus impairing the maturation of the vitamin K-dependent clotting factors (ProT, FVII, FIX, FX, PC, PS). Actually, these drugs act only on the synthesis of new coagulation factors, without affecting the pre-existing ones. The VKAs display an opening prothrombotic effect, by initially blocking PC and PS, followed by a delayed antithrombotic effect, through the impairment of ProT, FVII, FIX, FX Gla domain maturation [**39**]. If rapid anticoagulation is required, due to this early collateral effect, warfarin is co-administered with a parental anticoagulant, like heparin. Common side effects, as bleeding, can be reversed with the administration of vitamin K, FVIIa, fresh frozen plasma or ProT complex concentrates (PCC) [**40**;**41**].

In the fibrinolytic system, inactive plasminogen is converted to plasmin by tissue plasminogen activator (tPA) or urokinase. Active plasmin, in turn, proteolytically degrades the fibrin matrix, thus destroying the thrombus. tPA is characterized by low affinity towards circulating plasminogen, but high affinity for fibrin. After generating the stable bimolecular [tPA-fibrin] complex, plasminogen is activated only on the thrombus surface. Alteplase, an un-modified form of human tPA, along with reteplase and tenecteplase, modified analogues of tPA, are the most common drugs in this class [**42**;**43**]. These agents are used in case of pre-existent thrombi, for the treatment of acute cerebrovascular accidents, myocardial infarction, pulmonary emboli, presence of thrombi in indwelling catheters. There are no precise laboratory indexes to quantify the anticoagulant effect of the fibrinolytic drugs. The insurgence of haemorrhagic states is highly variable, and it is not efficiently reverted by the administration of blood products, as in the other cases. Other agents, like tranexamic acid and ε-aminocaproic acid, impair fibrinolysis by competitively inhibiting plasminogen activation.

Factor Xa Inhibitors and Direct Thrombin Inhibitors (DTIs)

FXa inhibitors (apixaban, rivaroxiban) act on this coagulation factor both free, clot-associated and in the prothrombinase complex [**44**] in a dose-dependent fashion [**45**]. These drugs are used for the prophylaxis and treatment of venous thromboembolism, for the prophylaxis of embolic disease in non-valvular atrial fibrillation, and as alternative coagulants in case of HIT.

On the other hand, direct thrombin inhibitors (DTIs) down-regulate αT catalytic activity without the need of a cofactor, as in case of heparin [**46**]. These drugs, either administered parenterally (argatroban) or orally (dabigatran), are used for the prophylaxis and treatment of venous

thromboembolism and acute coronary syndrome, and for prophylaxis of thrombus formation in non-valvular atrial fibrillation.

For both these classes, no specific laboratory parameters are available to monitor their effective anticoagulant impact. As in the case with all the anticoagulants, the most common adverse reaction is haemorrhage. For FXa inhibitors, thrombocytopenia was also reported: the molecular mechanism of its insurgence remains unclear [**37**]. DTIs have been reported to induce gastrointestinal bleeding and intracranial haemorrhage, in a dose-dependently way [**47**;**48**]. Bleeding can be reversed after the administration of FVIIa or PCC. Due to the limited evidence-based data, even in this case no specific antidotes exist. Both these drug categories include natural anticoagulants from hematophagous organisms.

Natural Anticoagulants from Hematophagous Organisms

A new hot trend in the development of anticoagulants is the purification or engineering of natural substances from hematophagous animals. To obtain blood meals avoiding the clotting, these organisms are armed with potent pharmacologically active molecules to overcome the hosts' response systems. The molecular heterogeneity displayed is huge and constantly expanding, since extensive efforts have been performed in the isolation and characterization of these compounds. Hematophagous animals consists mainly on arthropods (*Ixodidia*, *Dipteria*, *Hemiptera*, *Phthiraptera*, *Siphonaptera*), annelids in the subclass of leeches (*Hirudinea*), nematodes such as hookworms, and even mammals like vampire bats. Although the duration, behaviour and mechanisms of their feeding habits is different, they all face the mechanical (skin, vessel walls) and chemical defences of their hosts, including the haemostatic, inflammatory and immunologic systems. The pharmacological weapons used to overcome these defence responses include vasodilators, anticoagulants, antiplatelets, immunesuppressors and anti-inflammatory compounds [**49**;**50**;**51**;**52**].

Among all, anticoagulant hirudin from the medicinal leeches and bivalirudin (designed based on hirudin) are the most popular compounds. In the past decades, the clinical use of hirudin remained restricted because of its leakage in the natural source (≈20 μg/leech head). Now, advanced methods of peptide synthesis and of genetic engineering are providing sufficient amounts of hirudin in a purified form. This natural compound is thus becoming more and more pharmacologically interesting.

Hirudin

Among natural anticoagulants, hirudin is the most potent and specific thrombin inhibitor. This small polypeptide derives from the salivary glands of the blood sucking medicinal leech, and was first biochemically characterized by Markwardt [**53**]. This protein presents several isoforms: hirudin variants HV1, HV2 and HV3 are extracted from *Hirudo medicinalis* [**54**;**55;56**]. On the other side, HM1 and HM2 derive from *Hirudinaria manillensis*, also called buffalo leech, a specie significantly more specialized for mammalian parasitism [**57**;**58**;**59**].The primary structures of hirudin isoforms from *H. medicinalis* show significant sequence similarities (60-75%) to those of *H. manillensis* (**Fig. 1**). All the variants consist in a single polypeptide chain (65-66aa), in which a hydrophobic N-terminal core is composed by two β-sheets tightly packed in a compact structure. In particular, six Cys residues in highly conserved positions are engaged in a pattern of disulphide bonds peculiar for this class of serine proteases inhibitors [**60**] (**Fig. 2**). On the other hand, the C-terminal tail is highly acidic and de-structured. HV1, HV2 and HV3 present a sulphate Tyr63; in HM1 and HM2 this negative charge is supplied by an extra Asp in the C-terminal tail. Hirudin interacts with thrombin in an extremely tight complex, characterized by an inhibition constant of 10^{-11}-10^{-14} M [**61**]. Due to this dramatically high affinity, hirudin can bind the serine protease both free and in the thrombus-bound state [**62**].

.

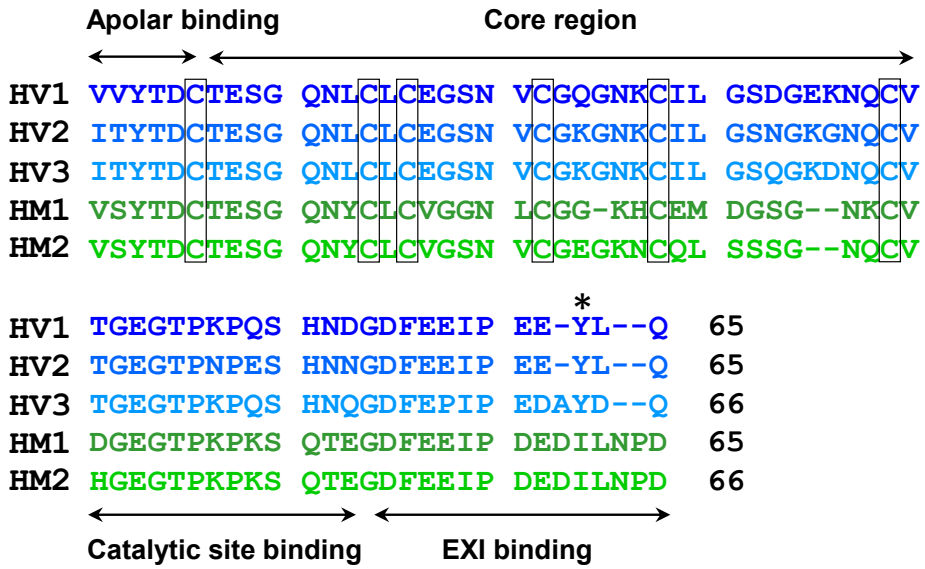

Figure 1 [adapted from Sohn et al., 2001]. Amino acid sequence alignment of hirudin variants HV1, HV2, HV3 from *Hirudo medicinalis* and HM1, HM2 from *Hirudinaria manillensis*, displayed in different colours. The sequences, of 65-66 amino acids, present a high degree of similarity. The six conserved Cys residues are boxed, while a star highlights the sulphated Tyr63 present in the *H. medicinalis* isoforms (*). Black arrows indicate the core N-terminal region, and the segments involved in the apolar binding, interaction with catalytic site, or exosite I.

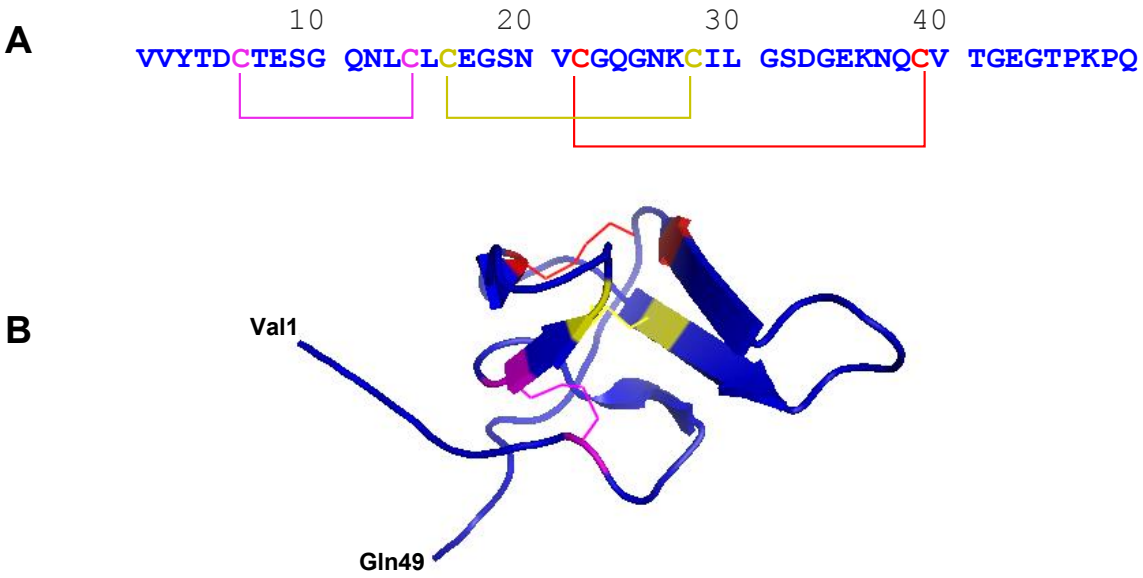

Figure 2. (A) Amino acidic sequence and (B) three-dimensional structure (pdb: 5hir) of hirudin HV1(1-49) from *H. medicinalis*. The N-terminal core is tightly packed by three highly conserved disulphide bridges, here displayed as coloured lines: Cys6-Cys14, in magenta; Cys16-Cys28 in yellow; Cys22-Cys39 in red. The C-terminal de-structured tail could not be crystallized in this model.

Due to its important pharmacological implications, the [hirudin-αT] complex was deeply studied through structural and biochemical investigations, both by X-ray crystallography [**63**;**64**] and by NMR studies [**65**]. The N-terminal domain covers αT active site, and through its first three amino acids extensively penetrates into the catalytic pocket of the enzyme. Notably, this tripeptide alone realizes about half of the total contacts observed for the binding of the core domain (1-47) to αT, accounting for ≈30% of the total free energy of binding (**Fig. 3A, B**).

Val / Ile 1 - NMR studies suggest that the first N-terminal residue is almost fully exposed to the solvent and highly flexible in free hirudin [**66**]. Conversely, in the αT-bound state, Val/Ile1 is completely buried into the active site, fixed into a single side-chain conformation [**64**]. In particular, the NH_2 group of residue 1 is engaged in an hydrogen bond with the Oγ of the catalytic Ser195, while its side-chain makes numerous hydrophobic contacts with Tyr60a and Trp60d, shaping the S2 site of the enzyme.

Val / Thr / Ser 2 - Hirudin residue 2, very flexible in the free molecule, is located at the entrance, without penetrating, the primary specificity S1 site (i.e. Asp 189). In conclusion, the occupancy of the S1 site is not strictly required for the binding.

Tyr 3 - Tyr3, highly conserved through the hirudin family [**67**] is characterized by a well-defined conformation both in the free- and in the bound-state. In detail, in the complex, the side chain of Tyr3 projects into the apolar S3 site: Hδ in the edge of the aromatic ring interacts with the π-electron cloud of the aromatic ring of Trp215.

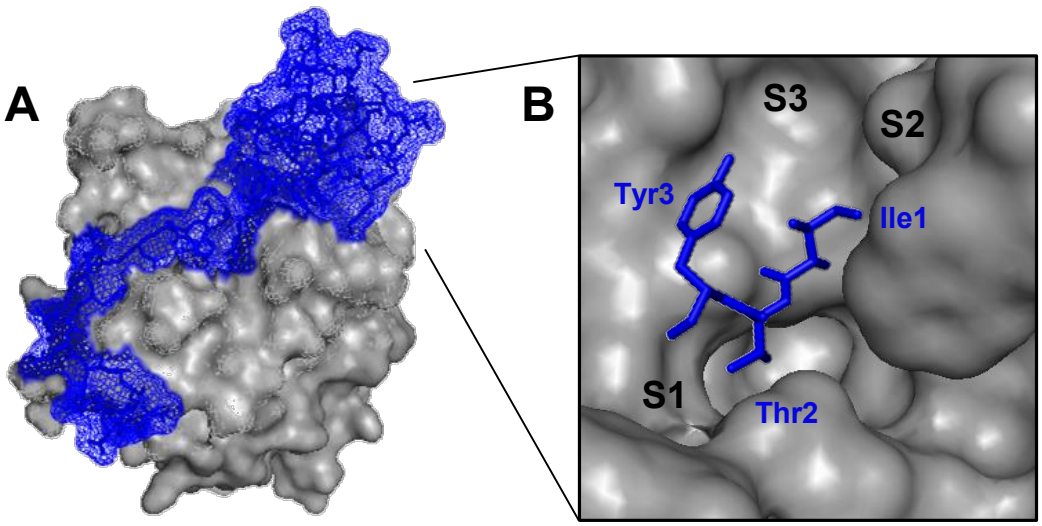

Figure 3. (A) Three-dimensional structure of [αT-HV2] complex (pdb: 4htc) and (B) detail of the interaction between hirudin N-terminal tripeptide (ITY) with αT catalytic cleft. In both the panels HV2 is displayed in blue, as sticks, while αT as a grey surface. Hirudin N-terminal tripeptide realizes half of the interactions of the compact (1-47) core. In detail, Ile1 enters the specificity site S2, Thr2 points, without penetrating, specificity site S1, while Tyr3 contacts with the large apolar specificity site S3.

On the other side, hirudin C-terminal segment lies in a long groove, extending from the active site pocket, flanked by thrombin loops (70-80) and (35-39) (**Fig. 3A**). This flexible unfolded region is engaged in both ionic and hydrophobic interactions with the fibrinogen binding site [**67**].

Hirudin is an excellent probe for the allosteric properties of αT, because it covers ≈12% of the available area of the enzyme upon formation of the complex [**64**]. Hirudin binds ≈30-fold more tightly to αT *fast* form, rather than the *slow* form [**68**]. Hirudin N-terminal domain (1-47), obtained either by peptide synthesis or by limited proteolysis [**69**] maintains the binding to the active site, although it is less active of about $2 \cdot 10^5$-fold, still showing a certain preference for αT *fast* form. Also the C-terminal domain alone, produced by peptide synthesis, retains the interaction to the fibrinogen binding site.

REFERENCES

[1] Collen D. Potential approaches for therapeutic intervention of thrombosis by fibrinolytic agents. Semin Thromb Hemost 1988 Jan;14(1):95-99.

[2] Girolami A, Simioni P, Scarano L, Girolami B. Venous and arterial thrombophilia. Haematologica 1997 Jan-Feb;82(1):96-100.

[3] Esmon CT. Basic mechanisms and pathogenesis of venous thrombosis. Blood Rev 2009 Sep;23(5):225-229.

[4] van der Poll T, Herwald H. The coagulation system and its function in early immune defense. Thromb Haemost 2014 Oct;112(4):640-648.

[5] Lane DA, Grant PJ. Role of hemostatic gene polymorphisms in venous and arterial thrombotic disease. Blood 2000 Mar 1;95(5):1517-1532.

[6] Smirnov MD, Safa O, Esmon NL, Esmon CT. Inhibition of activated protein C anticoagulant activity by prothrombin. Blood 1999 Dec 1;94(11):3839-3846.

[7] Rosendaal FR, Reitsma PH. Genetics of venous thrombosis. J Thromb Haemost 2009 Jul;7 Suppl 1:301-304.

[8] Esmon CT. Inflammation and thrombosis: the impact of inflammation on the protein C anticoagulant pathway. Haematologica 1995 Mar-Apr;80(2 Suppl):49-56

[9] Schwarz HP, Fischer M, Hopmeier P, Batard MA, Griffin JH. Plasma protein S deficiency in familial thrombotic disease. Blood 1984 Dec;64(6):1297-1300.

[10] Kunz G, Ireland HA, Stubbs PJ, Kahan M, Coulton GC, Lane DA. Identification and characterization of a thrombomodulin gene mutation coding for an elongated protein with reduced expression in a kindred with myocardial infarction. Blood 2000 Jan 15;95(2):569-576.

[11] Biguzzi E, Merati G, Liaw PC, Bucciarelli P, Oganesyan N, Qu D, et al. A 23bp insertion in the endothelial protein C receptor (EPCR) gene impairs EPCR function. Thromb Haemost 2001 Oct;86(4):945-948.

[12] Drake TA, Morrissey JH, Edgington TS. Selective cellular expression of tissue factor in human tissues. Implications for disorders of hemostasis and thrombosis. Am J Pathol 1989 May;134(5):1087-1097.

[13] Faust SN, Levin M, Harrison OB, Goldin RD, Lockhart MS, Kondaveeti S, et al. Dysfunction of endothelial protein C activation in severe meningococcal sepsis. N Engl J Med 2001 Aug 9;345(6):408-416.

[14] Esmon CT. Inflammation and the activated protein C anticoagulant pathway. Semin Thromb Hemost 2006 Apr;32 Suppl 1:49-60.

[15] Shreeniwas R, Ogawa S, Cozzolino F, Torcia G, Braunstein N, Butura C, et al. Macrovascular and microvascular endothelium during long-term hypoxia: alterations in cell growth, monolayer permeability, and cell surface coagulant properties. J Cell Physiol 1991 Jan;146(1):8-17.

[16] Closse C, Seigneur M, Renard M, Pruvost A, Dumain P, Belloc F, et al. Influence of hypoxia and hypoxia-reoxygenation on endothelial P-selectin expression. Haemostasis 1996 Oct;26 Suppl 4:177-181.

[17] Myers DD, Hawley AE, Farris DM, Wrobleski SK, Thanaporn P, Schaub RG, et al. P-selectin and leukocyte microparticles are associated with venous thrombogenesis. J Vasc Surg 2003 Nov;38(5):1075-1089.

[18] Falati S, Liu Q, Gross P, Merrill-Skoloff G, Chou J, Vandendries E, et al. Accumulation of tissue factor into developing thrombi in vivo is dependent upon microparticle P-selectin glycoprotein ligand 1 and platelet P-selectin. J Exp Med 2003 Jun 2;197(11):1585-1598.

[19] Lowe GD, Rumley A, Woodward M, Morrison CE, Philippou H, Lane DA, et al. Epidemiology of coagulation factors, inhibitors and activation markers: the Third Glasgow MONICA Survey. I. Illustrative reference ranges by age, sex and hormone use. Br J Haematol 1997 Jun;97(4):775-784.

[20] Abdollahi M, Cushman M, Rosendaal FR. Obesity: risk of venous thrombosis and the interaction with coagulation factor levels and oral contraceptive use. Thromb Haemost 2003 Mar;89(3):493-498.

[21] Sidney S, Petitti DB, Soff GA, Cundiff DL, Tolan KK, Quesenberry CP,Jr. Venous thromboembolic disease in users of low-estrogen combined estrogen-progestin oral contraceptives. Contraception 2004 Jul;70(1):3-10.

[22] Lim W, Eikelboom JW, Ginsberg JS. Inherited thrombophilia and pregnancy associated venous thromboembolism. BMJ 2007 Jun 23;334(7607):1318-1321.

[23] Bick RL. Cancer-associated thrombosis. N Engl J Med 2003 Jul 10;349(2):109-111.

[24] de Groot PG, Derksen RH. Pathophysiology of the antiphospholipid syndrome. J Thromb Haemost 2005 Aug;3(8):1854-1860.

[25] Koh CY, Kini RM. Anticoagulants from hematophagous animals. Expert Rev Hematol 2008 Dec;1(2):135-139.

[26] Ajjan R, Grant PJ. Coagulation and atherothrombotic disease. Atherosclerosis 2006 Jun;186(2):240-259.

[27] Gross PL, Weitz JI. New anticoagulants for treatment of venous thromboembolism. Arterioscler Thromb Vasc Biol 2008 Mar;28(3):380-386.

[28] Gray E, Mulloy B, Barrowcliffe TW. Heparin and low-molecular-weight heparin. Thromb Haemost 2008 May;99(5):807-818.

[29] Cranenburg EC, Schurgers LJ, Vermeer C. Vitamin K: the coagulation vitamin that became omnipotent. Thromb Haemost 2007 Jul;98(1):120-125.

[30] Weitz JI. Emerging anticoagulants for the treatment of venous thromboembolism. Thromb Haemost 2006 Sep;96(3):274-284.

[31] Abrams PJ, Emerson CR. Rivaroxaban: a novel, oral, direct factor Xa inhibitor. Pharmacotherapy 2009 Feb;29(2):167-181.

[32] Greinacher A, Warkentin TE. The direct thrombin inhibitor hirudin. Thromb Haemost 2008 May;99(5):819-829

[33] Warkentin TE, Greinacher A, Koster A. Bivalirudin. Thromb Haemost 2008 May;99(5):830-839.

[34] Yeh RW, Jang IK. Argatroban: update. Am Heart J 2006 Jun;151(6):1131-1138.

[35] Eriksson BI, Smith H, Yasothan U, Kirkpatrick P. Dabigatran etexilate. Nat Rev Drug Discov 2008 Jul;7(7):557-558.

[36] Douketis JD. Pharmacologic properties of the new oral anticoagulants: a clinician-oriented review with a focus on perioperative management. Curr Pharm Des 2010;16(31):3436-3441.

[37] Gresham C, Levine M, Ruha AM. Case files of the Medical Toxicology Fellowship at Banner Good Samaritan Medical Center in Phoenix, AZ: a non-warfarin anticoagulant overdose. J Med Toxicol 2009 Dec;5(4):242-249.

[38] Crowther MA, Warkentin TE. Bleeding risk and the management of bleeding complications in patients undergoing anticoagulant therapy: focus on new anticoagulant agents. Blood 2008 May 15;111(10):4871-4879.

[39] Ageno W, Gallus AS, Wittkowsky A, Crowther M, Hylek EM, Palareti G, et al. Oral anticoagulant therapy: Antithrombotic Therapy and Prevention of Thrombosis, 9th ed: American College of Chest Physicians Evidence-Based Clinical Practice Guidelines. Chest 2012 Feb;141(2 Suppl):e44S-88S.

[40] Tran HA, Chunilal SD, Harper PL, Tran H, Wood EM, Gallus AS, et al. An update of consensus guidelines for warfarin reversal. Med J Aust 2013 Mar 4;198(4):198-199.

[41] DeLoughery EP, Lenfesty B, DeLoughery TG. The use of recombinant factor VIIa in warfarin patients with traumatic brain injury: a retrospective case-control study. Blood Coagul Fibrinolysis 2013 Apr;24(3):317-320.

[42] Shehab N, Sperling LS, Kegler SR, Budnitz DS. National estimates of emergency department visits for hemorrhage-related adverse events from clopidogrel plus aspirin and from warfarin. Arch Intern Med 2010 Nov 22;170(21):1926-1933.

[43] Hirsh J, O'Donnell M, Eikelboom JW. Beyond unfractionated heparin and warfarin: current and future advances. Circulation 2007 Jul 31;116(5):552-560.

[44] Weitz JI, Eikelboom JW, Samama MM, American College of Chest Physicians. New antithrombotic drugs: Antithrombotic Therapy and Prevention of Thrombosis, 9th ed: American College of Chest Physicians Evidence-Based Clinical Practice Guidelines. Chest 2012 Feb;141(2 Suppl):e120S-51S.

[45] Kubitza D, Becka M, Roth A, Mueck W. Dose-escalation study of the pharmacokinetics and pharmacodynamics of rivaroxaban in healthy elderly subjects. Curr Med Res Opin 2008 Oct;24(10):2757-2765.

[46] Yee DL, O'Brien SH, Young G. Pharmacokinetics and pharmacodynamics of anticoagulants in paediatric patients. Clin Pharmacokinet 2013 Nov;52(11):967-980.

[47] Eikelboom JW, Wallentin L, Connolly SJ, Ezekowitz M, Healey JS, Oldgren J, et al. Risk of bleeding with 2 doses of dabigatran compared with warfarin in older and younger patients with atrial fibrillation: an analysis of the randomized evaluation of long-term anticoagulant therapy (RE-LY) trial. Circulation 2011 May 31;123(21):2363-2372.

[48] Connolly SJ, Ezekowitz MD, Yusuf S, Eikelboom J, Oldgren J, Parekh A, et al. Dabigatran versus warfarin in patients with atrial fibrillation. N Engl J Med 2009 Sep 17;361(12):1139-1151.

[49] Ribeiro JM. Blood-feeding arthropods: live syringes or invertebrate pharmacologists? Infect Agents Dis 1995 Sep;4(3):143-152.

[50] Ribeiro JM, Francischetti IM. Role of arthropod saliva in blood feeding: sialome and post-sialome perspectives. Annu Rev Entomol 2003;48:73-88.

[51] Salzet M. Anticoagulants and inhibitors of platelet aggregation derived from leeches. FEBS Lett 2001 Mar 16;492(3):187-192.

[52] Champagne DE. Antihemostatic strategies of blood-feeding arthropods. Curr Drug Targets Cardiovasc Haematol Disord 2004 Dec;4(4):375-396

[53] Markwardt F. Hirudin; an inhibitor of blood coagulation from medical leeches. Blut 1958 Jun;4(3):160-161.

[54] Dodt J, Seemuller U, Maschler R, Fritz H. The complete covalent structure of hirudin. Localization of the disulfide bonds. Biol Chem Hoppe Seyler 1985 Apr;366(4):379-385.

[55] Harvey RP, Degryse E, Stefani L, Schamber F, Cazenave JP, Courtney M, et al. Cloning and expression of a cDNA coding for the anticoagulant hirudin from the bloodsucking leech, Hirudo medicinalis. Proc Natl Acad Sci U S A 1986 Feb;83(4):1084-1088.

[56] Tripier D. Hirudin: a family of iso-proteins. Isolation and sequence determination of new hirudins. Folia Haematol Int Mag Klin Morphol Blutforsch 1988;115(1-2):30-35.

[57] Electricwala A, Hartwell R, Scawen MD, Atkinson T. The complete amino acid sequence of a hirudin variant from the leech Hirudinaria manillensis. J Protein Chem 1993 Jun;12(3):365-370.

[58] Scacheri E, Nitti G, Valsasina B, Orsini G, Visco C, Ferrera M, et al. Novel hirudin variants from the leech Hirudinaria manillensis. Amino acid sequence, cDNA cloning and genomic organization. Eur J Biochem 1993 May 15;214(1):295-304.

[59] Bagdy D, Barabas E, Graf L, Petersen TE, Magnusson S. Hirudin. Methods Enzymol 1976;45:669-678.

[60] Thornton JM. Disulphide bridges in globular proteins. J Mol Biol 1981 Sep 15;151(2):261-287.

[61] Stone SR, Hofsteenge J. Kinetics of the inhibition of thrombin by hirudin. Biochemistry 1986 Aug 12;25(16):4622-4628.

[62] Hoffmann A, Markwardt F. Inhibition of the thrombin-platelet reaction by hirudin. Haemostasis 1984;14(2):164-169.

[63] Rydel TJ, Ravichandran KG, Tulinsky A, Bode W, Huber R, Roitsch C, et al. The structure of a complex of recombinant hirudin and human alpha-thrombin. Science 1990 Jul 20;249(4966):277-280.

[64] Rydel TJ, Tulinsky A, Bode W, Huber R. Refined structure of the hirudin-thrombin complex. J Mol Biol 1991 Sep 20;221(2):583-601.

[65] Folkers PJ, Clore GM, Driscoll PC, Dodt J, Kohler S, Gronenborn AM. Solution structure of recombinant hirudin and the Lys-47----Glu mutant: a nuclear magnetic resonance and hybrid distance geometry-dynamical simulated annealing study. Biochemistry 1989 Mar 21;28(6):2601-2617.

[66] Nicastro G, Baumer L, Bolis G, Tato M. NMR solution structure of a novel hirudin variant HM2, N-terminal 1-47 and N64-->V + G mutant. Biopolymers 1997 Jun;41(7):731-749.

[67] Steiner V, Knecht R, Bornsen KO, Gassmann E, Stone SR, Raschdorf F, et al. Primary structure and function of novel O-glycosylated hirudins from the leech Hirudinaria manillensis. Biochemistry 1992 Mar 3;31(8):2294-2298.

[68] Naski MC, Fenton JW,2nd, Maraganore JM, Olson ST, Shafer JA. The COOH-terminal domain of hirudin. An exosite-directed competitive inhibitor of the action of alpha-thrombin on fibrinogen. J Biol Chem 1990 Aug 15;265(23):13484-13489.

[69] Di Cera E, Dang QD, Ayala YM. Molecular mechanisms of thrombin function. Cell Mol Life Sci 1997 Sep;53(9):701-730. De Filippis V, Vindigni A, Altichieri L, Fontana A. Core domain of hirudin from the leech Hirudinaria manillensis: chemical synthesis, purification, and characterization of a Trp3 analog of fragment 1-47. Biochemistry 1995 Jul 25;34(29):9552-9564.

CHAPTER 4.2

Expression, Purification and Characterization of Soluble and Active Hirudin in *E. coli* by SUMO Fusion Expression System

INTRODUCTION

Hirudin, the most potent and specific α-thrombin (αT) natural inhibitor, deriving from the salivary glands of the medicinal leech, was first biochemically characterized by Markwardt [**1**]. Hirudin presents several isoforms: hirudin variants HV1, HV2 and HV3 are extracted from *Hirudo medicinalis* [**2**;**3**;**4**]. On the other side, HM1 and HM2 derive from *Hirudinaria manillensis*, also called buffalo leech, a specie significantly more specialized for mammalian parasitism [**5**;**6**;**7**]. All the variants consist in a single polypeptide chain (65-66aa), composed by a hydrophobic N-terminal *core*, cross-linked by three disulphide bridges, and by an acidic unfolded C-terminal tail. In detail, hirudin HV1 (65aa, 7.0kDa) presents the disulphide bridges Cys6-Cys14, Cys16-Cys28, Cys22-Cys39 and a sulphated Tyr63. While its polypeptide sequence was identified in 1976 [**8**], its complete primary structure was unravelled only few years later, by Dodt and co-workers [**2**].

Hirudin interacts with thrombin in an extremely tight complex, characterized by an inhibition constant of 10^{-11}-10^{-14}M [**8**]. Due to this dramatically high affinity, hirudin can bind the serine protease both free and in the thrombus-bound state, thus preventing fibrin generation, platelets activation, and amplification of the clotting cascade by factors Va, VIIIa and XIIIa [**9**]. The complex between hirudin and thrombin, described both by X-ray crystallography [**10**;**11**] and by NMR studies [**12**], unravels a singular mode of serine protease inhibition. Hirudin amino-terminal domain occupies a hydrophobic pocket near the active site, composed by His57, Tyr60a, Leu99, Trp215 (chymotrypsinogen numbering). In detail, Val1 interacts with the specificity pocket P2, while Tyr3 is established in P3, leaving the primary specificity pocket P1 unoccupied [**13**]. On the other hand, the C-terminal segment lies in a long groove, extending from the active site pocket, flanked by thrombin loops (70-80) and (35-39). This flexible unfolded region is engaged in both ionic and hydrophobic interactions with the fibrinogen binding site [**14**]. Both N- and C-terminal fragments of hirudin, either produced by limited proteolysis or by peptide synthesis, maintain αT binding, with lower affinity. Moreover, the N-terminal region retains anti-thrombin activity. [**15**;**16**;**17**].

Owing to its remarkably stable anticoagulant properties [**18**], many efforts have been employed to develop hirudin as a pharmaceutical [**19**]. Although its relevant bleeding risks, hirudin offers some advantages over the more popular anticoagulant drug, heparin. In detail, the latter is not

active on clot-bound αT, it requires antithrombin III as a co-factor, and can elicit a severe immune reaction, heparin-induced thrombocytopenia (HIT) [**20**], while hirudin has no immune effects on erythrocytes [**21**]. Mainly, hirudin can be administered for the prophylaxis of deep vein thrombosis, in case of unstable angina pectoris, pulmonary embolism [**22**;**23**] and acute coronary syndromes [**24**;**25**]. During orthopaedic surgery, hirudin prevents venous thromboembolism [**26**;**27**]. Due to its anticoagulant properties, hirudin reduces synovial inflammation in arthritis and osteoarthritis [**28**] even by a topic, local administration [**29**]. Beyond these classical therapeutic purposes, hirudin is gaining an emerging role in the treatment of autoimmune diseases like multiple sclerosis [**30**], of the pregnancy complication preeclampsia [**31**] and it ameliorates intestinal radiation toxicity [**32**]. Moreover, hirudin and leech extracts are increasingly employed for cosmetic purposes, with both injectable and topic applications, during plastic surgery and for minor skin, tissue and circulatory traumas [**33**].

Since hirudin can be recovered only in trace amount from the natural source (≈20g/leech head) [**34**], in the past few decades a number of technological platforms have been developed to produce active hirudin in high purity. Some of the hosts tested have been bacteria (*Escherichia coli*, *Bacillus subtilis*, *Streptomyces lividans*), yeasts (*Saccharomyces cerevisiae*, *Pichia pastoris*, *Hansenula polymorpha*), infected insect cells, the fungus *Acremonium chrysogenum*, BHK cells and transgenic plants [**35**]. In this work, we focused our efforts on the production of soluble recombinant hirudin HV1 from *E. coli*. Among the systems available for the production of heterologous proteins, *E. coli* remains one of the most attractive because of its ability to grow rapidly and controlled, producing massive amounts of target proteins with inexpensive substrates. In the past, however, hirudin soluble expression in *E. coli* [**36**;**37**] resulted in low yields (≈1mg/l), attributable to the cytosolic degradation. Additionally, a mixture of two hirudins was produced: Met- and the less active Met+ at N-terminus [**38**]. To overcome these issues, we decided to express HV1 fused to SUMO protein [**39**].

SUMO (small ubiquitin-like modifier protein) is a ≈100aa specie involved in the modulation of proteins structure and function in eukaryotes, by covalent modification of the target [**40**;**41**;**42**]. Yeasts are characterized by a single SUMO gene (SMT3), while vertebrates carry three genes (SUMO-1; SUMO-2; SUMO-3) [**43**]. Conjugation to SUMO enhances proteins expression by increasing their folding and solubility in *E. coli* strains [**44**]. Recently, a hexa-histidine SUMO fusion construct has been shown to provide an efficient purification yield, by IMAC chromatography [**45**]. Moreover, after the expression, the fusion protein is released by SUMO specific proteases. Yeast SUMO proteases, Ulp1 and Ulp2, naturally recognize SUMO C-terminal region (-GGATY) and cleave it to give the mature protein (-GG) [**46**]. These enzymes are tremendously specific, since they recognize exclusively SUMO tertiary structure rather than a linear epitope, and require only the

terminal (-GG) sequence for the proteolysis. As a result, the conjugated recombinant proteins are released from SUMO starting with their natural N-terminus, without the retention of foreign amino acids downstream the cleavage site. This feature is crucial for hirudin, which requires the region (1-3) for its biological activity. In conclusion, SUMO conjugation represents an advancement in technological systems for soluble protein expression [**47**].

EXPERIMENTALS

Reagents

HV1 gene was synthesized in Prof. Negro's laboratory (Dept. of Biology - University of Padua), and cloned in a pET plasmid expression vector, containing the highly engineered His-tag SUMO (SMT3) gene. From here, we will refer to SUMO-HV1 as HV1 covalently linked by its N-terminal Val1 to the C-terminal segment (-GG) of His-tag SUMO, from SMT3 gene. Recombinant His-tag Ulp1 protease was engineered and expressed in Prof. Negro's laboratory. All salts, solvents and reagents of analytical grade were from Sigma (St. Louis, MO, USA). IMAC resin, used for the purification of the proteins of interest, was obtained from Biorad (Hercules, CA, USA). Human αT was purchased from Haematologic Technologies (Essex Junction, VT, USA), while the chromogenic substrate S2238 (D-Phe-Pip-Arg-pNA) was bought from Chromogenix (Milan, Italy). Endoproteinase GluC V8 from *Staphylococcus aureus* and thermolysin from *Bacillus thermoproteolyticus rokko* (not in commerce anymore) were obtained from Sigma (St. Louis, MO, USA). Trypsin from bovine pancreas was resourced from Promega (Milan, Italy).

Expression of SUMO-HV1

SUMO-HV1 expression vector was transformed by thermic shock into *E. coli* BL21*(DE3)pLysS cells. The transformed cells were selected on LB Agar supplemented with ampicillin (50μg/ml) overnight at 37°C. Protein expression was carried on in 500ml of LB Broth medium at room temperature (≈20°C), under vigorous shaking. Bacterial growth was monitored by measuring the absorbance at 600nm. When the O.D. of 0.7 was reached, the cells were induced with 1mM IPTG, and cultured overnight at room temperature. The bacteria were harvested by centrifugation at 6500rpm, for 20min at 4°C. The pellet was resuspended in 2ml of PBS, and stored at -20°C. A small amount of the *E. coli* suspension was collected to monitor SUMO-HV1 expression. The overall expression was checked on the whole pellet. On the other hand, the degree of soluble protein was tested on the supernatant deriving from bacteria sonication in PBS, in analytical scale. The samples were mixed with reducing GLB, boiled for 5min, and analysed in SDS-PAGE (4-12%

acrylamide), Coomassie stained. After the expression check, the pellet was resuspended in 100ml of buffer 40mM TRIS-HCl pH 8.0, 100mM NaCl and sonicated twice, 5ml to time. The cellular suspension was centrifuged at 10,000g, for 30min at 4°C: the collected supernatant was stored at 4°C for the purification.

Purification and Chemical Characterization of SUMO-HV1

The purification of SUMO-HV1 was performed by an IMAC chromatography. About 3ml of IMAC resin were washed with 10ml of 40mM TRIS-HCl pH 8.0, 100mM NaCl buffer, and added to the bacterial lysis supernatant (100ml). The interaction between Ni^{2+} ions and the histidine tag was achieved by slow stirring at 4°C for an hour. After sedimentation, the resin was loaded on a disposable column and conditioned with 60ml of the washing buffer. SUMO-HV1 was eluted by 10ml of 40mM TRIS-HCl pH 6.5, 100mM NaCl, 400mM imidazole. The collected fractions were pooled, dialyzed overnight versus 500ml of PBS and quantified by UV-Vis measurements at 280nm, using an absorption coefficient of $0.245 mg^{-1} \cdot cm^2$, calculated on the amino acidic composition of SUMO-HV1, assuming all the six Cys engaged in disulphide bridges.

Increasing amounts (3-7-15μg) of the purified SUMO-HV1 were added to non-reducing gel loading buffer, boiled for 3min, analysed by SDS-PAGE (4-12% acrylammide) and Coomassie stained. The degree of purification was quantified by a densitometric analysis, achieved with the free software ImageJ. *In situ* tryptic digestion confirmed SUMO-HV1 amino acidic sequence. An aliquot of 50μg was analysed by RP-HPLC from Jasco (Tokyo, Japan) on a C4 Vydac analytical column (4.6x150mm, 5μm, 300Å) (Hesperia, CA, USA) at a flow rate of 0.8ml/min. The sample was eluted with a linear acetonitrile-0.078% TFA gradient of 20-55% in 50min. The material collected from the two major peaks was lyophilized in Savant SpeedVac concentrator from ThermoScientific (Waltham, MA, USA) and analysed by high-resolution MS on a Xevo G2-S Q-TOF apparatus from Waters (Milford, MA, USA). The mass versus charge spectra were deconvoluted by the software MaxEnt1, yielding the species average mass values.

Cleavage of SUMO-HV1 and One-Step Purification of HV1

Recombinant HV1 was obtained from the bacterial cytosol by one-step IMAC purification. After a new expression trial of SUMO-HV1 (500ml), a fraction of the clear supernatant from cellular lysis (about 15mg of the fusion protein) was added to 3ml of conditioned IMAC resin and the derivatization was performed as detailed above. The resin was manually packed in a disposable column, which was connected to a peristaltic pump; the flow through (about 5ml) was collected for further analysis. The cleavage of SUMO-HV1 was achieved by 50μg of His-tag Ulp1 in 5ml of 50mM

TRIS-HCl pH 8.0, 150mM NaCl, 0.2% NP-40 (v/v), 5mM DTT, applied directly in the peristaltic circuit: the reaction was carried on for 6h at 28°C. After that, the flow through was collected, and the complete elution of the protein mixture was promoted by applying 5ml of 40mM TRIS-HCl pH 6.5, 300mM NaCl, 20mM imidazole.

An aliquot of 25µl from the three steps was cold precipitated in EtOH, resuspended in reducing gel loading buffer, boiled for 3min, and analysed by SDS-PAGE (4-16% acrylamide), Coomassie stained. Moreover, HV1 was further purified by RP-HPLC from Jasco (Tokyo, Japan) on a C4 Vydac semipreparative column (10x250mm, 5µm, 300Å) (Hesperia, CA, USA) at a flow rate of 1.5ml/min. An aliquot of 300µl of the second flow through was eluted with a linear biphasic acetonitrile-0.078% TFA gradient of 15-45% in 35min. The material collected from the major peak was lyophilized, and analysed again by RP-HPLC, in the same conditions detailed above.

Determination of HV1 Oxidation State

An aliquot of 30µg of purified HV1 was analysed by RP-HPLC from Jasco (Tokyo, Japan) on a C4 Vydac analytical column (4.6x150mm, 5µm, 300Å) (Hesperia, CA, USA) at a flow rate of 0.8ml/min. The sample was eluted with a linear acetonitrile-0.078% TFA gradient of 5-55% in 50min. The material collected from the major peak was analysed by high resolution MS, lyophilized and resuspended in 1ml of 100mM TRIS-HCl pH 7.4, 6M Gnd-HCl, 1mM EDTA, 125mM DTT for 90min at 37°C. This sample was analysed by RP-HPLC and by high resolution MS as detailed above.

Assignment of the Disulphide Bridges

Three progressive steps of limited proteolysis completed the detection of recombinant HV1 disulphide bridges. All the proteolysis mixtures were analysed by RP-HPLC from Jasco (Tokyo, Japan) on a C18 Vydac analytical column (4.6x250mm, 5µm, 300Å) (Hesperia, CA, USA) at a flow rate of 0.8ml/min, with a linear acetonitrile-0.078% TFA gradient.

First, about 100µg of hirudin from RP-HPLC, were collected and lyophilized. The full length protein was subjected to proteolysis by GluC V8 from *Staphylococcus aureus* in 200µl of PBS, with an enzyme:substrate ratio of 1:20 (w/w). The reaction, performed overnight at 37°C, was quenched by 5µl of H_2O-TFA 4%. The cleavage mixture was eluted by a 5-45% acetonitrile-0.078% TFA gradient in 45min; the major peak of the chromatogram was analysed high resolution MS and was identified as the N-terminal fragment (1-43).

In a second stage, lyophilized HV1(1-43) from the previous RP-HPLC step was resuspended in 200µl of PBS added with 5mM $CaCl_2$, and subjected to limited proteolysis by thermolysin from

Bacillus thermoproteolyticus rokko. The reaction, accomplished for 4h at 37°C in a protease:substrate ratio of 1:5 (w/w), was stopped by adding 5µl of H_2O-TFA 4%, and analysed in RP-HPLC with a 5-35% acetonitrile-0.078% TFA gradient in 45min. The chromatogram showed five major peaks, named Th1-Th5, and identified by experimental MS.

The lyophilized peptide identified as Th3 (**see Results**) was subjected to tryptic digestion in 200µl of PBS added with 5mM $CaCl_2$, overnight at 37°C. Unfortunately, the reaction has yet to be optimized.

Spectroscopic Studies

Protein concentration was determined by UV-Vis absorption at 280nm on a double-beam Jasco (Tokyo, Japan) V-630 spectrophotometer, equipped with a Peltier thermostat PAC-743, recording the spectra from 350nm to 240nm in PBS buffer. The absorption coefficient of 0.481 $mg^{-1} \cdot cm^2$ was calculated on the amino acidic composition, assuming all the Cys engaged in the three disulphide bridges, as previously determined. The second-derivative spectra was calculated according to the Savitzky-Golay model.

Fluorescence emission measurements were carried out at 20°C in PBS on a Jasco (Tokyo, Japan) FP-6500 spectrofluorimeter, equipped with a thermostated cell holder, at a protein concentration of 15µM. Samples were excited at 275nm, while fluorescence spectra were recorded from 280nm to 500nm in a 1-cm pathlength quartz cell. The data were subtracted of the solvent contribution.

CD measurements were performed on a Jasco (Tokyo, Japan) model J-810 spectropolarimeter, equipped with a thermostated cell holder connected to a model RTE-111 (NesLab) water-circulating bath. Far- and near-UV CD spectra were recorded at protein concentrations ranging from 15µM to 90µM, using 2- or 5-mm pathlength quartz cells in the far- and near-ultraviolet regions, respectively. All the measurements were performed at 20°C in PBS buffer.

Anti-thrombin Activity of HV1

The anti-thrombin activity of the fusion protein SUMO-HV1 and of the recombinant HV1 were measured by an enzymatic assay, using the chromogenic substrate S2238. Increasing hirudin concentrations (0, 25, 50, 250, 1000, 2000pM) were incubated for 20min at 37°C with 100pM αT in buffer HBS. After adding 20µM of S2238, in a final volume of 800µl, the absorbance at 405nm was recorded for 8min at 37°C on a Jasco (Tokyo, Japan) V-630 spectrophotometer, equipped with a Peltier thermostat PAC-743. The slopes v_i/v_0 of the curves were plotted against hirudin

concentrations, and the experimental data were interpolated with a tight binding equation [**48**] (**equation 1**), giving the apparent inhibition constant K_i^{app}:

$$\frac{v_i}{v_0} = 1 - \frac{([E]+[I]+K_i^{app}) - \sqrt{(([E]+[I]+K_i^{app})\text{^}2 - 4[E]\cdot[I])}}{2\cdot[E]} \qquad \textbf{(Eq. 1)}$$

where v_i is the slope of the curve in the presence of the concentration [I] of inhibitor; v_0 is the slope of the curve in the absence of inhibitor; [E] is the enzyme (αT) concentration; [I] is the inhibitor (SUMO-HV1 or HV1) concentration; K_i^{app} is the apparent inhibition constant of hirudin on αT.

Since HV1 inhibits αT activity with a competitive behaviour, the K_i^{app} was corrected according to **equation 2**:

$$K_i^{app} = K_i \cdot \left(1 + \frac{[S]}{K_m}\right) \qquad \textbf{(Eq. 2)}$$

where K_i is the real inhibition constant of HV1 on αT; [S] is the substrate (S2238) concentration; K_m is the Michaelis-Menten constant of αT on S2238.

A

```
        10         20         30         40         50
MRGSHHHHHH GMASMSDSEV NQEAKPEVKP EVKPETHINL KVSDGSSEIF

        60         70         80         90        100
FKIKKTTPLR RLMEAFAKRQ GKEMDSLRFL YDGIRIQADQ TPEDLDMEDN

       110        120        130        140        150
DIIEAHREQI GGVVYTDCTE SGQNLCLCEG SNVCGQGNKC ILGSDGEKNQ

       160        170
CVTGEGTPKP QSHNDGDFEE IPEEYLQ
```

B

Figure 1. (A) Amino acid sequence and (B) schematic representation of SUMO-HV1 in its colour coded architecture domains. The His-tag region (14aa, 1.7kDa) is highlighted in pink, SUMO (98aa, 11.3kDa) in violet, while hirudin HV1 (65aa, 7.0kDa) in blue. SUMO sequence is based on SMT3 yeasts gene; notably, HV1 N-terminal Val1 is covalently attached to the C-terminal (-GG) SUMO segment.

RESULTS AND DISCUSSION

Recombinant pET SUMO-HV1 Expression Vector

HV1 from the leech *Hirudo medicinalis* is a small protein (65aa, 7.0kDa) characterized by the presence of three disulphide bridges in its N-terminus [**2**]. Since the reducing conditions of the bacterial cytosol allow disulphide bond formation in only few cases [**49**], the gene of interest was fused to the C-terminus of SUMO tag to increase the expression of recombinant HV1 in *E. coli* strains in soluble form [**47**]. SUMO amino acid sequence was based on the yeast SMT3 gene, and engineered to optimize bacterial expression. The insertion of a hexa-histidine sequence before SUMO N-terminus allows efficient purification yields by IMAC chromatography [**45**]. The HV1 gene was cloned into the pET SUMO expression vector downstream the His-SUMO partner and under strong interaction with the T7lac promoter. The translation confirmed the correct amino acidic sequence of both His-SUMO (112aa, 12862.4Da), ending with GG-, and HV1 (65aa, 6969.3Da) (**Fig. 1**).

Expression of SUMO-HV1

The SUMO expression vector was transformed into *E. coli* strains by thermic shock, and the cells were selected on LB Agar plates by ampicillin. The bacteria were inoculated in LB Broth at ≈20°C: reduction of cultivation temperature usually increases the amount of native protein, due to the decrease of the expression rate. When the O.D. at 600nm of 0.7 was reached, the cells were inducted with IPTG and cultured overnight. As shown in SDS-PAGE analysis (**Fig. 2A**), a remarkable degree of cytosolic soluble protein was achieved. The bacterial pellet, harvested by gentle centrifugation, was sonicated in a physiologic buffer in little aliquots. The collected supernatant, containing the cytosolic fraction, was stored at 4°C.

Purification and Characterization of SUMO-HV1 Fusion Protein

Since the SUMO tag contains an N-terminal hexa-histidine sequence, the fusion protein was isolated from the cytosolic fraction by a Ni^{2+}-affinity chromatography in batch. An on-off gradient (400mM imidazole, pH 6.5) allowed us to get the target protein in high purity. About 50mg of SUMO-HV1 were obtained from 500ml of LB Broth. The SDS-PAGE analysis of increasing sample loadings (**Fig. 2B**) revealed a yield of purification of about 91%; the identity of the specie of interest was confirmed by *in situ* tryptic digestion. Notably, both the fusion partners, due to their hydrophilic properties, are characterized by a distinctive electrophoretic mobility. His-SUMO is about 12.9kDa, but migrates at ≈18kDa; on the other side, natural HV1 is about 7.0kDa, but runs on SDS-PAGE as ≈14kDa. As a result, recombinant SUMO-HV1 in non-reducing conditions migrates at ≈28kDa, even if its average molecular weight, calculated from the amino acidic composition, is 19813.9Da.

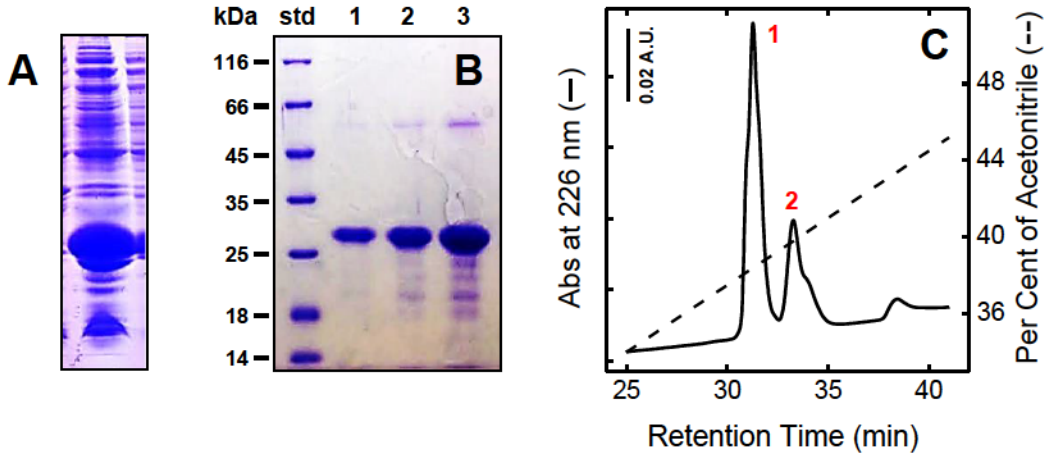

Figure 2. Expression, purification and chemical characterization of SUMO-HV1. (A) Electrophoretic analysis of SUMO-HV1 over-expression in the induced *E. coli* cells. An aliquot of the bacterial pellet was sonicated in an analytical scale and centrifuged. The supernatant was analysed by SDS-PAGE (4-12% acrylamide) under reducing conditions, and Coomassie stained. **(B) Electrophoretic analysis of IMAC-purified SUMO-HV1.** Increasing amounts of the fusion protein were analysed by SDS-PAGE (4-12% acrylamide) under non-reducing conditions, and Coomassie stained. Molecular weight protein standards (std*) was loaded in the left-handed lane. **Lane 1**: 3µg; **lane 2**: 7µg; **lane 3**: 15µg. **(C) RP-HPLC analysis of the purified SUMO-HV1.** An aliquot of 50µg of the IMAC-purified SUMO-HV1 was loaded on a C4 analytical column, eluted with a linear acetonitrile-0.078% TFA gradient of 20-55% in 50min, at flow rates of 0.8ml/min. The material collected from the two major peaks was analysed by high resolution MS.

The RP-HPLC analysis chromatogram of the IMAC-purified protein displays two major peaks, eluted at 38.3% and 39.8% of acetonitrile, respectively (**Fig. 2C**). Unexpectedly, high resolution MS analysis yielded an average molecular weight of 19876.9 a.m.u. for the main (**1**) peak, ≈69 a.m.u. bigger than the theoretical molecular weight, calculated on the amino acidic composition. Since *in situ* tryptic digestion matched 98% of the sequence, we can assume the generation of non-covalent adducts during the purification. On the other hand, the contaminant (**2**) peak displayed a *m/z* pattern typical of a non-protein material.

Purification of Recombinant HV1

After bacterial expression, the protein of interest was recovered in high purity from the cytosolic fraction by one-step IMAC chromatography, as shown from SDS-PAGE analysis in reducing conditions (**Fig. 3C**). About 15mg of SUMO-HV1 were derivatized to IMAC resin, and the proteolysis of the fusion protein was performed directly in the column, by applying His-tag Ulp1 in an enzyme:substrate ratio of 1:300 (w/w) (**Fig. 3A, B**).

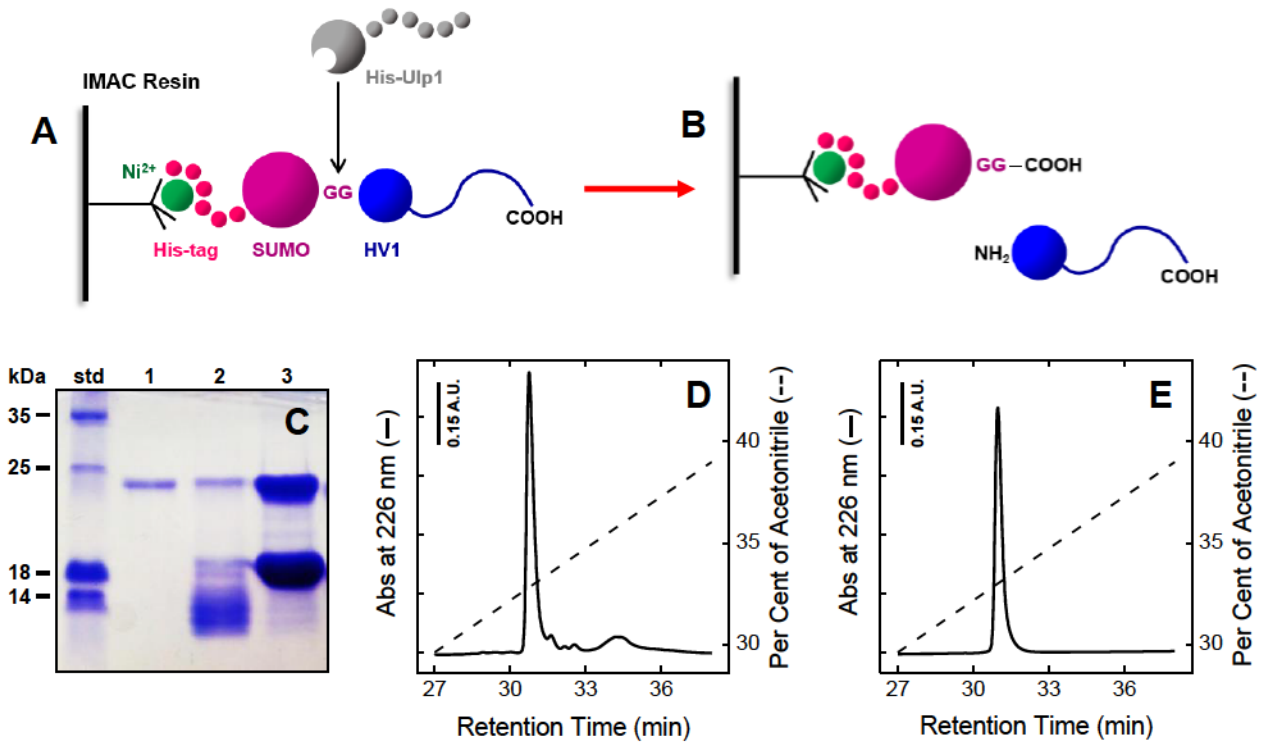

Figure 3. Purification and characterization of recombinant HV1. (A,B) Schematic representation of HV1 purification strategy. After saturating IMAC resin (3ml) with SUMO-HV1 (15mg) by Ni^{2+}-chelation to its His-tag, the cleavage of the fusion protein was performed *in situ* by His-tag recombinant Ulp1 (displayed in grey) in 5ml of proteolysis buffer (**see text**). The reaction was accomplished by recirculation for 6h at 28°C with a peristaltic pump, in an enzyme:substrate ratio of 1:300 (w/w). HV1 is collected in the flow through, while SUMO and the uncleaved SUMO-HV1 remain immobilized to the resin. **(C) Electrophoretic analysis of the IMAC chromatography purification steps.** Aliquots of 25µl of the eluted samples were analysed by SDS-PAGE (4-16% acrylamide) in reducing conditions and Coomassie stained. Molecular weight protein standards (std*) was loaded in the left-handed lane. **Lane 1**: flow through (5ml) before His-tag Ulp1 proteolysis; **lane 2**: flow through (5ml) after the proteolysis; **lane 3**: elution of the material chelated to the resin by 20mM imidazole and 300mM NaCl (5ml). **(D,E) RP-HPLC analysis of the IMAC purified HV1 fraction.** An aliquot of 300µl from the second flow through (**lane 2)** was loaded on a C4 semipreparative column, eluted with an acetonitrile-0.078% TFA gradient of 15-45% in 35min. The major peak at 30min was lyophilized and loaded again in the column.

After 6h of recirculation at 28°C, SUMO and the uncleaved SUMO-HV1 remain attached to the column, while HV1 is collected in the flow through (**Fig. 3C, lane2**). In these experimental conditions, the cleavage of the fusion protein is not complete, due to its immobilization on the column. Notably, the complete saturation of the IMAC resin, as demonstrated from the little loss of SUMO-HV1 before the proteolysis (**Fig. 3C, lane1**), is crucial for the proper purification of the protein of interest. Otherwise, His-tag Ulp1 would attach itself on the top of the column. Moreover, natural HV1 shows a certain degree of Ni^{2+} affinity, due to the surface-accessible His51. On the contrary, the full

resin saturation does not give chance to hirudin for the retention to the column. After Elution of HV1, the complete detachment of both SUMO and uncleaved SUMO-HV1 was promoted at high ionic strength (**Fig. 3C, lane3**). Both SUMO, HV1 and the fusion protein SUMO-HV1 exhibit a lower electrophoretic mobility, due to their hydrophilicity, as explained above. Moreover, hirudin migrates as a broad, non-focused band, due to the heterogeneous interactions of the highly negative, unfolded C-terminal tail with sodium dodecyl sulphate (**Fig. 3C**) [**50**]. After this first chromatographic step, HV1 is purified to an extent of 78%, as calculated from a densitometric analysis performed on the SDS-PAGE by the free software ImageJ.

The complete HV1 purification from the contaminants (His-tag Ulp1 and degradation products) was achieved by RP-HPLC in a semipreparative scale, as highlighted in **Fig. 3D, E**. The purification strategy described in this work is in accord to industrial scale purification methods adopted in the past years for soluble hirudin preparations, like the culture supernatant of yeasts. In previous works, recombinant hirudin was obtained in high purity (≈97%) in a couple of chromatographic steps, including ion-exchange chromatography, affinity chromatography, or even IMAC chromatography [**35**;**51**;**52**]. In particular, Bischoff and co-workers used high performance liquid chromatography to isolate recombinant hirudin produced by yeasts [**51**].

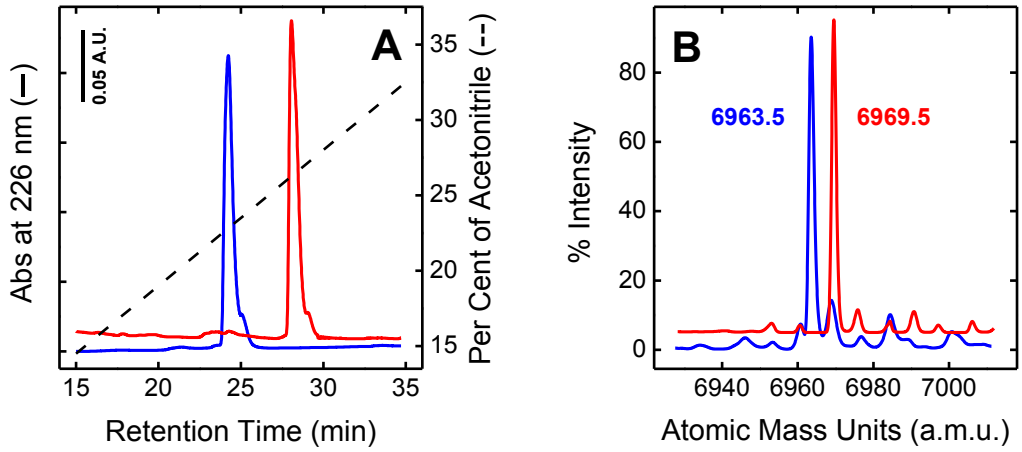

Figure 4. Determination of HV1 oxidation state. (A) RP-HPLC analysis of raw and reduced HV1. An aliquot of 30µg of RP-HPLC purified HV1 was re-loaded on a C4 analytical column, eluted with a linear acetonitrile-0.078% TFA gradient of 5-55% in 50min, at a flow rate of 0.8ml/min (—). The material collected from the major peak was lyophilized and subjected to a reducing treatment, by resuspension in 100mM TRIS-HCl pH 7.4, 6M Gnd-HCl, 1mM EDTA, 125mM DTT, for 90min at 37°C. This solution was analysed by RP-HPLC (—) as previously detailed. **(B) High resolution MS of the purified species.** Average molecular mass values of recombinant HV1 before (—) and after (—) reducing treatment differ of six units, as reported in the panel.

SUMO Fusion Strategy Allows HV1 Expression in the Fully Oxidized State

Although *E. coli* host stands out as the most attractive platform for heterologous protein expression, in most cases it fails the folding of eukaryotic proteins, resulting in the production of inclusion bodies. In this scenario, conjugation to SUMO, characterized by a hydrophobic core and by a hydrophilic surface, has been proved to enhance protein folding and solubility, by a detergent-like action [**44**;**46**]. In order to verify HV1 oxidation state, an aliquot of the protein of interest was purified in analytical scale by RP-HPLC. The material eluted from the major peak was analysed by high resolution MS, lyophilized, and subjected to a denaturing and reducing treatment. The reduced specie was loaded on RP-HPLC in the same experimental conditions and once again analysed by MS (**Fig. 4**). Purified HV1 from the raw cytosolic fraction yields an average experimental mass of 6963.5 a.m.u., in accord with the theoretical mass value of the specie with all the six Cys engaged in disulphide bridges (6963.5 a.m.u.). After the reducing treatment, the specie is eluted at a different retention time in RP-HPLC, and yields an experimental average mass of 6969.5 a.m.u., six units bigger, comparable with the presence of six free Cys. These experimental data confirm that hirudin cleaved from SUMO-HV1 is characterized by a fully oxidised state. It remains unclear whether the fusion protein bears disulphide bonds already in the *E. coli* cytosolic fraction, or if the oxidation process occurs in the mild oxidant conditions of IMAC purification.

Recombinant HV1 is Characterized by the Same Disulphide Bonds as the Natural Specie

The tight HV1 N-terminal region is characterized by three disulphide bonds: Cys6-Cys14, Cys16-Cys28, and Cys22-Cys39. The exact disulphides pairing in the native protein was first determined through a thermolytic digestion [**2**]. In our work, to assert the experimental pairing in recombinant HV1, three subsequent limited proteolysis steps were performed, according to the strategy accomplished by De Filippis and co-workers in 1995 [**16**]. First, fragment (1-43) was quantitatively obtained from the full length protein, by digestion with GluC V8 from *Staphylococcus aureus* (**Fig. 5A**). In these experimental conditions the proteases cleaves at C-terminals of Asp and Glu. The fragment (1-43), virtually correspondent to the N-terminal core, contains all the three disulphide bonds and is way less stable than the whole protein [**15**]. In a second stage, we utilized metalloproteinase thermolysin from *Bacillus thermoproteolyticus rokko*, which shows broad specificity, preferring cleavage on the amino-side of bulky hydrophobic residues. Thermolysin cleaves HV1 (1-43) in five major species, named Th1-Th5 (**Fig. 5B**), which identities were assigned by MS. The monoisotopic mass of the peptides, manually calculated, displayed an error <0.6 a.m.u., compared to the theoretical values (**Table 1A**).

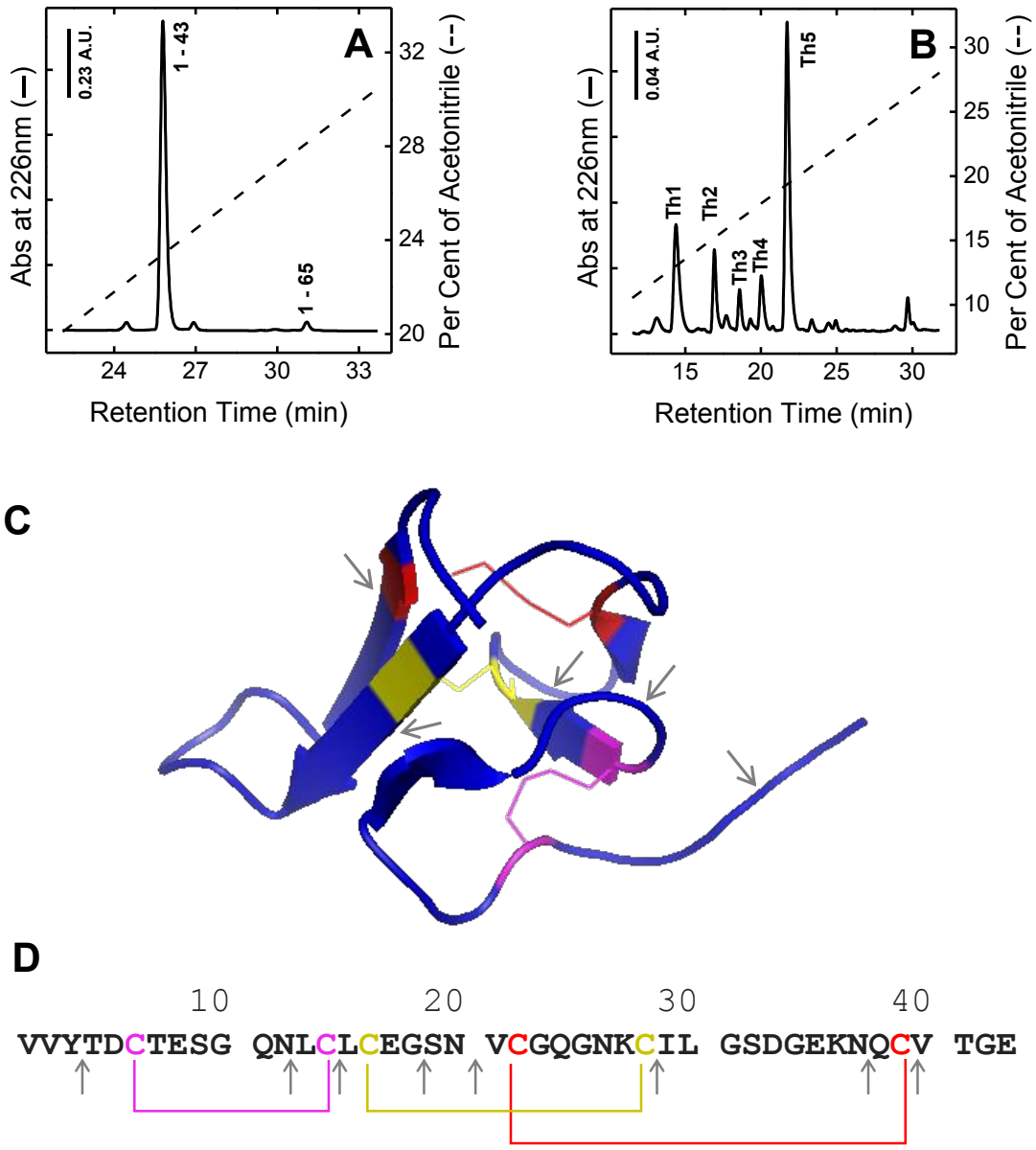

Figure 5. Assignment of recombinant HV1 disulphide bridges. The RP-HPLC analysis were performed on a C18 analytical column, with a linear acetonitrile-0.078% TFA gradient, at a flow rate of 0.8ml/min. **(A) Production of the HV1 N-terminal fragment (1-43) by GluC V8.** About 100µg of full length HV1 were subjected to proteolysis by endoproteinase GluC V8 in an enzyme:substrate ratio of 1:20 (w/w). The reaction, performed overnight in PBS buffer at 37°C, was analysed by RP-HPLC with a 5-45% gradient in 45min. The chromatogram shows a major peak, yielding an experimental average mass in accord to the theoretical molecular weight of fragment (1-43). **(B) Proteolytic digestion of fragment (1-43) by thermolysin.** Lyophilized fragment (1-43) from the previous step was dissolved in 200µl of PBS containing 5mM $CaCl_2$, and treated for 4h at 37°C with thermolysin, at a protease to substrate ratio of 1:5 (w/w). The reaction was analysed by RP-HPLC by a 5-35% gradient in 45min. Thermolysin cleaves HV1 (1-43) giving five major species, named Th1-Th5, as indicated in the panel. **(C) Three-dimensional (pdb: 5hir) and (D) amino acid sequence of HV1 (1-43).** The sites of proteolytic cleavages are stressed by grey arrows. The three disulphide bonds are displayed by different colours: Cys6-Cys14, in magenta; Cys16-Cys28, in yellow; Cys22-Cys39 in red.

	$MW_{monoisotopic}$ (a.m.u.)	Fragment
Th1	1185.43	4-12 13-14
Th2	1673.65	15-18 19-28 38-39
Th3	1472.59	15-18 21-28 38-39
Th4	931.46	29-37
Th5	379.21	1-3

Table 1. Identification of proteolytic peptides from fragment (1-43) digestion by thermolysin. The species composed of multiple sequences are linked by disulphide bridges. In all the measures, the experimental error was less than 0.6 a.m.u., compared to the theoretical MW.

Thermolysin proteolysis sites along HV1(1-43) sequence are indicated by grey arrows in panel **5C, D**: from the digestion it clearly emerges that only the bond Cys6-Cys14, contained in the peptide Th1, can be unequivocally assigned. On the other side, the nicked peptides Th2 and Th3 contain the four Cys residues located in position 16, 22, 28, 39, with two possibilities of pairing. Peptide Th3 was subjected by tryptic digestion in order to hydrolyse the peptide bond Lys27-Cys28, thus obtaining two fragments not linked by disulphide bridges. Unfortunately, the proteolytic conditions have still to be optimized. However, being the hirudin disulphide alignment absolutely peculiar, the probabilities of inverted pairing are extremely low.

Spectroscopic Studies

UV-Visible Absorption - The absorption spectrum of recombinant natural HV1, containing two Tyr (Tyr3, Tyr63) and a single residue of Phe (Phe56) is shown in **Fig. 6A**. As anticipated from its amino acidic composition, the spectra is dominated by the contribution of the Tyr residues, showing a maximal absorption at 275nm. The second-derivative spectra exhibits two maxima at 280nm and 290nm, and two minima at 275nm and 283nm, typical of a Tyr-containing protein [**53**].

Fluorescence - HV1 fluorescence was monitored by exciting the protein sample at 275nm, recording a maximum of emission intensity at 303nm, as expected (**Fig. 6B**).

Far-UV Circular Dichroism - As described by Otto & Seckler, recombinant hirudin shows a very low circular dichroism in the far-UV region ($[\theta]_{220nm} = 7.1 \pm 0.1 \cdot 10^2$ deg·cm^2·dmol^{-1}), indicative of a little content of secondary structure [**54**]. While hirudin C-terminal tail is flexible and unfolded, the N-terminal core is tightly packed in β-antiparallel turns. The β-like secondary structures are characterized by a minimum centred around 217-220nm, as identified in **Fig. 6C**, and by a positive band at 191-193nm [**55**;**56**]. The unusual sharp band detected at 205nm arises from the contribution of the side chain of Tyr3, constrained in the compact amino-terminal region.

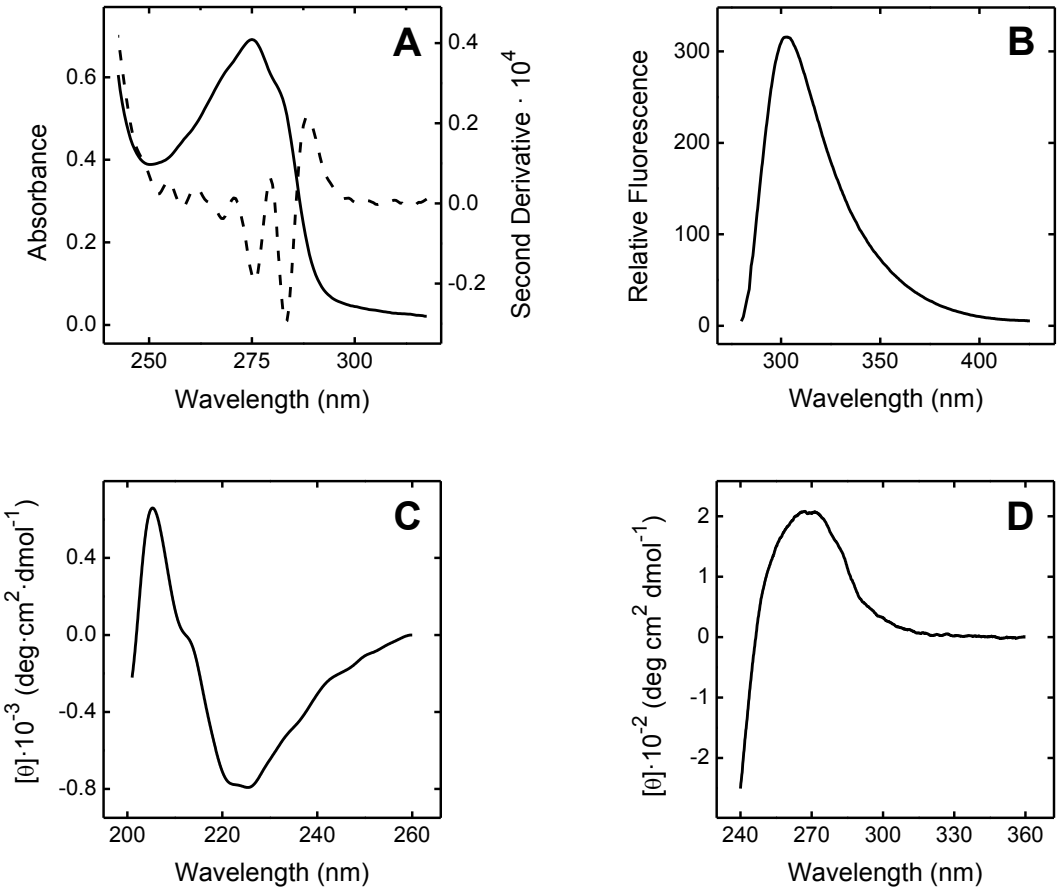

Figure 6. Spectroscopic characterization of recombinant natural HV1. (A) Ultraviolet absorption (**—**) and second-derivative spectra (---) of HV1. **(B)** Fluorescence emission of HV1, after exciting the sample at 275nm. As expected from the amino acid composition, both the absorption and the emission spectra are dominated by the contribution of the two Tyr residues. **(C)** Far-UV CD absorption reveals HV1 β-like structure, and the contribution of Tyr3, located in an asymmetric and rigid environment, for the sharp band at 205nm. **(D)** Near-UV CD spectra reflects the presence of three right-handed disulphide bridges and confirms the influence of Tyr3 for the fine structure bands. All these spectroscopic measurements were performed in PBS at room temperature.

In effect, as previously demonstrated from experimental measurements [**57**;**58**] and theoretical predictions [**59**], the more rigid and asymmetric is the environment, the more the aromatic chromophores contribute to the far-UV CD absorption.

Near-UV Circular Dichroism - The near-UV CD spectra of natural HV1 is nearly identical to those of full length HV3 [**54**], and of the fragment (1-47) of HM2 [**16**]. In particular, the intense positive band centred on 265nm is assigned to the contribution of the three disulphide bonds. Moreover, the signal indicates that the pairings are in right-handed conformation, in accord with the crystallographic structure of the [hirudin- αT] complex described by Rydel [**11**]. Superimposed over the disulphide background, the spectra is complicated by the vibrionic bands at 275nm and 282nm for Tyr3 contribution [**60**]. The appearance of these fine structure bands confirm that at least one Tyr (realistically Tyr3) is located in an asymmetric three-dimensional environment, as suggested from far-UV CD spectrum.

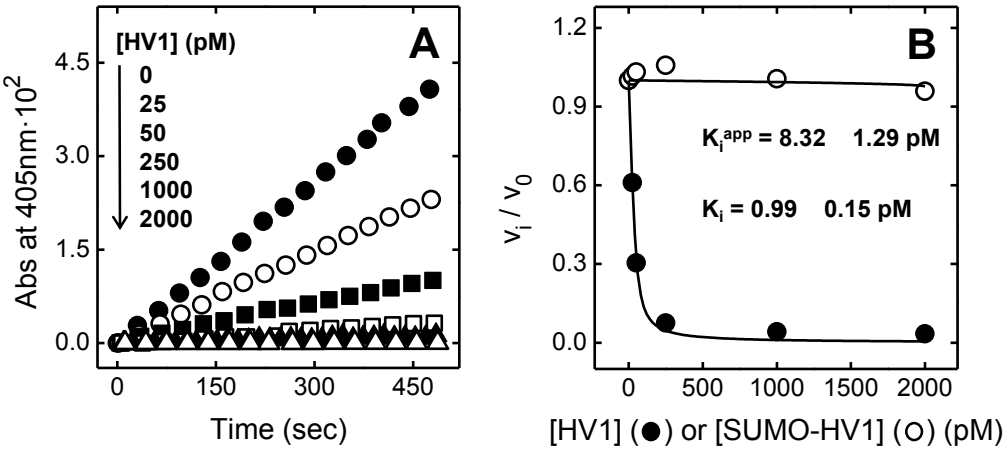

Figure 7. Functional characterization of recombinant SUMO-HV1 and natural HV1 on human αT. (A) Increasing concentrations of recombinant SUMO-HV1 or HV1 (0, 25, 50, 250, 1000, 2000pM) were pre-incubated at 37°C with 100pM αT in HBS for 20min. After adding 20μM of S2238 in a final volume of 800μl, the absorbance at 405nm was monitored at 37°C for 8min. Notably, in the presence of SUMO-HV1, αT proteolytic activity is retained (**data not shown**). **(B)** For each curve, the slope v_i, indicative for αT catalytic efficiency, was calculated. The ratios v_i/v_0 (slope in the absence of the inhibitor) were then plotted versus HV1(●) or SUMO-HV1(○) concentrations, and the data points were interpolated with **eq. 1**, giving an apparent K_i^{app} = 8.32±1.29pM for HV1. Since HV1 inhibits αT with a competitive behaviour, the effective K_i calculated by **eq. 2** was of 0.99±0.15pM.

Anti-thrombin Activity of HV1

HV1 activity on αT was measured by an enzymatic assay on the chromogenic substrate S2238 (D-Phe-Pip-Arg-pNA), and compared to SUMO-HV1. After thrombin cleavage, the synthetic peptide releases p-nitroaniline, absorbing the visible light at 405nm, in the yellow region of the spectrum (**Fig. 6A**). Being hirudin a slow tight binder, increasing amounts of SUMO-HV1 or HV1 were incubated with thrombin for 20min, before the chromogenic assay got started.

The experimental measurements clearly demonstrate that the fusion protein has no effects on αT activity (**Fig. 6B**). These data are in accord with the observation that the N-terminus of HV1 is crucial for the binding to thrombin. In particular, as observed in the crystallographic complex [**13**], Val1 and Tyr3 are engaged in hydrophobic interaction with αT specificity sites P2 and P3, respectively. Hence, it is reasonable that the fusion protein, being HV1 N-terminus covalently attached to SUMO-tag, retains no inhibitory activity towards the serine protease.

On the other hand, natural HV1 inhibits αT with an apparent constant K_i^{app} = 8.32±1.29pM. Since hirudin inhibits the serine protease in a competitive fashion, this value was corrected according to **equation 2**, assuming a K_m value of αT for S2238 of 2.71±.25pM in physiologic conditions [**61**]. The resulting K_i value of 0.99±0.15pM is about ten folds higher than natural HV1, in accord with previous observations. It has been demonstrated, indeed, that unsulphated hirudin, produced by recombinant technologies, retains anti-thrombin functions yet loosing ten-fold affinity [**62**].

CONCLUSIONS

Hirudin, from the salivary glands of the medicinal leech, is the most potent αT natural inhibitor, being characterized by remarkably stable anticoagulant properties. Nowadays, hirudin is gaining an emerging therapeutic role for the treatment of both the classical thrombotic disorders, and for non-canonical purposes, including plastic surgery and cosmetic procedures. Since hirudin can be recovered only in traces from its natural source, many efforts have been performed to develop convenient engineered platforms for its expression in massive amounts. Among all the hosts, *E. coli* is by far the most attractive; unfortunately, past attempts to express hirudin in the bacterial cells failed, due to protein misfolding and to its extensive degradation in the cytosol.

In this project, we optimized a novel strategy to express hirudin HV1 from the medicinal leech *Hirudo medicinalis* in *E. coli*, by conjugating the protein of interest to the C-terminal (-GG) of His-tag SUMO protein. The synthetic SUMO-HV1 fusion gene expression vector was transformed into BL21*(DE3)pLysS cells by thermic shock. The induction was performed in hypothermic conditions

to enhance the amount of soluble protein. After expression, 50mg of SUMO-HV1 were obtained from 500ml of LB Broth. Recombinant HV1 was purified to homogeneity by two chromatographic techniques: IMAC and RP-HPLC. After its immobilization to the IMAC resin, SUMO-HV1 was cleaved *in situ* by His-tag Ulp1, recirculating in a peristaltic pump. Native HV1, collected from the flow through, was further purified by RP-HPLC in a semipreparative scale. MS and fingerprinting analysis revealed that HV1 is expressed in a fully oxidized state, with the natural disulphide pairings Cys6-Cys14, Cys16-Cys28, and Cys22-Cys39. In a second stage, after a spectroscopic characterization, native HV1 was tested on αT activity, displaying an inhibition constant of 0.99±0.15pM in physiologic conditions (pH 7.4, 37°C). Since recombinant HV1 lacks of the sulphated Tyr63, this value is totally in accord to natural hirudin anti-thrombin activity.

REFERENCES

[1] Markwardt F. Hirudin; an inhibitor of blood coagulation from medical leeches. Blut 1958 Jun;4(3):160-161.

[2] Dodt J, Seemuller U, Maschler R, Fritz H. The complete covalent structure of hirudin. Localization of the disulfide bonds. Biol Chem Hoppe Seyler 1985 Apr;366(4):379-385.

[3] Harvey RP, Degryse E, Stefani L, Schamber F, Cazenave JP, Courtney M, et al. Cloning and expression of a cDNA coding for the anticoagulant hirudin from the bloodsucking leech, Hirudo medicinalis. Proc Natl Acad Sci U S A 1986 Feb;83(4):1084-1088.

[4] Tripier D. Hirudin: a family of iso-proteins. Isolation and sequence determination of new hirudins. Folia Haematol Int Mag Klin Morphol Blutforsch 1988;115(1-2):30-35.

[5] Electricwala A, Hartwell R, Scawen MD, Atkinson T. The complete amino acid sequence of a hirudin variant from the leech Hirudinaria manillensis. J Protein Chem 1993 Jun;12(3):365-370.

[6] Scacheri E, Nitti G, Valsasina B, Orsini G, Visco C, Ferrera M, et al. Novel hirudin variants from the leech Hirudinaria manillensis. Amino acid sequence, cDNA cloning and genomic organization. Eur J Biochem 1993 May 15;214(1):295-304.

[7] Bagdy D, Barabas E, Graf L, Petersen TE, Magnusson S. Hirudin. Methods Enzymol 1976;45:669-678.

[8] Stone SR, Hofsteenge J. Kinetics of the inhibition of thrombin by hirudin. Biochemistry 1986 Aug 12;25(16):4622-4628.

[9] Hoffmann A, Markwardt F. Inhibition of the thrombin-platelet reaction by hirudin. Haemostasis 1984;14(2):164-169.

[10] Rydel TJ, Ravichandran KG, Tulinsky A, Bode W, Huber R, Roitsch C, et al. The structure of a complex of recombinant hirudin and human alpha-thrombin. Science 1990 Jul 20;249(4966):277-280.

[11] Rydel TJ, Tulinsky A, Bode W, Huber R. Refined structure of the hirudin-thrombin complex. J Mol Biol 1991 Sep 20;221(2):583-601.

[12] Folkers PJ, Clore GM, Driscoll PC, Dodt J, Kohler S, Gronenborn AM. Solution structure of recombinant hirudin and the Lys-47----Glu mutant: a nuclear magnetic resonance and hybrid

distance geometry-dynamical simulated annealing study. Biochemistry 1989 Mar 21;28(6):2601-2617.

[13] Grutter MG, Priestle JP, Rahuel J, Grossenbacher H, Bode W, Hofsteenge J, et al. Crystal structure of the thrombin-hirudin complex: a novel mode of serine protease inhibition. EMBO J 1990 Aug;9(8):2361-2365.

[14] Naski MC, Fenton JW,2nd, Maraganore JM, Olson ST, Shafer JA. The COOH-terminal domain of hirudin. An exosite-directed competitive inhibitor of the action of alpha-thrombin on fibrinogen. J Biol Chem 1990 Aug 15;265(23):13484-13489.

[15] Vindigni A, De Filippis V, Zanotti G, Visco C, Orsini G, Fontana A. Probing the structure of hirudin from Hirudinaria manillensis by limited proteolysis. Isolation, characterization and thrombin-inhibitory properties of N-terminal fragments. Eur J Biochem 1994 Dec 1;226(2):323-333.

[16] De Filippis V, Vindigni A, Altichieri L, Fontana A. Core domain of hirudin from the leech Hirudinaria manillensis: chemical synthesis, purification, and characterization of a Trp3 analog of fragment 1-47. Biochemistry 1995 Jul 25;34(29):9552-9564.

[17] Ayala YM, Vindigni A, Nayal M, Spolar RS, Record MT,Jr, Di Cera E. Thermodynamic investigation of hirudin binding to the slow and fast forms of thrombin: evidence for folding transitions in the inhibitor and protease coupled to binding. J Mol Biol 1995 Nov 10;253(5):787-798.

[18] Zeymer U, Neuhaus KL, Wegscheider K, Tebbe U, Molhoek P, Schroder R. Effects of thrombolytic therapy in acute inferior myocardial infarction with or without right ventricular involvement. HIT-4 Trial Group. Hirudin for Improvement of Thrombolysis. J Am Coll Cardiol 1998 Oct;32(4):876-881.

[19] Markwardt F. The development of hirudin as an antithrombotic drug. Thromb Res 1994 Apr 1;74(1):1-23.

[20] Warkentin TE, Levine MN, Hirsh J, Horsewood P, Roberts RS, Gent M, et al. Heparin-induced thrombocytopenia in patients treated with low-molecular-weight heparin or unfractionated heparin. N Engl J Med 1995 May 18;332(20):1330-1335.

[21] Markwardt F. Hirudin as alternative anticoagulant--a historical review. Semin Thromb Hemost 2002 Oct;28(5):405-414.

[22] Corral-Rodriguez MA, Macedo-Ribeiro S, Pereira PJ, Fuentes-Prior P. Leech-derived thrombin inhibitors: from structures to mechanisms to clinical applications. J Med Chem 2010 May 27;53(10):3847-3861.

[23] Fischer KG. The role of recombinant hirudins in the management of thrombotic disorders. BioDrugs 2004;18(4):235-268.

[24] Eikelboom J, White H, Yusuf S. The evolving role of direct thrombin inhibitors in acute coronary syndromes. J Am Coll Cardiol 2003 Feb 19;41(4 Suppl S):70S-78S.

[25] van de Loo A, Bode C. Hirudin in acute coronary syndromes. Semin Thromb Hemost 2002 Oct;28(5):459-466.

[26] Eriksson BI, Dahl OE. Prevention of venous thromboembolism following orthopaedic surgery: clinical potential of direct thrombin inhibitors. Drugs 2004;64(6):577-595.

[27] Weltermann A, Kyrle PA, Eichinger S. Novel anticoagulants for the prevention and treatment of venous thromboembolism. Wien Med Wochenschr 2003;153(19-20):426-433.

[28] Scott DL, Berry H, Capell H, Coppock J, Daymond T, Doyle DV, et al. The long-term effects of non-steroidal anti-inflammatory drugs in osteoarthritis of the knee: a randomized placebo-controlled trial. Rheumatology (Oxford) 2000 Oct;39(10):1095-1101.

[29] Sokolov AV, Acquasaliente L, Kostevich VA, Frasson R, Zakharova ET, Pontarollo G, et al. Thrombin inhibits the anti-myeloperoxidase and ferroxidase functions of ceruloplasmin: relevance in rheumatoid arthritis. Free Radic Biol Med 2015 Sep;86:279-294.

[30] Han MH, Hwang SI, Roy DB, Lundgren DH, Price JV, Ousman SS, et al. Proteomic analysis of active multiple sclerosis lesions reveals therapeutic targets. Nature 2008 Feb 28;451(7182):1076-1081.

[31] Zhang Y, Ye YH, Peng W, Zhan Y. Correlation of oxidized low-density lipoprotein and lectin-like oxidized low-density lipoprotein receptor-1 with pre-eclampsia. Zhonghua Fu Chan Ke Za Zhi 2009 Feb;44(2):94-98.

[32] Wang J, Zheng H, Ou X, Albertson CM, Fink LM, Herbert JM, et al. Hirudin ameliorates intestinal radiation toxicity in the rat: support for thrombin inhibition as strategy to minimize side-effects after radiation therapy and as countermeasure against radiation exposure. J Thromb Haemost 2004 Nov;2(11):2027-2035.

[33] Abdualkader AM, Ghawi AM, Alaama M, Awang M, Merzouk A. Leech therapeutic applications. Indian J Pharm Sci 2013 Mar;75(2):127-137.

[34] Markwardt F. Biochemical basis for the control of anticoagulant and thrombolytic therapy. Folia Haematol Int Mag Klin Morphol Blutforsch 1970;94(2):116-128.

[35] Sohn JH, Kang HA, Rao KJ, Kim CH, Choi ES, Chung BH, et al. Current status of the anticoagulant hirudin: its biotechnological production and clinical practice. Appl Microbiol Biotechnol 2001 Dec;57(5-6):606-613.

[36] Dodt J, Schmitz T, Schafer T, Bergmann C. Expression, secretion and processing of hirudin in E. coli using the alkaline phosphatase signal sequence. FEBS Lett 1986 Jul 7;202(2):373-377.

[37] Harvey RP, Degryse E, Stefani L, Schamber F, Cazenave JP, Courtney M, et al. Cloning and expression of a cDNA coding for the anticoagulant hirudin from the bloodsucking leech, Hirudo medicinalis. Proc Natl Acad Sci U S A 1986 Feb;83(4):1084-1088.

[38] Courtney M, Loison G, Lemoine Y, Riehl-Bellon N, Degryse E, Brown SW, et al. Production and evaluation of recombinant hirudin. Semin Thromb Hemost 1989 Jul;15(3):288-292.

[39] Lu W, Cai X, Gu Z, Huang Y, Xia B, Cao P. Production and characterization of hirudin variant-1 by SUMO fusion technology in E. coli. Mol Biotechnol 2013 Jan;53(1):41-48.

[40] Johnson ES, Blobel G. Cell cycle-regulated attachment of the ubiquitin-related protein SUMO to the yeast septins. J Cell Biol 1999 Nov 29;147(5):981-994.

[41] Melchior F. SUMO--nonclassical ubiquitin. Annu Rev Cell Dev Biol 2000;16:591-626.

[42] Tatham MH, Jaffray E, Vaughan OA, Desterro JM, Botting CH, Naismith JH, et al. Polymeric chains of SUMO-2 and SUMO-3 are conjugated to protein substrates by SAE1/SAE2 and Ubc9. J Biol Chem 2001 Sep 21;276(38):35368-35374.

[43] Kawabe Y, Seki M, Seki T, Wang WS, Imamura O, Furuichi Y, et al. Covalent modification of the Werner's syndrome gene product with the ubiquitin-related protein, SUMO-1. J Biol Chem 2000 Jul 14;275(28):20963-20966.

[44] Malakhov MP, Mattern MR, Malakhova OA, Drinker M, Weeks SD, Butt TR. SUMO fusions and SUMO-specific protease for efficient expression and purification of proteins. J Struct Funct Genomics 2004;5(1-2):75-86.

[45] Zuo X, Li S, Hall J, Mattern MR, Tran H, Shoo J, et al. Enhanced expression and purification of membrane proteins by SUMO fusion in Escherichia coli. J Struct Funct Genomics 2005;6(2-3):103-111.

[46] Li SJ, Hochstrasser M. A new protease required for cell-cycle progression in yeast. Nature 1999 Mar 18;398(6724):246-251.

[47] Marblestone JG, Edavettal SC, Lim Y, Lim P, Zuo X, Butt TR. Comparison of SUMO fusion technology with traditional gene fusion systems: enhanced expression and solubility with SUMO. Protein Sci 2006 Jan;15(1):182-189.

[48] Morrison, J. F. (1969) *Biochim. Biophys. Acta*, 185, 269.

[49] Miele L, Cordella-Miele E, Mukherjee AB. High level bacterial expression of uteroglobin, a dimeric eukaryotic protein with two interchain disulfide bridges, in its natural quaternary structure. J Biol Chem 1990 Apr 15;265(11):6427-6435.

[50] Electricwala A, Sawyer RT, Jones CP, Atkinson T. Isolation of thrombin inhibitor from the leech Hirudinaria manillensis. Blood Coagul Fibrinolysis 1991 Feb;2(1):83-89.

[51] Bischoff R, Roecklin D, Roitsch C. Analysis of recombinant proteins by isoelectric focusing in immobilized pH gradients. Electrophoresis 1992 Apr;13(4):214-219.

[52] Rosenfeld SA, Nadeau D, Tirado J, Hollis GF, Knabb RM, Jia S. Production and purification of recombinant hirudin expressed in the methylotrophic yeast Pichia pastoris. Protein Expr Purif 1996 Dec;8(4):476-482.

[53] Balestrieri C, Colonna G, Giovane A, Irace G, Servillo L. Second-derivative spectroscopy of proteins. A method for the quantitative determination of aromatic amino acids in proteins. Eur J Biochem 1978 Oct 16;90(3):433-440.

[54] Otto A, Seckler R. Characterization, stability and refolding of recombinant hirudin. Eur J Biochem 1991 Nov 15;202(1):67-73.

[55] Brahms S, Brahms J. Determination of protein secondary structure in solution by vacuum ultraviolet circular dichroism. J Mol Biol 1980 Apr;138(2):149-178.

[56] Kelly SM, Price NC. The use of circular dichroism in the investigation of protein structure and function. Curr Protein Pept Sci 2000 Dec;1(4):349-384.

[57] Vuilleumier S, Sancho J, Loewenthal R, Fersht AR. Circular dichroism studies of barnase and its mutants: characterization of the contribution of aromatic side chains. Biochemistry 1993 Oct 5;32(39):10303-10313.

[58] Freskgard PO, Martensson LG, Jonasson P, Jonsson BH, Carlsson U. Assignment of the contribution of the tryptophan residues to the circular dichroism spectrum of human carbonic anhydrase II. Biochemistry 1994 Nov 29;33(47):14281-14288.

[59] Manning MC, Woody RW. Theoretical study of the contribution of aromatic side chains to the circular dichroism of basic bovine pancreatic trypsin inhibitor. Biochemistry 1989 Oct 17;28(21):8609-8613.

[60] Strickland EH. Aromatic contributions to circular dichroism spectra of proteins. CRC Crit Rev Biochem 1974 Jan;2(1):113-175.

[61] DiBella EE, Maurer MC, Scheraga HA. Expression and folding of recombinant bovine prethrombin-2 and its activation to thrombin. J Biol Chem 1995 Jan 6;270(1):163-169.

[62] Hofsteenge J, Stone SR, Donella-Deana A, Pinna LA. The effect of substituting phosphotyrosine for sulphotyrosine on the activity of hirudin. Eur J Biochem 1990 Feb 22;188(1):55-59.

APPENDIX

Appendix A

Abbreviations and Symbols

Å, Angstrom

aa, Amino acid

AD, Alzheimer's disease

Amp, Ampicillin

a.m.u., Atomic mass units

aPC, Active protein C

αSyn, Human α-synuclein

αT, Human α-thrombin

ATIII, Antithrombin

AU, Aggregation units

AUC, Area under the curve

BSA, Bovine serum albumin

β_TT, β-thrombin obtained by tryptic digestion

CD, Circular dichroism

ChCl, Choline chloride

Da, Dalton

DIC, Disseminated intravascular coagulation

DLS, Dynamic light scattering

DMSO, Dimethylsulfoxide

DTT, Dithiothreitol

EDTA, Ethylenediaminetetraacetic acid

ESI, Electrospray ionization

EtOH, Ethanol

F1·2, Prothrombin fragments 1 and 2

FI-FXIII, Coagulation factors

FIa-FXIIIa, Activated coagulation factors

Fmoc, Fluorenylmethoxycarbonyl

FpA/B, Fibrinopeptide A or B

Gla, γ-carboxyglutammic acid

Gnd-HCl, Guanidine hydrochloride

HBS, 20mM HEPES pH 7.4, 0.15M NaCl, 0.1% PEG-8000 (w/v)

HBS-$CaCl_2$, HBS added with 5mM $CaCl_2$

HBS-EP, 10mM HEPES pH 7.4, 0.15M NaCl, 50μM EDTA, 0.005% tween-20

HEPES, 4-(2-hydroxyethyl)-1-piperazine ethanesulfonic acid

HM2, Hirudin variant 2 from *Hirudinaria manillensis*

HV1, Hirudin variant 1 from *Hirudo medicinalis*

IMAC, Immobilized metal ions affinity chromatography

IPTG, Isopropyl-β-D-1-thiogalactopyranoside

K1-2, Kringle domain-1 or -2

LB, Lurea Bertani broth

LBs, Lewy Bodies

LC-MS, Liquid chromatography coupled to mass spectrometry

Lnk, Linker in prothrombin sequence

mIIa, Meizothrombin

MS, High-resolution mass spectrometry

MW, Molecular Weight

m/z, Mass to charge ratio

NF-κB, Nuclear factor kappa-light-chain-enhancer of activated B cells

NP-40, Nonyl-phenoxypolyetoxylethanol

NTA, Nitrilotriacetic acid

OD, Optical density

PARs, Protease activated receptors

PBS, 10mM TRIS-HCl, 0.15M NaCl

PC, Protein C

PD, Parkinson's disease

PEG, PolyEthylene Glycol

pNA, para-nitroanilide

Pre2, Prethrombin-2

ProT, Human prothrombin

PSGL-1, P-selectin glycoprotein ligand 1

SDS, Sodium Dodecyl Sulfate

SDS-PAGE, SDS-PolyAcrylamide Gel Electrophoresis

σPre2, Subtilisin-activated Pre2 or ProT

RP-HPLC, Reverse-phase high-pressure liquid chromatography

rT, Recombinant αT from *E. coli*

S2238, D-Phe-Pip-Arg-pNA

SPR, Surface plasmon resonance

SUMO, Small ubiquitin-like modifier protein

TBS, 10mM TRIS-HCl, pH 8.0

TCA, Trichloroacetic acid

TFA, Trifluoroacetic acid

TFPI, Tissue factor pathway inhibitor

TM, Thrombomodulin

TOF, Time-of-flight

TRIS, tris(hydroxymethyl)aminomethane

Ulp-1, Ubiquitin-like specific protease 1

UL-vWF, Ultra large von Willebrand Factor multimers

UV-Vis, Ultraviolet visible spectrophotometry

vWF, von Willebrand Factor

v/v, Volume/volume

w/v, Weight/volume

Appendix B

Amino Acids

Ala	A	Alanine
Arg	R	Arginine
Asp	D	Aspartic acid
Asn	N	Asparagine
Cys	C	Cysteine
Gly	G	Glycine
Gln	Q	Glutamine
Glu	E	Glutamic acid
His	H	Histidine
Ile	I	Isoleucine
Lys	K	Lysine
Leu	L	Leucine
Met	M	Methionine
Phe	F	Phenylalanine
Pro	P	Proline
Ser	S	Serine
Thr	T	Threonine
Tyr	Y	Tyrosine
Trp	W	Tryptophan
Val	V	Valine

Appendix C

Thrombin Numbering Scheme

Chym	T1h	F1g	G1f	S1e	G1d	E1c	A1b	D1a	C1	G2	L3	R4
Ch-A	1	2	3	4	5	6	7	8	9	10	11	12
Ch-B	-	-	-	-	-	-	-	-	-	-	-	-
ProT	285	286	287	288	289	290	291	292	293	294	295	296

Chym	P5	L6	F7	E8	K9	K10	S11	L12	E13	D14	K14a	T14b
Ch-A	13	14	15	16	17	18	19	20	21	22	23	24
Ch-B	-	-	-	-	-	-	-	-	-	-	-	-
ProT	297	298	299	300	301	302	303	304	305	306	307	308

Chym	E14c	R14d	E14e	L14f	L14g	E14h	S14i	Y14j	I14k	D14l	G14m	R15
Ch-A	25	26	27	28	29	30	31	32	33	34	35	36
Ch-B	-	-	-	-	-	-	-	-	-	-	-	-
ProT	309	310	311	312	313	314	315	316	317	318	319	320

Chym	I16	V17	E18	G19	S20	D21	A22	E23	I24	G25	M26	S27
Ch-A	37	38	39	40	41	42	43	44	45	46	47	48
Ch-B	1	2	3	4	5	6	7	8	9	10	11	12
ProT	321	322	323	324	325	326	327	328	329	330	331	332

Chym	P28	W29	Q30	V31	M32	L33	F34	R35	K36	S36a	C37	Q38
Ch-A	49	50	51	52	53	54	55	56	57	58	59	60
Ch-B	13	14	15	16	17	18	19	20	21	22	23	24
ProT	333	334	335	336	337	338	339	340	341	342	343	344

Chym	E39	L40	L41	C42	G43	A44	S45	L46	I47	S48	D49	R50
Ch-A	61	62	63	64	65	66	67	68	69	70	71	72
Ch-B	25	26	27	28	29	30	31	32	33	34	35	36
ProT	345	346	347	348	349	350	351	352	353	354	355	356

Chym	W51	V52	L53	T54	A55	A56	H57	C58	L59	L60	Y60a	P60b
Ch-A	73	74	75	76	77	78	79	80	81	82	83	84
Ch-B	37	38	39	40	41	42	43	44	45	46	47	48
ProT	357	358	359	360	361	362	363	364	365	366	367	368

Chym	P60c	W60d	D60e	K60f	N60g	F60h	T60i	E61	N62	D63	L64	L65
Ch-A	85	86	87	88	89	90	91	92	93	94	95	96
Ch-B	49	50	51	52	53	54	55	56	57	58	59	60
ProT	369	370	371	372	373	374	375	376	377	378	379	380

Chym	V66	R67	I68	G69	K70	H71	S72	R73	T74	R75	Y76	E77
Ch-A	97	98	99	100	101	102	103	104	105	106	107	108
Ch-B	61	62	63	64	65	66	67	68	69	70	71	72
ProT	381	382	383	384	385	386	387	388	389	390	391	392

Chym	R77a	N78	I79	E80	K81	I82	S83	M84	L85	E86	K87	I88
Ch-A	109	110	111	112	113	114	115	116	117	118	119	120
Ch-B	73	74	75	76	77	78	79	80	81	82	83	84
ProT	393	394	395	396	397	398	399	400	401	402	403	404

Chym	Y89	I90	H91	P92	R93	Y94	N95	W96	R97	E97a	N98	L99
Ch-A	121	122	123	124	125	126	127	128	129	130	131	132
Ch-B	85	86	87	88	89	90	91	92	93	94	95	96
ProT	405	406	407	408	409	410	411	412	413	414	415	416

Chym	D100	R101	D102	I103	A104	L105	M106	K107	L108	K109	K110	P111
Ch-A	133	134	135	136	137	138	139	140	141	142	143	144
Ch-B	97	98	99	100	101	102	103	104	105	106	107	108
ProT	417	418	419	420	421	422	423	424	425	426	427	428

Chym	V112	A113	F114	S115	D116	Y117	I118	H119	P120	V121	C122	L123
Ch-A	145	146	147	148	149	150	151	152	153	154	155	156
Ch-B	109	110	111	112	113	114	115	116	117	118	119	120
ProT	429	430	431	432	433	434	435	436	437	438	439	440

Chym	P124	D125	R126	E127	T128	A129	A129a	S129b	L129c	L130	Q131	A132
Ch-A	157	158	159	160	161	162	163	164	165	166	167	168
Ch-B	121	122	123	124	125	126	127	128	129	130	131	132
ProT	441	442	443	444	445	446	447	448	449	450	451	452

Chym	G133	Y134	K135	G136	R137	V138	T139	G140	W141	G142	N143	L144
Ch-A	169	170	171	172	173	174	175	176	177	178	179	180
Ch-B	133	134	135	136	137	138	139	140	141	142	143	144
ProT	453	454	455	456	457	458	459	460	461	462	463	464

Chym	K145	E146	T147	W148	T149	A149a	N149b	V149c	G149d	K149e	G150	Q151
Ch-A	181	182	183	184	185	186	187	188	189	190	191	192
Ch-B	145	146	147	148	149	150	151	152	153	154	155	156
ProT	465	466	467	468	469	470	471	472	473	474	475	476

Chym	P152	S153	V154	L155	Q156	V157	V158	N159	L160	P161	I162	V163
Ch-A	193	194	195	196	197	198	199	200	201	202	203	204
Ch-B	157	158	159	160	161	162	163	164	165	166	167	168
ProT	477	478	479	480	481	482	483	484	485	486	487	488

Chym	E164	R165	P166	V167	C168	K169	D170	S171	T172	R173	I174	R175
Ch-A	205	206	207	208	209	210	211	212	213	214	215	216
Ch-B	169	170	171	172	173	174	175	176	177	178	179	180
ProT	489	490	491	492	493	494	495	496	497	498	499	500

Chym	I176	T177	D178	N179	M180	F181	C182	A183	G184	Y184a	K185	P186
Ch-A	217	218	219	220	221	222	223	224	225	226	227	228
Ch-B	181	182	183	184	185	186	187	188	189	190	191	192
ProT	501	502	503	504	505	506	507	508	509	510	511	512

Chym	D186a	E186b	G186c	K186d	R187	G188	D189	A190	C191	E192	G193	D194
Ch-A	229	230	231	232	233	234	235	236	237	238	239	240
Ch-B	193	194	195	196	197	198	199	200	201	202	203	204
ProT	513	514	515	516	517	518	519	520	521	522	523	524

Chym	S195	G196	G197	P198	F199	V200	M201	K202	S203	P204	F204a	N204b
Ch-A	241	242	243	244	245	246	247	248	249	250	251	252
Ch-B	205	206	207	208	209	210	211	212	213	214	215	216
ProT	525	526	527	528	529	530	531	532	533	534	535	536

Chym	N205	R206	W207	Y208	Q209	M210	G211	I212	V213	S214	W215	G216
Ch-A	253	254	255	256	257	258	259	260	261	262	263	264
Ch-B	217	218	219	220	221	222	223	224	225	226	227	228
ProT	537	538	539	540	541	542	543	544	545	546	547	548

Chym	E217	G219	C220	D221	R221a	D222	G223	K224	Y225	G226	F227	Y228
Ch-A	265	266	267	268	269	270	271	272	273	274	275	276
Ch-B	229	230	231	232	233	234	235	236	237	238	239	240
ProT	549	550	551	552	553	554	555	556	557	558	559	560

Chym	T229	H230	V231	F232	R233	L234	K235	K236	W237	I238	Q239	K240
Ch-A	277	278	279	280	281	282	283	284	285	286	287	288
Ch-B	241	242	243	244	245	246	247	248	249	250	251	252
ProT	561	562	563	564	565	566	567	568	569	570	571	572

Chym	V241	I242	D243	Q244	F245	G246	E247
Ch-A	289	290	291	292	293	294	295
Ch-B	253	254	255	256	257	258	259
ProT	573	574	575	576	577	578	579

In the **first row** the chymotrypsinogen numeration of thrombin is indicated; in the **second row** the numeration in which the first residue of the A-chain is designated as 1 is indicated.; in the **third row** the numeration in which the first residue of the B-chain is designated as 1 is indicated; finally, the **last row** show the numeration of prothrombin.